Agricultural University of Athens

Quaternary multi-proxy analysis of the paleoenvironment, paleogeography and active tectonics of the Corinth Isthmus

Ph.D. Thesis

2018

Aggelos E. Pallikarakis

Mineralogy and Geology Laboratory, Department of Natural Resources Management & Agricultural Engineering, Agricultural University of Athens

Supervisor: Associate Professor, Dr. Papanikolaou Ioannis

Quaternary multi-proxy analysis of the paleoenvironment, paleogeography and active tectonics of the Corinth Isthmus

Ph.D. Thesis

2018

Aggelos E. Pallikarakis

Mineralogy and Geology Laboratory, Department of Natural Resources Management & Agricultural Engineering, Agricultural University of Athens

Supervisor: Associate Professor, Dr. Papanikolaou Ioannis

Ph.D. Thesis

Quaternary multi-proxy analysis of the paleoenvironment, paleogeography and active tectonics of the Corinth Isthmus

Aggelos E. Pallikarakis

Supervisory committee:

Associate Professor **Papanikolaou Ioannis**, AUA, Department of Natural Resources Management & Agricultural Engineering, Laboratory of Mineralogy and Geology, (main supervisor),

Professor **Triantaphyllou Maria**, UOA, Faculty of Geology and Geoenvironment, Historical Geology and Palaeontology, (co-supervisor)

Professor **Reicherter Klaus**, RWTH (Aachen), (co-supervisor)

Examination committee:

Associate Professor. **Papanikolaou Ioannis**, AUA, Department of Natural Resources Management & Agricultural Engineering, Laboratory of mineralogy and Geology, (main supervisor),

Professor **Triantaphyllou Maria**, UOA, Faculty of Geology and Geoenvironment, Historical Geology and Palaeontology, (co-supervisor)

Professor **Reicherter Klaus**, RWTH (Aachen), (co-supervisor)

Professor **Koukouvelas Ioannis**, University of Patra· Department of Geology

Professor **Syrides Georgios**, AUTh, Department of Geology, Laboratory of Geology and Palaeontology

Associate Professor **Alexandris Stavros,** Department of Natural Resources Management & Agricultural Engineering, Laboratory of Agricultural Hydraulics

Assistant Professor **Dimiza Margarita,** UOA, Faculty of Geology and Geoenvironment, Historical Geology and Palaeontology,

Abstract

This Ph.D. aims to shed light upon the interaction between the tectonic movements and the paleoenvironmental changes. The goal is to determine the tectonic uplift and the significance of the regional uplift at the Corinth isthmus, to estimate the slip rate of the Kalamaki-Isthmia fault and reconstruct the paleoenvironment and the paleogeography of the study area following a multidisciplinary approach.

In the tectonically active region of Corinth Isthmus the paleoenvironment and paleogeography has been studied mainly through detailed field mapping, surface observations and data obtained from 11 borehole cores up to 70 m deep. The interplay between the glacioeustatic sea level changes and the active tectonics resulted into a complicated paleoenvironmental pattern and stratigraphic structure. As a result, a multi proxy analysis have been followed that incorporates paleoenvironmental and micropaleontological studies (foraminifera, nannofossils), magnetic susceptibility, absolute dating techniques (U/Th, luminescence), borehole and surface data, geological mapping.

Quantitative analysis of foraminiferal fauna assemblages (355 in total) extracted both from surface outcrops and 8 borehole cores were employed to describe the paleoenvironment and the regional paleodepth estimation. Three indexes have been used to accurately describe the paleoenvironmetal conditions in the examined samples and in particular the foraminifer's density (FD), the percentage of the broken/weathered specimens in each sample (BR ratio) and the relationship between small sized and large *Ammonia* spp. (A-ratio). Magnetic Susceptibility measurements, extracted only from the borehole cores, were also used as an independent methodology to describe the alternations in the sedimentary sequences, while the results were correlated with the findings deprived from foraminiferal analyses.

To determine the age of the sediments three different techniques were employed. Coral dating and luminescence dating techniques were used for absolute dating and

calcareous nannofossils assemblages for relevant dating, with the latter offering a higher reliability.

Based on the data obtained both from the borehole sequences and the examined surface outcrops that have been successfully correlated, a 3-D spatial and temporal distribution of the sediments at the eastern part of the Canal has been described.

Furthermore, based on the ages supported by the nannofossils assemblages and the glacioeustatic sea level curve, the uplift rate of the Eastern part of the Corinth Isthmus has been re-interpreted following an independent approach compared to existing published rates. It is interesting that even though a different approach than previous researchers have followed, approximately the same results have been proposed adding credibility to the existing uplift rates.

The most important active fault that crosses the Corinth Canal has been studied in detail. Also in the basis of the ages proposed both from previous corals data and through nannofossils assemblages, the fault's activity has been estimated verifying a relatively low slip-rate but active fault. Based on the slip rates of the major faults which influence the area; a model has been developed describing the significance of each fault and the influence of the regional uplift to the total uplift rate of the study area, where a regional uplift of approximately 0.34±0.04 mm/yr is required in order to explain the stratigraphy of the boreholes and the paleoenvironmental pattern.

Finally, based on age constraints provided by nannofossils assemblages correlated with the glacioeustatic sea level changes and the uplift rate of the area, the paleogeography at the eastern part of the Corinth Isthmus during Pleistocene has been reconstructed, from MIS 9 (~330 ka) till the present day.

Key words: Paleoenvironment, Paleogeography, Benthic foraminifera, Calcareous nannofossils, Active faults

Περίληψη

Η παρούσα διατριβή έχει σαν αντικείμενο μελέτης την αλληλεπίδραση μεταξύ των τεκτονικών κινήσεων και των παλαιοπεριβαλλοντικών εναλλαγών σε μια περιοχή. Ο σκοπός της εργασίας είναι η μελέτη του ρυθμού τεκτονικής ανύψωσης στην περιοχή μελέτης, του ρυθμού ολίσθησης του ρήγματος Καλαμακίου-Ισθμίων, καθως και η μελέτη και ανακατασκευή του παλαιοπεριβάλλοντος και της παλαιογεωγραφίας στον Ισθμό της Κορίνθου.

Η περιοχή έρευνας είναι η ενεργή τεκτονικά περιοχή της Κορίνθου και κυρίως η περιοχή του Ισθμού, όπου μελετήθηκε μέσω λεπτομερούς χαρτογράφησης της περιοχής, καθώς και δεδομένων από 11 πυρήνες γεωτρήσεων βάθους μέχρι 70 μ. Η έντονη αλληλεπίδραση μεταξύ των τεκτονικών διαδικασιών και των συνεχόμενων μεταβολών της στάθμης της θάλασσας οδήγησε σε ένα πολύπλοκο παλαιοπεριβαλλοντικό μοντέλο. Για την καλύτερη και πληρέστερη ανάλυση των δεδομένων, αξιοποιήθηκαν διαφορικές μεθοδολογίες.

Η ανάλυση των συγκεντρώσεων της μικρό πανίδας τόσο από επιφανειακά δείγματα όσο και από τους πυρήνες γεωτρήσεων ήταν η βασική μεθοδολογία που χρησιμοποιήθηκε για την περιγραφή του παλαιοπεριβάλλοντος. Τρεις δείκτες χρησιμοποιήθηκαν για την ακριβέστερη περιγραφή του παλαιοπεριβάλλοντος και πιο συγκεκριμένα η πυκνότητα των τρηματοφόρων (FD), το ποσοστό των σπασμένων / φθαρμένων τρηματοφόρων σε κάθε δείγμα (BR) και σχέση μεταξύ μικρού και μεγάλου μεγέθους *Ammonia* spp. (A-ratio). Παράλληλα, μετρήθηκε η μαγνητική επιδεκτικότητα στις γεωτρήσεις και έγινε συσχέτιση των παρατηρούμενων εναλλαγών με τις μεταβολές του παλαιοπεριβάλλοντος.

Για τον χρονολογικό προσδιορισμό της ιζηματογένεσης χρησιμοποιήθηκαν τρεις διαφορετικές τεχνικές. Για τον απόλυτο προσδιορισμό της ηλικίας έγινε χρονολόγηση κοραλλιών που βρέθηκαν στα δείγματα των γεωτρήσεων καθώς και μέσω της φωταύγειας των ιζημάτων. Ο σχετικός προσδιορισμός της ηλικίας των ιζημάτων έγινε μέσω της βιοστρωματογραφίας καθώς αναλύθηκαν δείγματα ως προς το περιεχόμενο

τους σε ναννο απολιθώματα. Η τελευταία μεθοδολογία παρείχε τα πιο αξιόπιστα αποτελέσματα.

Με βάση τα δεδομένα που προέκυψαν τόσο από την ανάλυση των επιφανειακών δεδομένων όσο και τα δεδομένα από τις γεωτρήσεις, έγινε η τρισδιάστατη χωρική και χρονική κατανομή των ιζημάτων στο ανατολικό τμήμα της Διώρυγας.

Επιπλέον, με βάση τις εκτιμώμενες ηλικίες έγινε ο επαναπροσδιορισμός του ρυθμού της ανύψωσης του ανατολικού τμήματος του ισθμού της Κορίνθου. Είναι ενδιαφέρον το γεγονός πως παρόλο που έχει ακολουθηθεί μια διαφορετική προσέγγιση σε σχέση με προηγούμενες έρευνες, προκύπτουν περίπου τα ίδια αποτελέσματα, επιβεβαιώνοντας τους προτεινόμενους ρυθμούς ανύψωσης από προηγούμενες μελέτες.

Μελετήθηκε μέσω λεπτομερούς χαρτογράφησης το ρήγμα Καλαμάκι – Ίσθμια το σημαντικότερο ενεργό ρήγμα που τέμνει το κανάλι του Ισθμού της Κορίνθου. Με βάση τις ηλικίες που προτείνονται από την παρούσα διατριβή, εκτιμήθηκε η δραστηριότητα του ρήγματος, επιβεβαιώνοντας έναν σχετικά χαμηλό ρυθμό ολίσθησης ενός κατά άλλα ενεργού ρήγματος. Με βάση την ανάλυση της επίδρασης των σημαντικότερων ρηγμάτων που επηρεάζουν την περιοχή, επιβεβαιώνεται η σημασία της γενικότερης τεκτονικής ανύψωσης της περιοχής.

Με βάση τον σχετικό προσδιορισμό της ηλικίας των ιζημάτων και τις ευστατικές μεταβολές της στάθμης της θάλασσας και την τεκτονική ανύψωση της περιοχής, προσδιορίστηκε η παλαιογεωγραφία στο ανατολικό τμήμα του Ισθμού της Κορίνθου κατά το Τεταρτογενές, με έμφαση κυρίως από MIS 9 (~ 400 ka) μέχρι σήμερα.

Λέξεις κλειδιά: Παλαιοπεριβάλλον, Παλαιογεωγραφία, Βενθονικά τρηματοφόρα, Ασβεστολιθικό νανοπλαγκτόν, Ενεργά ρήγματα.

Acknowledgments

First and foremost, I would like to thank my supervisor Assoc. Prof. Ioannis Papanikolaou for his guidance and most important for his patience all these years. His motivations and his support were essential for accomplishing this Ph.D. thesis.

I am also deeply grateful for the constant support and guidance from Prof. Maria Triantaphyllou.

Special thanks must be made to Prof. Klaus Reicherter for being my committee member.

Furthermore, I am deeply thankful to Prof. Ioannis Koukouvelas, Prof. Georgios Syrides, Assoc. Prof. Stauros Alexandris and Assist. Prof. Margarita Dimiza.

I am also grateful to my colleagues Georgios, Maria, Sofia, Stella, Manolis, Spyros and Olga for their assistance. I would also like to thank my friend and colleague Dr. Psomiadis for his assistance with the DEM of the study area.

I would like to thank my colleagues from the laboratory of Archaeometry / Paleoenvironment & Archaeometallurgy of N.C.S.R. Demokritos, Dr. Bassiakos, Dr. Athanasas and Dr. Tsakalos, for their assistance during luminescence analysis.

Furthermore, I would like to thank Dr. Scholz from the Max Planck Institute for Chemistry in Mainz for ^{230}Th/U corals dating.

I would to thank the Edafomichaniki SA for offering the boreholes cores from the Corinth area which were examined in this PhD thesis

I would like to thank the Academy of Athens scholarship (Mitsopoulos Fund) for their financial support all these years.

Finally I would like to thank my family and my friends for their support all these years and dedicate this work to them.

Table of Contents

1 Introduction

1.1 Introduction

The morphology of the coastal areas is constantly influenced mainly by three major processes (e.g. Emery & Myers, 1994; Nichols, 1999). The first process is tectonic activity, the second is glacioeustatic sea-level changes and the third is sediments' accumulation and/or erosion at the coastal areas. Additional processes may also apply locally (e.g. sea currents) but are considered of secondary importance. The interplay of these three processes results into the constant shifting of the coastline either seawards (regression) or landwards (transgression).

Seawards movement of the coastline (regression, Fig. 1-1) is caused either by sediments accumulation, relative sea level fall or tectonic uplift of the coastal area (forced regression) (e.g. Collier, 1990). Relative sea level rise will force the coastline to move landwards (transgression) (e.g. Nagendra et al., 2011; Scarponi et al., 2014). These changes to the shoreline cause different sedimentary patterns which can be preserved in the vertical stacking of strata as changes in facies going up through a succession (e.g. Amorosi et al., 2014a; Nichols, 1999). A deepening upwards pattern is described as a transgression succession (e.g. Collier, 1990; Emery and Myers, 1996; Nichols, 1999; Scarponi et al., 2014), while the opposite pattern is described as a regression sequence.

Sequence stratigraphy of the sediments is based on the identification of specific strata stacking patterns and characterization of bounding surfaces (Amorosi et al., 2014b). The identification of these depositional trends can be relatively difficult within a borehole sequence considering the lack of geometric constraints and scarcity of sedimentary structures. In such cases the description of the fossil organisms preserved in the core can be used to describe the paleoenvironmental alternations within the core and through them stratigraphical interpretation of the sediments (e.g. Amorosi et al., 2014a, b).

Furthermore, data on fault activity and slip-rates can be extracted from paleoenvironmental analysis and interpretations based on correlating morphological surfaces and stratigraphic data extracted from the surface or boreholes (Yasuhara et al., 2005; Ferranti et al., 2011; Papanikolaou et al., 2015). Papanikolaou et al. (2015) made a pioneer use of paleoenvironmental indicators for extracting the slip-rate of the Kalamaki-Isthmia fault, based on the correlation between the footwall and hangingwall horizons, indicating that only minor displacement of several metres has been accumulated over the last 175 kyrs, suggesting that this structure progressively dies out.

The Corinth Gulf is a fine example to examine these processes since all three factors influence the area. The Gulf is one of the most active and one of the fastest extending regions not only in Greece but worldwide (up to 20 mm/year that diminishes to 8 and 4 mm/year towards its eastern end) (e.g. Billiris et al., 1991; Briole et al., 2000), dominated by major active fault systems, such as the Xylokastro (e.g. Armijo et al., (1996)), the Eliki fault (e.g. Koukouvelas et al., 2005) and the South Alkyonides Fault System (SAFS) (e.g. Morewood and Roberts, 1997, 1999; Collier et al., 1998). The glacioeustatic sea level changes have constantly shifted the coastline landwards and seawards, influencing the type and the duration of the sedimentation. Furthermore, the drainage system (e.g. Rachiotis) supplies coarse sediments in the Corinth Gulf, resulting into successively packages of fluvial – torrential and marine layers.

The latter can be observed in the Corinth Canal, a 6.3 km long and up to ~ 90 m high mega – trench (Marinos and Tsiambaos, 2008; Papantoniou et al., 2008), excavated during 1893. The described sediments in the Canal (e.g. Collier, 1990) combined with the data obtained from 11 boreholes, all of them drilled at the eastern part of the Canal; offer an opportunity for a detailed study of the sedimentological processes and syn sedimentary faults in a highly complicated environment.

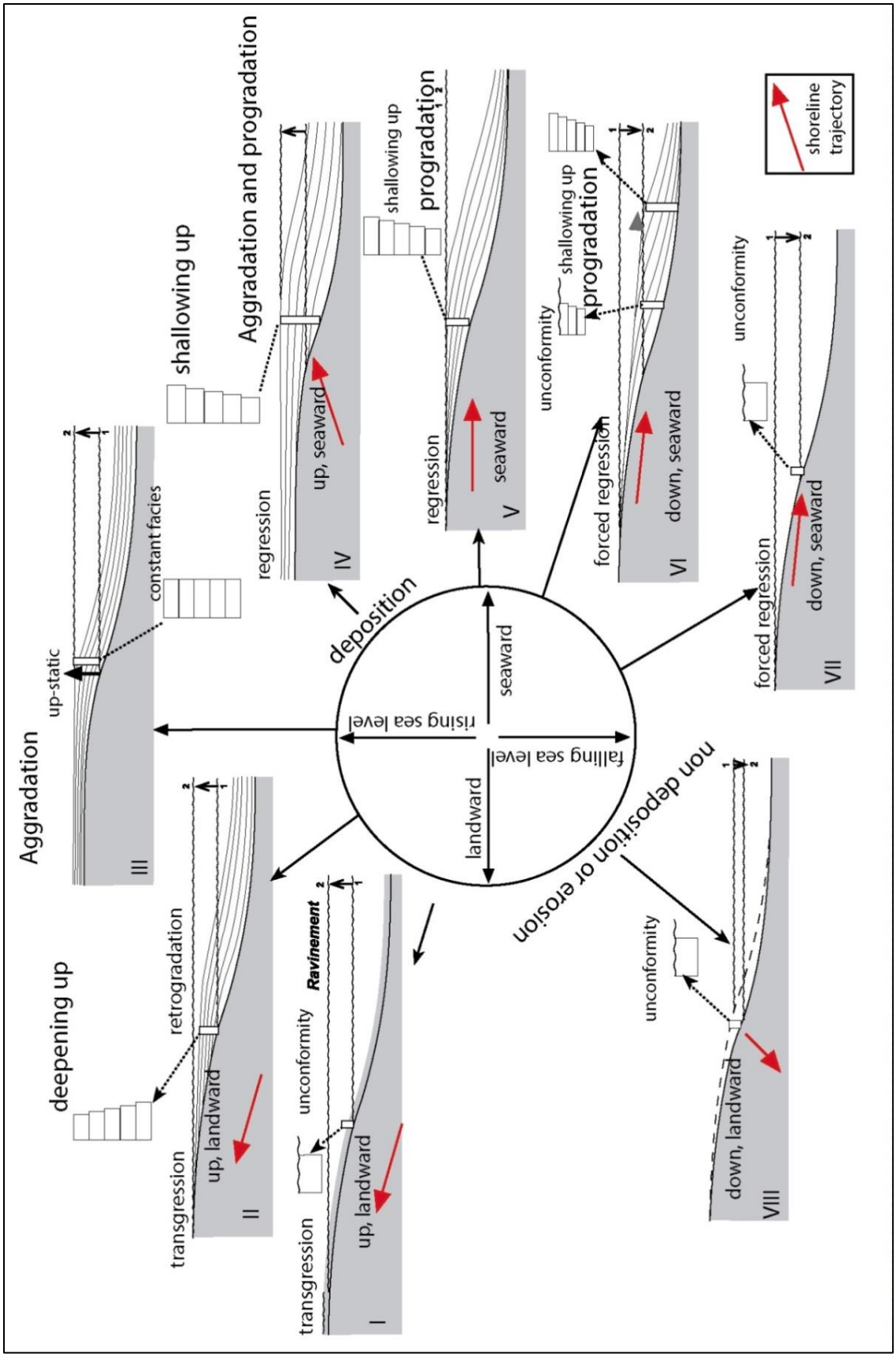
shoreline trajectory
rising sea level
seaward
falling sea level
landward
deposition
non deposition or erosion
Aggradation
up-static
constant facies
III
deepening up
retrogradation
transgression
up, landward
II
Ravinement
unconformity
transgression
up, landward
I
shallowing up
Aggradation and progradation
regression
up, seaward
IV
shallowing up
progradation
regression
seaward
V
unconformity
shallowing up
progradation
forced regression
down, seaward
VI
unconformity
forced regression
down, seaward
VII
unconformity
down, landward
VIII

Figure 1-1. *Nichols (1999) has simple presented the various possible sedimentation patterns as a result of the interplay of the three major factors which control them. In cases I and II transgression sequences (sea level rise and/or limited sediment accumulation) will occur, while coastline moves landwards. In cases III the equilibrium between sea level rise and the sedimentation will lead into constant facies and the coastline will remain standstill (a rare scenario though). In cases IV to VII the coastline will shift seawards (regression and forced regression).*
Εικόνα 1-1. *Ο Nichols (2009) παρουσίασε με απλό τρόπο τα διάφορα πιθανά μοτίβα της ιζηματογένεσης ως προϊόν της αλληλεπίδρασης των τριών βασικών παραγόντων που τις ελέγχουν. Στις περιπτώσεις I και II παρατηρείται η άνοδος της στάθμης της θάλασσας με την ακτογραμμή να κινείται προς την ξηρά. Στις περιπτώσεις III παρατηρείται ισορροπία ανάμεσα στον ρυθμό ανόδου της στάθμης της θάλασσας και τον ρυθμό ιζηματογένεσης με την ακτογραμμή να παραμείνει στάσιμη (σπάνιο σενάριο). Στις περιπτώσεις IV έως VII η ακτογραμμή θα μετατοπιστεί προς την θάλασσα (απόσυρση)*

The scientific community has deployed numerous tools (foraminifera, ostracods, echinoderms, mollusks, diatoms etc.) to examine the paleoenvironmetal conditions (salinity, temperature, depth, chemistry, pollution etc.) (e.g. Benson, 1976; Nurnberg et al., 1996; Campeau et al., 1999; Keller et al., 2002; Martin et al., 2002; Debenay et al., 2005; Regenberg et al., 2009; Ivanova et al., 2012; Dimiza et al., 2016), tectonic movements (e.g. Avnaim – Katav et al., 2012; 2013), natural hazards (e.g. Cundy et al., 2000; Mischke et al., 2012), the glacioeustatic sea level changes (e.g. Kemp et al., 2012) climate change (e.g. Zubakov and Borzenkov 1988; Howell et al., 1990; Jalut et. al., 1997) etc.

Benthic foraminifera assemblages are the most common and essential paleontological tool since are considered a sensitive indicator of paleoenvironmental variations in nearshore to shallow marine environments. Several researches have used the foraminiferal assemblages to reconstruct the paleoenvironment and the paleogeography of an area early from the Paleozoic (e.g. Ershova et al., 2016) till the Quaternary (e.g., Scott and Medioli, 1980; Triantaphyllou et al., 2003, 2010; Murray, 2007; Pavlopoulos et al., 2007; Koukousioura et al., 2012; Avnaim – Katav et al., 2012, 2013, 2015).

Even though that active tectonic areas are not preferable for paleontological and paleoenvironmetal research since the sediments are often disturbed and not in situ position, foraminiferal assemblages and the paleoenvironmetal changes can also be helpful in such challenging environments. Cundy et al. (2000) through foraminiferal analysis described the subsidence caused by the Atalanti Fault during the 1894 rupture. Yasuhara et al. (2005) provided a robust method for reconstruction of the Holocene seismic history using ostracods assemblages within cores, since through them they reconstructed the relative sea-level curve showing seismic subsidence during the Holocene. Ferranti et al. (2011) also used different paleoenvironments described within borehole cores and correlated them to study the tectonic subsidence in Calabria (Southern Italy) caused by active faults during the Holocene. Avnaim – Katav et al. (2012, 2013) through the paleoenvironmetal description of borehole cores complied after foraminiferal analysis estimated the vertical offset of Carmel fault in Israel coast during Early to Middle Pleistocene. Yeager et al. (2012) through lithostratigraphic and biostratigraphic description of borehole cores estimated the vertical offset and the growth of an active fault in Louisiana (USA). Active fault movements were examined as well by Feagin et al. (2013) in Texas area also thought foraminiferal analysis and paleogeographical description of borehole cores.

A scientific tool which is also used with the paleoenvironmental analysis is Magnetic susceptibility (MS) of the sediments. MS depends mostly on mineral composition and grain size (e.g., Mullins 1977, Oldfield; 1991, Da Silva et al., 2009; Reicherter et al., 2010). In general, iron bearing minerals lead to high values of MS (dimensionless SI units).Several researchers have employed MS signal along with other methods to examine paleoenvironmental alternations (e.g. Ghilardi et al., 2008; Lézin et al., 2012; Sonnenburg et al., 2013; Danelian et al., 2014; Maselli et al., 2014), sedimentology studies (e.g. Waldmann et al., 2014), natural hazards (e.g. Reicherter et al., 2010; Goff et al., 2012), active tectonics (e.g. Braun et al., 2015; Drahor and Berge, 2017) etc.

The paleoenvironmental reconstruction of an area though would be incomplete without data constraining the sediments' age. Several scientific tools have been used in the past in order to estimate the age of sedimentary sequences (corals, mollusks,

foraminifera etc.) examined through many different techniques ($^{234}U/^{238}U$, ^{14}C, $^{230}Th/^{238}U$, OSL, IRSL etc.). Every methodology offers both advantages and disadvantages since it is constrained by significant physical parameters. The preferable technique is determined by the requested chronological framework of the study area, while the aim of the researchers is to develop more accurate, faster and less expensive dating methodologies.

For the examination of the Middle-Upper Pleistocene (the last ~ 350 ka) $^{234}U/^{238}U$ in corals stems is the most common methodology followed by the majority of the researchers. Several studies applied $^{234}U/^{238}U$ dating in corals to estimate the uplift in tectonically active areas (e.g. Collier et al., 1992; Vita-Finzi, 1993; Dia et al., 1997; Houghton et al., 2003; Kershaw et al., 2005; Roberts et al., 2009). Apart from corals stems, $^{234}U/^{238}U$ is applied in other fossils as well (e.g. mollusks, ostracods). Considering that the chemistry of the surrounding environment poses significant influence to the chemical components of the samples, the results have to be examined with precautions (e.g. Scholz et al., 2004; Scholz and Mangini, 2007).

Optical and Infra-red Luminescence dating (OSL and IRLS respectively) techniques are also applied to determine the age of the sediments. Luminescence techniques offer the possibility of dating sediments' even ~1 Ma ago and therefore have a significant advantage against $^{234}U/^{238}U$ dating. The main principal of these techniques is to estimate how long has been since sediments' grains were exposed to sunlight and therefore when the sediment was deposited

There are several techniques that can be used to measure mineral's luminescence where Quartz and feldspar are most commonly used, since both of them are abundant in nature, are resistant in weathering and their signal is more stable during time.

A significant limitation of luminescence dating is that the minerals' grains were not completely bleached from their previous exposure to sunlight. It is often observed that

the signal of the feldspar is weak and the Quartz's signal saturated[1], cases which is not possible to apply OSL and IRSL to estimate the sediments' age.

Luminescence dating is commonly used in archaeology (e.g. Lang & Wagner, 1996; Folz et al., 2001) paleoenvironment reconstruction and sea level changes (e.g. Pope et al., 2008; Pawley et al., 2010; Reimann et al., 2011; Ozturk et al., 2016) active tectonics (e.g. Porat et al., 1997, 2009; Chen et al., 2009; Mayo et al., 2009; Rizza et al., 2011; Tsodoulos et al., 2016).

Calcareous nannofossils assemblages are also a useful scientific tool for paleoenvironmental studies, since constitute a significant component of the marine micro fauna (Dimiza et al., 2011) and have a world-wide distribution in modern oceans. Through them it is possible to study climate conditions and environmental parameters (e.g. Triantaphyllou et al., 2009; Dimiza et al., 2011; Triantaphyllou, 2014), paleoenvironmental conditions (e.g. Triantaphyllou, 2015), stratigraphy (e.g. Triantaphyllou, 2013; Athanasiou et al., 2015; Foroughi et al., 2017). Their appearance is widely used during the last decades in marine biostratigraphy and the biozonation of calcareous nannofossils was established by several researchers in the past, while their presence is widely used to determine the chronological framework of an area (e.g. Martini, 1971; Raffi et al., 2006; Rio et al., 2010; Backman et al., 2012).

Arai et al. (2014) based on the age implied by calcareous nannofossils, estimated the vertical displacements of normal faults at the Ryukyu Island Arc (West Pacific) the last 265 ka. Chen et al. (2015) deployed both planktonic foraminifera and calcareous nannofossils analysis to demonstrate the tectonic evolution of the oblique collision between the North Luzon Arc and the Eurasian Continent margin. Clauzon et al. (2015) examined the evolution of the Roussillon Basin during Miocene in respect with the active tectonics of the area, also based in foraminiferal and calcareous nannofossils assemblages.

[1] *See chapter 4 for a description and an explanation of the methodology and its principals.*

For this Ph.D. three different methodologies have been followed to define the chronological framework of the sedimentation processes, determining the rates of the tectonic movements and the paleogeography of the study area. Two techniques were used for absolute dating ($^{230}Th/^{238}U$ dating in corals stems, OSL and IRSL luminescence dating to samples extracted from borehole cores) and one for relevant dating (the biozonation of calcareous nannofossils, combined with the glacioeustatic sea level changes and the regional uplift). The latter comprises the innovation of this research. Considering as well that few researchers have analyzed the paleoenvironment for studying the active tectonics of an area, this study distinguishes from them since the most valuable and reliable results, deprive mainly through nannofossils and afterwards through the $^{230}Th/U$-method.

1.2 Scope of study

This study aims to estimate the activity of the Kalamaki-Isthmia fault located at the eastern margin of the Corinth canal, examine the uplift rate of the area and offers an estimation of the regional uplift rate of the area. The low slip rate of the Kalamaki-Isthmia fault is confirmed and the uplift rate of the area since MIS 7 was re-examined following a different and independent methodology, compared with the methodologies followed by previous researchers.

Furthermore, the detail description of the paleoenvironmental alternations at the eastern part of the Corinth Isthmus has been examined through different methodologies. The studied area is a complex area influenced both by glacioeustatic sea level changes and tectonic movements leading into a complicated lithosedimentary pattern with alternating beds of marls, sands and gravels. The 3D model of the area was reconstructed showing the spatial and temporal distribution of the strata. Finally the paleogeography of the eastern part of the Corinth Isthmus area has been reconstructed.

The study is focused on the detailed examination of 11 boreholes drilled in either sides of the Kalamaki-Isthmia fault. Boreholes Bh-6 and Bh-3 (which was longest of them,

70.20 m long), were drilled at fault's footwall while the rest towards the immediate hangingwall of the fault. Eight of them were examined in detail, while for the rest only lithological description was obtained. Overall, 355 samples were extracted from the total 373 m long borehole cores and were examined for their foraminiferal contend. The Magnetic Susceptibility (MS) of the sediments has been measured (986 measurements) also assisting in the paleoenvironmental interpretation of the sedimentary sequences. Furthermore, specific samples were examined for nannofossils assemblages[2]. Through the biozonation established by several researchers before age constrains of the described sediments were implied. Furthermore, an area of ~15 km^2 was detailed mapped in depth (1:5000 scale) and 249 measurements of the tectonic and stratigraphic features were obtained. In addition, 99 outcrop samples were extracted for further laboratory examination (foraminiferal and nannofossils assemblages).

Six samples were examined for OSL and IRSL in the laboratory of Archaeometry / Paleoenvironment & Archaeometallurgy of N.C.S.R. Demokritos. The poor quality of the samples resulted into no scientifically significant result. Coral stems found within the boreholes were dated through U^{238}/ Th^{234} . The value of the results limit their possible age to be older than 175 ka, since the processes of diagenesis have significantly influence the chemistry of the samples.

The dating difficulties were overcome based on the glacioeustatic sea level curve and the uplift rate of the area. The combination of these along with the biozonation as was implied by nannofossils assemblages, resulted into a specific age period were sedimentation could occur ranging from MIS 5.5 to MIS 7.5.

---

[2] *Nannofossils thrive into relatively deeper marine environments. After the detailed paleoenvironmetal description the samples indicating more open marine conditions, based on the palaeobathymetry as well, were examined for nannofossils. Samples of lagoonal or coastal environments were barren confirming the previous statement.*

1.3 Chapters – Outline of the Ph.D. thesis

The first chapter of this thesis introduces the reader to the sedimentation processes. The main factors which influence the sedimentology and therefore the coastal morphology of an area are highlighted based on previous researches. The Corinth Gulf is mentioned as a fine example where all three factors influence the processes. Furthermore, every methodology which has been used in this multi-proximal study is briefly mentioned and described through examples of previous researchers. Finally, the scope of this study is presented a well as the different procedures which have been followed.

The second chapter describes the paleoclimate, the paleotemperature and their influence to the glacioeustatic sea level changes. Furthermore, the influence of the paleotemperature conditions is also mentioned.

The third chapter describes the area of Corinth and Saronic Gulf, where this research is focus on. These active extensional regions have been studied in detailed by several researchers, especially after the 1981 Alkyonides earthquakes sequence and the previous studies regarding these Gulfs are briefly described. Previous researchers have focused not only on the active tectonics and the seismicity, but also to the paleoenvironment, the sedimentology and the paleogeography of these areas as well. The unique Corinth Canal, also offers an opportunity to study in detail the sedimentological processes of the area, influenced by active syn-sedimentary faults.

The forth chapter describes all the different methodologies which have been applied in this multi-proxy study. The basis of this thesis are 11 boreholes and surface samples, located at the eastern part of the Corinth Canal and more specific, foraminifera and calcareous nannofossils assemblages extracted through them. In addition through a Bartington MS2 system with the MS2K sensor the magnetic susceptibility of the sediments has been measured. The results (MS measurements and foraminiferal assemblages), have been statistically analyzed. Through detailed mapping the lithologies of the area and the Kalamaki-Isthmia fault have been described, while

samples extracted from surface outcrops have also been examined for their micro- and nanno- fossils assemblages. Finally, in order to establish the chronological framework of the sedimentation processes, two independent methodologies have been deployed; $^{230}Th/^{238}U$ to coral stems found in growth position in two boreholes and OSL / IRSL techniques to undisturbed sediments extracted from three borehole cores.

In chapter five, the detailed analysis of the 11 boreholes cores is presented. Several lithological alternations have been described, ranging from fine marine sediments to coarse fluvial gravels. Eight of them were analyzed for their micro and nanno paleontological contend. In each borehole, the results of the detailed foraminiferal analysis are provided, as well as the A-ratio, BR-ratio and FD index of the described foraminifera. Furthermore, the results of the calcareous nannofossils analysis from 6 boreholes are also presented. The MS measurements extracted from borehole cores are presented and correlated with the described lithological alternations within the sequences.

In chapter six the detailed mapping of the study area is described. The eastern part of the Corinth Canal has been detailed described (1:5000 scale) where different lithological sequences have been identified, varying from coarse fluvial sediments to fine clayey marine horizons. Samples extracted from surface outcrops have been analyzed for their nanno and micro paleontological content. Tectonic fractures and fault planes have also been described.

In chapter seven the statistical analysis both of the micropaleontological analysis and the MS measurements is presented. Foraminiferal assemblages have been subjected into two way cluster analysis (Q-mode, R-mode) to highlight the biofacies (Ward's method and Euclidean distances as a similarity index). Based on the results, three distinct groups have been identified; each of one represents a different ecology and depositional environment. Furthermore, a non-metric multi-dimensional scaling (MDS) ordination was used to identify to correlation among the assemblages. MS measurements have been subjected firstly to a Kolmogorov-Smirnov normality test to examine if the measured MS values follow a normal distribution or not, based on the described lithology and the estimated paleoenvironment of the cores; and a Pearson

correlation test to examine if there is any correlation among the described lithology, the paleoenvironment and the measured MS values.

In chapter eight the paleoenvironmental interpretations both of the borehole sequences and of the surface outcrops have been combined. Based on the two-way cluster analysis described before, all the indexes (BR-, FD-, and A-ratio), the results presented in chapter five have been refined. Based on the lithological description and the MS values (for boreholes), the paleoenvironment has been described. Furthermore, based on the ecology of the described foraminifera the regional depositional depth has been estimated both in borehole cores and in surface outcrops.

In chapter nine, the applied dating techniques have been described. *Cladocora caespitosa* corals stems have been dated with the ^{230}Th/U-method at the Max Planck Institute for Chemistry in Mainz, while six samples, selected from three boreholes, have been selected for OSL and IRSL dating. Furthermore, based on the nanno fossils assemblages, the biozonation of the sediments has been established and through them thresholds of the possible age of the sediments has been estimated.

In chapter ten, a case study of the Saronic Gulf is presented. Three boreholes located at the Piraeus coastal plain where examined for the micropaleontological content. Palynological, molluscan and magnetic susceptibility analysis which has been performed by Triantaphyllou et al. (2016) has been a guide to correlate the paleoenvironments described in these boreholes, with the boreholes located at the Corinth Canal. The correlation of the paleoenvironmental patters in both cases is important for validating the analysis performed in boreholes from the Canal.

In chapter eleven, the outcomes of this research have been discussed. Through the borehole descriptions, the estimated paleoenvironment and palaeobathymetry, the surface outcrops and the exposed strata at the Corinth Canal, a 3-D model showing the spatial and temporal distribution of the strata at the eastern part of the Corinth canal has been constructed. Furthermore, based on the glacioeustatic sea level curve, the uplift rate of the area and the ages proposed mostly through the nanno fossils assemblages, the relative age of the sediments is estimated. Through these ages the activity of the

Kalamaki-Isthmia fault is estimated and the uplift rate of the area is interpreted. Furthermore, the major faults which influence the area are also described. Based on their slip rates a model is proposed describing the significance of each fault to the total uplift and/or subsidence of the area, while the influence of the regional tectonic uplift is also determined. Furthermore, the paleogeography of the eastern part of the Corinth Isthmus is reconstructed, during the Quaternary. Finally, the followed methodologies are also an important outcome from this PhD, since this multi – proxy analysis proved to be a very good correlation methodologies (quantitative benthic foraminiferal analysis, with nanno fossils assemblages and magnetic susceptibility data) and a promising paleoenvironmental tool box for study of the paleoenvironment and paleogeography. However, their constrains (e.g. absence of absolute dates) are also mentioned

The final chapter of this PhD presents the conclusions concerning both the paleogeography and the active tectonics of the area, while significant outcomes concerning the relative age of the sediments are also highlighted.

The last part of this study includes lists of the presented figures and tables as well as all the cited bibliography. In the included appendixes a brief definition of the abbreviations mentioned in the text is provided (Appendix A), a detailed description of the foraminiferal analysis both in boreholes and in surfaces samples (Appendixes B , C) of the MS values extracted from the borehole cores (Appendix D), as well as an extended version in Greek (Appendix E).

2 Sea level changes and paleotemperatures

The research of the climate and environmental conditions has always been an intriguing issue for the scientific community, both for the past (e.g. De Blasio et al., 2015; Eldevik et al., 2016) and for the present day (e.g. Alexandris et al., 2008; Karavitis et al., 2015). The scientific community has recently comprehended the significance of the paleoclimate conditions, their connection with the glacioeustatic sea level changes and the cyclicity of the relative sea level rise or fall.

A breakthrough for the better understating of this phenomenon was the conception of different cycles of the Earth's orbit (Fig. 2-1). The scientific community refers to them as the Milankovitch's cycles (Milankovitch, 1941), which are the collective effects of changes in the Earth's variations in eccentricity (influencing the distance from the sun); axial tilt (obliquity, the angle between an Earth's rotational axis and its orbital axis) and precession (the change in the orientation of the rotational axis of Earth) (Fig. 2-1). These cycles of the Earth's orbit resulted in cyclical variation in the solar radiation reaching the Earth and trigger significant changes in the Northern Hemisphere ice volume (Shackleton, 2000) and therefore to the paleoclimate, to the paleogeography, to the paleoenvironment and the sea level glacioeustatic changes (e.g. Shackleton, 1967; Broecker and Van Donk, 1970; Imbrie and Imbrie, 1980; Imbrie et al., 1993; Shackleton, 2000; Tzedakis et al., 2017).

These cycles have recently been modeled by Tzedakis et al. (2017). The astronomical periodicities of obliquity (axial tilt, ~41 ka) and precession (~23 ka) as well as the maximum in boreal summer insolation, with perihelion (when Earth is nearest to the Sun) at the northern summer solstice, have influenced the cumulative solar energy the last 600 ka[3]. Even though that during the perihelion the earth is at shorter distance from

[3] *Mean daily insolation on 21 June at 65° N is often used as a predictor of glacial changes, because it represents maximum values at a sensitive time of the year at a critical latitude for ice-sheets*

the sun, its orbit is faster compared to its orbit during the aphelion. The latter influences the cumulative solar energy that reaches to earth. Based in these cycles Tzedakis et al (2017) mentioned that not every astronomical event has lead into an interglacial period, as was initially thought to and developed a robust taxonomy of interglacials, continued interglacials and interstadial for the entire Quaternary. They have defined a threshold of the effective solar energy required to result into an interglacial period (Fig. 2-2).

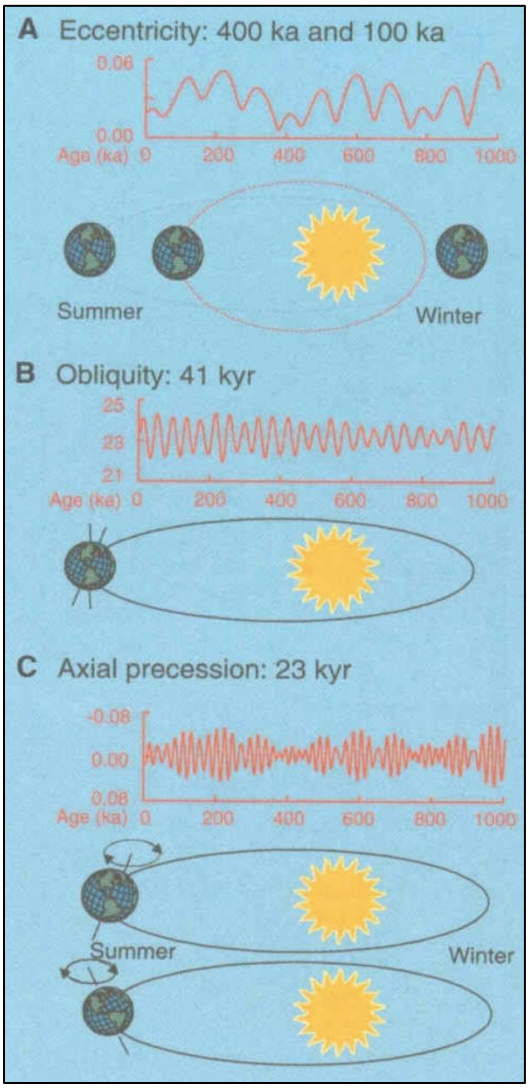

Figure 2-1. *Variation of the Earth's eccentricity, obliquity and precession the last 1000 ka (Zachos et al., 2001).*

Εικόνα 2-1. *Οι εναλλαγές της κλίσης του άξονα και της περιστροφής της γης τα τελευταία 500 χιλιάδες χρόνια (Zachos et al., 2001)*

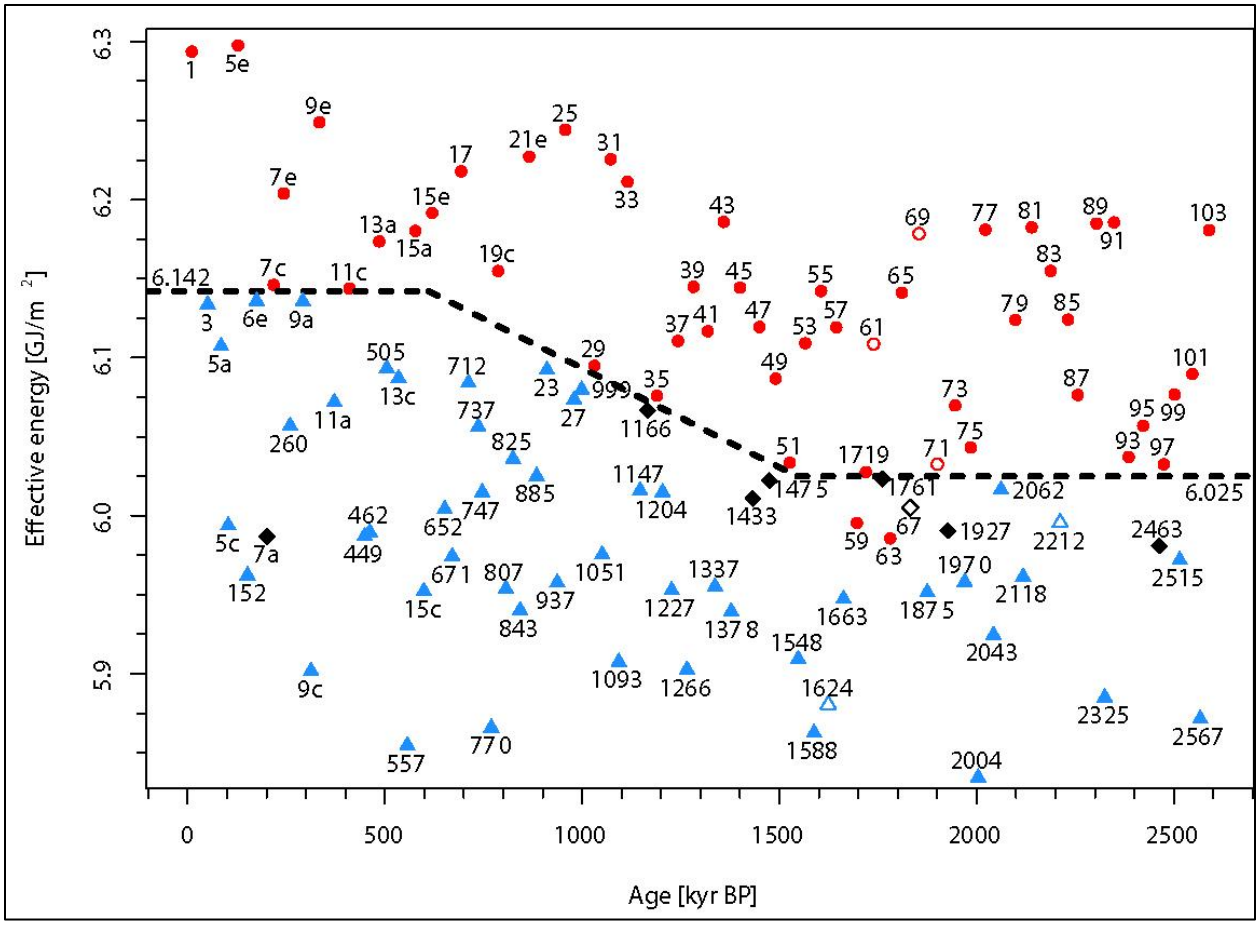

Figure 2-2*. The effective energy at each insolation peak during the past 2.6 Myr based on the classification proposed by Tzedakis et al. (2017) to separate the complete deglaciated (highstands) from incomplete and no deglaciated periods (lowstands). Interglacial (red circles) are seperated by the two horizontal lines with a ramp from interstadial and glacial (light blue triangles) periods (Tzedakis et al., 2017).* ***Εικόνα 2-2.*** *Τα παγετώδη (μπλε τρίγωνα) και μεσοπαγετώδη διαστήματα (κόκκινοι κύκλοι) όπως έχουν διαχωριστεί από τους Tzedakis et al. (2017) τα τελευταία 2.6 εκ. χρόνια με βάση την ηλιακή ενέργεια που δέχεται η γη.*

The foraminiferal analyses have significantly assisted for the detailed study not only of the sea level fluctuations, but of the paleoclimate and paleotemperature conditions as well, based on chemical proxies that can be measured in foraminiferal tests to reconstruct past environments. A common method for estimating ice-volume fluctuations and the associated glacioeustatic sea level changes involves correcting the benthic oxygen isotope ($d^{18}O$) records for temperature in order to isolate that part of the

signal that reflects ice volume (e.g. Urey, 1947; Emiliani, 1955; Shackleton, 1967; Waelbroeck et al., 2002). The basic principles of using oxygen isotopic abundance ratio changes as a means of estimating past temperatures is *"that since small isotopic fractionation which takes place when a carbonate is deposited slowly from aqueous solution is temperature dependent, the temperature of deposition may be estimated by measuring the extent of the isotopic fractionation"* (e.g. Urey, 1947; Emiliani, 1955; Shackleton, 1967; Shackleton and Opdyke, 1973). Waelbroeck et al. (2002) mentioned that "*The shell $^{18}O/^{16}O$ ratio is a function of both the isotopic composition and the temperature of the water in which the foraminifera develops. Therefore, assuming that deep water temperature does not vary too much over time, the benthic $^{18}O/^{16}O$ ratio ($d^{18}O_b$, expressed in ‰) can be used as a first order proxy for global ice volume"* (Figs 2-3, 2-4).

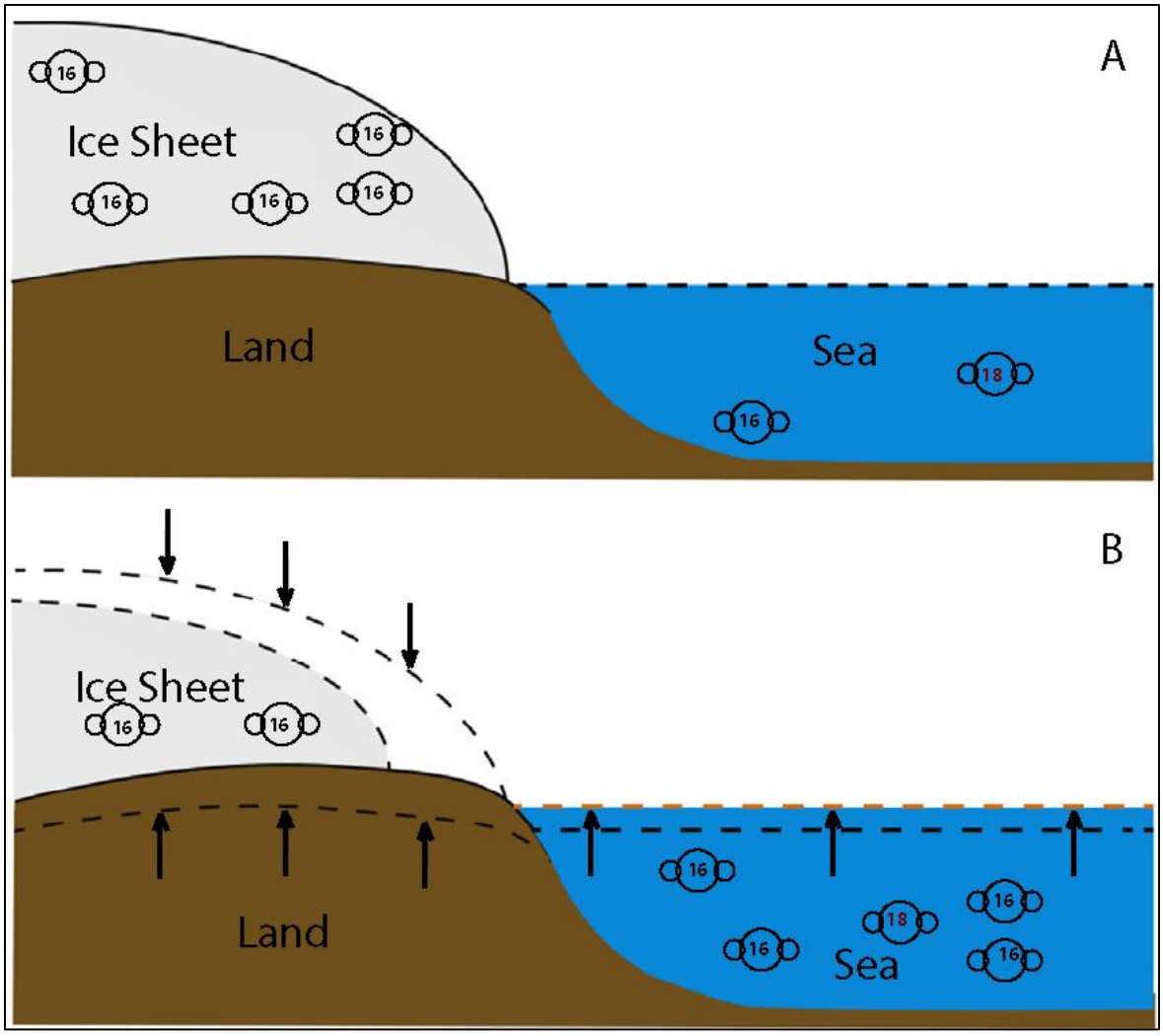

Figure 2-3. *A schematic representation of the interaction between ice sheets, land and sea. A) During glaciation the ratio $^{18}O/^{16}O$ is high since ^{16}O is trapped within he glaciers b) During deglaciation the water returns to the sea resulting into sea level rise and isostatic uplift of the land (modified from de Boer et al. 2017). The ratio$^{18}O/^{16}O$ is lower since the melting of the glaciers release ^{16}O to the atmosphere.*
Εικόνα 2-3. *Σχηματική απεικόνιση της αλληλεπίδρασης των καλυμμάτων πάγου, της ξηράς κα της θάλασσας. Α) Παγετώδης περίοδος κατά την οποία ο λόγος $^{18}O/^{16}O$ είναι αυξημένος, καθως το ^{16}O δεσμεύεται στους παγετώνες Β) Κατά την αποπαγετοποίηση λόγο προσφοράς νερού ανεβαίνει η στάθμη της θάλασσας ενώ παρατηρείται ισοστατική ανύψωση της ξηράς που ήταν καλυμμένη με πάγο. Το λιώσιμο των πάγων έχει σαν αποτέλεσμα την απελευθέρωση ^{16}O στην ατμόσφαιρα και μείωση το λόγου $^{18}O/^{16}O$ (Τροποποιημένο από de Boer et al. 2017)*

During marine highstands the benthic oxygen isotope ($d^{18}O$) records were higher than marine lowstands (e.g. Shackleton, 2000; Waelbroeck et al., 2002; Siddall et al., 2003, Fig. 2-5b). Shackleton and Opdyke (1973) mentioned (based on Emiliani (1961)) that isotopic temperature fluctuations during the last 200 ka range from ~30 ^{o}C (marine highstands) to ~20 ^{o}C (marine lowstands). On the same line, Waelbroeck et al. (2002) modeled deep water temperature fluctuations ~ 5 ^{o}C for the last 400 ka (Fig. 2-5a). Furthermore, during the highstand MIS 5e, MIS 7 and MIS 9 the estimated temperatures were similar or even higher than the present day (e.g. Hoffman et al., 2017; Vaughn and Caissie, 2017).

The temperature conditions influence the chemical composition, the growth size and growth rate of the fossils (e.g. Skirbekk et al., 2016; Mine et al., 2017). The knowledge on the conditions of foraminifer's growth has been extracted from laboratory studies under controlled conditions (e.g. Lombard et al., 2009). Lombard et al. (2009) mentioned that *"growth rate is generally quantified by the number of chambers precipitated within the observation period (as chamber d^{-1} or µm d^{-1}), for each studied foraminifera"*. Higher temperatures lead into relative thicker and bigger foraminifera and marine fossils in general (e.g. Lombard et al., 2009, Evans et al., 2016). Lombart e al. (2009) have modeled the growth rates of eight foraminifera species, related to the temperature (Fig. 2-6). They have analyzed the growth rates through a mechanistic formulation, showing that the temperatures which favor the growth rates range from ~20 ^{o}C to ~28 ^{o}C. In extreme temperatures (>28 ^{o}C) the growth rates decrease (e.g. Nigam et al., 2008; Lombard et al., 2009; Prazeres et al., (2016). Nigam et al. (2008) have also indicated that ~27 ^{o}C is the most favorable temperature for *R. leei* to thrive.

The connection among the number of the population, the number of the species and the paleotemperatures have also implied by De Blasio et al. (2015). Based on a spatio-temporal discrete-time Markov process model of macroevolution featuring population formation, speciation and extinction, they have shown a correlation among higher biodiversity, foraminifer's prosperity and higher temperatures the last 10 Ma.

Vaughn and Caissie (2017) have also mentioned that changes in the species dominance for MIS 5e should be expected considering that temperatures during the last interglacial were characterized as being warmer than today.

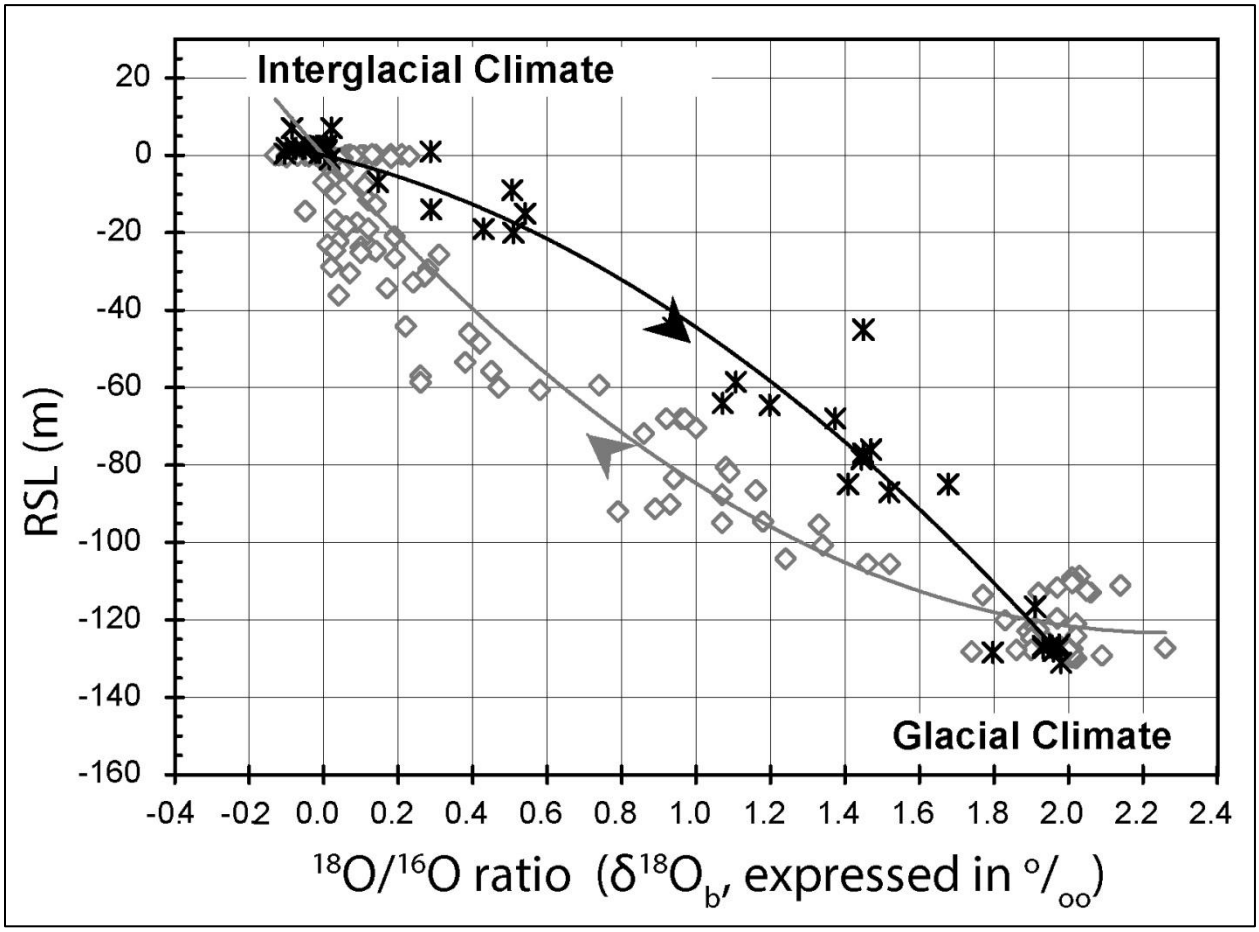

Figure 2-4. *The relative sea level (RSL) estimates versus the $\delta^{18}O_b$ measurements over the last glacial period (last 22 kyr). Notable the $\delta^{18}O_b$ is higher during the glacial time.*
Εικόνα 2-4. *Η μεταβολή στη στάθμης της θάλασσας (RSL) σε σχέση με το $\delta^{18}O_b$ κατά την τελευταία παγετώδη περίοδο, που εμφανίζονται και μεγαλύτερες τιμές.*

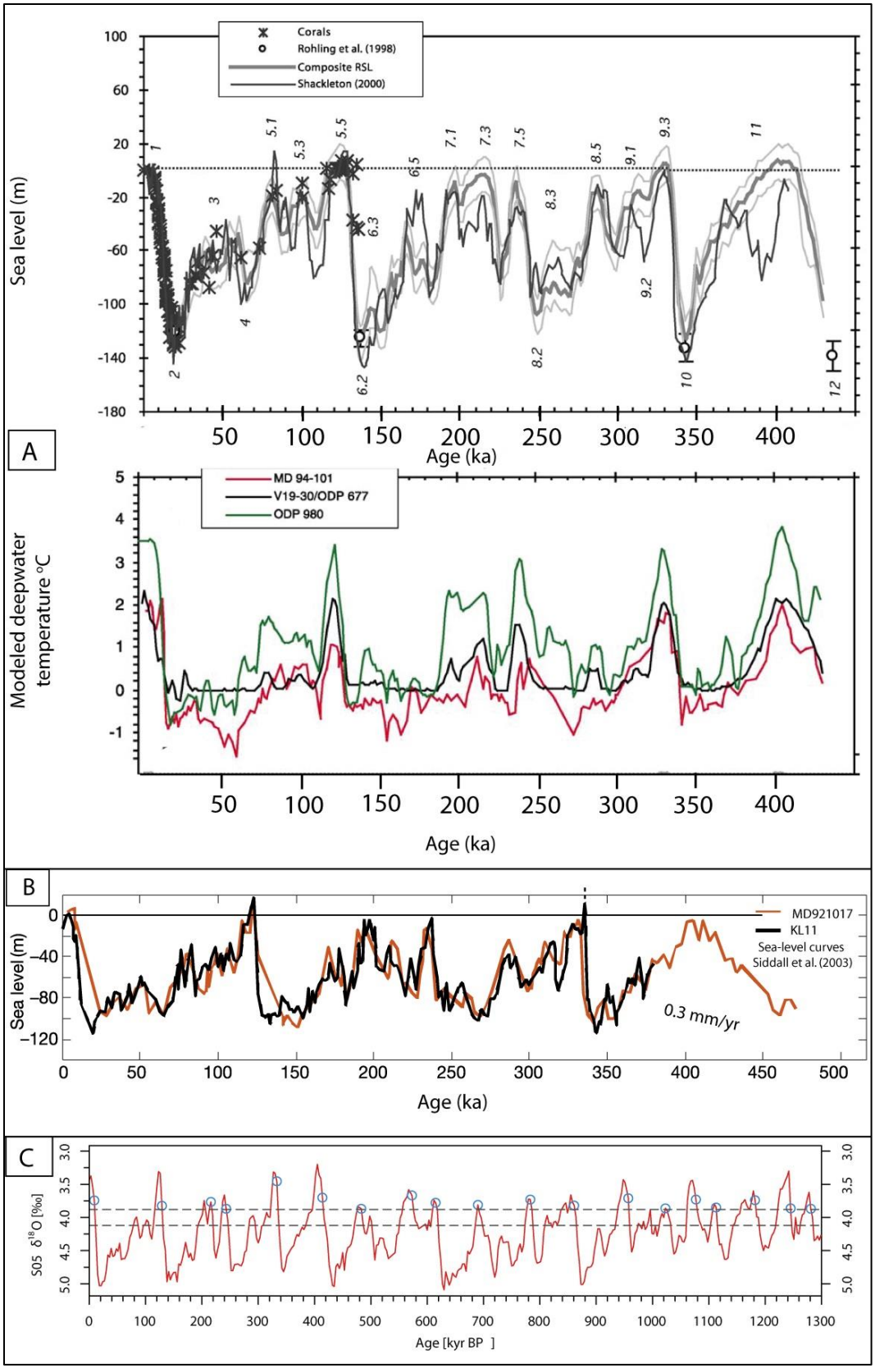
A
Sea level (m)
Corals
Rohling et al. (1998)
Composite RSL
Shackleton (2000)
Age (ka)
Modeled deepwater temperature °C
MD 94-101
V19-30/ODP 677
ODP 980
Age (ka)
B
Sea level (m)
MD921017
KL11
Sea-level curves
Siddall et al. (2003)
0.3 mm/yr
Age (ka)
C
SO5 δ18O [‰]
Age [kyr BP]

Figure 2-5. *A) The relative sea level curve (up) and the modeled deep water temperature fluctuations ~ 5 ^{o}C (down) the last 400 ka (modified from Waelbroeck et al., 2002). B) The glacioeustatic sea level change curve by Siddall et al. (2003), which has been used in this thesis. C) The definition of the interglacial periods (blue circles) from Tzedakis et al. (2017) the last 1300 ka.*

Εικόνα 2-5. *Α) Η καμπύλη μεταβολής της στάθμης της θάλασσας (επάνω) και οι διακυμάνσεις της θερμοκρασίας(~ 5 ^{o}C) στους ωκεανούς (κάτω) τα τελευταία 400 χιλιάδες χρόνια (τροποποιημένη από Waelbroeck et al., 2002). Β) Η καμπύλη μεταβολής της στάθμης της στάθμης της θάλασσας από Siddall et al. (2003), η οποία χρησιμοποιήθηκε και στην παρούσα διατριβή. C) Τα μεσοπαγετώδη διαστήματα (μπλε κύκλοι) από Tzedakis et al. (2017) τα τελευταία 1300 χιλιάδες χρόνια*

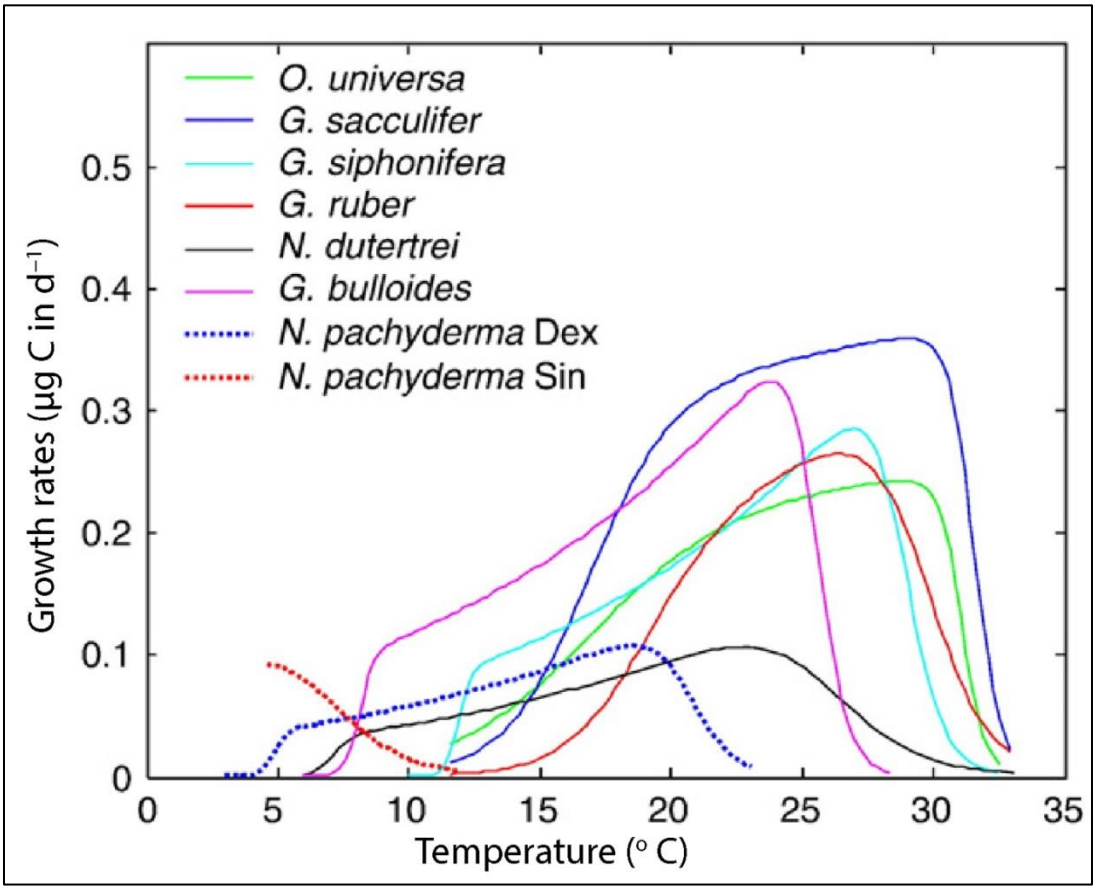

Figure 2-6. *Comparison of the modelled growth rate (d^{-1}) of the different foraminifera species in relation to experimental temperature (°C) (Lombard et al., 2009). Notable, higher than ~30^{o} the growth rate plummets.*

Εικόνα 2-6. *Το μοντέλο που συσχετίζει τον ρυθμό ανάπτυξης τρηματοφόρων σε σχέση με την θερμοκρασία, με σαφή μείωση για τις θερμοκρασίες πάνω από 30^{o} (Lombard et al., 2009).*

3 Study area

3.1 Introduction

The Alpine orogenesis which started during the Eocene resulted to the collision of the Eurasian plate with the African plate and the submersion of the latter under the former. This collision has led to the destruction of the Tethys Ocean. The area of Greece is one of the most active tectonic areas in Europe (e.g. Papanikolaou and Royden, 2007; Vassilakis et al., 2011) with complicated geological conditions within the active margin of the Eurasian Plate behind the active Hellenic arc and trench system. This system, which is running from the Ionian Sea to the W and SW of the Hellenic peninsula to the Libyan and Levantine seas to the S and SE, is part of the convergence zone between the African and Eurasian plates (Papanikolaou and Royden, 2007). The subduction northeastward of the Ionian Sea lithosphere occurs at ~35mm/yr (Kahle et al., 2000; McClusky et al., 2000; Nyst and Thatcher, 2004) while along the northern Hellinides subduction occurs at the slower rate of ~4 ± 2 mm/yr (Hollenstein et al., 2006).

The Aegean region is the result of recent extension (e.g. Armijo et al., 1996; Place et al., 2007; Bell et al. 2009). The main origin of this extension is highly debated and is attributed to the gravitational collapse of the Hellenic orogenic belt (e.g. Place et al., 2007; Jolivet, 2001; Le Pourhiet et al., 2003), the back arc thinning (trench roll-back[4]) induced by subduction of the African plate at the Hellenic Trench (e.g. McKenzie, 1972,1978; Doutsos et al.1988; Doutsos and Piper, 1990) and the recent tectonic activity of the North Anatolian Fault (NAF) (Dewey & Sengor, 1979; Armijo et al., 1996). Duermeijer et al. (2000) though paleomagnetic data suggested that *"the western Aegean arc underwent a clockwise rotation phase which took place between ~0.8 Ma till recent on Zakynthos and at least ~1.8 Ma on the Peloponnesus"*.

[4]*The subduction zone moves backwards relative to the motion of the plate which is being subducted, the trench is pulled backwards and the overriding plate is stretched and becomes thinner resulting in the back-arc basin.*

Corinth rift as well as the Saronic Gulf is the result of these extension processes. Papanikolaou and Royden (2007) mentioned the Central Hellenic Shear Zone a transtensional shear zone which crosses the older structures of the Hellenic thrust belt and connects to the modern trench. They mentioned that "*the motion of the Aegean block is accommodated by a zone of right slip in the northern Aegean that continues westward into a broad zone of dextral and extensional shear along a southwest trending zone that crosses central Greece. This active deformation zone reaches from the North Anatolian Fault in the east to the northern end of the Hellenic trench in the west (Kahle and Muller, 1993; Kahle et al., 1995, 2000; McClusky et al., 2000; Goldsworthy et al., 2002). Most of the modern seismicity associated with extensional deformation of the Aegean region is also concentrated along the Central Hellenic Shear Zone, most famously in the area near the Gulf of Corinth"*. Place et al. (2007) mentions that "*The propagation of this fault into the Aegean region modified the regional tectonic stress field whereby the Corinth Rift may be considered as one of the graben structures linking the NAF to the Hellenic subduction zone"* .

Several studies based on GPS points have estimated the extension rate of the Corinth Gulf (e.g. Billiris et al., 1991; Davies et al., 1997); while evidences strongly indicate that the extension rate of the western part is higher than the eastern. Clark et al. (1997), Avallone et al. (2004), Nyst and Thatcher (2004), McNeill and Collier (2004), Chousianitis et al. (2013) mentioned that the opening velocity of the central and western part of the gulf is approximately 15 to 20 mm/yr, relatively higher than the eastern part which is approximately 5 to 7 mm/yr. Vassilakis et al. (2011) also mentions an extension "*14 ± 2 mm/yr at the western part of the Corinth Gulf, where most of it is relayed to the northwest along a prominent zone of left-slip and extension through Lake Trichonis and the Amphilochia fault zone (11 ± 2 mm/yr) while the remaining displacement across the western Gulf of Corinth is relayed into 7 ± 2mm/yr of right-slip on the southwest-striking Achaia fault zone"*.

Both seismic and geodetic observations indicate that the opening of the rift developed firstly in the eastern and central part, and then propagated westward (e.g. van Hinsbergen & Schmid 2012). Apart from the Corinth Gulf, the Saronic Gulf area is also

under extensional regime. Chousianitis et al., (2013) has mentioned extension rates ~ 25 ns/yr for the Saronic Gulf.

3.2 Geology

The geology of the Corinth Gulf consists of the alpine and the post alpine sediments, mostly Plio-Pleistocene sediments. The dominant geological Units of the alpine basement are Boeotian Unit, Tripolis Unit and Pelagonian Unit (e.g. Bornovas et al., 1972, 1984; Gaitanakis et al., 1985).

3.2.1 Alpine bedrock

The eastern part of the Corinth Gulf comprises mostly of the Upper Triassic to Lower Cretaceous limestones/dolomites, the Boeotian flysch of the Boeotian Unit (and ophiolite nappes Perachora peninsula). Southern than the Agios Vassileios fault the area comprises of Triassic to Jurassic Pelagonian Unit limestones and Eocene to Cretaceous limestones of the Tripoli Unit (e.g. Bornovas et al., 1972, 1984; Gaitanakis et al., 1985).

3.2.2 Post Alpine sediments

Above the alpine basement the deposited Plio-Pleistocene sediments (mainly at the southern part of the Gulf), have recorded the paleogeographical evolution of the Corinth rift. A complicated lithological pattern of gravels and conglomerates, sand and sandstone, marls and silts has been described by several researchers; as well as the different paleoenvironments which these facies represent. Ori (1989) has mention the presence of lacustrine deposits form fine grained marls to coarse gravels, partially

influenced by the sea water, mostly at the south eastern part of the Gulf. Several researchers have thoroughly described the sedimentology of the central and western part of the Gulf, dominated by ~ 1 km thick Gilbert-type fan deltas (e.g. Dart et al., 1994; Malartre et al, 2004; Ford et al., 2007, 2012; Rohais et al., 2008; Backert et al., 2010). A complex sedimentary pattern has been described in these Gilbert-type fan deltas consisting of fine grained fluvial-lacustrine sediments, to coarse conglomerates and turbidites; described, as topsets, foresets, bottomsets and pro-delta which are correlated with regressive glacio-eustatic interglacial periods (Ford et al., 2007).

Elevated marine deposits have been described at the southeastern part of the Gulf, the marine terraces. Marine terraces have been firstly described by Deperet (1913) as steps, attributed to a single faulted Tyrrhenian terrace. Keraudren (1970- 72), Keraudren & Sorel (1987), Keraudren et al. (1995) mentioned the existence of more than one terrace, describing 20 terraces. Using U/Th dating methods, as well as micropaleontological data, they have estimated the age of the terraces and have correlated them with glacio eustatic sea level changes the last 330 ka. Armijo et al. (1996) have re-examined the described terrace sequence mentioned by Keraudren & Sorel (1987) and through them they estimated the uplift of the area and the influence of the Xylokastro fault. Doutsos & Piper (1990) have also implied that not all terraces have a marine origin but are lacustrine facies, when the Corinth Gulf was regulated at the Rio Strait. Westaway (1996, 2002) has also described the terraces of the same area mentioning in his conclusions that not all terraces have a marine origin.

Saronikos Gulf also displays a complicated morphology a product of its complicated geology correlated both to its neotectonic evolution and the Quaternary volcanic intrusions (Papanikolaou et al., 1988, 1989; Nomikou et al., 2013). A shallow N–S platform divides the Gulf into a western and an eastern part by, an observation which it's crucial to the paleogeographical evolution of the Gulf (Drakatos et al., 2005) (see chapter 8). *This zone comprises several volcanic outcrops of Plio-Quaternary age, representing the northwestern edge of the Hellenic volcanic arc* (Pe-Piper and Piper, 2002 Nomikou et al., 2013).

Towards the southern margin of the gulf (Methana), as well as at the emerged islands at the Gulf (e.g. Aegina), the volcanic activity resulted in to a complicated geological pattern with both sedimentary and volcanic rocks*. Volcanisms initiated in the area of Aegina 4.4 Myr ago and continued for a long period until 2 Myr ago (Nomikou et al., 2013), while at the peninsula of Methana, volcanic activity started ~ 0.9 Myr ago and continues until recent historical times 2.2 kyr ago*. Volcanic outcrops have also described along the coastal area of northwestern Saronikos Gulf at Agioi Theodori–Soussaki in western Attica. It is interesting to mention the presence of sub-merged active volcano Pausanias (Pavlakis et al., 1990; Nomikou et al., 2013)

3.2.3 Faults

The area of the Corinth Gulf is influenced by major fault structures. Even though that several researchers have described the gulf as an asymmetric half graben due to the dominance of north-dipping faults (e.g. Myrianthis 1982; Brooks and Ferentinos, 1984; Keraudren and Sorel, 1987; Ori, 1989; Sorel, 2000; Stefatos et al., 2002; Moretti et al., 2003), more recent seismic reflection profiles have revealed both N- and S-dipping offshore faults, (e.g. Stefatos et al., 2002; Moretti et al., 2003; Papatheodorou et al., 2003; McNeill et al., 2005; Zygouri et al., 2008).

Several researchers have studied both the offshore and the onshore faults at the eastern part of the Corinth Gulf (e.g. Doutsos & Piper, 1990; Armijo et al., 1996; Roberts & Koukouvelas, 1996; Collier et al., 1998; Perissoratis et al., 2000; Stefatos et al., 2002; Pantosti et al., 2004; Sakellariou et al.; 2007; Leeder et al., 2008; Gobo et al., 2014; Hemelsdael & Ford, 2015; Koukouvelas et al., 2017; Deligiannakis et al., in press).

Among them the Kenchreai (~0.2 mm/yr), the Agios Vassileios (~0.15 mm/yr) and the Loutraki (~0.5 mm/yr) faults subside the area of Corinth Isthmus, while more distal faults such as SAFS (~2 mm/yr) and the Xylokastro faults uplift it (Fig. 3-1) (e.g. Papanikolaou et al., 1988, Papanikolaou et al., 1989; Papanastassiou and Gaki-Papanastassiou, 1994; Armijo et al., 1996; Roberts, 1996; Morewood and Roberts, 1997, 1999;

Goldsworthy and Jackson, 2001; Sakellariou et al., 2007; Zygouri et al., 2008; Roberts et al., 2009, 2011; Charalampakis et al., 2014; Koukouvelas et al., 2017; Deligiannakis et al., in press). The south dipping fault of Kenchreai and north dipping Loutraki fault form a tectonic graben in which minor faults have deformed the Isthmus area forming the secondary horst of Corinth isthmus within the major graben

The Kenchreai and Agios Vassileios faults influence not only the Corinth, but also the Saronic Gulf as well (Fig. 3-1). Bell et al., (2009) mentioned that "*in the easternmost rift, the Megara basin faults, Kechriaie fault and other N-dipping faults bordering the NW Saronic Gulf which may be considered ancestors to the currently active Skinos and Pisia faults of the Perachora peninsula".* A significant segment of these faults are off shore (Papanikolaou et al., 1988, 1989; Deligiannakis et al., in press; Koukouvelas et al., 2017). Jackson (1999) mentioned that the Kenchreai fault has Upper Pleistocene marine sediments on its hanging wall, Holocene scarps and the submerged harbor in its immediate hanging wall indicating that it is not completely dead.

In the Perachora peninsula at the eastern end of the Gulf, the E-W coastal faults (SAFS) cut the NW-trending normal fault system bounding the Megara basin. This indicates that "t*his fault was active during Pliocene and Lower Pleistocene times, but at present day shows no sign of activity since it is displaced by the ENE-WSW Skinos-Psatha fault segments that were partly ruptured during the 1981 earthquake sequence"* (in Roberts et al., 2011).

The change in activity from faults with NW-SE to E-W strikes happened within the last 1 Ma (Jackson, 1999). Furthermore, at the eastern part of the Perachora peninsula Rondoyanni and Marinos (2008) have described the Kakia Skala fault, as the northern margin of the Saronic Gulf.

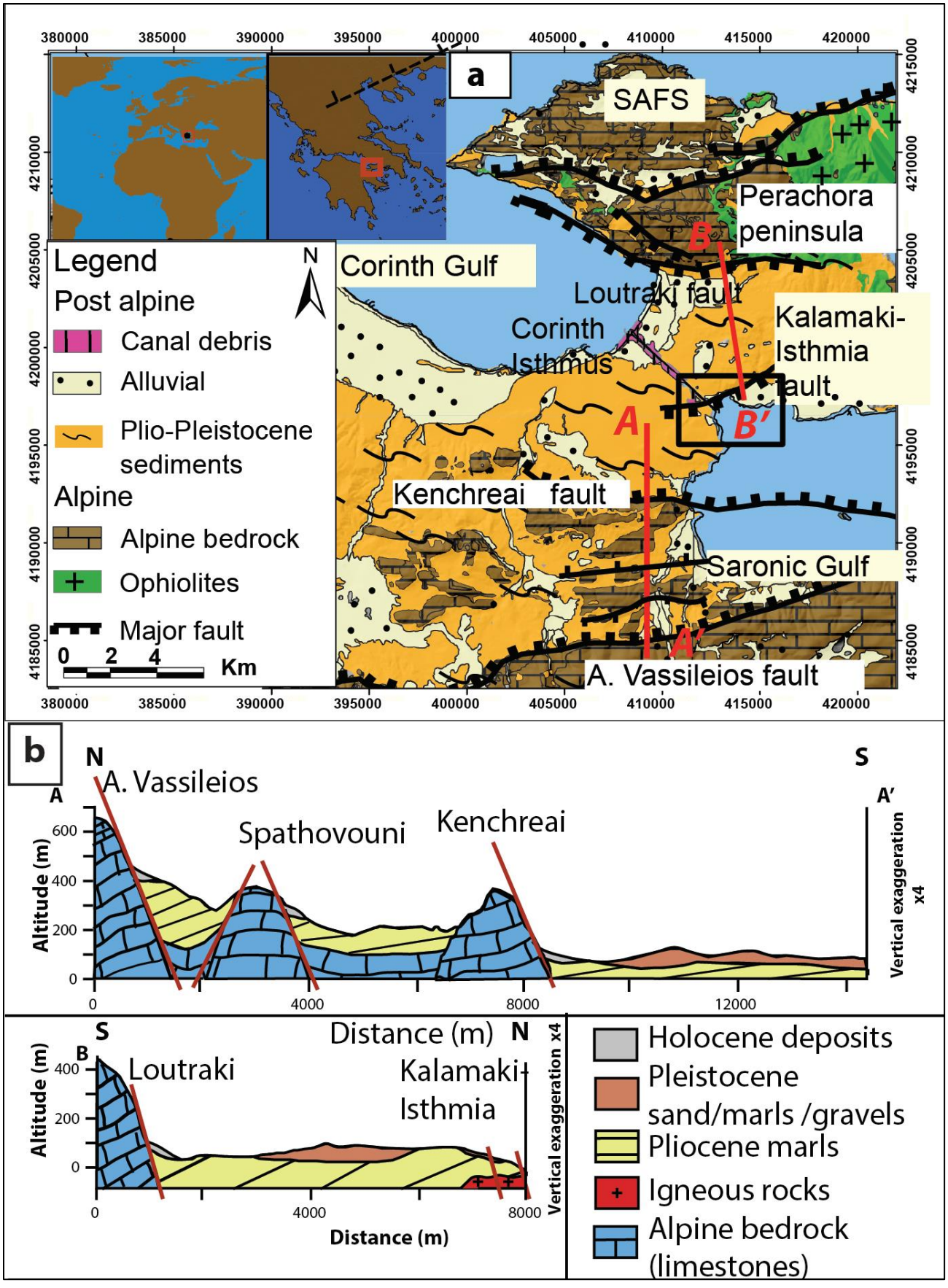
a
SAFS
Perachora peninsula
Corinth Gulf
Loutraki fault
Corinth Isthmus
Kalamaki-Isthmia fault
Kenchreai fault
Saronic Gulf
A. Vassileios fault
A
A′
B
B′
Legend
Post alpine
Canal debris
Alluvial
Plio-Pleistocene sediments
Alpine
Alpine bedrock
Ophiolites
Major fault
0 2 4 Km
N
380000 385000 390000 395000 400000 405000 410000 415000 420000
4215000 4210000 4205000 4200000 4195000 4190000 4185000
b
N
S
A
A′
A. Vassileios
Spathovouni
Kenchreai
Altitude (m)
0 200 400 600
0 4000 8000 12000
Vertical exaggeration x4
S
N
B
Distance (m)
Loutraki
Kalamaki-Isthmia
Altitude (m)
0 200 400
0 4000 8000
Distance (m)
Vertical exaggeration x4
Holocene deposits
Pleistocene sand/marls /gravels
Pliocene marls
Igneous rocks
Alpine bedrock (limestones)

Figure 3-1. *Simplified geological map showing the lithology of the area, grouped into Plio-Pleistocene clayey to gravely sediments, alpine bedrock (Triassic-Jurassic Boeotian and Pelagonian limestones as well as the Boeotian flysch) and the Upper Cretaceous Ophiolitic nappe; as well as the major faults of the area (South Alkyonides Fault System (SAFS), Loutraki, Ag. Vassileios and* Kenchreai *faults) and the Kalamaki-Isthmia fault (modified from Bornovas et al., 1972, 1984; Gaitanakis et al., 1985; Papanikolaou et al., 1989, 1996). The black box indicates the area where the boreholes were drilled. (b) Cross sections A-A' and B-B' at the eastern area of the Corinth, exaggerated in the vertical axis by 4.*

Εικόνα 3-1. *Απλοποιημένος γεωλογικός χάρτης της περιοχής της Κορίνθου με την λιθολογία της περιοχής ομαδοποιημένη σε Πλιο -Πλειστοκαινικά αργιλικά και κροκαλοπαγή ιζήματα, στο αλπικό υπόβαθρο και στους Άνω Κρητιδικούς Οφιολίθους. Επισημαίνονται τα σημαντικότερα ρήγματα της περιοχής (ζώνη Αλκυονίδων, Λουτρακίου, Αγ. Βασιλείου και Κεχριών) και το ρήγμα Καλαμάκι-Ίσθμια (τροποποιημένο από τους Bornovas et al., 1972, 1984, Gaitanakis et al. 1985, Papanikolaou et αϊ., 1989, 1996). Το μαύρο πλαίσιο υποδεικνύει την περιοχή όπου έγιναν οι γεωτρήσεις. (β) Τομές Α-Α και Β-Β' στην ανατολική περιοχή της Κορίνθου, όπου είναι μεγεθυμένος ο κάθετος άξονας επί 4.*

3.3 Paleogeographical evolution of the Corinth and Saronic Gulfs

Most researchers mention that the paleogeographical evolution of the Corinth Rift can be divided into two phases (e.g. Ori, 1989; Sorel, 2000; Jolivet et al., 2003, 2010; Flotte´ et al., 2005; Bell et al., 2009). Most researchers suggested that this Proto Gulf (first stage) was a lacustrine to shallow marine intracontinental sea, which was probably drained southeastward to the Argos Gulf and the subsidence rate never exceeded the sedimentation rate. This proto-Gulf stage is marked by lacustrine facies deposition from Pliocene to Lower Pleistocene, observable even 40 km south of the southern coast of the Gulf. During the second stage (The last 1 Ma), the Gulf has taken its present form, with the northwards migration of the major faults and the deep marine deposits, including turbidity flows.

The development of the easternmost Corinth Gulf is also mentioned by Leeder et al. (2002), where the Proto-Corinth rift during the Pliocene and the Corinth Gulf with its present form during the Pleistocene. Westaway, (1996; 2002) mentioned for the transition from the proto- Corinth Gulf to the present Gulf "*that the ca. 80 m of water loading when the lacustrine basin was flooded by the sea 0.9 Ma ago caused a positive lithostatic pressure anomaly to the brittle crust and this caused out flow of the lower crust to the beneath the Plio-Pleistocene basin farther south*".

Bell et al. (2009) suggested a four stages evolution of the Corinth Gulf. Stage 1 is from ~4 Ma till ~2.2 Ma ago, where the Megara basin was the easternmost part of the rifting. Stage 2 is from 1-2 Ma to 0.4 Ma ago, where activity focused on the Mamoussia Pirgaki fault resulting to the deposition 1.5 km thick Gilbert fan deltas (from Collier & Jones, 2003). Stage 3 is from 0.4 Ma till the present form of the Corinth Gulf. In this stage dominant faults of the central rift (Derveni and Likoporia) experienced an increase in displacement and in slip rate. Slip rates exceed of those the west and east (Eliki, Xylokastro). Recent Holocene activity is described as stage 4, where microseismicity is concentrated in Aigion and Rio graben (from Doutsos et al., 1988). Sakelariou et al. (2007) suggested that the current basin, together with the actively forming Gilbert-type deltas at the present sea level, may represent a third phase in the evolution of the Gulf

of Corinth, something that is also suggested by Moretti et al. (2003) and Ford et al. (2012).

The Saronic Gulf has also undergone significant changes during the Quaternary. Collier (1990) mentioned the Quaternary collapse of the Saronic Gulf, where marginal faults (e.g. Kakia Skala, Kenchreai, Agios Vassileios) were more active (Leeder et al., 2008). A point of interest in the western coast of the Gulf, is the submerged harbor of Kenchreai (e.g. Mourtzas et al., 2014; Mourtzas and Kolaiti, 2014; Kolaiti and Mourtzas, 2016). This Roman infrastructure is submerged ~ 0.70 m beneath the sea surface and even though that the Kenchreai fault's activity might be partially responsible for that, sea level rise and liquefactions which occurred in the area could also have submerged the harbor (Koukouvelas et al., 2017).

Glacioeustatic sea level changes have also influenced the morphology of the Gulf at least since upper Pleistocene. Lykousis, (2009) mentioned the presence of a paleolake at least during the last sea level lowstand (MIS 2), at the western part of the Saronic Gulf, while during the glacioeustatic sea level lowstands during the last 400 ka subaerial conditions are mentioned for the entire Saronic Gulf. The presence of a lake is also mentioned in Lykousis et al., (2007) where aragonite crystals have been identified since the last glacioeustatic lowstand.

3.4 Uplift

The northern coast of the Peloponnese has been uplifted the last 2.2 Ma. This is documented in the deep fluvial incision and the uplifted Plio-Pleistocene sediments. Several researchers have studied and described the marine, fluvial and the Gilbert Fan Deltas sediments uplifted up to 1200 m above the present sea level at the western part of the Gulf (e.g. Ori, 1989; Gobo et al., 2014; Demoulin et al., 2015; Malartre et al., 2004; Dart et al., 1994; Ford et al., 2007, 2012 and Bell et al., 2009).

At the southern part of the Gulf the uplift of the marine terraces have been described by several researchers (e.g. Keraudren & Sorel, 1987; Keraudren et al., 1995; Armijo et al., 1996; Westaway, 1996, 2002). Researchers have described and correlated marine terraces with the glacioeustatic sea level change during the Upper-Middle Pleistocene and the have estimate an uplift rate approximately at 1.5 mm/yr the last 500.000 years at the central part of the southern Gulf of Corinth, which diminishes at 0.3 mm/yr at the eastern part.

The uplift of the Perachora peninsula during the Holocene – Upper Pleistocene is also examined by several researchers. Kershaw & Guo (2001), estimated the Holocene uplift through cyanobacterial mounds while Leeder et al. (2003) through marine shorelines. Paleoshorelines of the Perachora peninsula were studied by Roberts et al. (2009) and Cooper et al. (2007) as well. According to Cooper et al. (2007), the estimated uplift rate during the Holocene from the highest notches is up to 0.55 mm/yr. Roberts et al. (2009) has also mapped and examined the different heights of the raised paleoshorelines and marine terraces across the footwall of the South Alkyonides fault system. They suggested that the southernmost area of Perachora peninsula has been uplifted with a rate approximately 0.15 mm/yr, during the Pleistocene till the last 200 ka towards its center and diminish towards its tips. They also suggested that the slip rate of the SASF has accelerated and the last 200 ka the area is uplifted with a 0.51 mm/yr rate. Uplifted terraces have been described by Morewood & Roberts, (1999) in Perachora peninsula as well, Charalampakis et al. (2014) by correlating the bedrock beneath the Lechaion Gulf and the adjacent mountains through sequence stratigraphy interpretation of seismic profiles from the Lechaion Gulf, suggested an cumulative average slip rate of 0.9 mm/yr or less, over the last 4 Ma. Turner et al. (2010) tested various rival hypotheses concerning the evolution of the eastern tip of Corinth and the uplift of this area, proposing a 0.31 mm/yr uplift rate at Lechaion Gulf. Finally, they also suggested that the north coast of Lechaion Gulf uplift cannot be solely explained by footwall uplift but it is due to isostatic uplift that probably affects the whole of the southern Gulf of Corinth rift.

Collier et al. (1992) and Dia et al. (1997) through corals dating, have estimated the uplift rate of the Isthmus Canal approximately at 0.3 mm/yr (Corinth Canal) and 0.45 mm/yr at Examilia (southwards the city of Corinth) over the last 200 ka.

It is clear that the Corinth Gulf is a highly active tectonic region, where the southern coast is constantly uplifted, at least during Pleistocene. Uplift rates though, are not the same at every section of the Gulf. Most researchers suggest that the central part of the Gulf is uplifted at a higher rate (1.5–2 mm/yr) than the western or the eastern part (0.3–0.8 mm/yr) (e.g. Keraudren & Sorel, 1987; Keraudren et al., 1995; Pirazzoli et al., 2004; Westaway, 1996, 2002; Armijo et al., 1996; McMurray & Gawthorpe, 2000; Leeder et al., 2008).

The origin of southern Corinth Gulf rift and Peloponnese's uplift is highly debated. Le Pichon & Angelier, (1979) suggested that uplift is caused by sediment underplating, by intrusion and thrusting from the Hellenic subduction zone and Cretan forearc (Leeder & Mack, 2007). Leeder et al. (2003, 2008) and Leeder & Mack, (2007), suggested that the regional uplift of Peloponnesus and the Southern Gulf is due to deeper tectonic processes, a view also held by Moretti et al. (2003). Leeder & Mack, (2007) suggested that the uplift is attributed to buoyancy of the underlying African flat slab, as augmented by local footwall uplift along the southern margin to the Gulf of Corinth. McMurray & Gawthorpe, 2000 mentioned that "*Collier et al. (1992) suggested that the uplift is of regional origin while Armijo et al. (1996) conclude that the observed uplift between Xylokastro and Corinth is due to local uplift in the footwall of the Xylokastro fault. However, the presence of uplifted marine terraces between Xylokastro and Akrata, in the hanging wall of the Xylokastro fault (as mapped by Armijo et al. 1996), suggests that the Xylokastro fault cannot be the only cause of uplift in the northern Peloponnesus".* Westaway (1996, 2002) mentioned the contribution of the isostatic response to the uplift rate of the area., suggesting that "*the main effect in this locality is southward lower-crustal flow from beneath the modern Gulf interior to beneath the PGCB, driven by pressure variations at the base of the brittle layer caused by the sediment loading in the Gulf and the unloading of the Proto Gulf Corinth Basin caused by its erosion. Sediments began to be rapidly eroded from former depocentres and re-deposited in adjacent*

localised topographic lows. The thermal response to this change from slow sedimentation to more rapid erosion or sedimentation enabled the associated isostatic and lower-crustal flow responses and the resulting changes in relief to be determined".

3.5 Seismicity

The region of the Corinth Gulf is one of the most seismically active regions in Greece where significant historical and reported earthquake events have been described (e.g. Scranton,1957; Noller et al., 1997; Papazachos & Papazachou, 1997). Sachpazi et al. (2003) mentioned 10 events in the Corinth Gulf of M≥5 since 1965. Roberts & Koukouvelas (1996) mention that the Gulf of Corinth has hosted 11 earthquakes of magnitude M_s>5.8 the last 100 years, while Koukouvelas et al. (2017) mentioned the existence of 11 historical events (6.0 ≤Mw≤ 6.9) and 5 reported events from 1850 to 1981 (5.0 ≤Mw≤ 6.) at the eastern part of the Corinth.

Much of the interest in the area was spurred after the earthquake sequence of since it was an excellent opportunity to observe the effects from an earthquake sequence in 1981, with well recorded earthquake effects and primary surface ruptures. Three earthquakes on February 24, with 6.7 Ms, on February 25, with 6.4 Ms and on March 4, with 6.4 Ms, occurred. The epicenters of the first two earthquakes were at the Alkyonides Basin in the eastern Gulf of Corinth, while the third one was at the Kapareli fault (e.g. Jackson et al., 1982; Taymaz et al., 1991; Collier et al., 1998).

Jackson et al. (1982) and Mariolakos et al. (1982) were among the first who have mapped and described the effects from these earthquakes. They have identified surface ruptures both in Kapareli and Schinos-Pisia faults tracing surface ruptures approximately 25 km long. Maximum observed displacements were approximately 1.5 m high. Hubert et al. (1996) described and mapped the effects from the earthquakes, modeled the vertical displacement caused by these events and the Coulomb stress transfer due to the earthquakes. They have implied that the first earthquake might have triggered the others.

The vertical slip rate at SAFS was studied both by Pantosti et al. (1996) and Collier et al. (1998), through trenching methods. In an active alluvial fan at Bambakies, approximately at the center of the fault system and more specifically at the easternmost end of the Schinos surface rupture, a trench was excavated in order to identify paleosoil horizons. Pantosti et al. (1996) identified and dated three layers attributed to paleoearthquakes at 1295 AD and at 590 AD estimating the vertical slip rate at minimum of 1 mm/yr. Collier et al. (1998) repeated the procedure two years afterwards at the same area where two more trenches were excavated. Earthquake recurrence was estimated at 700 years (trench 1), to 330 years (trench 3). Displacement per event has been estimated at 0.5 m, while vertical slip rate has been calculated to 2-3 mm/yr.

3.6 The Corinth Canal – Isthmus

The Corinth Canal offers a unique opportunity to study the sediments accumulation of the Isthmus (Fig. 3-2). Several researchers have described in detail the lithological patterns of the strata (e.g. Freyberg, 1973; Collier, 1990; Collier & Dart, 1991; Collier & Thomson, 1991; Gawthorpe et al., 1994), have established the age framework of the sediments (e.g. Collier et al., 1990; Dia et.al, 1997; Pierini et al., 2016), or have estimated the uplift rate of the Isthmus area (e.g. Collier et.al, 1990; Dia et.al, 1997).

Freyberg (1973) was among the first to describe the sedimentology of the Isthmus Canal, recognizing that eustatic variation had influenced facies patterns in the canal are, describing two marine to Pleistocene freshwater ‘cycles’ in the canal section.

Collier & Dart (1991) have thoroughly described the sediments at the NE part of the Canal, separating them into three major Groups, the Lower Pliocene Group crops out in the Asprakhomata- Kalamona and Charalampos, the Trapeza- Isthmos Group outcrops in the Trapeza-Isthmos fault block and Holocene fan-delta which is exposed on the Kalamaki fault block (Fig. 3-3a). The Charalampos marl Formation, a silty-grey mudstone with packages of sandstones and conglomerate, in which Gaitanakis et al. (1985) mentioned the presence of freshwater *Viviparus* and *Melanopsis* macrofauna,

indicating lacustrine to alluvial environments. The Charalampos conglomerate Formation consists of coarsening upwards conglomerate above the marl Formation, (either in transition from marl to conglomerate, or by erosion where the researchers have mentioned lignite horizons between them), describing fluvial packages of a fan delta. The white marl Formation is a thick calcareous siltstone which also contains freshwater or marine fauna (e.g. *Viviparus*, *Cyprideis*, *Cardium*).

Kitrinovuni sand Formation (Fig. 3-3) contains two facies of fluvial systems (one of sandstone with siltstone and one of coarse sands) while Koudounistra Formation consists of red chert and ultrabasic clasts conglomerate. The Drosia and Koudounistra conglomerates consist of a coarsening upwards pattern ranging from marls to conglomerate sediments. The uplifted sediments by the Kalamaki Isthmia fault were not described in detail. The researchers refer only to the Trapeza- Isthmus group without further examination suggesting a Pliocene-Pleistocene age.

Collier & Thomson (1991) have thoroughly described the sediments at the central part of the Corinth Canal, describing Upper Pleistocene marine facies including beach to offshore conglomerates and sandstones with wave-modified sedimentary structures. They mentioned planar and cross bedded sandstones and conglomerate facies, associated with a beach to offshore transition; variable laminated siltstone to sandstone, associated with shallow marine deposits. Oolitic sandstone facies were related with shallow and high energy marine environments, while transverse and linear dunes with deeper marine deposits.

The researchers have also reconstruct the paleogeography of the area during the MIS 7 (200 ka) suggesting that a marine connection periodically existed through the Corinth Isthmus based on active faults and glacio-eustatic sea level highstand.

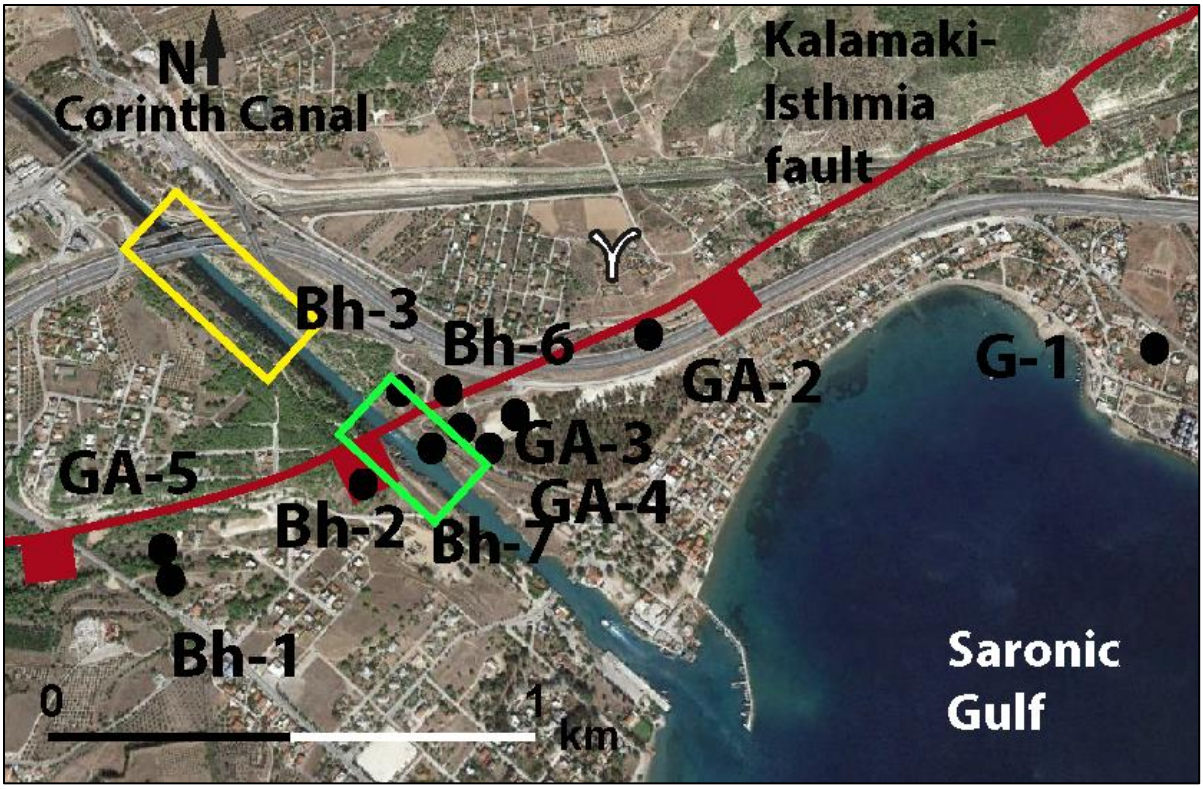

Figure 3-2. *View of the Corinth Canal, where boreholes were drilled, using Google Earth imagery from August 2014. The area where Collier et al. (1992) sampled corals is indicated with the white coral symbol, while the yellow box indicates where the photos of the canal in figure 12-4 and the green box the photos in figure 11-3 were taken.*
Εικόνα 3-2. *Άποψη του καναλιού της Κορίνθου, όπου έγιναν και οι γεωτρήσεις, βασισμένη στις εικόνες του Google Earth από τον Αύγουστο του 2014. Υποδεικνύεται η περιοχή όπου οι Collier et al. (1992) χρονολόγησαν τα κοράλλια (λευκό κοράλλι), ενώ το κίτρινο και το πράσινο πλαίσιο υποδεικνύει την περιοχή οπού λήφθηκαν οι φωτογραφίες του καναλιού από τις εικόνες 12-4 και 11-3 αντίστοιχα.*

They also mentioned that the uplifted strata by the Kalamaki-Isthmia fault are tilted towards NW implying the recent activity of the fault. Finally, they have mentioned the presence of a marine terrace, northwards than the canal, at 150 m height. By analogy with the terraces of the southern Corinth Basin and the beach cycles of the central Corinth they suggested an uplift rate 0.4–0.8 mm/yr.

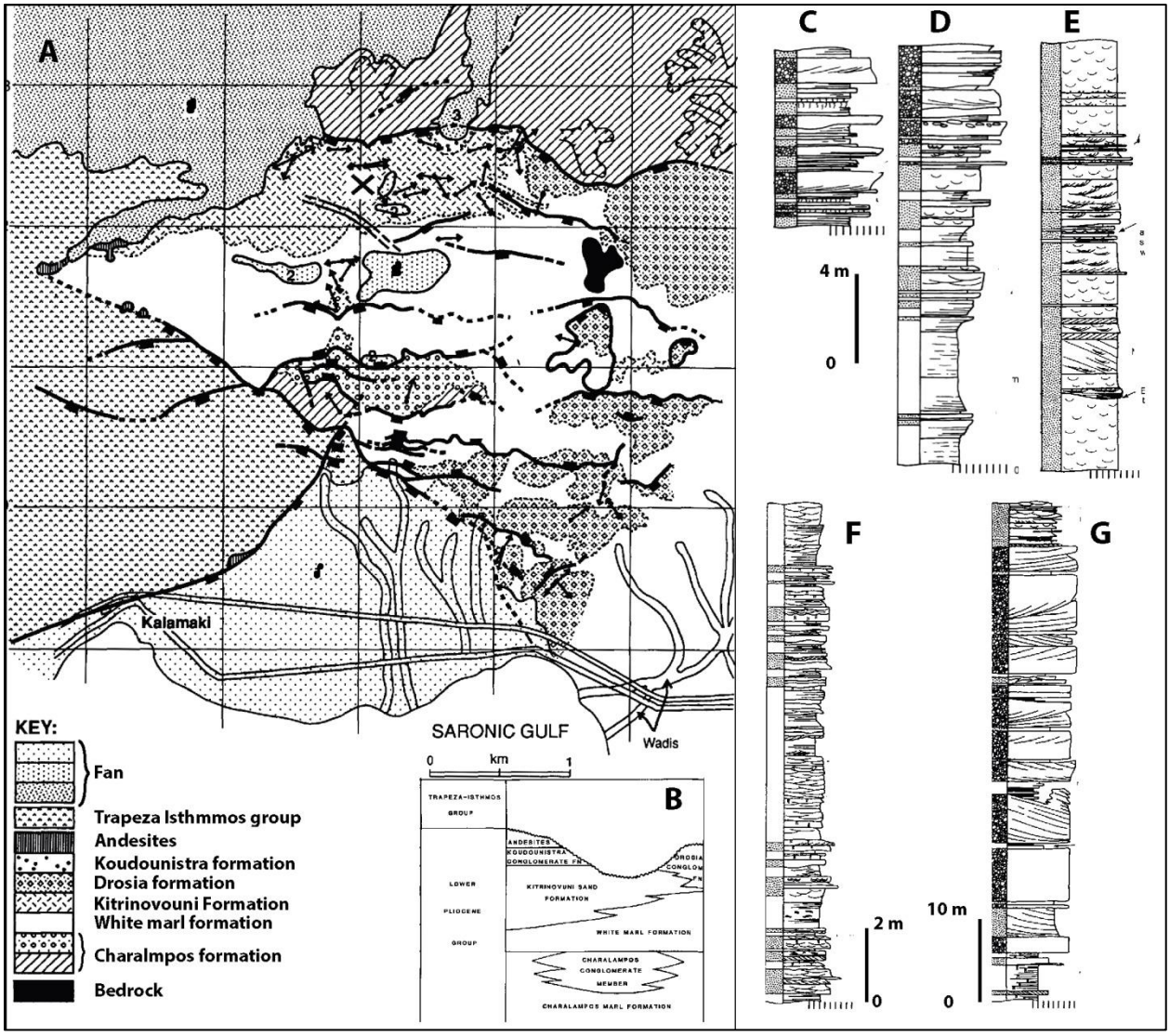

Figure 3-3. *A) The geological map showing the lithological formation eastern the Corinth Canal. B) Stratigraphic scheme for the Lower Pliocene to Pleistocene outcrops C-G) Sedimentary logs of the described lithological formations. C) Koudounistra Formation, D) Drosia Formation, E) Kitrinovuni Formation, F) Charalampos Formation, White marl Formation. (Modified from Collier & Dart, 1991).*
Εικόνα 3-3. *Α) Ο γεωλογικός χάρτης της περιοχής ανατολικά της Διώρυγας. Β) Σχηματική απεικόνιση της στρωματογραφίας της περιοχής. C-G) Στρωματογραφικές στήλες των μελετημένων λιθολογιών C) σχηματισμοί Κουδουνίστρας, D) σχηματισμοί Δροσιάς, Ε) σχηματισμοί Κιτρινοβουνίου, F) σχηματισμοί Χαραλάμπου, G) σχηματισμοί Λευκής μάργας (από Collier & Dart, 1991)*

Collier (1990) described five subsequences at the Corinth Canal. He mentioned that Corinth Marls, previously described by Freyberg (1973), to be the oldest sediments exposed in the canal section, also mentioning an upwards transition within the central horst block from freshwater or brackish to marine facies. Coral dating from this section were not useful, since due to limitations of the methodology their expected age is older than 350 ka. Above the Marls he described the 1stsubsequence, which consists of conglomerates with ophiolite clasts, (coastal paleoenvironment) fining upwards to sandy layers (shallow marine with fresh water influence). The 2ndsubsequence consists of beach- to shoreface set a, fining upwards to shallow marine mudstones. Corals dated from with this subsequence have shown an age ~312 ka, placing them at MIS 9. The 3rd subsequence consists of fining upwards sands, of marine origin. Corals dated form this subsequence indicated an age ~205 ka, placing them at MIS 7. The 4th subsequence was described at the NW part of the Canal interpreted as the product of another marine transgression. The 5th subsequence is described and interpreted as coastal, recent (Holocene) deposits.

Gawthorpe et al. (1994) and McMurray & Gawthorpe (2000) have also studied the sediments formations from the Corinth Canal. McMurray & Gawthorpe (2000) described the facies stacking patterns of the attached shoreface sequences from the Corinth Canal mentioning shoaling and coarsening upward facies stacking pattern. Between the basal contact of the first sequence overlying Corinth Marls a prominent palaeocliff approximately 1.75 m high, was interpreted as evidence of subaerial exposure prior to transgression. Gawthorpe et al. (1994) mentioned that these sequences in the south-east of the isthmus consist of foreshore conglomerates while to the north-west consist of lower shoreface sands; suggesting that the general facies stacking pattern within the sequences is one of progradation with limited aggradation. Furthermore, the researchers based on the described exposed sequences on the isthmus suggested that *“they display a distinctive stacking pattern and form one sequence set which each sequence is located further basinward of the previously deposited sequences and the sequence boundaries converge and become coincident in the up-dip direction (to the south-east). Thus this sequence set offlaps to the north-west and is considered here to represent a forced regressive sequence set*”.

Several researchers have estimated the age of the sediment sequences based on corals dating (e.g. Collier et al., 1992; Dia et al., 1997; Pierini et al., 2016). In Collier (1990) corals' dating indicated an age of the Corinth Marl older than 350 ka, of the 2nd subsequence ~312 ka and of the 3rd subsequence ~205 ka. In Collier & Dart (1991) and Collier et al. (1992) corals samples were also dated from Examilia village, southern than the Canal, implying an age ~205 ka. Samples from the same area were dated by Dia et al. (1997) as well, suggesting an age ~330. They have also dated corals from Perachora Peninsula, as well as from the Corinth Canal, demonstrating ages similar with these in Collier (1990). Based on these dates Collier (1990) and Collier et al. (1992), suggested an uplift rate for the Corinth Canal, approximately 0.3 mm/yr. Pierini et al. (2016) through *Pecten* specimens used for IcPD dating suggested approximately ages with Collier (1990)[5].

[5] *>350 ka for MIS 11, ~311 ka for MIS 9 and ~205 for MIS 7.*

4 Materials and methods

4.1 Surface mapping

Detailed surface mapping was focused mainly on the eastern part of the Corinth Canal at the footwall and the hangingwall of the Kalamaki Isthmia fault, describing the lithology and the tectonic features of the area. In total 149 measurements of the strata inclination and 91 of the tectonic features were extracted. Furthermore, 99 samples extracted from sandy, clayey and even gravely outcrops were examined for their micropaleontological and 32 samples were examined for their nannofossils content.

4.2 Boreholes

Eleven boreholes were drilled[6] in either sides of Kalamaki-Isthmia fault (~ 373 m total length), offering unique data. Boreholes Bh-6 and Bh-3 (which was the longest of them, 70.20 m long), were drilled at fault's footwall while the rest towards the immediate hangingwall of the fault (Fig. 3-2). Eight of them were examined in detail, while for the rest only lithological description was obtained.

4.3 Foraminifera

In total 355 samples extracted from boreholes and from surface outcrops have been analyzed for their micropaleontological content (256 from the borehole cores and 99 samples from surface outcrops), where each sample (20 g dry weight) was treated with H_2O_2 to remove the organic matter, to disaggregate silt and clay and subsequently was

[6] *The boreholes were drilled from Edafomichaniki SA, for geotechnical research.*

washed through a 125 μm sieve and dried at 60 °C. A subset containing approximately 200 benthic foraminifera for each sample when this was feasible was obtained using an Otto microsplitter. The microfauna have been identified under a Leica APO S8 stereoscope (Appendix B).

The affinities of the foraminiferal assemblages to environmental (mostly salinity) conditions can be evaluated on foraminiferal test size (e.g. Murray, 1991; Melis and Violanti, 2006; Koukousioura et al., 2012). In order to quantify this observation, biometric measurements were performed on *Ammonia* spp. tests distinguishing them in two size categories: small (<0.5 mm) and large (>0.5 mm). Therefore, the use of the ratio between large (L) and small (S) *Ammonia* tests is established as A-ratio: A=100 x L/(S +L) and it is used for estimating paleosalinity conditions (Koukousioura et al., 2012). Additionally, a broken-reworked ratio, BR=100 x broken-reworked/ (normal + broken-reworked) was calculated in order to better evaluate high energy paleoenvironments; high numbers of broken foraminiferal specimens indicate strong nearshore hydrodynamics (e.g. Vilela and Koutsoukos, 1992; Geslin et al., 2002). For data analysis, foraminiferal species relative abundances are expressed as percentage (%) of the assemblage. Foraminiferal diversity was determined through Fisher's alpha (α) index which was calculated using the Past.exe 1.23 software package (Hammer et al., 2001; Cosentino et al., 2017) (Appendix C).

The percentage of planktonic foraminifera (%P) within the total foraminiferal assemblage has been estimated, if it was feasible, according to Avnaim-Katav et al. (2013) based on Van Der Zwaan et al. (1990) and Van Hinsbergen et al. (2005) and was used as a proxy for palaeobathymetry.

4.4 Nannofossils

63 samples of fine-grained sediments (32 extracted from surface outcrops and 31 from the borehole cores were examined by Scanning Electron Microscopy (SEM) for their calcareous nannoplankton content. A small amount of sediment (~1 mg) per sample

was dissolved in buffered solution and filtered on Whatman cellulose nitrate filters (47mm diameter, 0.45μm pore size), using a vacuum filtration system. The filters were open dried and stored in plastic Petri dishes. A piece of each filter approximately 8x8 mm^2 was attached to a copper electron microscope stub using a double-sided adhesive tape and coated with gold. The filter pieces were examined using a Jeol JSM 6360 Scanning Electron Microscope (SEM, Faculty of Geology & Geoenvironment, National and Kapodistrian University of Athens[7]). A working magnification of 1200x was used throughout the analysis. A total of 300 coccoliths were counted per sample (e.g. Thierstein et al., 1977; Triantaphyllou, 2015). The definition of the *Emiliania huxleyi* NN21a biozone (Martini, 1971) is based on the first appearance of specimens of the species that is the midpoint of the slope of the initial increase of species in counts of 300 coccoliths (Thierstein et al., 1977; Rio, et al., 1990).

4.5 Magnetic Susceptibility

Magnetic Susceptibility within the core is measured with the Bartington MS2 system with the MS2K sensor (see also Reicherter et al., 2010). In total, 986 MS measurements have been carried out from different lithological alternations within the cores. The Magnetic Susceptibility (MS) of sediments depends mostly on mineral composition and grain size. In general, iron bearing minerals lead to high values of MS (dimensionless SI units) (e.g., Mullins, 1977; Oldfield, 1991; Da Silva et al., 2009; Reicherter et al., 2010; Maselli et al., 2014). Terrestrial deposits are often characterized by higher amounts of such minerals compared to marine sediments and therefore MS measurements can help to distinguish between different sedimentary environments (Appendix D).

[7] *Magnification: 8X to 300,000X, resolution: 4.0nm (at 20kV),*

4.6 ^{230}Th/U-dating of fossil corals

Seven coral stems from a colony in borehole Bh-7 were selected for ^{230}Th/U-dating. Sample preparation and mass spectrometric analysis were performed at the Max Planck Institute for Chemistry, Mainz. Sample preparation and chemical separation of U and Th isotopes was performed as described by Yang et al. (2015). Uranium and Th isotopes were analysed by multi-collector inductively coupled plasma mass spectrometry (MC-ICP-MS, Nu Plasma). Analytical details can be found in Obert et al. (2016). Details about the calibration of the mixed U-Th spike are given by Gibert et al. (2016). All ages were corrected for potential detrital contamination assuming an average upper continental crust ^{232}Th/^{238}U weight ratio of 3.8 for the detritus and ^{230}Th, ^{234}U and ^{238}U in secular equilibrium. All activity ratios were calculated by using the half-lives reported by Cheng et al. (2000).

4.7 Luminescence

4.7.1 Introduction

Six samples from three boreholes were selected for OSL and IrSL dating, based on the quality of the samples[8] (Bh-1, 5.25 m, 6.05 m, Bh-3, 20.5 m, 21.25 m, Bh-7, 20.65 m, 33.45 m). Following the conventional laboratory practices, (e.g., Preusser et al., 2008) samples were prepared for obtaining quartz and feldspar coarse-grains at the laboratory of Archaeometry / Paleoenvironment & Archaeometallurgy of N.C.S.R. Demokritos.

[8] *The examined samples should be undisturbed and without any fractures that could have allowed the sun light to pollute the sample. Furthermore each sample should have enough material for analysis considering that a significant eternal layer was removed.*

Luminescence is the physical procedure, in which light is emitted by the crystals of a mineral. As long as grains are exposed to daylight, there is no luminescence signal. Daylight or heat above several hundred ^{o}C, erases any energy that was previously absorbed. After their deposition, grains are affected by radioactive isotopes such as (^{238}U/^{235}U, ^{40}K and ^{232}Th) and grains slowly begin to accumulate luminescence signal. There is excitation of the atoms in the crystal lattice due to ionizing radiation. Consequently, the activated electrons "jump" at higher states. Many of them are captured at specific electronic levels, which are called electron traps (e.g. Chen & Mckeever 1997; Krbetschek et al. 1997; Preusser et al., 2008).

All luminescence techniques aim to determine the energy (the electrons) that the grains have absorbed, since their last exposure to daylight. To achieve this mineral's grains are technically stimulated at a laboratory. The recorded energy which is measured is referred as the palaeodose. This energy is measured in Gy (Gray), which is the absorbed energy per mass of mineral ($J*kg^{-1}$). By dividing this energy with the dose rate, the age of the mineral is estimated. Dose rate is the "amount of energy deposited per mass of mineral due to radiation exposure acting on the sample over a certain time ($Gy\ a^{-1}$)" (Preusser et al., 2008).

Sediments that have been deposited more years have more electrons trapped within their crystal lattice. When these electrons are stimulated, emit an amount of light. The density of this light is measured to estimate the luminescence of the minerals. It should be mentioned that the amount of stimulated electrons, is a combination of the time that the sediment was trapped and the environment (which affect the dose rate) (e.g. Preusser et al., 2008).

4.7.2 Processing of the samples

Chemical Treatment

The external part of each sample (approximately 1 cm thick) was removed, material that may have been affected by solar radiation. The rest of samples was powdered and treated with hydrochloric acid (HCl) 10%. Afterwards the samples were washed up five times with tap water, one with distilled water and one with ethyl alcohol so any remains of HCL was washed away and any carbonate material was removed from the sample. The time of treatment with HCL depends on the content of carbonate in the sample.

Afterwards the material was dried and sieved and was treated with hydrogen peroxide (H_2O_2) 10%, removing any organic particles from the samples. The samples were re-washed three times with tap water, one with distilled water and one with ethyl alcohol for inactivating any residual H_2O_2 left. The time of treatment with H_2O_2 depends on the content of the organic in the sample.

Then the samples were treated with hydrofluoric acid (HF) for removing the outer surface of quartz grains, which had accepted the effect of particle "a" and to increase the purity of the quartz and feldspar in the samples. Quartz was obtained from the fractions which was treated with HF40% for 40 minutes, while feldspar was obtained from the fractions which was treated with HF 10% for 90 minutes. All samples were treated with HCL 10% for 15 minutes and were washed with distilled water seven times then with alcohol and were dried. Finally, with a powerful magnet any remains of magnetic minerals were removed.

Signal Measurements

For measuring the omitted signal single aliquot measurements were used, consisting of a monolayer of quartz or feldspar grains mounted on stainless steel discs of 10 mm diameter using silicone oil as an adhesive. The quartz and feldspar grains covered the

central 5 mm diameter portion of each disc, corresponding to several hundred grains per aliquot (e.g. Tsakalos et al., 2016).

All measurements were carried out on a Risø TL-DA 15 luminescence reader fitted with a Thorn EMI photomultiplier tube. Irradiation was from a calibrated 90Sr/90Y β source. Feldspar grains were stimulated by infrared light diodes emitting at 870 nm and the detected luminescence signal in the blue-violet region (320-460 nm) was achieved with a Schott BG39/Corning 7-59 filter combination. Infrared light stimulation was at 290 °C, right after a 50 °C stimulation for 100s, showing significant anomalous fading (Thiel et al., 2011; Tsakalos et al., 2016).Quartz grains were similarly examined using blue LEDs (470 nm) for stimulating the aliquots and a 7.5 mm Hoya U-340 filter for the signal detection filter mounted in front of the photomultiplier tube.

For the estimation of the sediments' age the dose rate of the relevant elements was determined separately. The calculation of the dose rates (U, Th and K) was based on analytical data obtained by Inductively Coupled Plasma Mass Spectrometry (ICP-MS; ACME laboratories, Canada) and using the "The Dose Rate calculator (DRc)" software developed by Tsakalos et al. (2016). This program uses the conversion factors proposed by Guérin et al. (2012) and the attenuation factors (due to water content) for alpha radiation by Aitken (1985), beta by Nathan and Mauz (2008), and gamma by Guérin et al. (2012). DRc also calculates the cosmic rays contribution to the total dose rate (according to Prescott and Stephan, 1982; Prescott and Hutton, 1988, 1994) using the altitude and latitude of the sampling sites, present day depth and the density of the overburden. The final dose rates are obtained by correcting for etching of the grains and the grain size**.**

4.7.3 Quartz OSL methodology

For the examination of the quartz grains the 'double-SAR' ('post-IR blue') protocol as described and outlined by Roberts and Wintle (2001) and Banerjee et al., (2001) was followed.

Firstly, the aliquot is given a small beta (test dose) irradiation which is less than the natural De value. The OSL response (TN) to this test dose is used to normalize the natural signal. The aliquot is then given a range of "regeneration" doses (R1-R2) and the resulting OSL decay curves (L1-L2) are measured. Each measurement of regenerated dose-response is followed by the application of a test beta doses, and subsequent measurement of the OSL response to that test dose (T1-T2) allows LX/TX to be determined for each regeneration dose step.

4.7.4 Feldspar IRSL methodology

Thiel et al. (2011) have briefly and simply described the procedure followed for the IRSL signal measurements in the following table

Table 1. The typical procedure followed for IRSL signal measurements (Thiel et al., 2011). Πίνακας 1. Η τυπική διαδικασία υπολογισμού του εκλυόμενου σήματος μέσω υπέρυθρης φωταύγειας.

Step	Procedure
1	Give dose
2	Preheat for 60 s at 320 ^{0}C
3	IR stimulation for 200 s at 50 ^{0}C
4	IR stimulation for 200 s at 290^{0}C
5	Give test dose, DT
6	Preheat for 60 s at 320^{0}C,

7	IR stimulation for 200 s at 50 ^{0}C
8	IR stimulation for 200 s at 290 ^{0}C
9	IR stimulation for 100 s at 325 ^{0}C
10	Return to 1

4.8 Statistical analysis

For data analysis, foraminiferal species relative abundances are expressed as percentage (%) of the assemblage. Foraminiferal diversity was determined through Fisher's alpha (*α*) index was calculated using the Past.exe 1.23 software package (Hammer et al., 2001; Cosentino et al., 2017).

Hierarchical cluster analysis, an algorithmic approach to find discrete groups with varying degrees of (dis)similarity in a data set represented by a (dis)similarity matrix, has been used for a detailed analysis of the results. Foraminiferal species are subjected into two-way cluster analysis (Q-mode, R-mode) to highlight biofacies (Scarponi et al., 2014). Samples (Q-mode) and taxa (R-mode) were clustered by the hierarchical cluster analysis (Ward's method and Euclidean distances as a similarity index) to determine species associations and to assess the ecological affinity among different groups. Biofacies were identified by a Q-mode cluster sharing a distinctive cluster(s) of taxa (R-mode), well represented in the Q-mode cluster (Scarponi et al., 2014). To examine only significant suites of taxa, R-mode clusters are examined only to species that exceeded 3% of the assemblage in at least one of the samples. Samples in the text are expressed as the centered value of the depth core from which the surface was extracted (e.g., sample Bh-1 from 9.60–9.70 m is referred to as Bh-1, 9.65 m).

A non-metric multi-dimensional scaling (MDS) ordination was used to identify significant groups (Avnaim-Katav *et al*., 2013).The object of nonmetric MDS is to find the coordinates of the points in two-dimensional space, so that there is a good agreement

between the observed proximities and the inter-point distances. (Fahrmeir and Hamerle, 1984) MDS attempts to represent as closely as possible the pairwise dissimilarity between the values into two-dimensional space.

A Kolmogorov-Smirnov normality test was used to examine if the measured MS values follow a normal distribution or not, based on the described lithology and the estimated paleoenvironment of the cores. Finally, a Pearson correlation test was compiled to examine if there is any correlation among the described lithology, the paleoenvironment and the measured MS values.

5 Corinth Canal borehole data

5.1 Introduction

Eleven boreholes were drilled in either sides of Kalamaki-Isthmia fault (~ 373 m total length) (Table 2). Boreholes Bh-6 and Bh-3 (which was the longest of them, 70.20 m long), were drilled towards the footwall of the fault while the rest towards the immediate hangingwall of the fault (Fig. 3-2, 5-1). Eight of them were examined in detail, while for the remaining three only lithological description was obtained. Borehole Bh-7 intersected the main fault plane at approximately 36 m core depth, exhibiting a 12 m thick deformation zone (from 33 m to 45 m core depth with several meters of cataclastites, containing fragments of limestone and tectonic breccia).

Figure 5-1. *Images from the drilled cores. (A) Borehole GA-4 from 18.30 m till 19.20 m, showing the transition from fluvial (gravels) to marine (silt). (B) Borehole GA-4 from 33.00 m to 33.90 m, showing the transition from gravels to sitly sand. (C) Borehole GA-5 from 28.60 m to 29.70 m, showing the transition from marine (clayey sand) to fluvial gravels.*

Εικόνα 5-1. *Χαρακτηριστικές εικόνες από τους πυρήνες των γεωτρήσεων . (Α) Γεώτρηση GA-4 από 18,30 μ. έως 19,20 μ., που φαίνεται τη μετάβαση από το ποταμοχειμάρεια σε θαλάσσια ιζήματα. (Β) Γεώτρηση GA-4 από 33,00 m έως 33,90 m, που φαίνεται η μετάβαση από χονδρόκοκκο σε λεπτότερο υλικό. (Γ) Γεώτρηση GA-5 από 28,60 μ. έως 29,70 μ., που φαίνεται η μετάβαση από θαλάσσια (αργιλώδη άμμο) σε ποταμοχειμάρεια ιζήματα.*

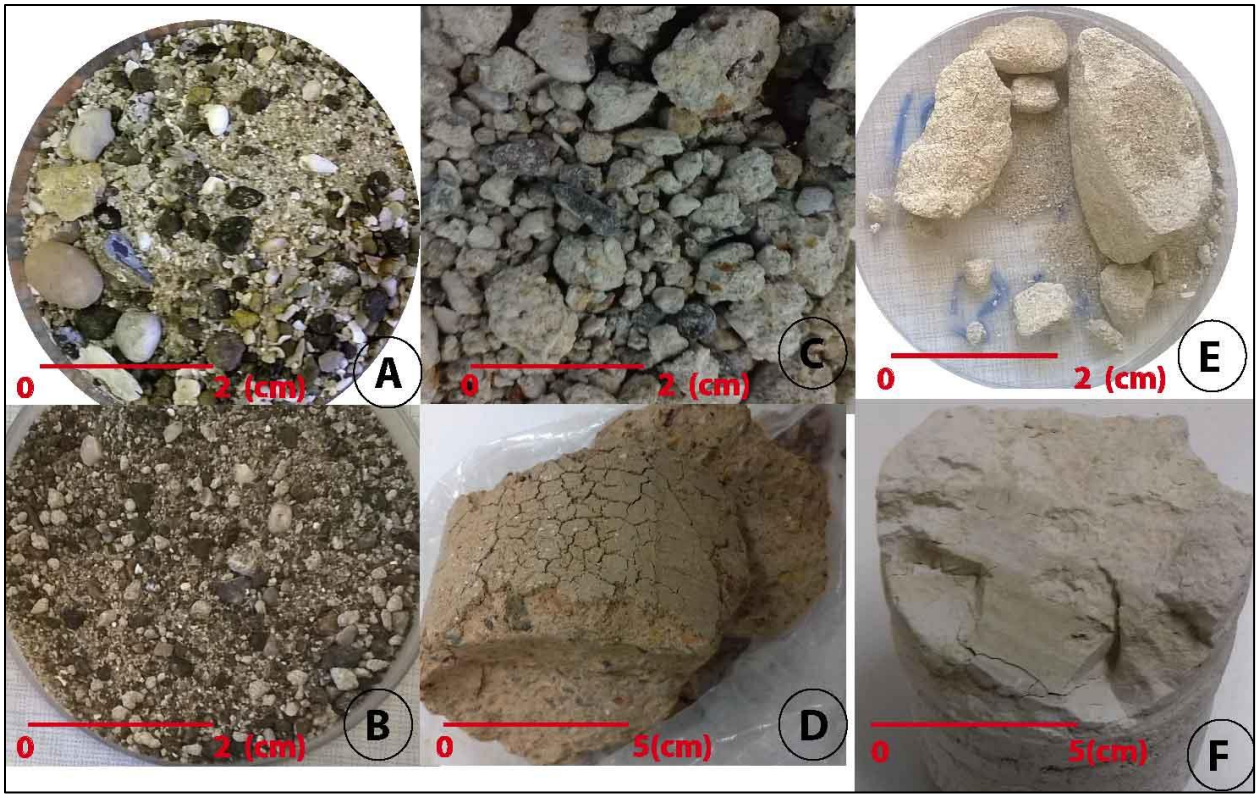

Figure 5-2. *Examples of the analyzed samples A) Gravels with ophiolite fragments (sample Bh-3 28.05 m), B) & C) Gravels (samples Bh-3 42.85 m and Bh-3 66.55 m respectively), D) Reddish clay (sample Bh- 15.25 m), E) Sand (sample Bh-3 49.65 m), F) Clay (sample Bh-3 37.55 m).*

Εικόνα 5-2. *Χαρακτηριστικά παραδείγματα των δειγμάτων που αναλύθηκαν Α) Χαλίκια με θραύσματα οφιολίθου (δείγμα Bh-3 28,05 m), Β) & C) Χαλίκια (δείγματα Bh-3 42,85 m και Bh-3 66,55 m αντίστοιχα) 15.25 m), Ε) Άμμος (δείγμα Bh-3 49.65 m), F) Άργιλος (δείγμα Bh-3 37.55 m).*

Table 2. The altitude, the depth and the coordinates (EGSA87) of the studied boreholes. The error of the coordinates is ± 2. Πίνακας 2. Το υψόμετρο, το βάθος και οι συντεταγμένες (EGSA87) των γεωτρήσεων (εκτιμώμενο σφάλμα ± 2).

Borehole	Altitude (m)	Depth (m)	X	Y
Bh-1	16.00 ±0.5	31.00	412040	4197081
Bh-2	15.00 ±5	49.00	412211	4197061
Bh-3	19.20 ±0.5	70.10	412269	4197153
Bh-4	20.50 ±5	30.50	412380	4197275
Bh-6	27.00 ±5	40.60	412366	4197115
Bh-7	16.10 ±0.5	57.00	412300	4197198
G-1	20.00 ±0.5	20.00	414642	4197778
G-2	19.00 ±0.5	10.50	413605	4197811
GA-2	35.00 ±0.5	14.00	412648	4197422
GA-3	20.80 ±0.5	15.20	412566	4197259
GA-4	21.10 ±0.5	45.50	412392	4197216
GA-5	19.90 ±0.5	30.00	412048	4197104

5.2 Stratigraphy — lithological description

In each borehole lithological alternations of sand, clay, clayey sand, conglomerate, marl and fragments of limestone have been recognized. It is remarkable that among these layers for all boreholes, there is no significant correlation. The latter strongly indicates that there are major lateral alternations and lithological variations. Conglomerate and layers with gravels contain pebbles and sub-angular clasts, indicating a high energy depositional environment. Ophiolites found within were probably transferred by torrents and sourced from the Gerania Ophiolitic nappes (e.g. Gawthorpe et al., 1994). Therefore, these strata can be ascribed to a fluvial–torrential paleoenvironment. Sandy

layers can be ascribed to various paleoenvironments from coastal to marine (Figs 5-1, 5-2).

5.3 Micro- and nanno- paleontological analysis

The studied benthic foraminiferal assemblages are relatively abundant and moderately preserved. In total 26 different species were described (Fig. 5-3) both from the surface and the borehole samples. Calcareous nannoplankton specimens have been identified through SEM analysis, within certain horizons of the examined boreholes (Fig. 5-4). From the 31 examined samples 15 of them proved to be rich in calcareous nannoplankton. In all these samples approximately the same species were identified. Samples were dominated by the presence of small *Reticulofenestra* spp. (~40%) and small *Gephyrocapsa* spp. (~30%) coccoliths, while *Emiliania huxleyi* specimens were relatively scarce (5-8% of the total assemblage), but consistently present.

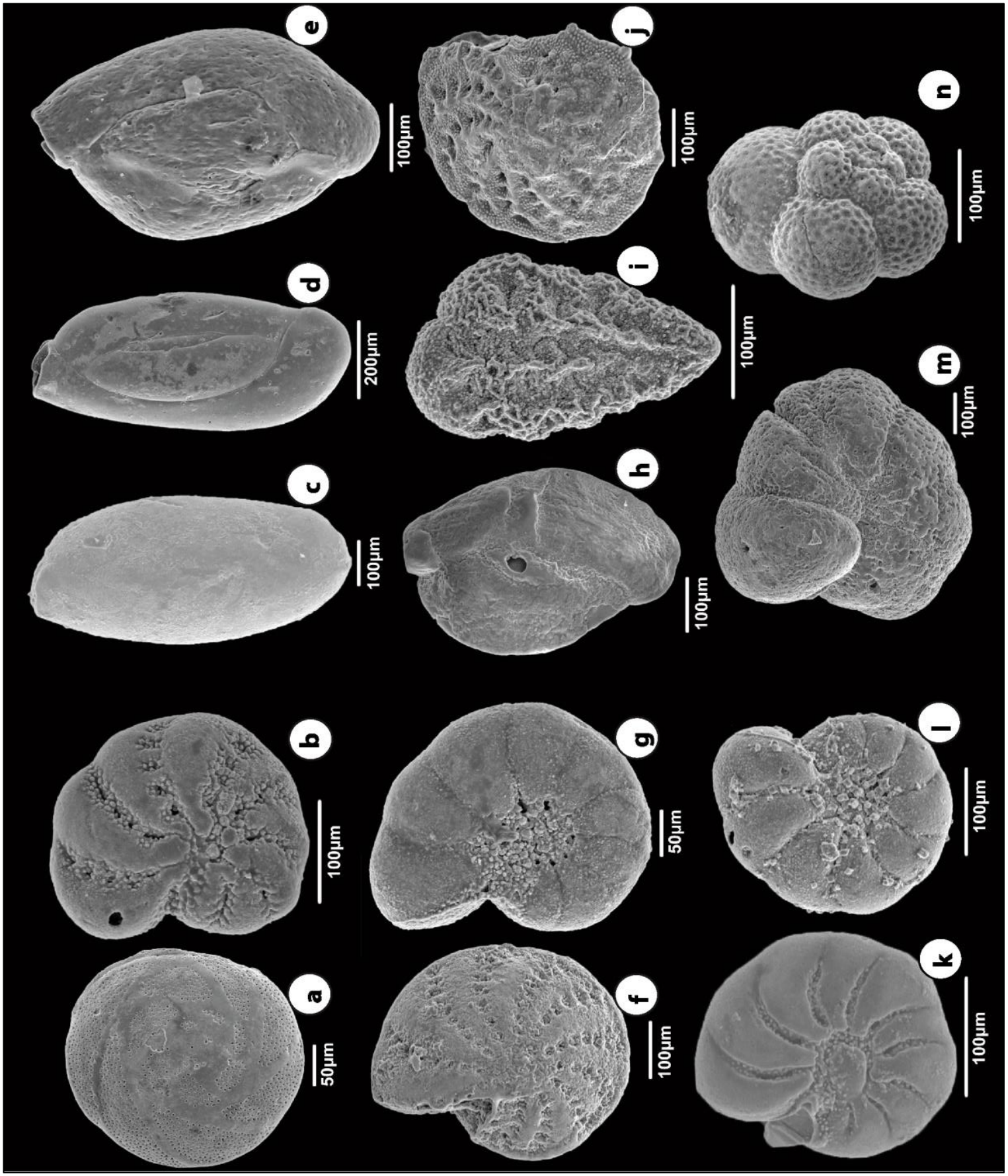
a
50µm
b
100µm
c
100µm
d
200µm
e
100µm
f
100µm
g
50µm
h
100µm
i
100µm
j
100µm
k
100µm
l
100µm
m
100µm
n
100µm

Figure 5-3. *Foraminiferal specimens under a Scanning Electron Microscopy (SEM). a) Rosalina bradyi (Cushman), spiral side (Bh-3, 19.85 m), b) Elphidium granosum (d'Orbigny), side view (Bh-3, 19.85 m), c-e) Quinqueloculina spp. (GA-4, 25.55 m, GA-2, 12.95 m, Bh-7, 26.55 m) f) Elphidium crispum (Linné), side view (Bh-3, 11.45 m). g) Haynesina depressula (Walker and Jacob), side view (Bh-3, 18.05 m). h) Quinqueloculina spp. (GA-4 31.05 m). i) Bolivina spp. (Linné), (GA-2, 12.95 m). j) Elphidium crispum (Linné), side view (Bh-1, 13.15 m). k-l). Haynesina depressula (Walker and Jacob), side view (Bh-7,22.35 m and spiral view GA-2, 6.35 m). m) Lobatula lobatula (Walker and Jacob), umbilical side (GA-4, 31.05 m). n) Globigerinoides spp. (Cushman), spiral side (Bh-3, 36.35 m).*

Εικόνα 5-3. *Χαρακτηριστικά τρηματοφόρα που περιγράφηκαν α) Rosalina bradyi (Cushman), σπειροειδής πλευρά (Bh-3, 19,85 m), b) Elphidium granosum (d'Orbigny), πλάγια όψη (Bh-3, 19,85 m), c-e Quinqueloculina spp. (GA-4, 25,55 m, GA-2, 12,95 m, Bh-7, 26,55 m) στ) Elphidium crispum (Linné), πλάγια όψη (Bh-3, 11,45 m). g) Haynesina depressula (Walker and Jacob), πλάγια όψη (Bh-3, 18,05 m). η) Quinqueloculina spp. (GA-4 31,05 m). i) Bolivina spp. (Linné), (GA-2, 12,95 m). j) Elphidium Crispum (Linné), πλάγια όψη (Bh-1, 13,15 m). k-1). Haynesina depressula (Walker and Jacob), πλάγια όψη (Bh-7,22,35 m και σπειροειδής όψη GA-2, 6,35 m). m) Lobatula lobatula (Walker and Jacob), ομφαλική πλευρά (GA-4, 31,05 m). n) Globigerinoides spp. (Cushman), σπειροειδής πλευρά (Bh-3, 36,35 m*

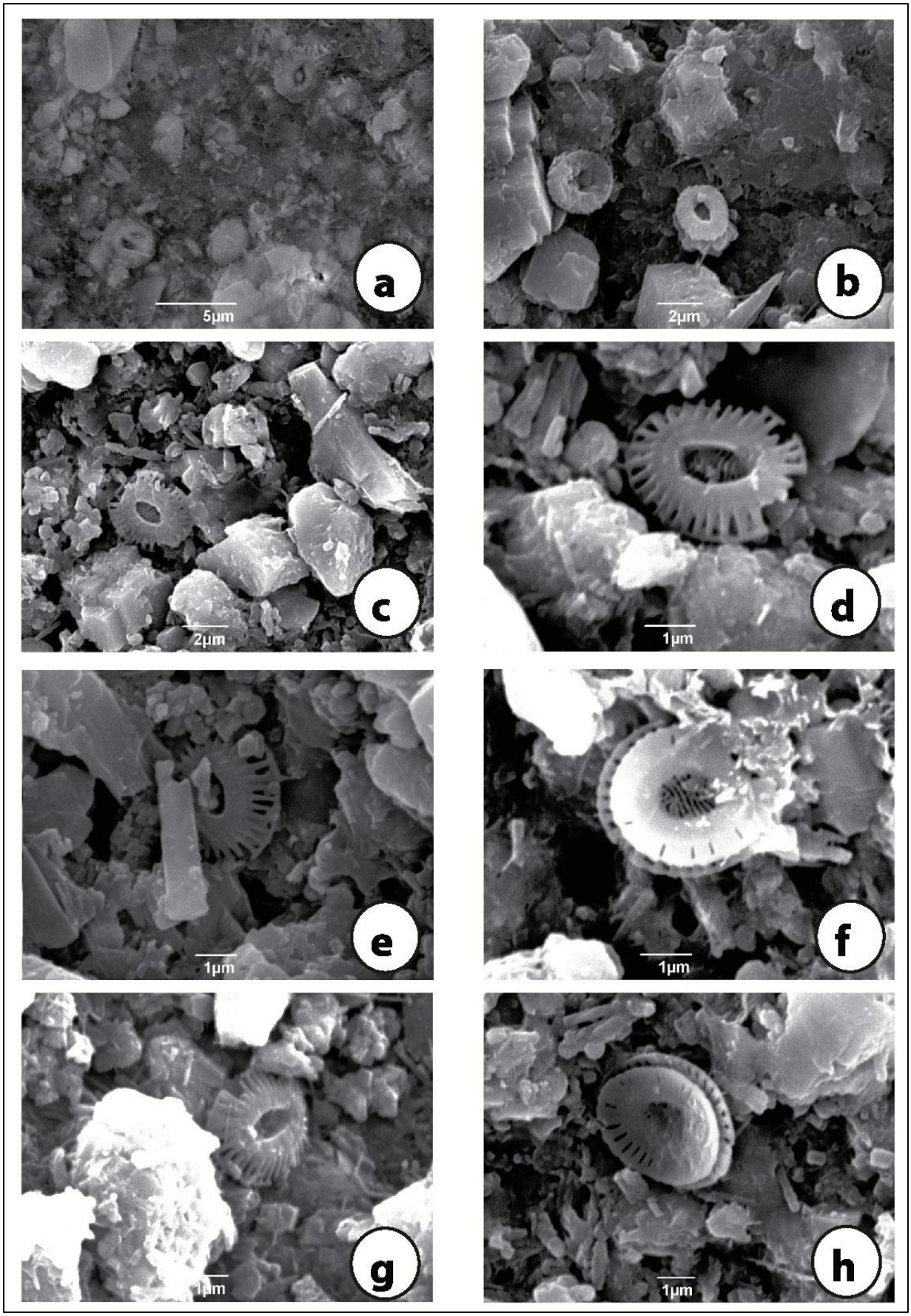
a
5μm
b
2μm
c
2μm
d
1μm
e
1μm
f
1μm
g
1μm
h
1μm

Figure 5-4. *Nannoplankton identified under a Scanning Electron Microscopy (SEM) a) Gephyrocapsa spp. and Emiliania huxleyi coccolith distal side (Bh-7 26.55 m), b) Reticulofenestra spp. coccolith distal side (GA-4 35.65 m), c-e) Emiliania huxleyi coccolith proximal side (Bh-3 8.75 , 35.65 m), f-h) Emiliania huxleyi coccolith distal side (sample Bh-3 20.75 m).*

Εικόνα 5-4. *Χαρακτηριστικά δείγματα νανοπλαγκτόν που περιγράφηκαν (SEM) a) Gephyrocapsa spp. και την ανώτερη πλευρά Emiliania huxleyi (Bh-7 26,55 m), b) Reticulofenestra spp. (Bh-3 8,75, 35,65 m), f-h) άνω πλευρά της Emiliania huxleyi (δείγμα Bh-3 20,75 m).*

5.4 Magnetic Susceptibility Analysis

The magnetic susceptibility (MS) of sediments depends mostly on the mineral composition and grain size (e.g., Mullins 1977, Oldfield, 1991, Da Silva et al., 2009, Reicherter et al., 2010, Pallikarakis et al., 2015). In general, iron bearing minerals lead to high values of MS (dimensionless SI units). Terrestrial deposits are often characterized by higher amounts of such minerals compared to marine sediments; therefore MS measurements can help to distinguish between different sedimentary environments. Overall, the described lithology within the boreholes is in agreement with the MS measurements taken. The extracted data show clear difference between coarse and fine sediments. Higher values are measured at gravely layers, while clayey and sandy layers have less magnetic susceptibility. Ophiolite clasts within the sediments are responsible for higher values, since they contain magnetic minerals.

5.5 Boreholes description

The analysis of the boreholes, located at the eastern part of the Corinth Canal (Fig. 3-2), is presented below

5.5.1 Borehole Bh-1

Lithology

Borehole Bh-3 consists of clay, clayey sands and sand, irrupted by gravely layers, several meters thick (Fig. 5-5, table 3).

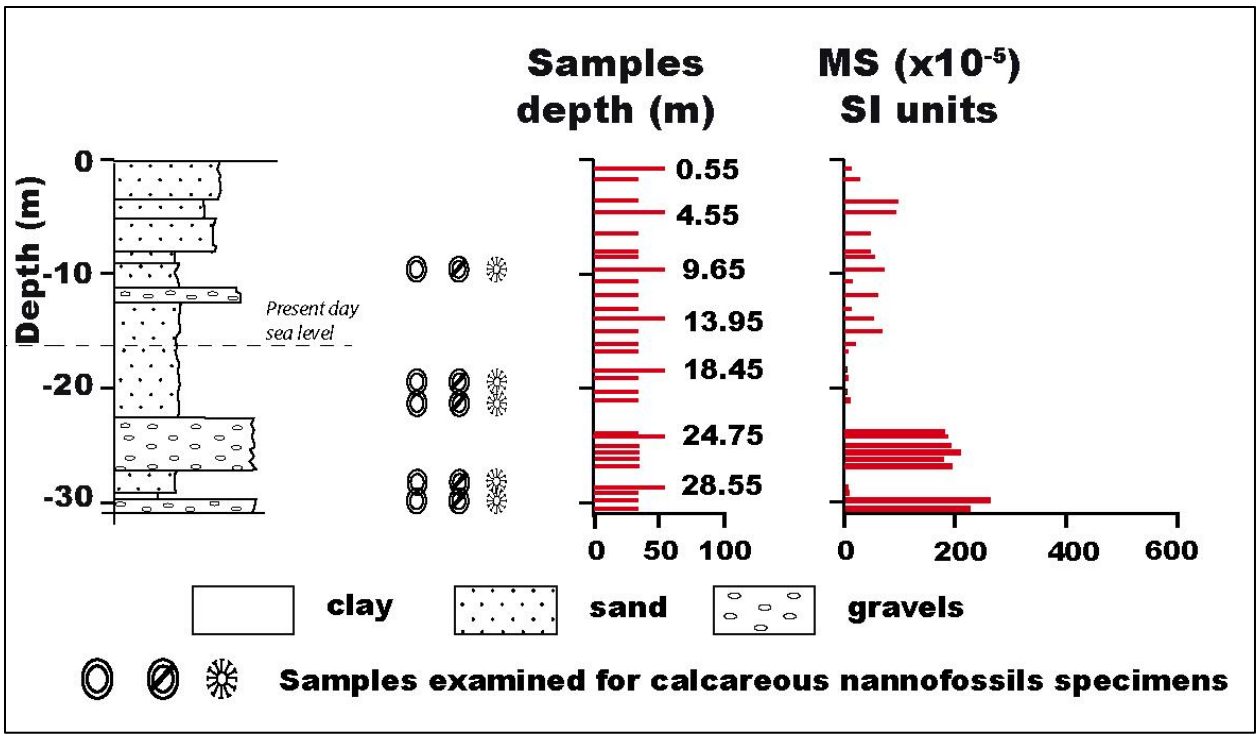

Figure 5-5. *Lithological description of Bh-1, showing the extracted samples based on their depth from the surface, the samples examined for calcareous nannofossils and the measured Magnetic Susceptibility of the sediments.*
Εικόνα 5-5. *Η λιθολογική περιγραφή της γεώτρησης Bh-1, τα δείγματα που εξετάστηκαν σε σχέση το βάθος τους από την επιφάνεια και αυτά που εξετάστηκαν για νανοαπολιθώματα καθως και η μετρηθείσα μαγνητική επιδεκτικότητα των ιζημάτων.*

Table 3. Lithological description of borehole Bh-1 and samples extracted from the borehole based on their depth from the surface. Πίνακας 3. Η λιθολογική περιγραφή και τα δείγματα που αναλύθηκαν στην Bh-1.

Depth (m)	Lithology	Samples Bh-1 (depth, m)
0.00–3.50	Top soil and gravely terrestrial formation	0.55, 1.45
3.50–11.20	Brown–beige fine to coarse sand.	3.05, 4.55, 6.95, 8.15, 8.55, 9.65, 10.65
11.20-12.50	Gravels with coarse sand	11.85
12.50–22.60	Sand	13.15, 13.95, 15.15, 16.25, 16.75, 18.45, 19.15, 20.35, 21.05
22.60–27.20	Gravels with coarse sand	23.95, 24.75, 25.35, 25.95, 26.75
27.20–29.10	Sand	28.55
29.10–29.70	Clay	29.25
29.70–31.00	Gravels with coarse sand	29.85, 30.65

Microfauna

Of the total examined samples, 16 were relatively rich in foraminiferal species (~200 specimens were counted per sample) with an FD-index ranging from ~60 to ~400 forams/g, while benthic foraminifera were absent in 5 samples and just few broken specimens were found in 7 samples, with FD-index < 2 forams/g (gravel layers). Fisher's alpha index values ranged from α=0 (sample Bh-1, 28.55 m) to α=5.43 (sample Bh-1, 18.45 m); higher values were observed particularly in the central part of the borehole (from 16.00 to 21.00 m core depth).

In general, the foraminiferal fauna is dominated by species with calcareous test. Thirteen benthic foraminiferal taxa made up more than 95% of the total assemblage: *Ammonia beccarii*, *Ammonia tepida*, *Rosalina bradyi*, *Cibicides refulgens*, *Elphidium crispum, Elphidium complanatum*, *Elphidium granosum*, *Haynesina depressula*, *Neoconorbina terquemi, Asterigerinata mammilla* and *planorbis, Discorbis* spp. and miliolids (Fig. 5-6). In particular, *A. tepida* was the dominant species with an average abundance ~18% (maximum relative abundance 92% sample Bh-1, 29.25 m). *Ammonia beccarii* were present in all samples comprising almost 8% of the assemblages (maximum relative abundance 20% Bh-1, 18.45 m). The epiphytic species, *R. bradyi*, *Discorbis* spp. and *C. refulgens*, were generally well represented, with maximum relative abundance values of 18% (maximum relative abundance 37% sample Bh-1, 13.95 m), ~2.5% (maximum relative abundance 11% sample Bh-3, 11.85 m) and 10% (maximum relative abundance 27 %Bh-1, 11.85 m) respectively. Among the *Elphidium* taxa, *E. granosum* (average abundance ~10% and maximum relative abundance ~18 % sample Bh-1, 28.55 m) was the most common species, followed by *E. Crispum* (average abundance ~3.3 and maximum relative abundance ~12% sample Bh-1, 22.35 m) and *E. complanatum* (average abundance ~3% and maximum relative abundance ~8% sample Bh-1, 19.15 m). *H. depressula* was also well represented with an average abundance 13% (maximum relative abundance 31% Bh-1, 28.55 m). Other taxa such as *Aubignina perlucida* and *N. terquemi* were also traced, with maximum relative abundances of 11% (sample Bh-1, 11.85 m), and 20% (Bh-1, 18.45 m) respectively. Miliolids were present in all samples comprising almost 17% of the assemblages

(maximum relative abundance 29% Bh-1, 9.65 m). *Asterigerinata* (*mammilla* and *planorbis*) were represented, with maximum relative abundances of 12% (sample Bh-1, 28.75 m), and 13% (Bh-1, 18.45 m) respectively.

BR-ratio ranges from 4–10 (samples Bh-1, 13.15 m, 20.15 m), up to 40 (samples Bh-1, 21.05 m, 28.55 m depth). In general, gravely layers have a higher percentage of broken species than clays. A-ratio ranges from very low values (8.6 at sample Bh-1, 8.55 m) to high values (80–90 at the interval 10.00–20.00 m core depth).

MS

Magnetic Susceptibility in Bh-1 sediments ranges from 5 to 267 ×10-5 (SI units) (Fig. 5-5). The interval 23.50 to 30.00 m core depth has relatively high MS values ranging from 181 to 267 ×10-5 (SI units)(average value 212 ×10-5 (SI units), interrupted by a thin layer at 28.00 to 29.5 m core depth with an average value 8×10-5 (SI units). The interval 23.50 to 16.50 m core depth MS values range from 5 to 12×10-5 (SI units), with an average value 7×10-5 (SI units). Till the surface at 0.00 m the MS values range from 15 to 99×10-5 (SI units), with an average value at 52×10-5 (SI units).

Calcareous Nannoplankton

Calcareous nannoplankton specimens have been identified through SEM analysis in certain levels of borehole Bh-1 (Fig. 5-5). Five samples were examined four of which proved to be rich in relatively well-preserved nannofossils (samples Bh-1, 9.65, 19.15, 20.35, 28.55 m depth were rich in nannofossils, while sample Bh-1 29.75 m depth was barren. All samples, were dominated by the presence of small Reticulofenestra spp. (~35%) and small Gephyrocapsa spp. (~30%) coccoliths, while Emiliania huxleyi specimens were relatively scarce (10-15% of the total assemblage), but consistently present.

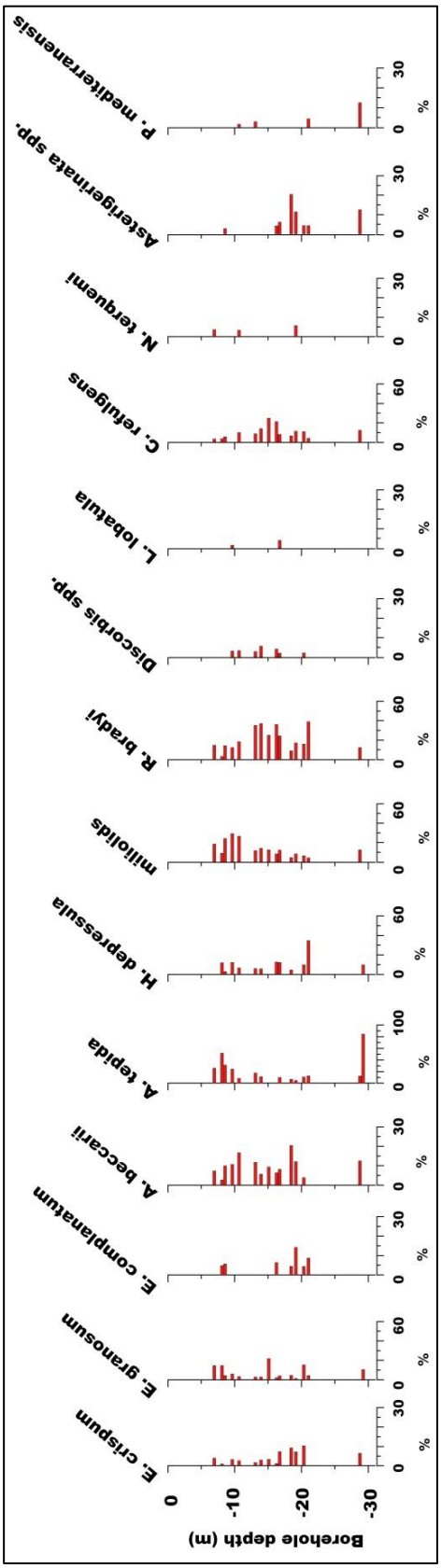

Figure 5-6. *Diagram showing the relative abundances of the most significant (>3%) recorded benthic foraminiferal species in borehole Bh-1.*

Εικόνα 5-6. *Διάγραμμα των συγκεντρώσεων των κυριότερων τρηματοφόρων (>3%)*

5.5.2 Borehole Bh-2

Lithology

Borehole Bh-2 was not examined in detail and only a description of borehole's lithology is available (Fig. 5-7, Table 4).

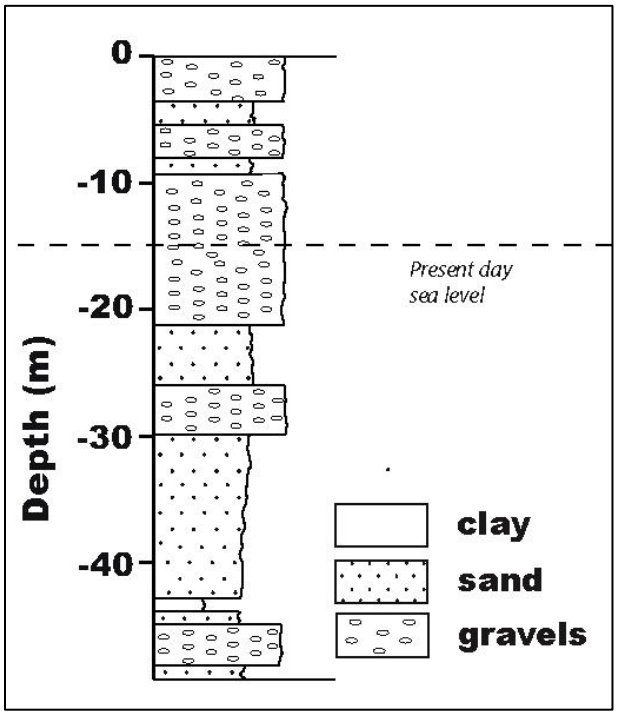

Figure 5-7. *Lithological description of Bh-2.*
Εικόνα 5-7*. Η λιθολογία της γεώτρησης Bh-2.*

Table 4 Lithological description of borehole Bh-2. Πίνακας 4. Η λιθολογική περιγραφή στην Bh-2.

Depth (m)	Lithology
0.00–3.60	Top soil and gravely terrestrial formation
3.60–5.40	Fine to coarse sand.
5.40–8.00	Gravels with coarse sand
8.00–9.30	Sand
9.30–21.20	Gravels with coarse sand
21.20–25.90	Sand
25.90–30.00	Gravels with coarse sand
30.00–42.80	Sand
42.80–43.80	Clay
43.80–44.90	Sand
44.90–48.10	Gravels with coarse sand
48.10–49.00	Sand

5.5.3 Borehole Bh-3

Lithology

Borehole Bh-3 consists of clay, clayey sands and sand, irrupted by gravely layers, several meters thick (Fig. 5-8, table 5).

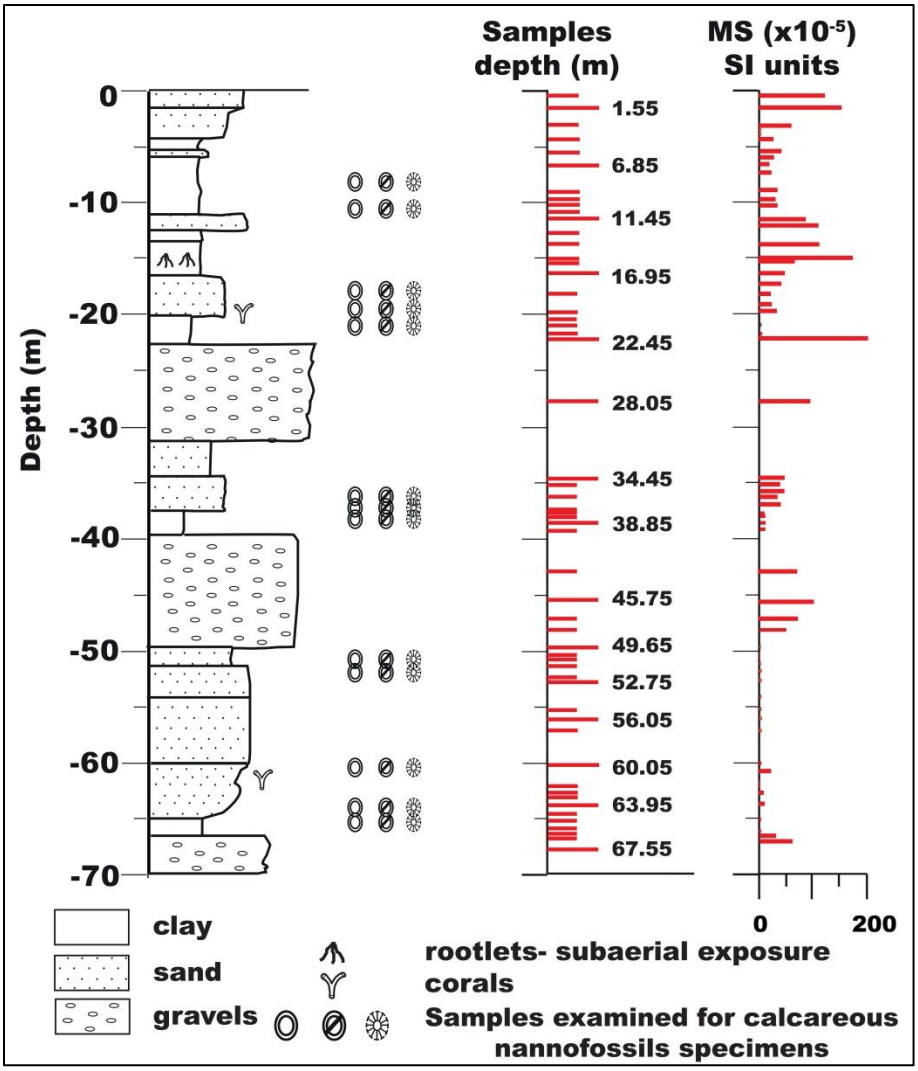

Figure 5-8. *Lithological description of Bh-3, showing the extracted samples based on their depth from the surface, the samples examined for calcareous nannofossils and the measured Magnetic Susceptibility of the sediment.*

Εικόνα 5-8*. Η λιθολογική περιγραφή της γεώτρησης Bh-3, τα δείγματα που εξετάστηκαν σε σχέση το βάθος τους από την επιφάνεια και αυτά που εξετάστηκαν για νανοαπολιθώματα καθως και η μετρηθείσα μαγνητική επιδεκτικότητα των ιζημάτων.*

Table 5 Lithological description of borehole Bh-3 and samples extracted from the borehole based on their depth from the surface. Πίνακας 5. Η λιθολογική περιγραφή και τα δείγματα που αναλύθηκαν στην Bh-3.

Depth (m)	Lithology	Samples Bh-3 (depth, m)
0.00–1.50	Top soil and gravely terrestrial formation	0.55, 1.55
1.50–4.70	Brown–beige fine to coarse sand.	3.05, 4.35
4.70–11.00	Clay to fine sand. At 5.40-5.70 m core depth and after 8.50 m core depth, contains fine gravels,	6.35, 6.85, 8.75, 9.35, 10.25
11.00–12.50	Coarse sand with gravels	11.45
12.50–13.00	Clay with few gravels.	12.75
13.00–16.50	Reddish clay with gravels	14.45, 15.25, 15.75, 16.35
16.50–20.00	Sand	18.05, 19.85
20.00–22.40	Clay with coral Cladocora caespitosa in living position.	20.75, 21.75
22.40–31.20	Gravels with coarse sand	22.45, 28.05
31.20–39.60	Clayey sand, interrupted by sand with few gravels	34.45, 35.65, 36.35, 37.55, 38.05, 38.75, 39.25
39.60–49.60	Gravels	42.85, 45.75, 47.25, 48.05
49.60–60.00	Sand to coarse sand	49.65, 50.35, 51.15, 52.35, 52.75, 54.05,

		56.05, 57.15
60.00–62.00	Brown-beige coarse sand, coral fragments	60.15, 61.95
62.00- 66.50	Clay, clayey sand and sand which contains few gravels.	62.65, 63.95, 64.35, 65.35, 65.75, 66.25
66.50- 70.20	Coarse sand with gravels	66.55

Microfauna

Of the total examined samples, 23 were relatively rich in foraminiferal species (~200 specimens were counted per sample) with an FD-index ranging from ~50 to ~600 forams/g, while benthic foraminifera were absent in 17 samples (from reddish clay to sand layers), and just few broken specimens were found in 15 samples, with FD-index < 2 forams/g (gravel layers). Fisher's alpha index values ranged from α = 1.38 (sample Bh-3, 4.35 m) to α = 5.99 (sample Bh-3, 51.15 m); higher values were observed, particularly in the lower part of the borehole (from the 49.60‑54.50 m core depth), signifying higher biodiversity in these samples. In general, the benthic foraminiferal fauna was dominated by species with calcareous test.

Fourteen benthic foraminiferal taxa comprised >90% of the total assemblage: *Ammonia beccarii*, *Ammonia tepida*, *Rosalina bradyi*, *Cibicides refulgens*, *Elphidium crispum, Elphidium complanatum*, *Elphidium granosum*, *Haynesina depressula*, *Neoconorbina terquemi, Discorbis* spp., *Planorbulina mediterranensis, Asterigerinata* spp., *Lobatula lobatula*, and miliolids (Fig. 5-9). In particular, *A. tepida* was the dominant species with maximum relative abundance ~92% at sample Bh-3, 21.75 m. *Ammonia beccarii* was 206 a significant component in the lower sandy horizons of the borehole, with a maximum relative abundance of 40% at sample Bh-3, 49.45 m. Two epiphytic species, *R. bradyi* and *C. refulgens*, were generally well represented, with maximum relative abundance of 35% (sample Bh-3, 34.45 m) and 28% (sample Bh-3, 36.35 m),

respectively. Among the *Elphidium* species, *E. crispum* (maximum relative abundance 16%, Bh-3, 35.65 m) was the most common, followed by *E. granosum* (maximum relative abundance 18%, Bh-3, 19.85 m) and *E. complanatum* (maximum relative abundance 12%, Bh-3, 35.65 m). Other taxa such as *H. depressula* and *N. terquemi* were also traced, with maximum relative abundances of ~20% at sample Bh-3, 19.85 m, and ~15% at sample Bh-3, 52.75 m, respectively. Miliolids were present in most of the samples, with a maximum relative abundance of ~28% (Bh-3, 3.35 m). *Lobatula lobatula* and *Discorbis* spp. were also traced with maximum relative abundances of ~20% at sample Bh-3, 10.85 m, and ~10% at sample Bh-3, 52.35 m, respectively. *Asterigerinata* spp. (*mammilla* and *planorbis*) were also represented, with a maximum relative abundance of ~11% (Bh-3, 10.25 m). *Planorbulina mediterranensis* was described with a maximum relative abundance of ~5% (Bh-3, 8.75 m), whereas very well preserved planktonic foraminifera specimens were found at ~4% maximum relative abundance (Bh-3, 35.65 m).

BR-ratio ranged from 4‑6 (16.50‑22.40 m, 34.00‑37.00 m core depth) up to 75 (sample Bh-3, 14.05 m). In general, gravelly layers had a higher percentage of broken species than clays. A-ratio tests were performed in 13 samples and ranged from very low (0.3 at sample Bh-3, 21.75 m) to high values (~90 at the 50.75 m core depth sample). A low A-ratio is associated with the cluster I assemblage (mostly at the 16.50‑22.40 m core depth), whereas higher values are associated with cluster III assemblages (50.00‑52.00 m core depth).

Benthic foraminifera were absent (or just few broken specimens were found) in terrestrial sediments samples (gravel layers), whereas the rest studied samples were relatively rich in foraminiferal species. Fisher's alpha index values ranged from α=1.38 (sample Bh-3, 4.35 m) to *α*=5.99 (sample Bh-3, 51.15 m); higher values were observed particularly in the lower part of the borehole (from 49.60 m to 54.50 m core depth).

MS

Magnetic susceptibility in Bh-3 sediments ranged from 1 to 207 × 10^{-5} (SI units) (Fig. 5-8). Clayey and fine coarse sediments displayed lower MS signal than gravelly and

coarse sediments. Based on the measured signal of the sediments, in the lower part of the borehole (66.5-70.20 m core depth interval), the mean MS value was at 55 × 10^{-5} (SI units), whereas the49.60-66.50 m core depth varied from 1 to 18 × 10^{-5} (SI units), with a mean value at 2.8 × 10^{-5} (SI units). From the 39.60-49.60 m core depth, the MS signal ranged from 41 to 108 × 10^{-5} (SI units), with a mean value at 59.5 × 10^{-5} (SI units), whereas from the 31.20-39.60 m core depth, the MS signal exhibited values from 8 to 51 × 10^{-5} (SI units), with a mean value at 23 × 10^{-5} (SI units). From the 22.40-31.20 m core depth, the MS signal ranged from 98 to 207 × 10^{-5} (SI units), with a mean value at 105 × 10^{-5} (SI units), whereas from the 16.50-22.40 core depth the MS signal varied from 4 to 50 × 10^{-5} (SI units), with a mean value at 28 × 10^{-5} (SI units). From the 11.00-16.50 m core depth, the MS signal ranged from 70 to 176 × 10^{-5} (SI units), with a mean value at 110 × 10^{-5} (SI units), whereas from the 3.00-11.00 m core depth, the MS signal exhibited values from 3 to 61 × 10^{-5} (SI units), with a mean value at 23 × 10^{-5} (SI units). The MS signal in the upper 3.30 m of the borehole ranged from 123 to 156 × 10^{-5} (SI units) (mean 140 × 10^{-5} [SI units]).

Calcareous Nannoplankton

Calcareous nannoplankton specimens have been identified through SEM analysis within certain levels of borehole Bh-3 at Corinth Isthmus. Eight of the studied samples proved to be rich in relatively well preserved nannofossils (samples Bh-3, 8.75, 10.25, 20.75, 35.65, 36.35, 51.15, 52.75, and 60.15 m), whereas the rest of the samples (Bh-3, 19.85, 21.75, 38.85, 63.95, and 64.35 m) were barren. All samples were dominated by the presence of small *Reticulofenestra* spp. (~40%) and small *Gephyrocapsa* spp. (~30%) coccoliths, whereas *Emiliania huxleyi* specimens were relatively scarce (5%-8% of the total assemblage), but consistently present.

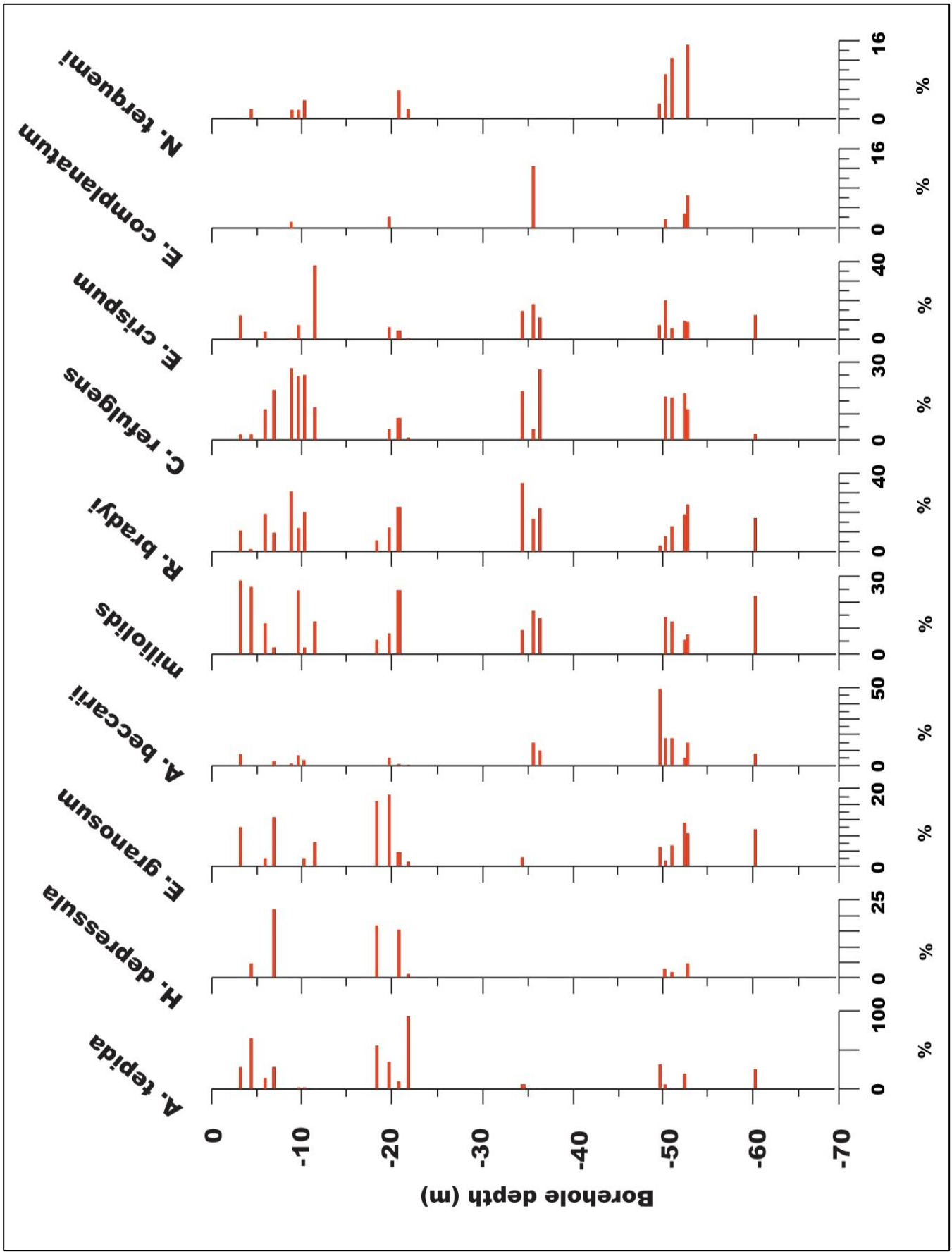
A. tepida
H. depressula
E. granosum
A. beccarii
miliolids
R. bradyi
C. reticulgens
E. crispum
E. complanatum
N. terquemi
Borehole depth (m)
0
-10
-20
-30
-40
-50
-60
-70
%
0
100
25
20
50
30
40
16

Figure 5-9. *Diagram showing the relative abundances of the most significant (>3%) recorded benthic foraminiferal species in borehole Bh-3.*
Εικόνα 5-9. *Διάγραμμα των συγκεντρώσεων των κυριότερων τρηματοφόρων (>3%) στην γεώτρηση Bh-3.*

5.5.4 Borehole Bh-4

Lithology

Borehole Bh-4 was not examined in detail and only a description of borehole's lithology is available (Fig. 5-10, table 6).

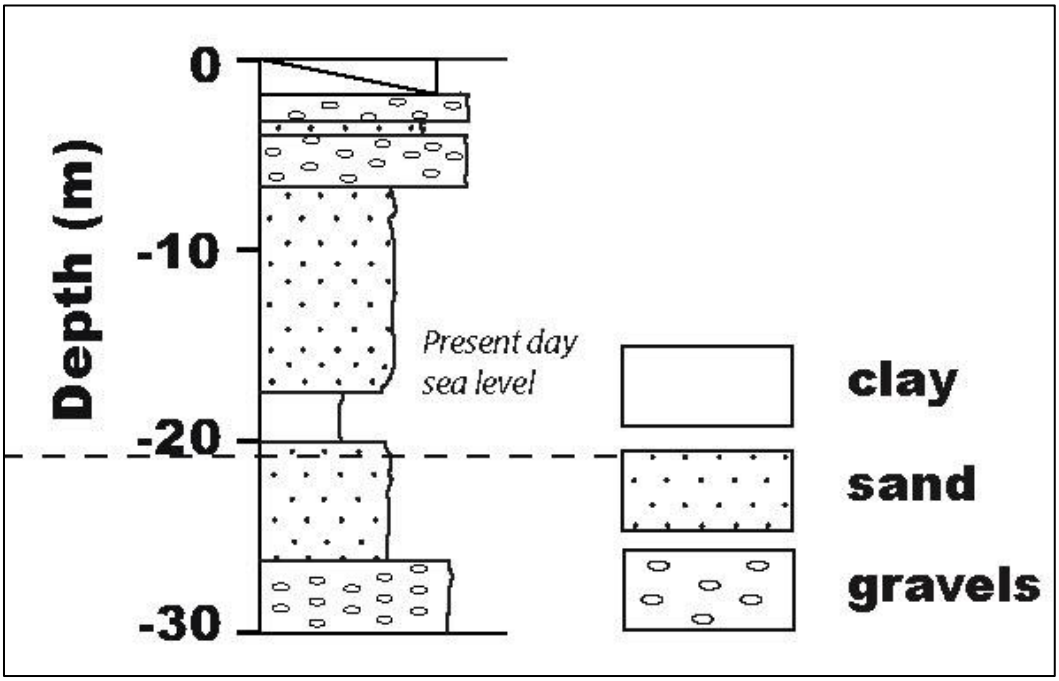

Figure 5-10. Lithological description of Bh-4.
Εικόνα 5-10. Η λιθολογική περιγραφή της γεώτρησης Bh-4.

Table 6. Lithological description of Bh-4. Πίνακας 6. Η λιθολογική περιγραφή στην Bh-4.

Depth (m)	Lithology
0.00–1.80	Man-made Canal debris
1.80–3.20	Gravels with coarse sand
3.20–3.90	Sand
3.90–6.70	Gravels with coarse sand
6.70–17.50	Sand
17.50–20.00	Clay
20.00–26.20	Sand
26.20–30.50	Gravels with coarse sand

5.5.5 Borehole Bh-6

Borehole Bh-6was not examined in detail and only a description of borehole's lithology is available (Fig. 5-11, table 7).

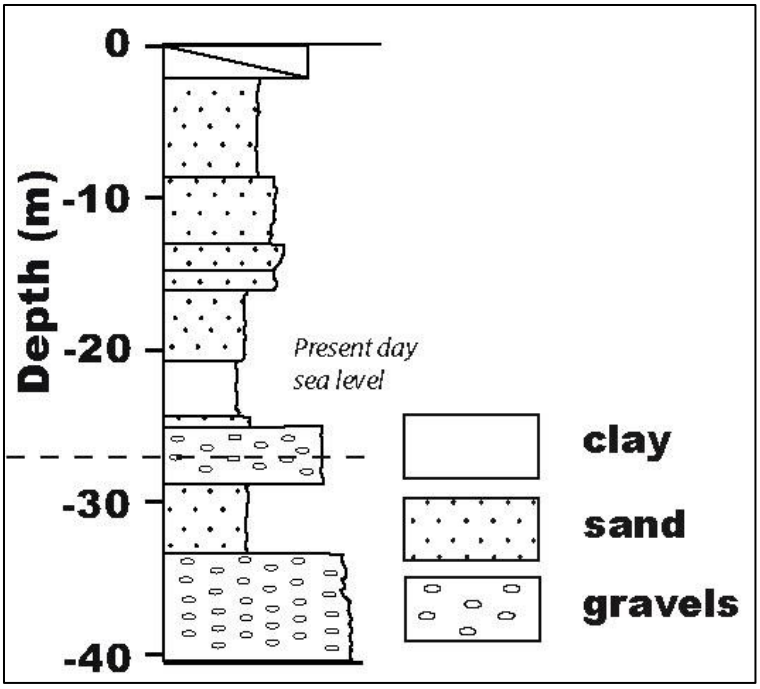

Figure 5-11. *Lithological description of Bh-6.*

Εικόνα 5-11. *Η λιθολογική περιγραφή της γεώτρησης Bh-6*

Table 7. Lithological description of Bh-6. *Πίνακας 7. Η λιθολογική περιγραφή στην Bh-6.*

Depth (m)	Lithology
0.00–2.10	Man-made Canal debris
2.10–20.70	Fine to coarse sand.
20.70–24.30	Clay
24.30–25.10	Sand
25.10–28.80	Gravels with coarse sand
28.80–33.40	Sand
33.40–40.60	Gravels with coarse sand

5.5.6 Borehole Bh-7

Lithology

Borehole Bh-7 consists of clay, clayey sands and sand, irrupted by gravely layers, several meters thick (Fig. 5-12, Table 8).

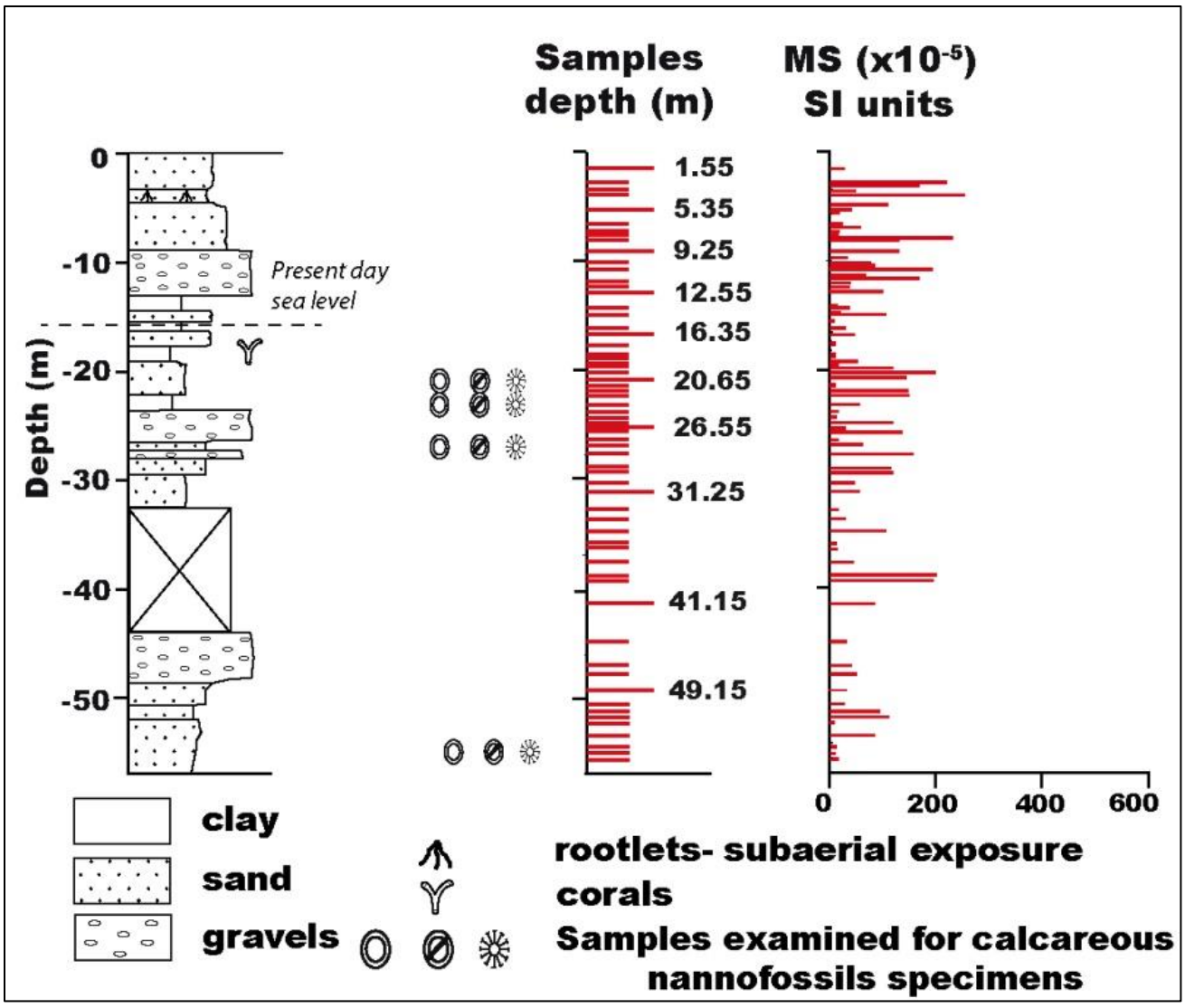

Figure 5-12. *Lithological description of Bh-7, showing the extracted samples based on their depth from the surface, the samples examined for calcareous nannofossils and the measured Magnetic Susceptibility of the sediments.*

Εικόνα 5-12. *Η λιθολογική περιγραφή της γεώτρησης Bh-7, τα δείγματα που εξετάστηκαν σε σχέση το βάθος τους από την επιφάνεια και αυτά που εξετάστηκαν για νανοαπολιθώματα καθως και η μετρηθείσα μαγνητική επιδεκτικότητα των ιζημάτων.*

Table 8. Lithological description of borehole Bh-7 and samples extracted from the borehole based on their depth from the surface. Πίνακας 8. Η λιθολογική περιγραφή και τα δείγματα που αναλύθηκαν στην Bh-7.

Depth (m)	Lithology	Samples Bh-7 (depth, m)
0.00–1.50	Top soil and gravely terrestrial sediments	–
1.50–9.00	Sand with low or no cohesion, interrupted by paleosoil layer at 5.00–5.20 m core depth	1.55, 2.85, 3.45, 3.95, 5.35, 6.95, 7.35, 7.65, 8.15,
9.00–18.00	Sand to coarse sand containing few gravels	9.25, 10.25, 10.55, 11.65, 12.25, 12.55, 14.15,15.55, 16.35, 17.05,17.95,
18.00–19.00	Clay with coral Cladocora caespitosa in living position.	18.25, 18.55,
19.00–23.00	Sand	19.05, 19.55, 19.75, 19.85, 20.25, 20.75, 21.45, 21.95, 22.35, 22.75,
23.00–26.50	Gravels	23.25, 23.75, 24.35, 25.45,

		25.85,
26.50–33.00	Sand with medium cohesion, including a few gravels.	26.45, 26.85, 27.35, 28.55, 29.05, 29.45, 30.65, 31.05, 31.25,
33.00–45.00	Deformation zone of the fault. The upper part of the deformation zone lies within a layer of silty sand. The main fault plane was found at 36.00 m, whereas the cataclastic zone continues from 39.00 m down to 45.00 m where the deformation zone ends.	33.45, 34.55, 34.95, 35.95, 36.45, 37.65, 38.75, 39.35, 41.15, 44.65,
45.00–57.00	Successive undeformed alterations of cohesive sand and gravels	46.85, 47.65, 49.15, 50.55, 51.35, 51.75, 52.35, 53.45, 54.25,54.75, 55.05, 55.55

Microfauna

Of the total examined samples, 25 were relatively rich in foraminiferal species (~200 specimens were counted per sample) with an FD-index ranging from ~50 to ~650

forams/g, while benthic foraminifera were absent in 32 samples (from reddish clay to sand layers), and just few broken specimens were found in 11 samples, with FD-index < 2 forams/g (gravel layers). Fisher's alpha index values ranged from α=0.68 (sample Bh-7, 23.25m) to α=5.55 (sample Bh-7, 17.95 m).

In general, the foraminiferal fauna is dominated by species with calcareous test. Twelve benthic foraminiferal taxa made up more than 95% of the total assemblage: *Ammonia beccarii, Ammonia tepida, Rosalina bradyi, Cibicides refulgens, Elphidium crispum, Elphidium complanatum, Elphidium granosum, Haynesina depressula, Neoconorbina terquemi, Discorbis spp.* and miliolids (Fig. 5-13). In particular, *A. tepida* was the dominant species, with average relative abundance ~27% of the foraminiferal fauna (more than 50% at the interval 19.00–24.00 m core depth). *A. beccarii* were present in all samples, comprising almost 6.5% of the assemblages (maximum at Bh-7, 17.95 m depth). The epiphytic species, *R. bradyi*, *Discorbis spp*. and *C. refulgens*, were generally well represented, with maximum relative abundance values of ~61% (sample Bh-7, 16.35 m), ~12% (sample Bh-7, 17.95 m) and ~19% (Bh-7, 17.95 m) respectively. Among the Elphidium taxa, *E. crispum* (maximum abundance ~30%, Bh-7, 26.85) was the most common species, followed by *E. granosum* (~30%, Bh-7, 19,75) and *E. complanatum* (~10% Dh-7, 26.85). *H. depressula* was also well represented with an average abundance 7% (mostly at the interval 19.00–24.00 m core depth). *N. terquemi* was represented (with a maximum abundance ~8% Bh-7, 2.85). Miliolids were present in all samples comprising almost 15 % of the assemblages (maximum relative abundance ~40% Bh-7, 20,75). Other taxa such as *Aubignina perlucida, Asterigerinata spp., Bolivina spp., Planorbulina spp.* and *Textularia spp.* were traced but were relatively scarce. Furthermore, ostracod specimens have been recorded at the interval 49.00–56.00 m core depth.

BR-ratio ranges from 4–10 (at the interval 14.00–24.00 m core depth), up to 75 (Bh-7, 8.15 m depth). In general, gravely layers have a higher percentage of broken species than clays. A-ratio ranges from very low values (~5 at sample Bh-7, 22.35 m) to high values (~57 at sample Bh-7, 17.55 m).

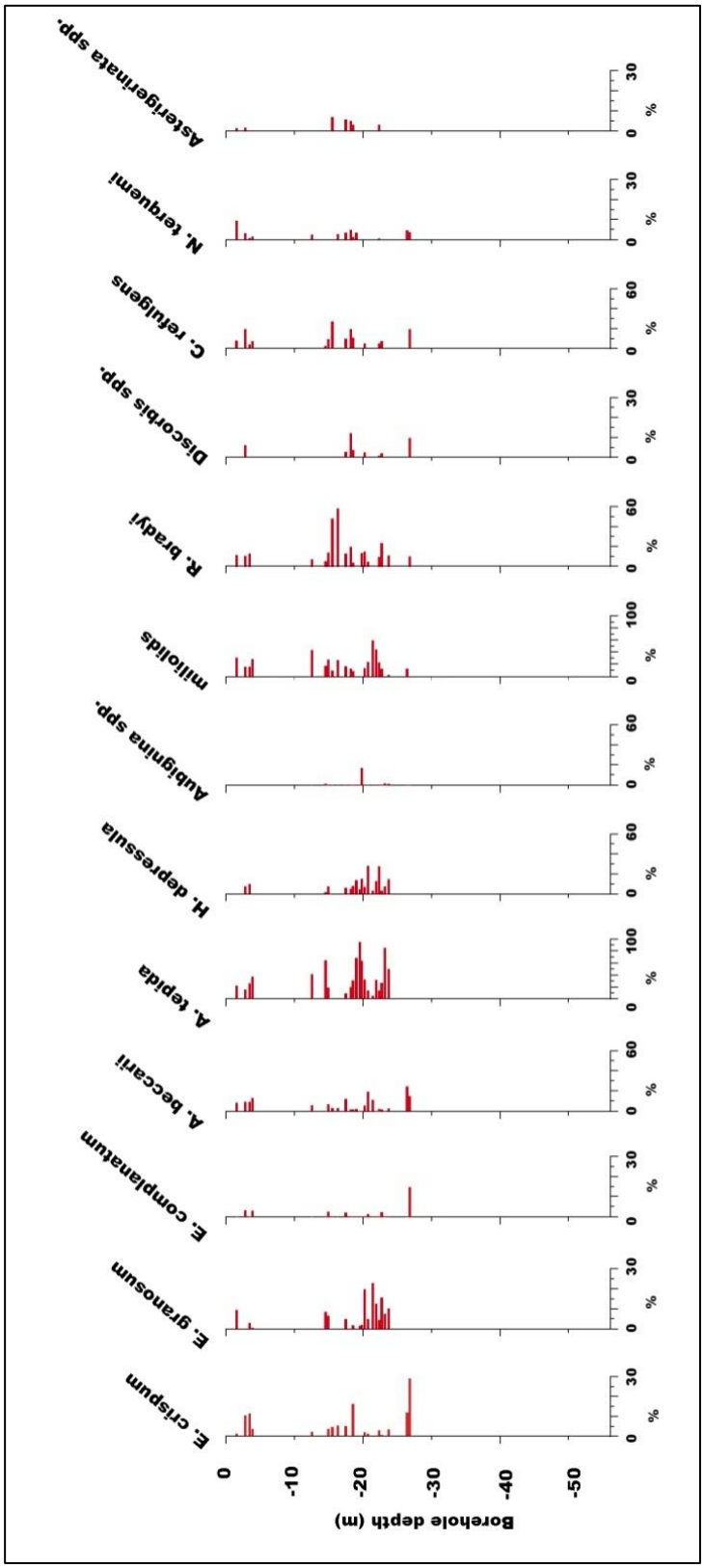

*Figure **5-13**. Diagram showing the relative abundances of the most significant (>3%) recorded benthic foraminiferal species in borehole Bh-7.*

***Εικόνα 5-13**. Διάγραμμα των συγκεντρώσεων των κυριότερων τρηματοφόρων (>3%) στην νεώτηση Bh-7.*

MS

Magnetic Susceptibility in Bh-7 sediments ranged from 2 to 245 $\times 10^{-5}$ (SI units) (Fig. 5-12). The lower part of the borehole from 49.00 to 56.00 m core depth MS values ranged from 5 to 101 $\times 10^{-5}$ (SI units) (average value 37 $\times 10^{-5}$ (SI units). From 49.00 to 45.00 m core depth MS values ranged from 46 to 76 $\times 10^{-5}$ (SI units) (average value 60 $\times 10^{-5}$ (SI units), while at the deformation zone of the fault[9] the MS values ranged from 2 to 195 $\times 10^{-5}$ (SI units) (average value 55 $\times 10^{-5}$ (SI units). The interval 24.00–33.00 m core depth was characterized by relatively higher MS values ranging from 50 to 150 $\times 10^{-5}$ (SI units) (average value 83 $\times 10^{-5}$ (SI units), interrupted by a thin layer at 26.00–27.00 m core depth with lower values (~25 $\times 10^{-5}$ (SI units)). The MS values at the interval 24.00–14.00 m core depth ranged from 2 to 180 $\times 10^{-5}$ (SI units) with an average value at 55 $\times 10^{-5}$ (SI units). The MS values at the interval 14.00–5.50 m core depth ranged from 35 to 200 $\times 10^{-5}$ (SI units) with an average value at 75 $\times 10^{-5}$ (SI units). Finally, the interval 1.50–5.50 m core depth was characterized by relatively low MS values (from 2 to 45 $\times 10^{-5}$ (SI units)) and the top 1.50 m of the borehole sequence by higher MS values (~245 $\times 10^{-5}$ (SI units)).

Calcareous Nannoplankton

Calcareous nannoplankton specimens have been identified through SEM analysis in certain levels of borehole Bh-7. Four samples were examined where two of them proved to be rich in relatively well-preserved nannofossils (samples Bh-7 22.35 and 26.85 m were rich in nannofossils, while samples Bh-7 21.45 and 54.75 m core depth were barren). All samples, were dominated by the presence of small *Reticulofenestra* spp. (~50%) and small *Gephyrocapsa* spp. (~30%) coccoliths, while *Emiliania huxleyi* specimens were relatively scarce (~5–10% of the total assemblage), but consistently present (Fig. 5-12).

[9] *33.00–45.00 m core depth*

5.5.7 Borehole G-1

Lithology

Borehole G-1 consists mainly of gravels and gravely sand (Fig. 5-14, table 9).

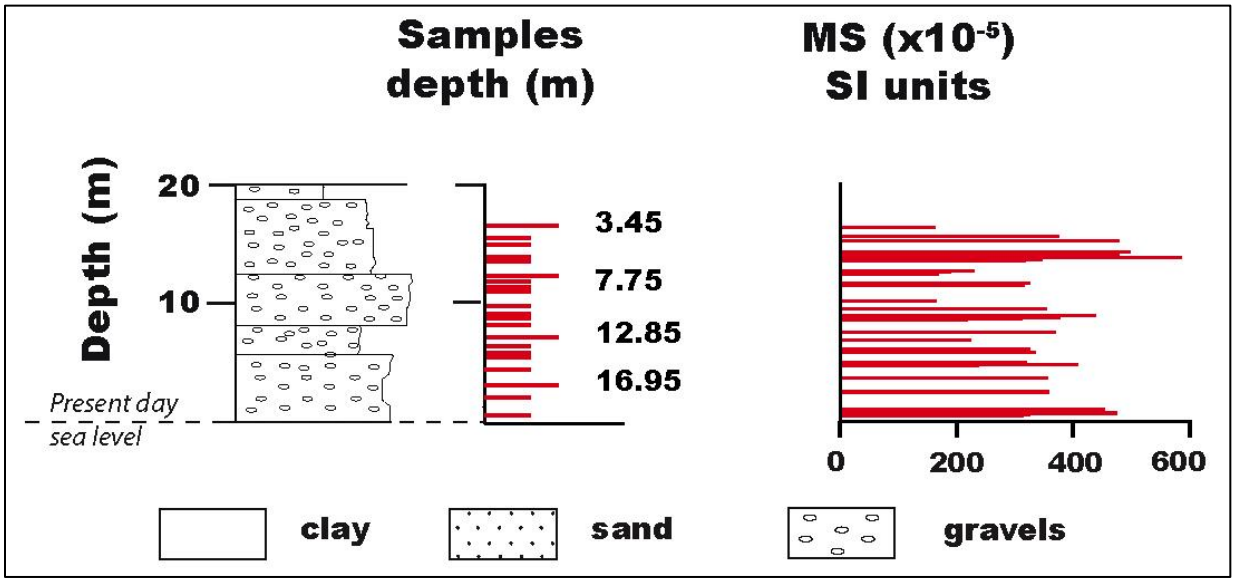

Figure 5-14*. Lithological description of G-1, showing the extracted samples based on their depth from the surface and the measured Magnetic Susceptibility of the sediments.* ***Εικόνα 5-14****. Η λιθολογική περιγραφή της γεώτρησης G-1, τα δείγματα που εξετάστηκαν σε σχέση το βάθος τους από την επιφάνεια και η μετρηθείσα μαγνητική επιδεκτικότητα των ιζημάτων*

Table 9. Lithological description of borehole G-1 and samples extracted from the borehole based on their depth from the surface. Πίνακας 9. Η λιθολογική περιγραφή και τα δείγματα που αναλύθηκαν στην G-1.

Depth (m)	Lithology	Samples G-1 (depth, m)
0.00–1.30	Sand with few gravels	–
1.30–8.00	Coarse sand with gravels	3.45, 4.55, 5.05, 6.55, 7.75, 7.95
8.00–12.00	Gravels	8.55, 9.05, 10.25, 10.95, 11.45, 11.75
12.00–14.50	Coarse sand with gravels	12.85, 13.65, 14.25
14.50–20.00	Gravels	14.65, 15.65, 16.95, 18.05, 19.75

Microfauna - MS

In borehole G-1 no or few broken and weathered foraminifera have been found. The highest values of magnetic susceptibility have been measured in G-1, compared with the measured signal from the other examined boreholes, ranging from 75 to 582×10^{-5} (SI units) (Fig. 5-14).

5.5.8 Borehole GA-2

Lithology

Borehole GA-2 consists mainly of clay and clayey sand. Few gravels are described at the upper part of the borehole (Fig. 5-15, table 10).

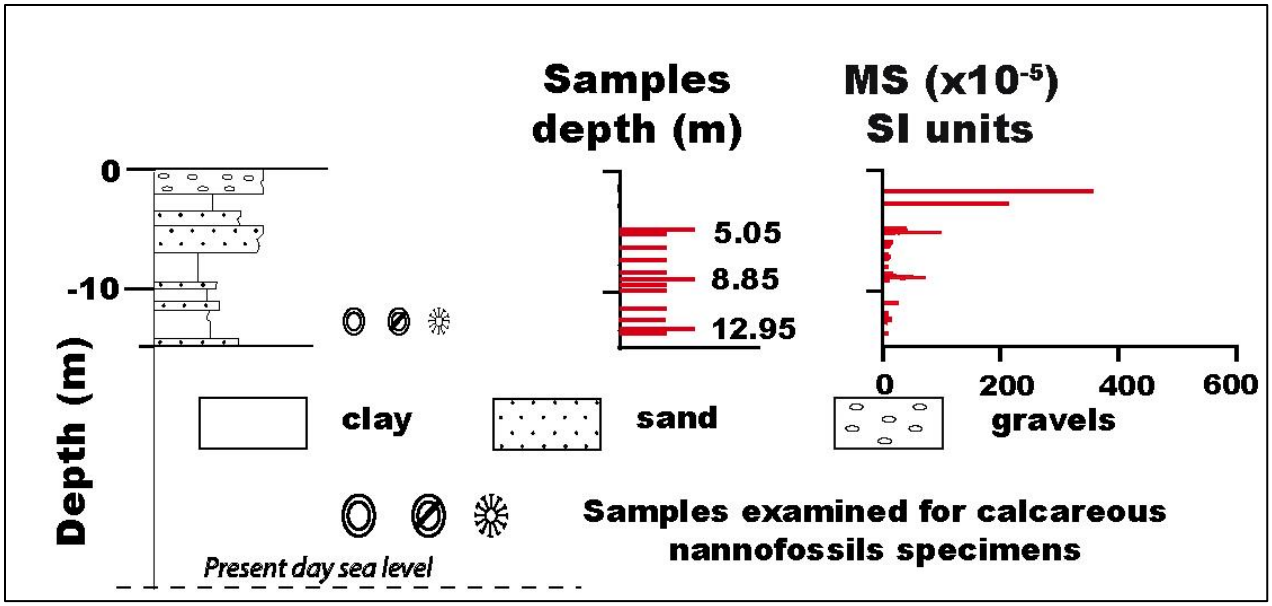

Figure 5-15*. Lithological description of GA-2, showing the extracted samples based on their depth from the surface, the samples examined for calcareous nannofossils and the measured Magnetic Susceptibility of the sediments.*
Εικόνα 5-15. *Η λιθολογική περιγραφή της γεώτρησης GA-2, τα δείγματα που εξετάστηκαν σε σχέση το βάθος τους από την επιφάνεια και αυτά που εξετάστηκαν για νανοαπολιθώματα καθως και η μετρηθείσα μαγνητική επιδεκτικότητα των ιζημάτων.*

Table 10. Lithological description of borehole GA-2 and samples extracted from the borehole based on their depth from the surface. Πίνακας 10. Η λιθολογική περιγραφή και τα δείγματα που αναλύθηκαν στην GA-2.

Depth (m)	Lithology	Samples GA-2 (depth, m)
0.00–3.80	Coarse sand with few gravels	–
3.80–5.30	Brown–beige fine sand formation	5.05
5.30–7.30	Fine sand with a few gravels	5.45, 6.35

7.30–9.90	Clay	7.55, 8.25, 8.85, 9.05, 9.35
9.90–10.30	Sandstone	-
10.30–11.45	Clay	11.15
11.45–12.30	Sandstone	-
12.30–13.80	Clay	12.35, 12.95, 13.55
13.80–14.00	Sandstone	-

Microfauna

Of the total examined samples, 11 were relatively rich in foraminiferal species (~200 specimens were counted per sample) with an FD-index ranging from ~30 to ~200 forams/g, while benthic foraminifera were absent in one sample (Fig. 5-16). In general, the foraminiferal fauna is dominated by species with calcareous specimens. Fisher's alpha index values ranged from α=2.32 (sample GA-2, 2.55 m) to α=5.69 (sample GA-2, 12.95 m). Eleven foraminiferal taxa made up approximately 90% of the total assemblage: *Elphidium crispum, Elphidium complanatum, Elphidium granosum, Ammonia beccarii, Ammonia tepida, Aubignina perlucida, Rosalina bradyi, Cibicides refulgens, Haynesina depressula, Asterigerinata mammilla* and *planorbis* and miliolids. In particular, *A. tepida* was the dominant species with average abundance ~ 26% comprising more than 56% at 2.50–6.50 m core depth. *Ammonia beccarii* was a significant component mostly in the lower sandy horizons of the borehole with average abundance ~5% (maximum relative abundance 22% at 12.00–13.00 m core depth). Epiphytic species, *R. bradyi* and *C. refulgens* were generally well represented with average relative abundance 11% and 15% respectively and maximum relative abundance 20% and 26% respectively (at 12.00–13.00 m core depth). *Asterigerinata* spp. was also represented with at an average abundance~ 4% and maximum relative abundance 16% at GA-2, 7.45 m. Among the *Elphidium* taxa, *E. granosum* (average

abundance ~15% and maximum relative abundance 24% at GA-2, 7.45 m depth) was the most common species, followed by *E. crispum* (3% and maximum relative abundance ~7% at 12.35 m) and *E. complanatum* (2% and maximum relative abundance ~5% at 12.35 m). Other taxa such as *H. depressula* (~5%) and *A. perlucida* (~2.3%) also occurred, with maximum relative abundance 13% and ~4% at sample GA-2, 6.35 m. Miliolids were present with maximum relative abundance values of 7% at sample GA-2, 12.95 m. Other species had a circumstantial appearance (*e.g. Textularia* spp. (5% at sample GA-2, 7.45 m), *Nonnion* spp. (3% at sample GA-2, 7.45 m), *Planorbulina mediterranensis* (3% at sample GA-2, 8.35 m).

BR-ratio was relatively low ranging from 3–9. A-ratio ranges from low values (1–55 at the interval 2.50–6.40 m core depth) to higher values (5–25 at the interval 6.40–13.00 m core depth).

MS

Borehole GA-2, had relatively low MS values ranging from 1 to 68 $\times 10^{-5}$ (SI units) (average value ~13 $\times 10^{-5}$ (SI units), except from the surface sediments with average MS value at 288×10^{-5} (SI units) (Fig. 5-15).

Calcareous Nannoplankton

Calcareous nannoplankton specimens have been identified through SEM analysis in one sample examined in borehole GA-2 rich in relatively well-preserved nannofossils (sample GA-2 12.95 m depth).Sample was dominated by the presence of small Reticulofenestra spp. (~52%) and small Gephyrocapsa spp. (~41%) coccoliths, while Emiliania huxleyi specimens were relatively scarce (~8% of the total assemblage), but consistently present.

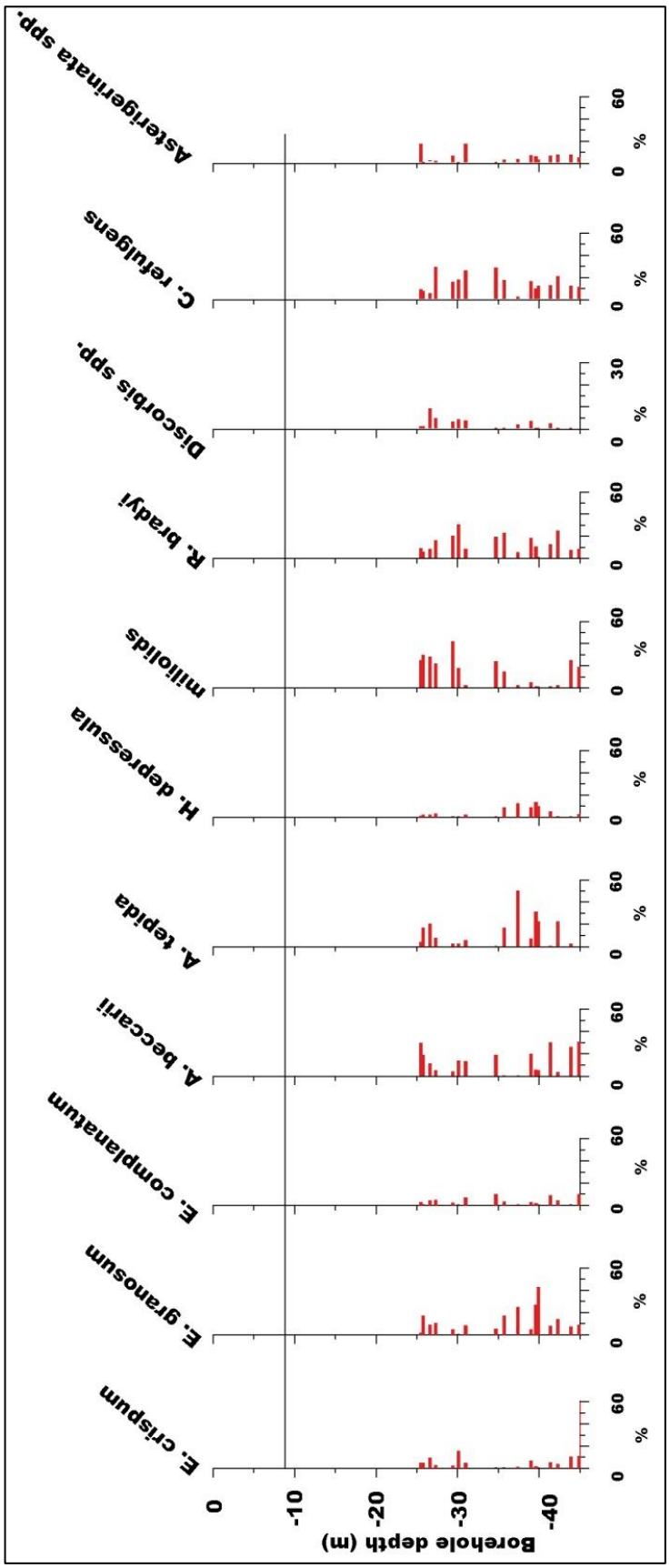

Figure 5-16*. Diagram showing the relative abundances of the most significant (>3%) recorded benthic foraminiferal species in borehole GA-2.*

Εικόνα 5-16*. Διάγραμμα των συγκεντρώσεων των κυριότερων τρηματοφόρων (>3%) στην γεώτρηση GA-2.*

5.5.9 Borehole GA-3

Lithology

Borehole GA-3 consists mainly of gravels while the upper 5.20 m of the core were described as re-deposited excavated canal debris (Fig. 5-17, table 11).

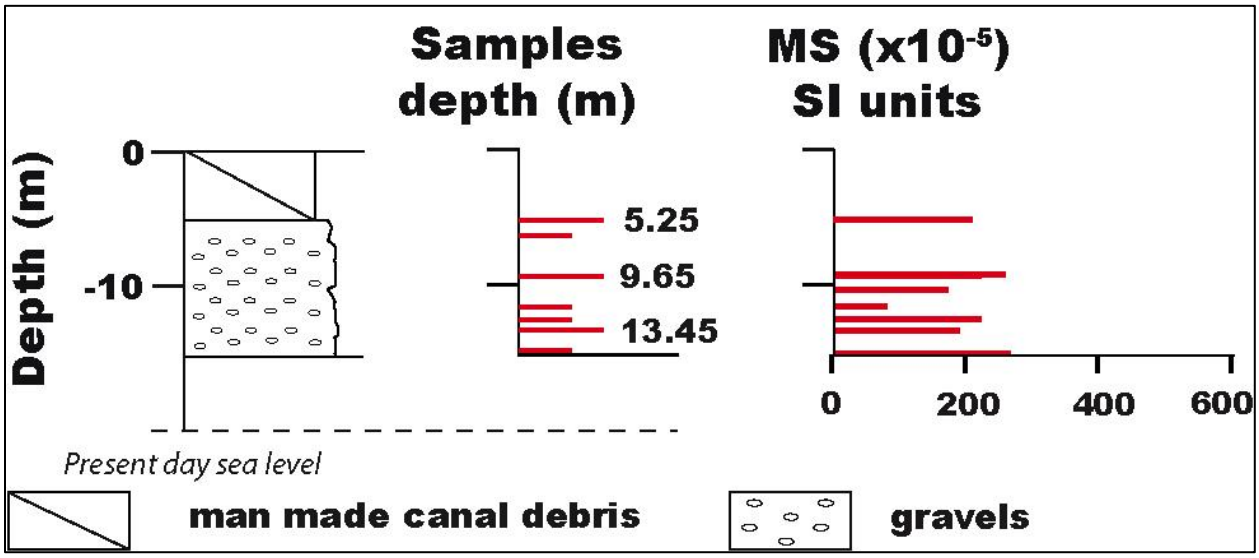

Figure 5-17. *Lithological description of GA-3, showing the extracted samples based on their depth from the surface and the measured Magnetic Susceptibility of the sediments.* ***Εικόνα 5-17****. Η λιθολογική περιγραφή της γεώτρησης GA-3, τα δείγματα που εξετάστηκαν σε σχέση το βάθος τους από την επιφάνεια και η μετρηθείσα μαγνητική επιδεκτικότητα των ιζημάτων*

Table 11. Lithological description of borehole GA-3 and samples extracted from the borehole based on their depth from the surface. Πίνακας 11. Η λιθολογική περιγραφή και τα δείγματα που αναλύθηκαν στην GA-3.

Depth (m)	Lithology	Samples GA-3 (depth, m)
0.00–5.20	Man-made Canal debris	–
5.20–15.20	Gravels	5.25, 6.75, 9.65, 11.65, 12.65, 13.45, 15.05

Microfauna & MS

Generally, in GA-3 few or no foraminifera were found mostly miliolids, *Cibicides* spp., *Rosalina* spp. and *Elphidium* spp.

MS

In Borehole GA-3, relatively high values of magnetic susceptibility were measured, ranging from 75 to 262 $\times 10^{-5}$ (SI units) with average MS value at 198 $\times 10^{-5}$ (SI units) (Fig. 5-17).

5.5.10 Borehole GA-4

Lithology

Borehole GA-4 consists of alternations of clays, sands gravels while the upper 8.80 m of the core were described as re-deposited excavated canal debris (Fig. 5-18, table 12).

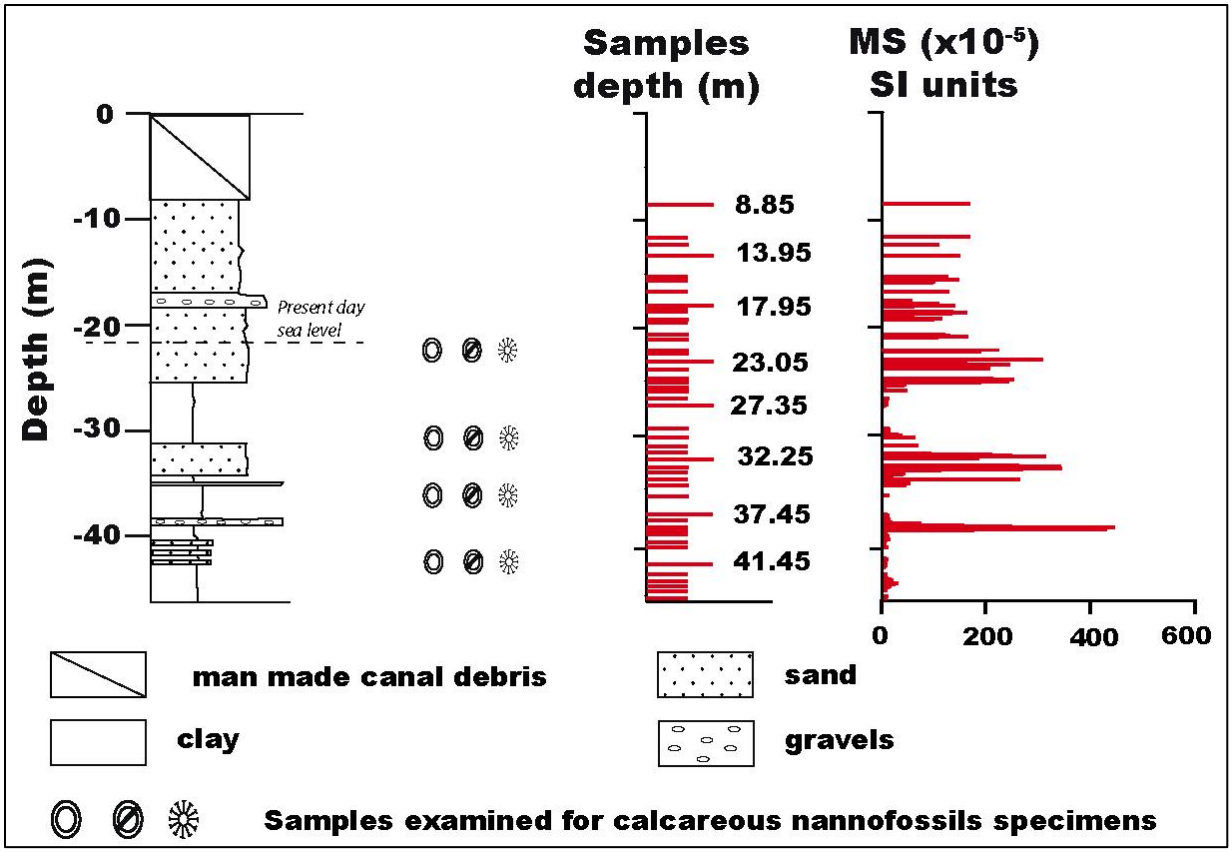

Figure 5-18. *Lithological description of GA-4, showing the extracted samples based on their depth from the surface, the samples examined for calcareous nannofossils and the measured Magnetic Susceptibility of the sediments.*
Εικόνα 5-18. *Η λιθολογική περιγραφή της γεώτρησης GA-4, τα δείγματα που εξετάστηκαν σε σχέση το βάθος τους από την επιφάνεια και αυτά που εξετάστηκαν για νανοαπολιθώματα καθως και η μετρηθείσα μαγνητική επιδεκτικότητα των ιζημάτων*

Table 12. Lithological description of borehole GA-4 and samples extracted from the borehole based on their depth from the surface. Πίνακας 12. Η λιθολογική περιγραφή και τα δείγματα που αναλύθηκαν στην GA-4.

Depth (m)	Lithology	Samples GA-4 (depth, m)
0.00–8.50	Man-made Canal debris	–
8.50–16.50	Reddish sand fine sand to clay	8.85, 10.95, 11.65, 12.25, 13.95, 15.25, 15.55
16.50–18.40	Gravels	16.65, 17.95, 18.15, 18.35
18.40–25.10	Coarse sand	19.25, 19.35, 20.75, 21.05, 22.05, 22.25, 23.05, 23.95, 24.85, 25.15
25.10–31.20	Clay	25.55, 25.85, 26.65, 27.35, 29.45, 30.15, 31.05,
31.20–34.20	Sand	32.25, 32.95, 33.45, 33.85
34.20–45.50	Alternations of clay with sand and gravels	34.25, 34.75, 35.75, 37.45, 38.35, 38.45, 38.80, 38.85, 39.05, 39.65, 39.95, 41.45, 42.35, 43.45, 43.95, 44.95, 45.05

Microfauna

Of the total examined samples, 17 were relatively rich in foraminiferal species (~200 specimens were counted per sample) with an FD-index ranging from ~40 to ~680 forams/g, while benthic foraminifera were absent in 17 samples (from reddish clay to sand layers), and just few broken specimens were found in 15 samples, with FD-index < 2 forams/g (gravel layers) (Fig. 5-19). Fisher's alpha index values ranged from α=2.99 (sample GA-4, 37.45 m) to α=6.00 (sample GA-4, 39.05 m).

In general, the foraminiferal fauna is dominated by species with calcareous specimens. Thirteen benthic foraminiferal taxa made up more than 95% of the total assemblage: *Ammonia beccarii, Ammonia tepida, Rosalina bradyi, Cibicides refulgens, Elphidium crispum, Elphidium complanatum, Elphidium granosum, Haynesina depressula, Neoconorbina terquemi, Asterigerinata mammilla and planorbis, Discorbis* spp. and miliolids (Fig. 5-19). In particular, miliolids were the dominant species present in all samples comprising almost 15% of the assemblages(maximum ~54% at sample GA-4, 25.15 m).*A. tepida* was, comprising more than 12% of the foraminiferal fauna (maximum ~49% at sample GA-4, 37.45 m). *A. beccarii* was present in all samples comprising almost 13% of the assemblages (maximum ~29% at sampleGA-4, 41.45 m). The epiphytic species, *R. bradyi* (~12%) and *C. refulgens* (~14%) were generally well represented, with maximum relative values at 30% (sample GA-4, 30.15 m) and ~27% (sample GA-4, 27.35 m) respectively. *Discorbis* spp. was represented mostly at the interval 26.00–31.0 m core depth (maximum ~8%) with average values ~3%. Among the *Elphidium* taxa, *E. granosum* (average abundance ~11% and maximum ~40% at sample 39.95 m) was the most common species, followed by *E. Crispum* (average abundance ~4% and maximum ~14% at sample 30.15 m) and *E. complanatum* (average abundance ~3% and maximum ~9% at sample 34.75 m). *H. depressula* was also well represented with an average abundance 3.3%. *Lobatula lobatula* and *Asterigerinata mammilla* and *planorbis* were also represented with average values approximately ~1% and 1.5% respectively. Other species had a circumstantial appearance (*e.g. Textularia* spp. (4.7% sample GA-4, 43.95 m), *Conurbella* spp. (3% sample GA-4, 43.95 m).

BR-ratio ranges from 5–10 at the intervals 27.00–31.00 m core depth, up to 40 (sample GA–4, 22.25 m). In general, gravely layers have a higher percentage of broken species than clays. A-ratio ranges from very low values (~5 at the interval 39.00–44.00 m core depth) to higher values (~ 50 at the interval 25.00–31.00 m core depth).

MS

Magnetic Susceptibility in GA-4 sequence ranged from 1 to 442 $\times 10^{-5}$ (SI units) (Fig. 5-18). At the interval 39.00 m to 45.50 m core depth, MS values ranged from 1 to 27 $\times 10^{-5}$ (SI units) (average value ~6 $\times 10^{-5}$ (SI units)). In the interval 38.40–39.00 m core depth MS values ranged from 126 to 442 $\times 10^{-5}$ (SI units) (average value 276 $\times 10^{-5}$ (SI units). The interval 33.30 m –38.40 m core depth was characterized by relatively low MS values ranging from 4 to 50 ×10-5 (SI units) (average value ~25 $\times 10^{-5}$ (SI units), while the MS values at the interval 33.30–30.00 m core depth ranged from 70 to 343 $\times 10^{-5}$ (SI units) with an average value at 19 $\times 10^{-5}$ (SI units). The MS values at the interval 30.00–25.10 m core depth ranged from 1 to 76 $\times 10^{-5}$ (SI units) with an average value at 13 $\times 10^{-5}$ (SI units). Finally, the MS values at the interval 8.50 m –25.10 m core depth ranged from 16 to 310 $\times 10^{-5}$ (SI units) with an average value at 111$\times 10^{-5}$ (SI units). Man-made debris from the excavation of the Corinth Canal comprising the upper 8.50 m of the borehole have not been examined. .

Calcareous Nannoplankton

Calcareous nannoplankton specimens have been identified through SEM analysis in certain levels of borehole GA-4. Four samples were examined where two of them proved to be rich in relatively well-preserved nannofossils (samples GA-4 31.05 and GA-4 41.45 m depth were rich in nannofossils, while samples GA-4 22.25 and GA-4 35.75 m depth were barren. All samples, were dominated by the presence of small *Reticulofenestra* spp. (~48%) and small *Gephyrocapsa* spp. (~43%) coccoliths, while *Emiliania huxleyi* specimens were relatively scarce (~4–8% of the total assemblage), but consistently present.

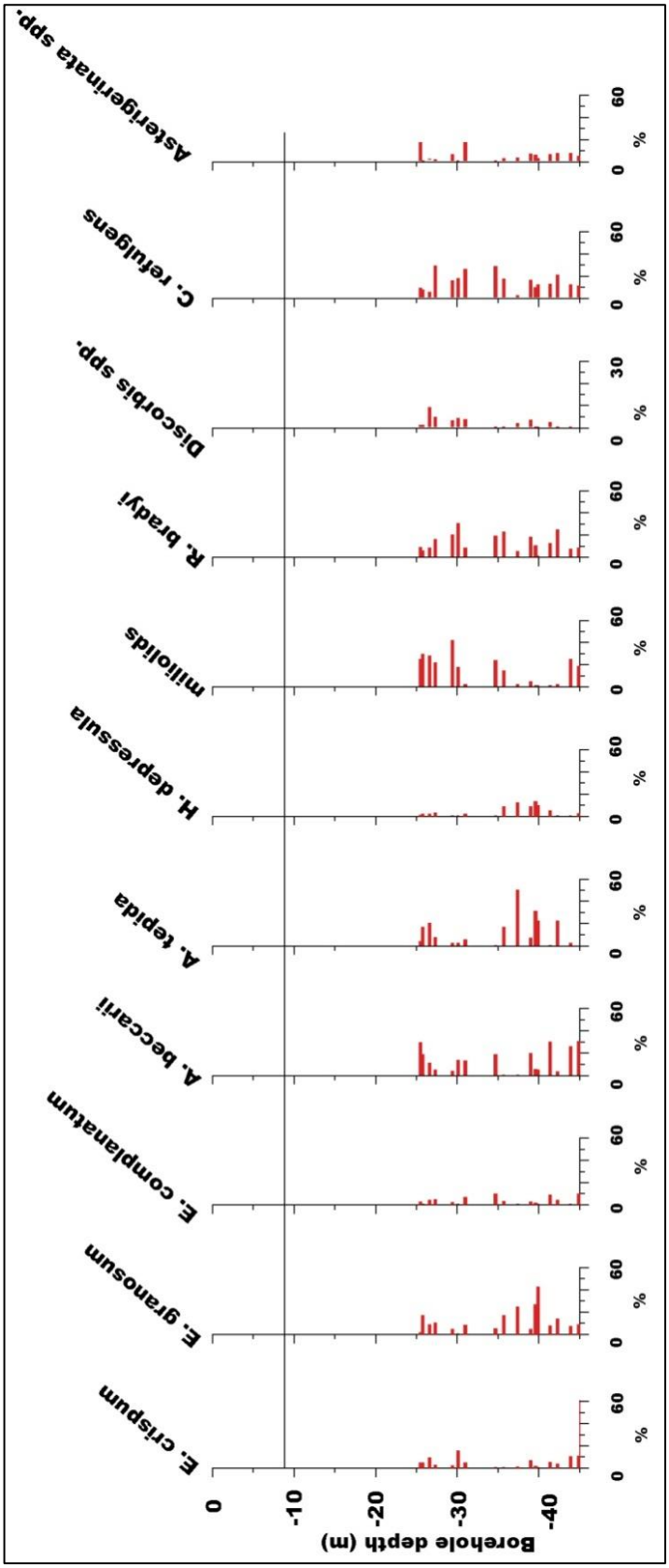

Figure 5-19. *Diagram showing the relative abundances of the most significant (>3%) recorded benthic foraminiferal species in borehole GA-4.*

Εικόνα 5-19. *Διάγραμμα των συγκεντρώσεων των κυριότερων τρημματοφόρων (>3%) στην γεώτρηση GA-4*

5.5.11 Borehole GA-5

Lithology

Borehole GA-5 consists mostly of sands and gravels and to a lesser degree of clays (Fig. 5-20, table 13).

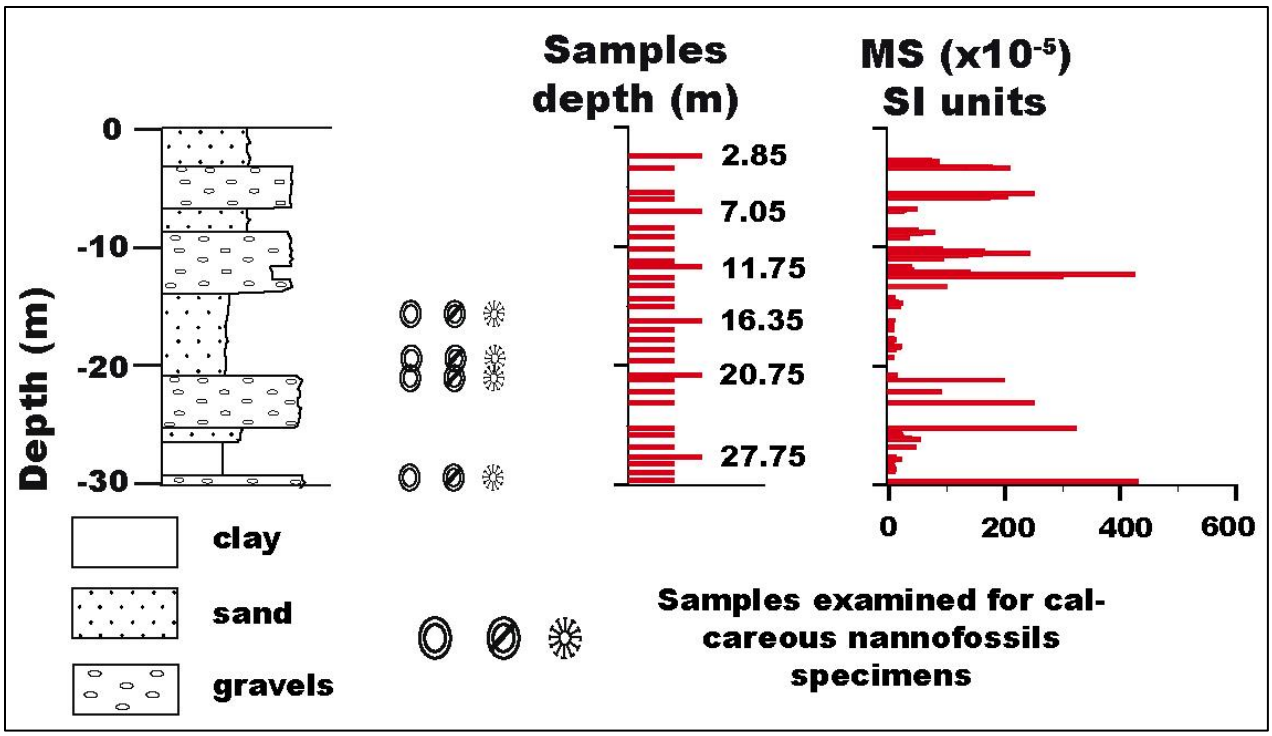

Figure 5-20*. Lithological description of GA-5, showing the extracted samples based on their depth from the surface, the samples examined for calcareous nannofossils and the measured Magnetic Susceptibility of the sediments.*
Εικόνα 5-20*. Η λιθολογική περιγραφή της γεώτρησης GA-5, τα δείγματα που εξετάστηκαν σε σχέση το βάθος τους από την επιφάνεια και αυτά που εξετάστηκαν για νανοαπολιθώματα καθως και η μετρηθείσα μαγνητική επιδεκτικότητα των ιζημάτων*

.

Table 13. Lithological description of borehole GA-5 and samples extracted from the borehole based on their depth from the surface. Πίνακας 13. Η λιθολογική περιγραφή και τα δείγματα που αναλύθηκαν στην GA-5.

Depth (m)	Lithology	Samples GA-5 (depth, m)
0.00–2.70	Top soil and gravely terrestrial formation	–
2.70–3.20	Sand	2.85
3.20–6.80	Gravels and sand	3.55, 5.65, 6.05
6.80–8.70	Sand	7.05, 8.65
8.70 –11.70	Sand	9.35, 10.25, 11.25, 11.65,
11.70–13.80	Gravels and sand	11.75, 12.65, 13.35
13.80–20.80	Sand	14.35, 15.15, 16.35, 17.05, 18.75, 19.35, 20.75
20.80–25.30	Gravels and sand	20.95, 22.15, 23.25
25.30–26.60	Sand	25.35, 26.05
26.60–29.30	Clay	26.95, 27.75, 28.25, 28.75
29.30–30.00	Gravels and sand	29.95

Microfauna

Of the total examined samples, 18 were relatively rich in foraminiferal species (~200 specimens were counted per sample) with an FD-index ranging from ~30 to ~720 forams/g, while benthic foraminifera were absent in 7 samples (from reddish clay to sand layers), and just few broken specimens were found in 5 samples, with FD-index < 2 forams/g. Fisher's alpha index values ranged from α=1.5 (sample GA-5, 28.25 m) to α=5.04 (sample GA-5, 11.25 m depth).

In general, the foraminiferal fauna is dominated by species with calcareous specimens. Thirteen foraminiferal taxa made up more than 80% of the total assemblage: *Ammonia beccarii*, *Ammonia tepida*, *Rosalina bradyi*, *Cibicides refulgens*, *Elphidium crispum, Elphidium complanatum*, *Elphidium granosum*, *Haynesina depressula*, *Aubignina perlucida, Asterigerinata* spp., *Bolivina* spp., *Discorbis* spp. and miliolids (Fig. 5-21). In particular, *A. tepida* was the dominant species (average abundance ~16%), constituting in some cases more than 65% of the foraminiferal fauna (sample GA-5, 28.25 m). *Ammonia beccarii* was a significant component of the foraminiferal fauna (~9%) with maximum relative abundance 31% at sample GA-5, 9.35 m. The epiphytic species, *R.bradyi* (~15%), *Discorbis* spp. (~7%)and *C. refulgens* (~10%), were generally well represented, with maximum relative abundance values 34% at GA-5 18.75 m depth, 14% at GA-5 11.75 m and 14 at GA-5 11.25 m depth respectively. Among the *Elphidium* taxa, *E. granosum* (average abundance ~15%) was the most common species, followed by *E. crispum* (3.5%) and *E. complanatum* (~1%) (maximum ~30% at sample GA-5, 17.85 m, ~11% at sample GA-5, 20.75 m and ~8% at sample GA-5, 27.75 m respectively. Other taxa such as *H. depressula* and *Asterigerinata* spp. also occurred, with average abundances 5% and ~5.2% respectively (maximum at samples GA-5, 28.25 m and 17.05 m respectively). *Bolivina* spp. was also represented with maximum relative abundance value at 10% (sample GA-5, 14.25 m). Miliolids were present in all samples comprising almost 10% of the assemblages (maximum ~27% at sample GA-5, 2.85 m. Other species had a circumstantial appearance (*e.g. Hyalinea baltica* (3.1% sample GA-5, 3.55 m), *Conurbella* spp. (3,5% sample GA-5, 20.75 m).

BR-ratio ranges from 3–7 (2.00–4.00 m, 7.00–10.00 m core depth), to 45 (17.00–20.00 m core depth). In general, gravely layers have a higher percentage of broken species than clays, which is expected since gravely layers require higher energy. A-ratio ranges from very low values (2.5 at sample GA-5, 8.65 m) to higher values (28 at sample GA-5, 17.85 m).

MS

Magnetic Susceptibility in GA-5sequence ranged from 3 to 430 $\times 10^{-5}$ (SI units) (Fig. 5-20). At the interval 29.30–30.00 m core depth MS values ranged from 395 to 430 $\times 10^{-5}$

(SI units) (average value 412 $\times 10^{-5}$ (SI units). At the interval 26.60–29.30 m core depth MS values ranged from 3 to 20 $\times 10^{-5}$ (SI units))(average value 10 $\times 10^{-5}$ (SI units), while at the interval 25.30–26.60 m core depth from 20 to 60 $\times 10^{-5}$ (SI units) (average value 30 $\times 10^{-5}$ (SI units). The MS values at the interval 20.80–25.30 m core depth ranged from 90 to 323 $\times 10^{-5}$ (SI units) with an average value at 215 $\times 10^{-5}$ (SI units). The MS values at the interval 13.80–20.80 m core depth ranged from 3 to 22 $\times 10^{-5}$ (SI units) with an average value at 9 $\times 10^{-5}$ (SI units). The MS values at the interval 8.70–13.80 m depth ranged from 25 to 424 $\times 10^{-5}$ (SI units) with an average value at 105 $\times 10^{-5}$ (SI units).MS values at the interval 6.80–8.70 m depth ranged from 13 to 78 $\times 10^{-5}$ (SI units), with an average value at 37 $\times 10^{-5}$ (SI units). At the upper part of the borehole sequence MS values ranged from 20 to 208 $\times 10^{-5}$ (SI units), with an average value at 126 $\times 10^{-5}$ (SI units).

Calcareous Nannoplankton

Calcareous nannoplankton specimens have been identified through SEM analysis in certain levels of borehole GA-5. Four samples were examined where two of them proved to be rich in relatively well-preserved nannofossils (samples GA-519.35 and 27.75 m depth were rich in nannofossils, while samples GA-514.35 and 28.25 m depth were barren. All samples, were dominated by the presence of small *Reticulofenestra* spp. (~49%) and small *Gephyrocapsa* spp. (~41%) coccoliths, while *Emiliania huxleyi* specimens were relatively scarce (~5–10% of the total assemblage), but consistently present.

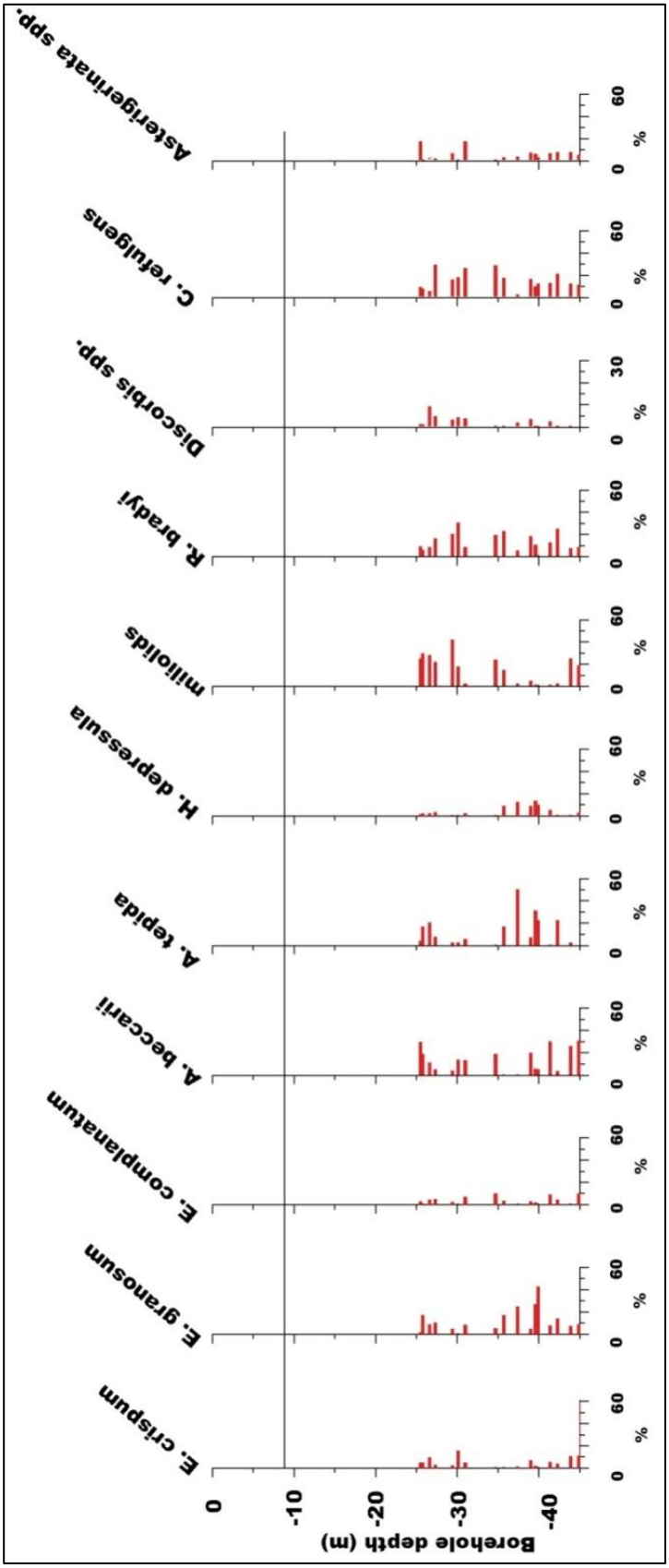

Figure 5-21*. Diagram showing the relative abundances of the most significant (>3%) recorded benthic foraminiferal species in borehole GA-5.*

Εικόνα 5-21*. Διάγραμμα των συγκεντρώσεων των κυριότερων τρηματοφόρων (>3%) στην γεώτρηση GA-5.*

6 ***Fieldwork mapping***

6.1 Introduction

The area which has been described and mapped in detailed is located at the Corinth Canal and lays between two major opposite dipping active normal faults (the Loutraki and the Kenchreai faults) that form a graben. It is mostly focused at the footwall and hangingwall of the Kalamaki–Isthmia fault. The excavated Corinth Canal offers a unique opportunity as "Mega-trench" to identify the sedimentary facies of the area. On the basis of a detailed field survey at 1:5.000 scale different lithologies ranging from coarse gravels containing Ophiolite cherts, coarse to fine sand, sandstones and clays, indicate a complicated lithological and consequently paleoenvironmental pattern that has been confirmed also by the detailed micropaleontological analysis.

6.2 Fieldwork mapping

For the detailed mapping of the area the first step was the identification of sedimentary facies, tectonic structures and specific points of interest (e.g. the locations where Collier et al. (1992), took corals samples for absolute dating), In doing so, a consistency between the previous studies and this one has been preserved. This area has also been stratigraphically described before (e.g. Freyberg, 1973; Bornovas et al., 1972, 1984; Gaitanakis et al., 1985 Collier and Dart, 1991). For instance, Collier and Dart has meticulously described the sedimentary facies northern than the Kalamaki-Isthmus fault, identifying a range of lithologies (from coarse to fine sediments), corresponding to different paleoenvironments. Unfortunately, the exact outcrops where Collier et al. (1992) dated corals ~ 205 ka old[10] have not been found since human activity has significant changed the landscape the last 30 years.

---

[10] *These were the corals which have been used to estimate the ~ 0.30 mm/yr uplift rate at the area*.

Since these sediments have been identified and described, samples have been extracted (99 in total) from every sedimentary formation. Each sample was marked through a handheld GPS, to secure the exact location and altitude of the formation and the extracted sample. Through these GPS points the detailed geological map has been compiled. All samples have been extracted from undisturbed and in situ outcrops. Furthermore the external and weathered outcrop has been removed before extracting the sample to secure the quality and the reliability of the sample. Apart from surface samples, tectonic measurements (32 measurements) have been extracted as well. Furthermore in two cases striations on the fault plane have also been extracted. Finally, 111 measurements of the strata inclination have been extracted from surface outcrops.

In general, the described lithologies can be grouped into two categories. The lower part, includes the magmatic rocks, the marl sediments and the siltstone/gravels alternations above them. The upper part consists of alternations of marls, sands and gravels, similar to the described lithologies within the boreholes, and the recent alluvial sediments.

Igneous rocks

Collier and Dart (1991) mention the presence of andesites at Kalamaki- Isthmia fault. By a hornblende concentrate extract igneous rocks were dated since Lower Pliocene (~2.7 to 4 Ma) (e.g. Fytikas et al., 1984; Collier and Dart, 1991).

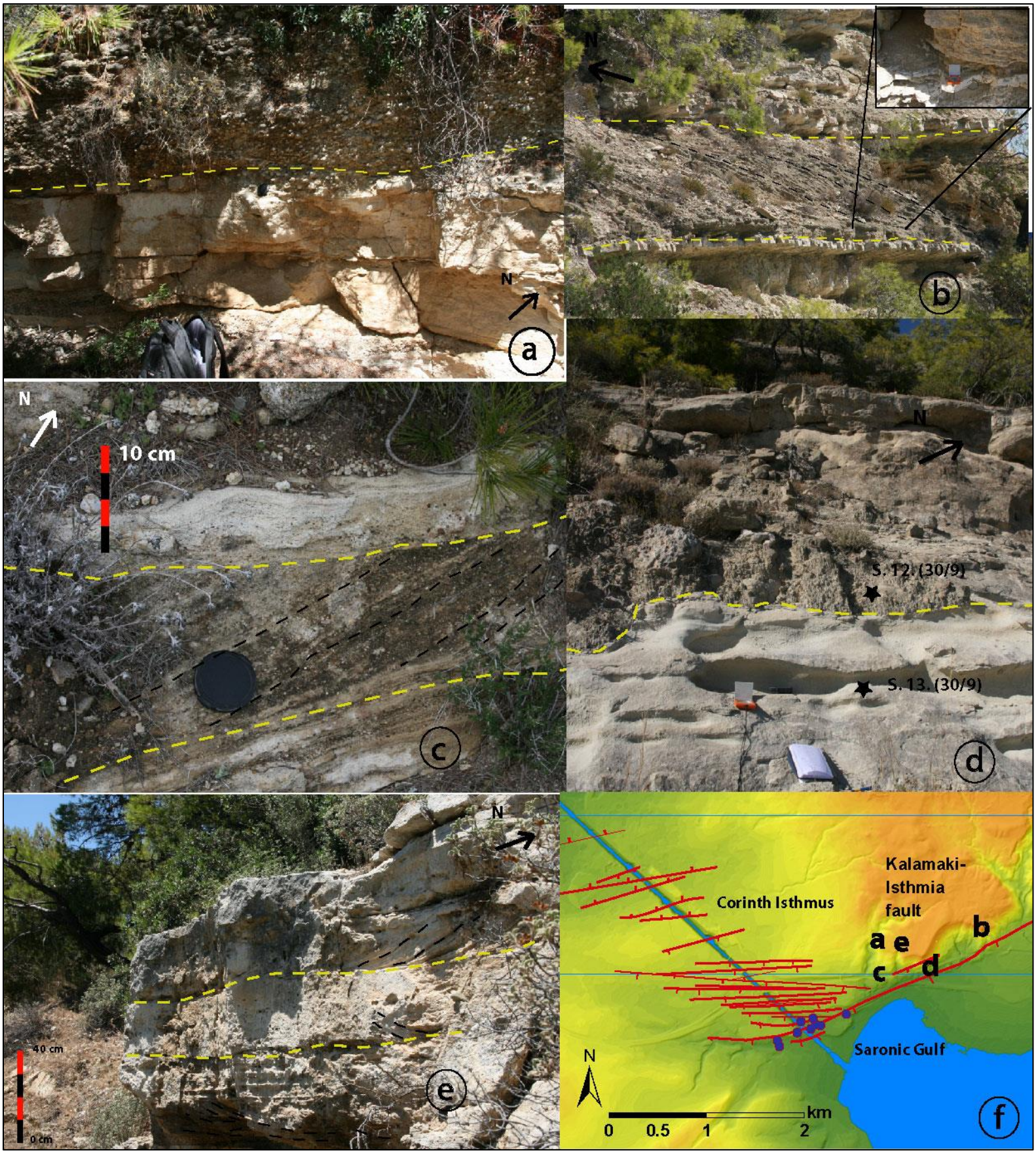
N
a
N
b
N
10 cm
c
N
S. 12. (30/9)
S. 13. (30/9)
d
N
40 cm
0 cm
e
Kalamaki-
Isthmia
fault
Corinth Isthmus
a e
b
c
d
Saronic Gulf
N
km
0 0.5 1 2
f

Figure 6-1*. a) Poorly sorted gravels with brown sand as matrix reflecting, possible fluvial conditions, above sandstone beds with cross bedded ripples reflecting a tidal intertidal conditions (Fine to coarse sand sediments), b) Packages of gravely sands with mudstones at the central part of the fault's footwall. With yellow colour is highlighted the surface between the mudstone-sand while with black colour the sand ripples, indicating paleo-deltaic conditions. (Planar cross-bedded mudstone / gravely sands sediments), c) Trough scours trend with cross-stratification layers of sand/clay indicating tidal/intertidal conditions (Fine to coarse sand sediments), d) Erosional surface between the gravely sands and the white marl defining unconformity (Marl sediments), e) Cross stratification in sandstone and mudstone indicating tidal intertidal conditions. The opposite direction of the stratification indicates different paleoflow direction (black lines) (Fine to coarse sand sediments), f) the location at the study area where the photos have been extracted.*

Εικόνα 6-1. *α) Μη ταξινομημένα χονδρόκοκκα υλικά με λεπτόκοκκη άμμο ως συνδετικό υλικό (πιθανές ποτάμιες αποθέσεις), πάνω από ψαμμίτη που υποδεικνύουν παλιρροιακές συνθήκες (Fine to coarse sand sediments), (β) Εναλλαγές λεπτόκοκκου με χονδρόκοκκου υλικού υποδεικνύοντας παλαιό-δελταϊκές συνθήκες (Planar cross-bedded mudstone / gravely sands sediments), γ) Εναλλαγές άμμου / αργίλου που δείχνουν παλιρροιακές συνθήκες. Η διαφορετική κατεύθυνση της διαστρωμάτωση υποδεικνύει διαφορετική κατεύθυνση της ροής. (Fine to coarse sand sediments), δ) Επιφάνεια ασυνέχειας μεταξύ της αμμώδους άμμου και αργίλου(Marl sediments), ε) Διαστρωμάτωση σε ψαμμίτη και άργιλο που δείχνει παλιρροιακές συνθήκες (Fine to coarse sand sediments), στ) Οι θέσεις των φωτογραφιών στο χάρτη.*

Marl sediments

The activity of the fault has revealed a white partially laminated marl formation towards the center of the fault in the immediate footwall where the maximum uplift is observed. These sediments are tilled towards NNW, while their inclination ranges from 30^{o}–40^{o}/~300^{o} (the lowermost layers), to ~10–20^{o}/~300^{o} (the uppermost layers). (Fig. 6-5). These formations corresponded to low energy, freshwater-dominated

paleoenvironments. Furthermore, the microfauna in the examined samples indicate brackish-oligohaline conditions partially influenced by marine waters (lagoonal).

Planar cross-bedded mudstone / gravely sands sediments

The northern part of the study area is characterized by alternations of thin layers of mudstones (5–10 cm thick) followed by 1-6 m thick cross- bedded layers of coarse sand and pebbles (Fig. 6-1b), above the marl sediments described before. Inclination of these packages vary from 20^{o}–30^{o}/~300^{o} (the lowermost layers), to 5o–10^{o}/~300^{o} (the uppermost layers), while cross-bedded sands dip at~50^{o} towards NE (~050^{o} to 075^{o}). Planar cross-stratification is seen across a scale range of 1-6 m, indicating paleo-flow from west to the east. Towards the center of the fault the uplifting and the erosional processes have revealed more than 70 m of successive alternations which overlie through erosional surface several meters of partially laminated (from few mm to several cm thick) marl layers. The described cross-bedding formation is most commonly encountered in river channels, deltas, estuaries and shallow marine environments where there are relatively strong, sustained flows (e.g. Nichols, 1999). Samples examined for their micropaleontological content indicated a high energy paleoenvironment, possible river-dominated deltaic facies.

Fine to coarse sand sediments

Towards the central and southern part of the Kalamaki-Isthmia fault area, mostly laminated fine grained sands to cross-stratified sandstones were identified (Figs 6-2a, c, e, 6-5). Trough scours and cross-stratified lenses or beds of gravels and sandy gravels locally interpose between the sands and marls, which may reflect unidirectional current activity as tidal/intertidal conditions and wave's activity (e.g. Collier and Thompson, 1991). Layers are generally tilted ~5^{o} to ~10^{0} towards NNW.

Recent alluvial sediments

The eastern part of the Kalamaki-Isthmia fault is covered by recent alluvial-fluvial sediments transferred by the drainage system, covering most of the fault's hangingwall (Figs 6-5 to 6-7).

6.3 Corinth Canal

The walls of the Corinth Canal, offers a unique opportunity to describe the sedimentary facies and the syn-sedimentary faults that have deformed them (Figs. 6-2, 6-3). After the identification of the sedimentary facies, the tectonic structures and several points of interest[11] in the Canal, samples have been extracted to verify the already described facies (e.g. Collier, 1990; Gawthorpe et al., 1994; McMurray & Gawthorpe, 2000). These results are also included in the detailed geological map (Figs 6-5 to 6-7).

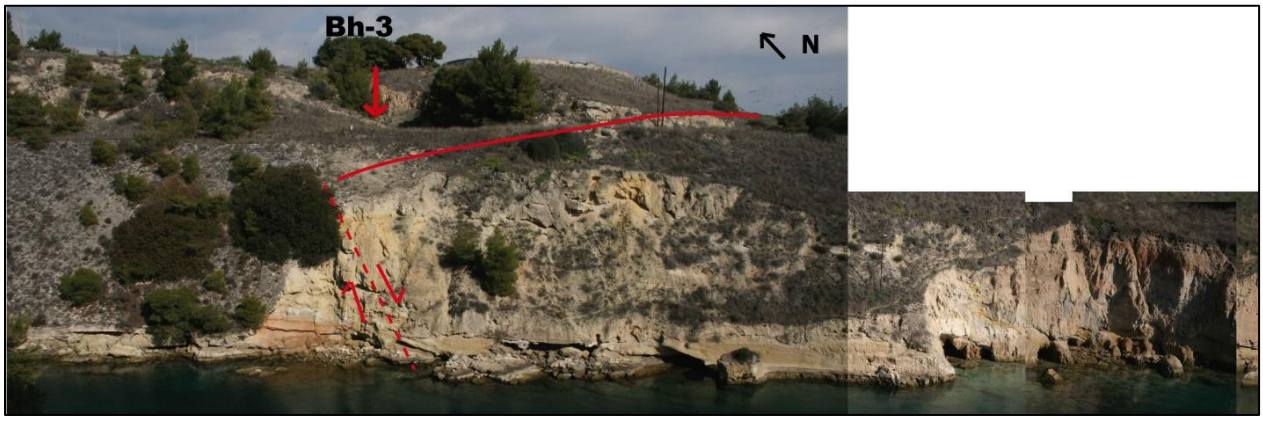

Figure 6-2*. Photomosaic of the easternmost tip of the Corinth Canal, showing the Kalamaki-Isthmia fault, the location where borehole Bh-3 was drilled and the sediments structure.*

Εικόνα 6-2*. Φωτομωσαϊκό του ανατολικού τμήματος της διώρυγας της Κορίνθου, που διακρίνεται το ρήγμα Καλαμάκι-Ίσθμια, η θέση όπου έγινε η γεώτρηση Bh-3 και τα επιφανειακά ιζήματα που διατηρούνται στη διώρυγα*

[11] *E.g. the palaeocliff described by Gawthorpe et al. (1994) and Murray & Gawthorpe (2000)*

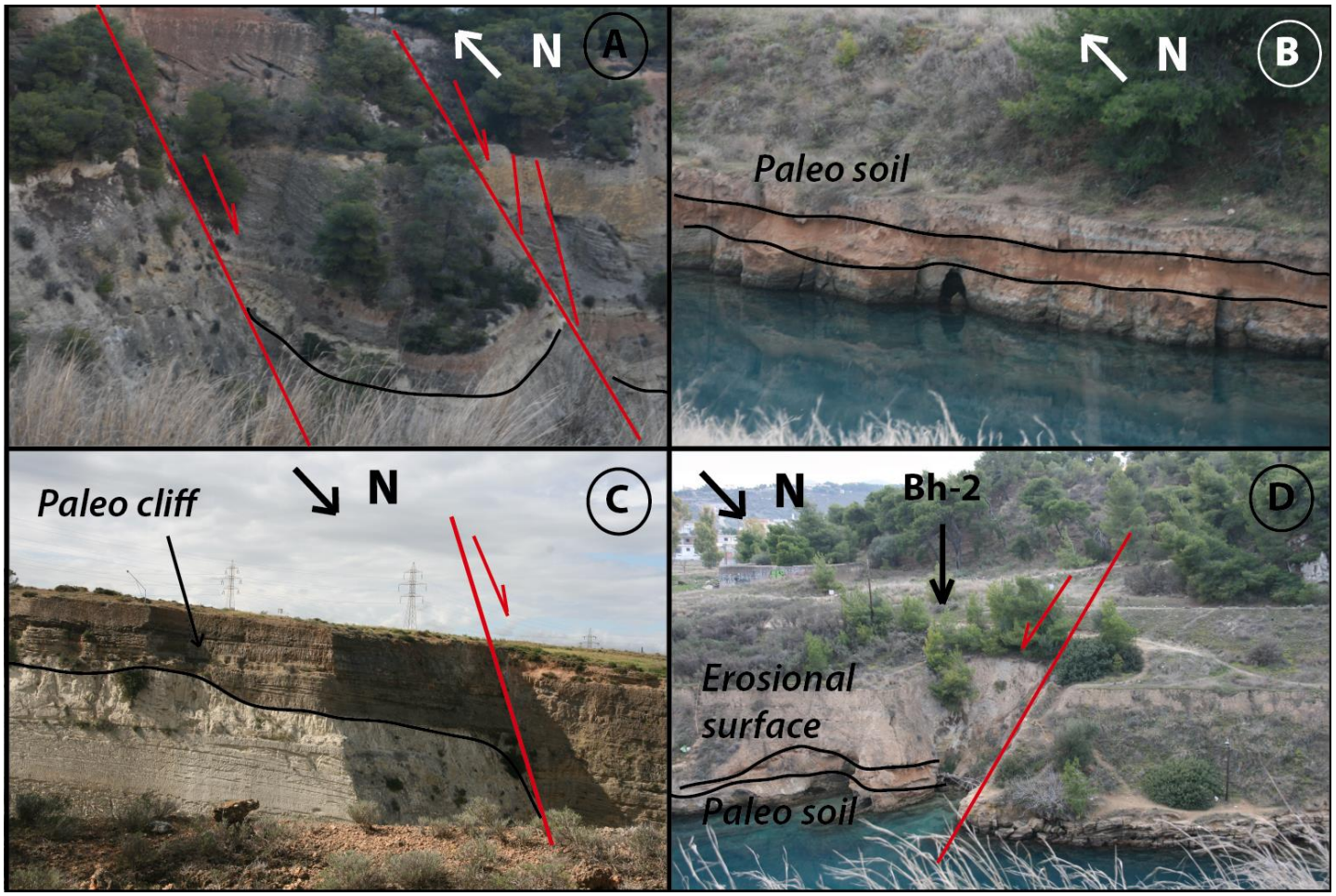

Figure 6-3. *A) Deformed sediments from faults intersecting the northern part of the Canal. B) Paleosoil horizon indicating subaerial exposure, visible from the Canal. C) The palaeocliff described by Gawthorpe et al. (1994) and Murray & Gawthorpe (2000) at the southern part of the Canal. A minor fault has displaced (~10 m) the coarse (dark brown) shoreface sequence. D) Paleosoil horizon exposed from the Canal. The Kalamaki-Isthmia fault is highlighted as well as the location where borehole Bh-2 was drilled.*

Εικόνα 6-3*. Α) Μετατοπισμένα στρώματα από ρήγματα που τέμνουν το βόρειο τμήμα του Καναλιού. Β) Παλαιοεδάφη που φαίνονται στην διατομή του Καναλιού. Γ) Ο παλαιό-κρημνός που περιγράφεται από τους Gawthorpe et al. (1994) και Murray & Gawthorpe (2000) στο νότιο τμήμα του Καναλιού, οπού ένα ρήγμα έχει μετατοπίσει (~ 10 m) τα ιζήματα. D) Παλαιοέδαφος που διακρίνεται στην διατομή του Καναλιού. Διακρίνεται το ρήγμα Καλαμάκι-Ίσθμια καθώς και η θέση όπου έγινε η γεώτρηση Bh-2.*

6.4 Kalamaki-Isthmia fault

Detailed mapping 1:5.000 of the Corinth Isthmus area revealed a fault system of parallel/subparallel fault segments, striking at ~ 060^{o} – 110^{o} and ~ 55^{o} – 70^{o} dipping towards SSE. The main fault trace strikes at 075^{o} and dips~65^{o} towards SSE. The fault plane was also traced 300 m southwards the Canal, striking at ~070^{o} also dips towards SSE (Papanikolaou et al., 2015).

The main fault trace has also been described in borehole Bh-7 at the interval from 33.00 m to 45.00 m core depth. Based on the distance between borehole Bh-7 and the fault trace an approximately 60^{o} dip is estimated. Secondary parallel structures are also described towards NW of the main fault plane that are synthetic to the main fault trace. Based on their characteristics these segments comprise a fault zone, the Kalamaki-Isthmia fault zone, indicating that the fault activity has progressively migrated eastwards towards the main Kalamaki-Isthmia fault trace (Papanikolaou et al., 2015).

Unfortunately, human infrastructures have heavily disturbed the natural terrain and it was not possible to identify a clear fault plane of the main Kalamaki-Isthmia fault trace near its center (national highway, railway and houses). Instead of this, several fault segments parallel or subparallel to the main structure were traced, either in the Corinth Canal or at the uplifted sediments of the Kalamaki-Isthmia footwall (Fig. 6-4).

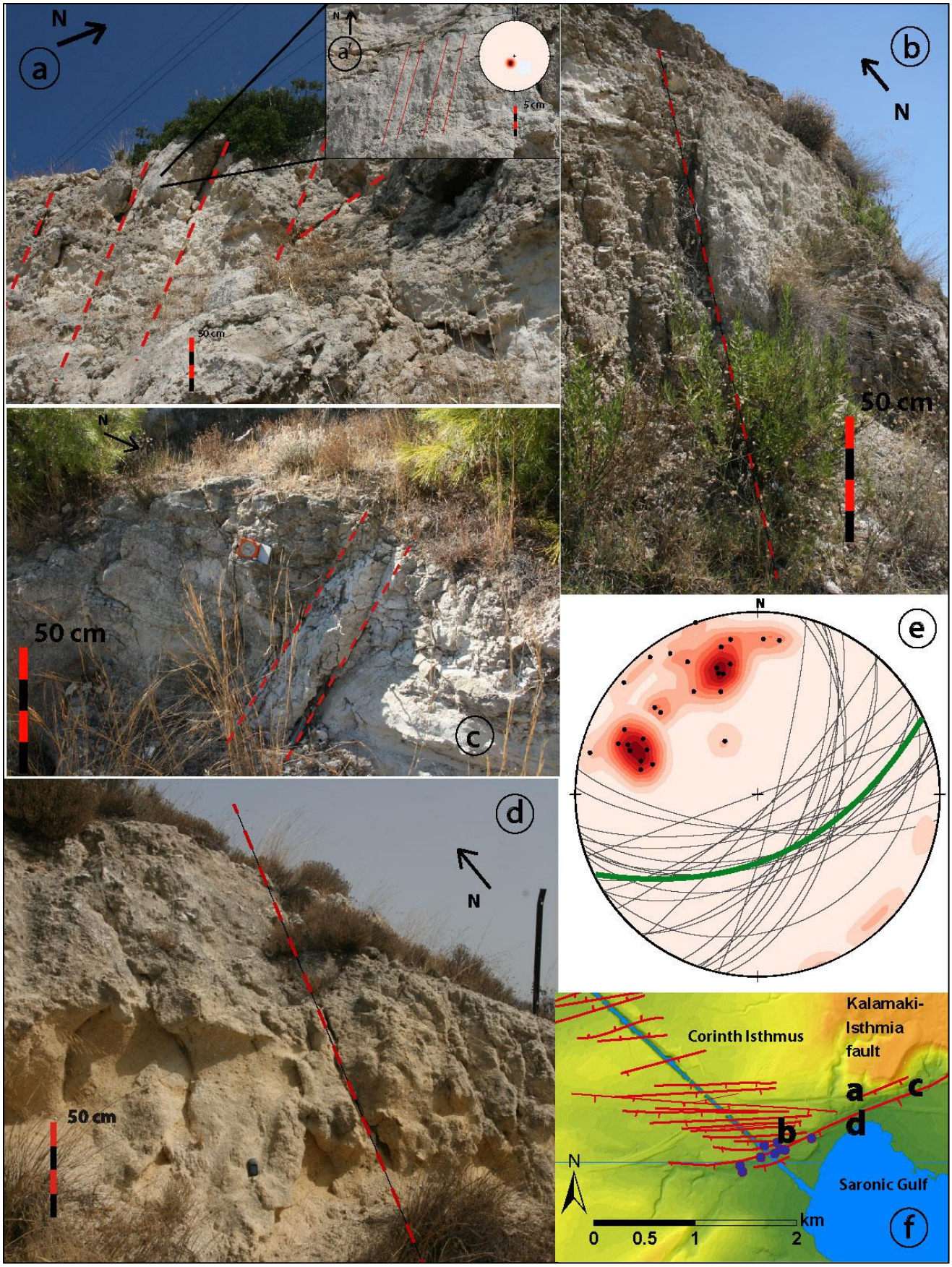
a
N
50 cm
5 cm
b
N
50 cm
c
N
50 cm
d
N
50 cm
e
N
f
Corinth Isthmus
Kalamaki-
Isthmia
fault
a
c
d
b
N
Saronic Gulf
km
0
0.5
1
2

Figure 6-4. *a-d) Photos of fault planes identified through detailed mapping, while in figure (a) striations measured on the fault plane plunge at 75° towards the SE. e) Stereographic projections of the measured fault planes and tectonic fractures with a mean ~130°/65° (green curve). f) The location at the study area where the images were extracted.*

Εικόνα 6-4. *Φωτογραφίες του ρήγματος Καλαμακίου-Ίσθμιων μέσω λεπτομερούς χαρτογράφησης, ενώ στο σχήμα (a) φαίνονται οι γραμμές προστριβής που κλίνουν 75 ° προς ΝΑ. ε) Στερεογραφικές προβολές των τεκτονικών επαφών με μέση τιμή ~ 130° / 65° (πράσινη καμπύλη). στ) Οι οι θέσεις λήψης των φωτογραφιών στην περιοχή μελέτης.*

Inclination measurements extracted from surface outcrops varied both along and across strike of the fault plane (Figs. 6-4 and 6-5). Sediments exposed on the immediate footwall and close to the center of the fault, dip ~30° to the NNW, indicating also that this tilt is due to the recent fault activity. Strata towards the center of the fault dip at ~30°, while these closer to its tip at 15° to the NNW. The latter indicates that the backtilting is controlled by the slip-rate variability from the center to the fault tip. In addition, older strata near the center of the fault in its immediate footwall dip at ~30°, whereas younger strata dip at ~10° (Fig. 6-5), indicating that this fault was active during sedimentation.

Stereographic projections of the measured faults plane and tectonic fractures with a mean ~130°/65° (green curve in Fig. 6-4e) reveals a local extensional NE-SW stress field. The major stress field of the area is an N-S extensional stress field northern (Loutraki fault) and southern than Corinth Isthmus (Kenchreai fault). This local extensional stress field is indeed what Gawthorpe et al. (2004) mentioned that the area of Corinth Isthmus is a transfer zone where the polarity of the major faults switches (Loutraki and Kenchreai).

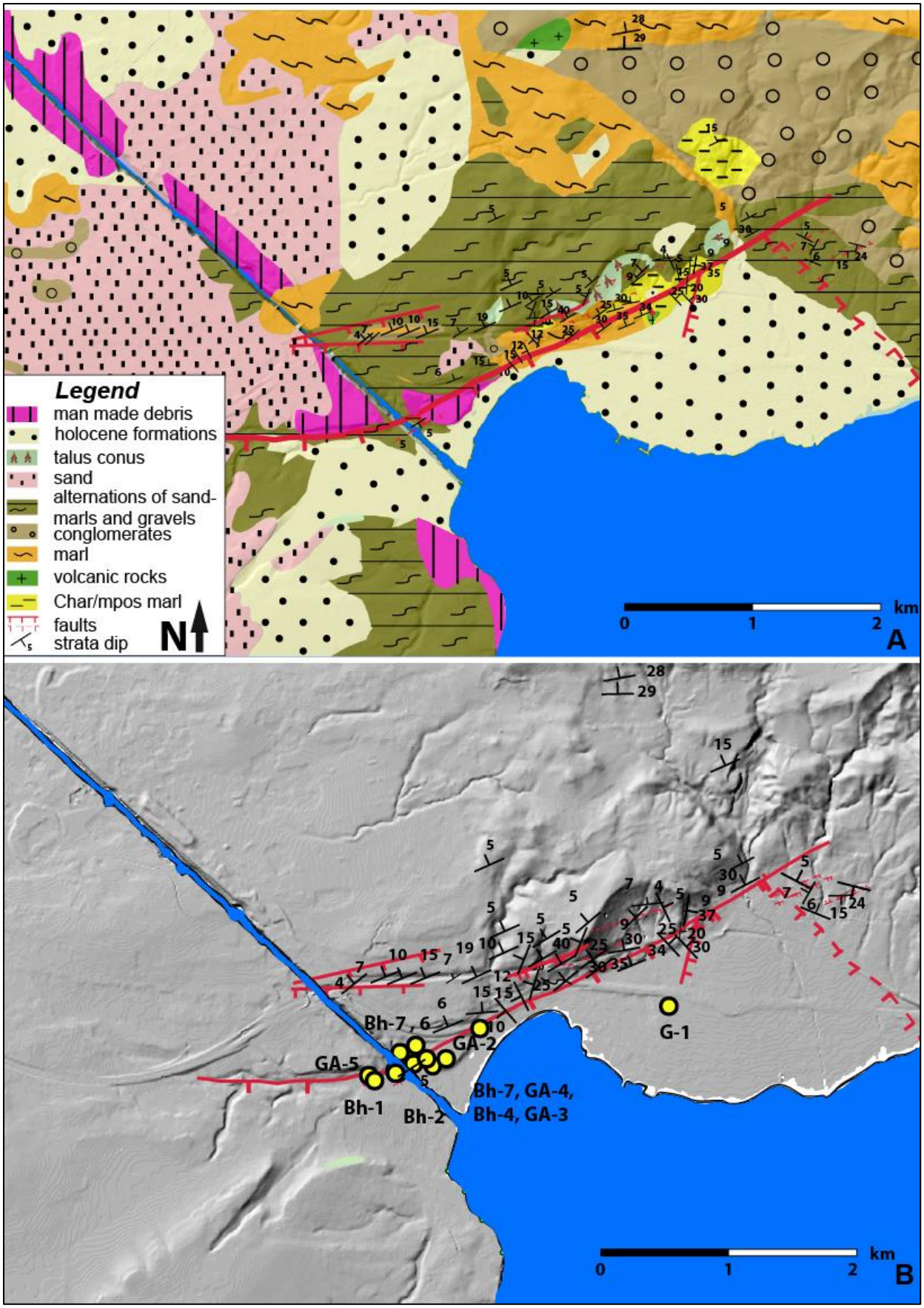
Legend
man made debris
holocene formations
talus conus
sand
alternations of sand-
marls and gravels
conglomerates
marl
volcanic rocks
Char/mpos marl
faults
strata dip
N
km
0
1
2
A
Bh-7, 6
GA-2
GA-5
Bh-1
Bh-2
Bh-7, GA-4,
Bh-4, GA-3
G-1
km
0
1
2
B

Figure 6-5. *(A) Geological map of the study area (based on Gaitanakis et al., 1985; Collier and Dart, 1991; this study). The location of the boreholes and the outcrops where the examined samples were extracted is indicated, as well as the inclination and the direction of the described strata (B).*

Εικόνα 6-5. *(A) Γεωλογικός χάρτης της περιοχής μελέτης (με βάση τους Gaitanakis et al., 1985, Collier and Dart, 1991, την παρούσα διατριβή). Φαίνεται η θέση των γεωτρήσεων, των επιφανειακών στρωμάτων, καθώς και η κλίση και η κατεύθυνση των στρωμάτων (B).*

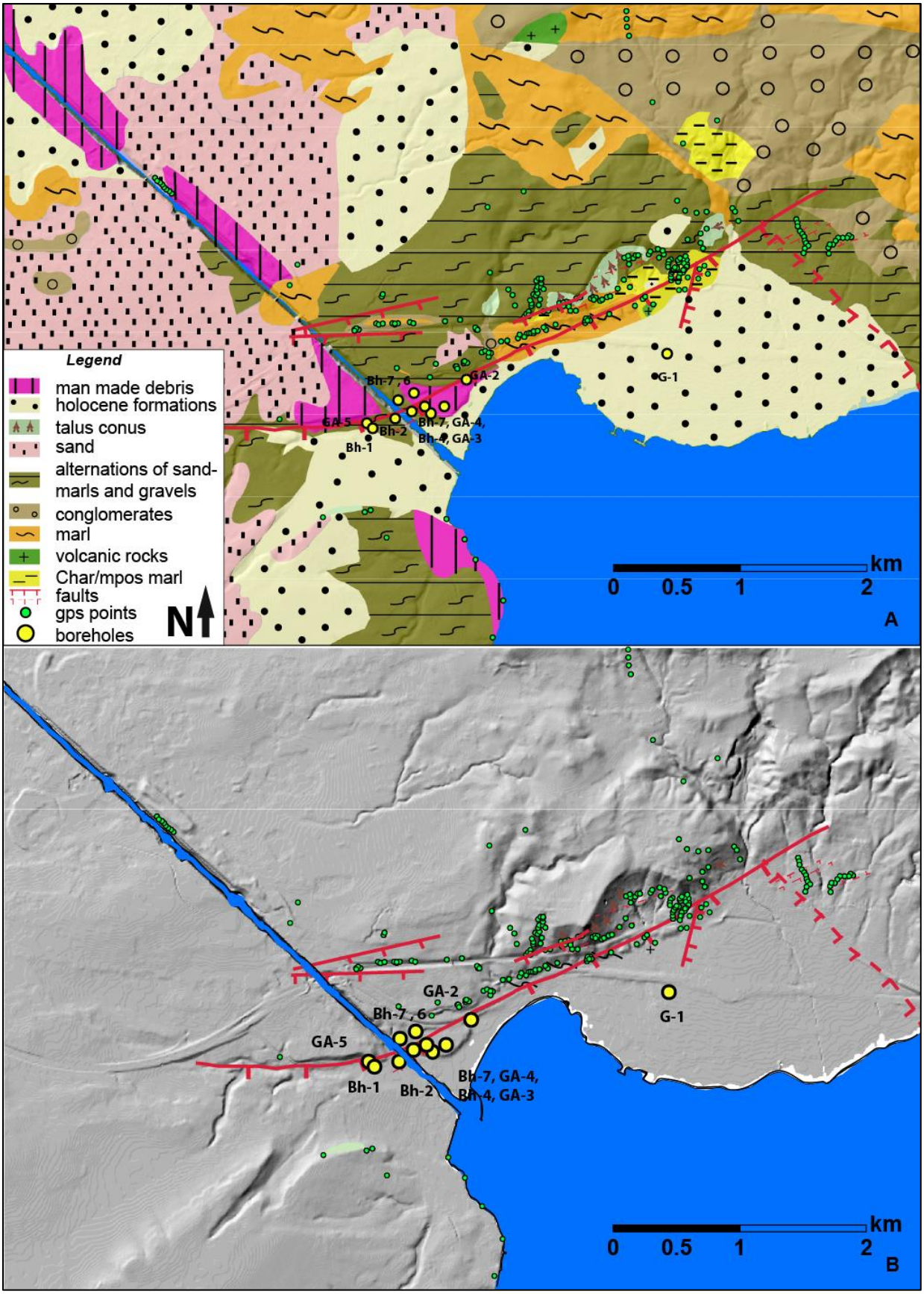
Legend
man made debris
holocene formations
talus conus
sand
alternations of sand-marls and gravels
conglomerates
marl
volcanic rocks
Char/mpos marl
faults
gps points
boreholes
N
Bh-7 , 6
GA-2
G-1
GA-5
Bh-2
Bh-1
Bh-7, GA-4,
Bh-4, GA-3
km
0 0.5 1 2
A
B

Figure 6-6. *(A) Geological map showing the location of all GPS points taken during field work (green dots), with the location of the boreholes (B).*
Εικόνα 6-6. *(A) Γεωλογικός χάρτης που επισημαίνεται η θέση των σημείων GPS που λήφθηκαν κατά την διαδικασία της χαρτογράφησης και η θέση των γεωτρήσεων που μελετήθηκαν (B).*

6.5 Micropaleontological analysis

In general the studied benthic foraminiferal assemblages were relatively abundant and moderately preserved. 32 samples were relatively rich in foraminiferal species (~200 specimens were counted per sample) with FD-index ranging from ~27 to ~198 forams/g. Benthic foraminifera were absent in 12 samples and just few broken specimens were found in 48 samples with FD-index <2 forams/g. Fisher's alpha index values ranged from α=0.69 (sample S.1/7/8) to α=5.61 (sample S.4/7/14).

In general, the benthic foraminiferal fauna was dominated by species with calcareous test. Fourteen benthic foraminiferal taxa comprised ≥ 90% of the total assemblage: *Ammonia beccarii, Ammonia tepida, Rosalina bradyi, Cibicides refulgens, Elphidium crispum, Elphidium complanatum, Elphidium granosum, Haynesina depressula, Neoconorbina terquemi*, *Discorbis* spp., *Planorbulina mediterranensis, Asterigerinata* spp., *Lobatula lobatula, Bolivina* spp. and miliolids (Fig. 6-7).

In particular, *A. tepida* was the dominant species with a maximum relative abundance of ~84% at sample S.1/7/8*. Ammonia beccarii* was also a significant component of the boreholes with maximum relative abundance ~45% at sample S.4/7/10. Two epiphytic species, *R. bradyi* and *C. refulgens*, were generally well represented, with maximum relative abundance of ~20% (sample S.17/7/7) and 27% (sample S.4/7/15) respectively. Among the *Elphidium* species, *E. crispum* (maximum relative abundance of ~30% S.4/7/16) was the most common, followed by *E. granosum* (maximum relative abundance of ~18% S.4/7/6) and *E. complanatum* (maximum relative abundance of ~10% S.1/9/7). Taxa such as *Haynesina* spp. (*depressula* and *germanica*) and *N.*

terquemi were also traced, with maximum relative abundances of ~16% at sample S.1/7/5 and ~27% at sample S.12/7/3 respectively. Miliolids were present with maximum relative abundance of ~46% at sample S.17/7/5. *Lobatula lobatula* and *Discorbis* spp. were also traced with maximum relative abundances of ~34% at sample S.25/9/2 and ~26% at sample S.1/7/4 respectively. *Asterigerinata* spp. (*mammilla* and *planorbis*) were also represented with maximum relative abundance of ~24% S.25/9/3. *P. mediterranensis* was described with maximum relative abundance of ~9% S.25/9/7.*Bolivina* spp. was also represented with maximum relative abundance of ~10% S.25/9/3.

The presented samples have relatively low BR-ratio ranged from 3.5 to ~15. A-ratio tests were performed in 10 samples and ranged from low (3.4 at sample S.1/7/8) to high values (~ 58 at sample S.17/7/7). Low A-ratio is associated with Cluster I assemblages, while higher values are associated with Cluster III assemblages (see chapter 7, Fig. 7-1).

It is interesting to mention the presence of ostracod representatives (e.g. *Cyprideis* spp.) recorded into marl sediments exposed at the central part of the fault's footwall, indicating an oligohaline-lagoonal paleoenvironment (e.g., Ben Rouina et al., 2016).

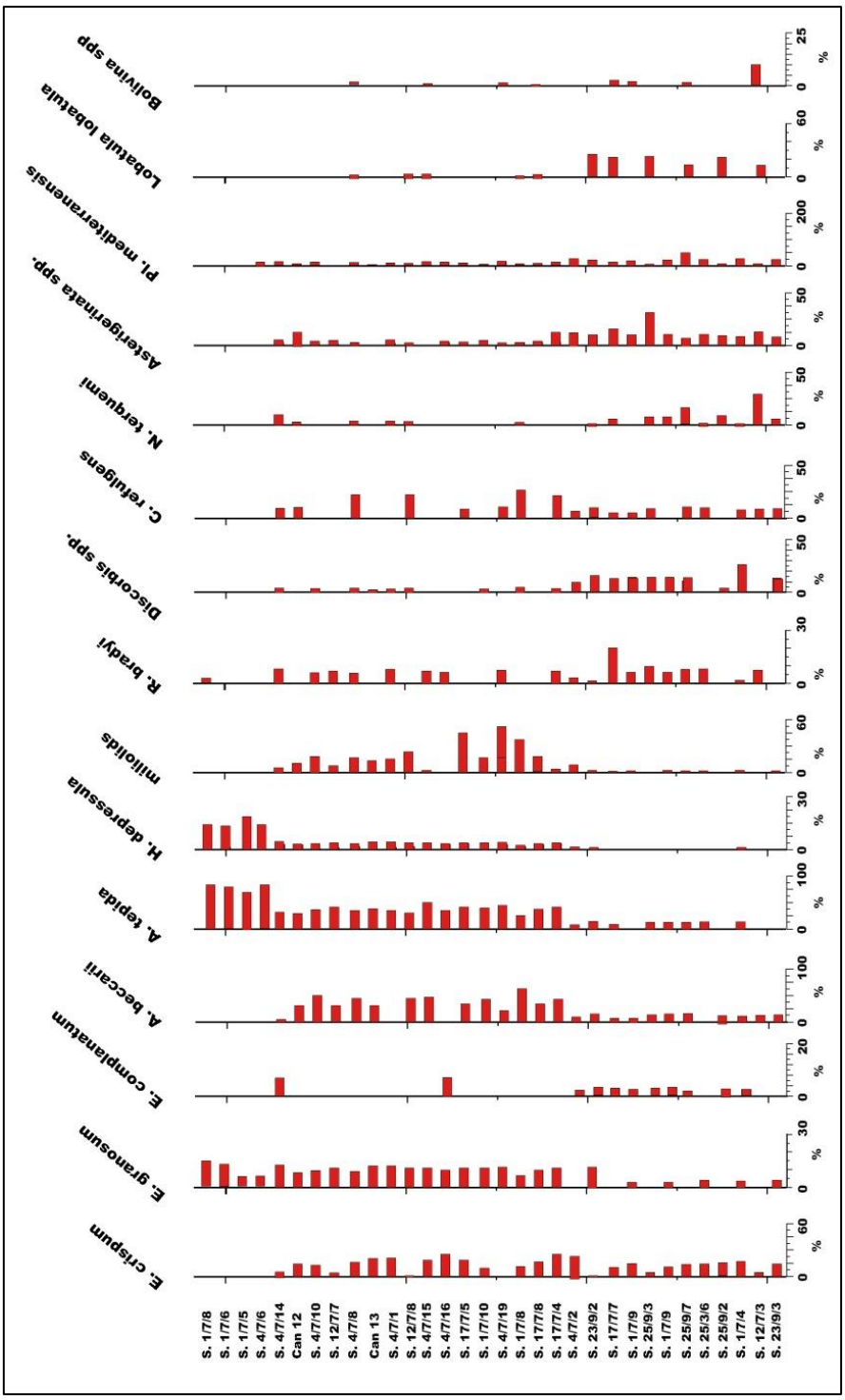

Figure 6-7. *Diagram showing the relative abundances of the most significant (>3%) recorded benthic foraminiferal species from the examined surface samples.* ***Εικόνα 6-7.*** *Διάγραμμα των συγκεντρώσεων των πιο σημαντικών τρηματοφόρων (>3%) στα επιφανειακά δείγματα.*

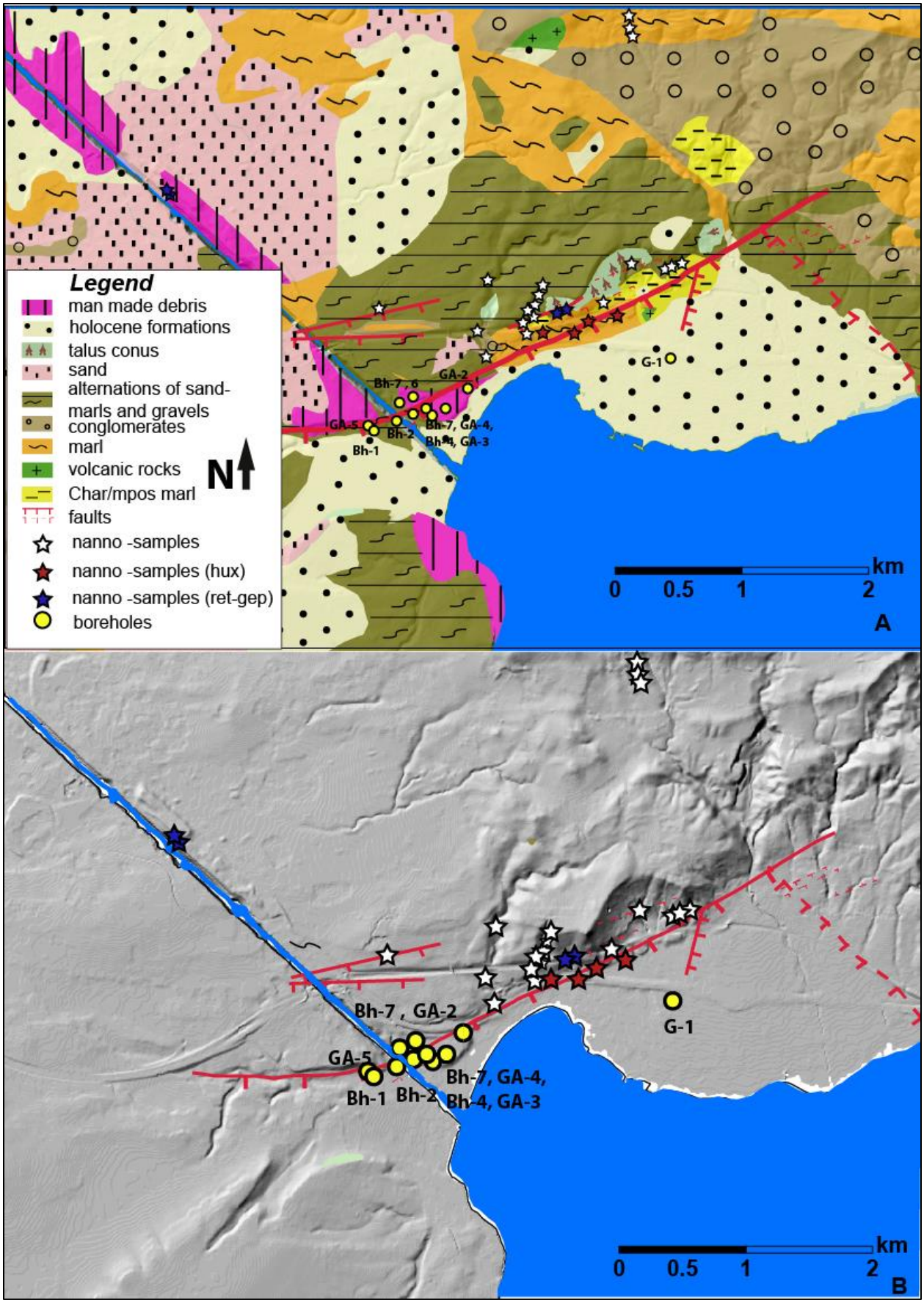
Legend
man made debris
holocene formations
talus conus
sand
alternations of sand-
marls and gravels
conglomerates
marl
volcanic rocks
Char/mpos marl
faults
nanno -samples
nanno -samples (hux)
nanno -samples (ret-gep)
boreholes
N
Bh-7 , 6
GA-2
GA-5
Bh-2
Bh-7, GA-4,
Bh-4, GA-3
Bh-1
G-1
km
0
0.5
1
2
A
Bh-7 , GA-2
GA-5
Bh-1
Bh-2
Bh-7, GA-4,
Bh-4, GA-3
G-1
km
0
0.5
1
2
B

Figure 6-8*. A) Geological map showing the location of the boreholes and the locations where the extracted samples have been analyzed for nanno fossils. With white color are highlighted the barren samples, with red the samples where E. huxleyi has been found and with blue the samples where only Reticulofenestra spp. and Gephyrocapsa spp. has been found (B).*

Εικόνα 6-8*. (Α) Γεωλογικός χάρτης που επισημαίνεται η θέση των γεωτρήσεων και των σημείων δειγματοληψίας για νάννο απολιθώματα. Με άσπρο χρώμα φαίνονται τα στείρα δείγματα, με κόκκινο αυτά που περιείχαν Ε. Huxleyi και με μπλε αυτά που είχαν μόνο Reticulofenestra spp. και Gephyrocapsa spp (Β).*

6.6 Calcareous nannofossils

From the total 32 samples examined (Fig. 6-8), 8 proved to be rich in relatively well-preserved nannofossils (samples S.17.7/5, S.17.7/6, S.23.9/2, S.25.9./3, S.25.9/2, Can.12, S. 4/7/17, S.12/7/3); while the rest were barren. In samples, S.17.7/5, S.17.7/6, 4/7/17 and Can.12 only small *Reticulofenestra* spp. (~60%) and small *Gephyrocapsa* spp. (~40%) coccoliths were identified. In samples S.23.9/2, S.25.9/3, S.25.9/2 and S.12/7/3, apart from small *Reticulofenestra* spp. (~45%) and small *Gephyrocapsa* spp (~33%), *E. huxleyi* specimens were relatively scarce (5-8% of the total assemblage), but consistently present.

7 Statistical analysis

7.1 Two way cluster analysis

Foraminiferal assemblages were subjected in to two-way cluster analysis (Q-mode, R-mode) to delineate biofacies and their occurrence, revealing three distinctive clusters (see also Pallikarakis et al., in press) (I, II, III) (Figs 7-1, 7-2). Cluster II and III have stronger correlation with each other than cluster I. R-mode analysis also delineates three distinctive Groups (A, B, C). Group A (*Ammonia tepida, Haynesina* spp, and *Elphidium granosum*) and Group B (*Elphidium crispum*, miliolids, *Ammonia beccarri, Cibicides refulgens* and *Rosalina bradyi*) have a stronger correlation than Group C (*Elphidium complanatum, Discorbis* spp., *Planorbulina mediterranensis, Asterigerinata* spp. and *Lobatula lobatula*). Two way cluster analysis allows a separation between those species that are more abundant and common in lagoonal environments (Group A) from those that prevail in shallow marine environments (Group C). Q- and R- mode analysis allowed the recognition of three biofacies (lagoonal Group A/Cluster II, transitional Group A/B with Cluster III and shallow marine Group B/C with cluster I). Distinct clusters are also described through multi-dimensional scaling (MDS) diagram (Fig. 7-3).

Furthermore, the presence of planktonic foraminiferal abundance recorded at several samples (e.g. Bh-3 35.65 m) despite been low in percentages (up to 4%), offers an additional valuable indicator for depositional depth between 40–80 m (Israel coast; Avnaim-Katav *et al*., 2013) confirming relatively deeper marine environments.

7.1.1 Cluster I (shallow marine assemblage, fresh water influence) Group B/C

The first biofacies is identified by Q-mode cluster I and R-mode Groups A and B (Figs 7-1, 7-2). R-mode Groups A and B combined indicated transitional conditions between lagoonal and shallow marine environments. The significant abundance of species tolerate to low salinity, salinity fluctuations or both (as *A. tepida* and *A. beccarri*) (Triantaphyllou et al., 2003, 2010; Melis and Violanti, 2006; Ruiz et al., 2006; Pavlopoulos et al., 2007), associated with the intense presence of miliolids, *C. refulgens* and *R. bradyi* that occupy the infralittoral and upper circalittoral zones (Sgarrella and Moncharmont Zei, 1993; Moulfi- El-Houari et al.,1999; Koukousioura et al., 2012), indicate shallow marine with freshwater input conditions. The latter is also indicated by the high A-ratio recorded values. Therefore Cluster I/Group A/B foraminiferal assemblage points to a transitional zone from lagoonal to shallow marine paleoenvironment and a mean depth of approximately 20–40 m.

7.1.2 Cluster II (shallow marine assemblage) Group A/C

The second biofacies is identified by Q-mode cluster II and R-mode Group B / Group C. Group B consists of a considerable variety of taxa dominated by *A. beccarii, R. bradyi, C. refulgens, E. crispum* and miliolids (Figs 7-1, 7-2). The high abundance of *A. beccarii*, combined with the constant presence of *E. crispum* implies resistance to lower salinities and/or salinity fluctuations (Triantaphyllou et al., 2003, 2010; Melis and Violanti, 2006; Ruiz et al., 2006; Pavlopoulos et al., 2007). However the widespread presence of infralittoral and circalittoral taxa (*e.g., C. refulgens, R. bradyi, miliolids*), indicate shallow marine paleoenvironments within a possible paleodepth of ca. 30 m (e.g., Sgarrella and Moncharmont Zei, 1993; Moulfi- El-Houari et al., 1999; Morigi et al., 2005; Rossi and Horton, 2009; Koukousioura et al., 2012).

Group C consists of a variety of taxa dominated by *E. complanatum, L. lobatula, Asterigerinata* spp., *P. mediterranensis*, *N. terquemi* and *Discorbis* spp.. Jorissen (1988)

suggested mean depositional depths between 30-60 m depth in Adriatic Sea for *Asterigerinata* spp*., C. refulgens* and *R. bradyi*, indicating relatively deeper marine environments. *Neoconorbina terquemi* flourish in a wide variety of depths from very shallow to deeper marine environments. Walker et al. (2011) described *N. terquemi* on inner shelf (~ 15 m depth) to outer shelf (~ 33 m depth) environments in Bermuda. Cosentino et al. (2017) mentions that *L. lobatula* and *P. mediterranensis* are indicative of a more densely vegetated sea-bottom environment and more stable salinity values (open marine conditions), while Van Voorthuysen (1973) mentions that *P. mediterranensis* abounds from <25 to 100 m depth in Piraeus, Greece.

Therefore, Cluster II–Group B/C foraminiferal assemblage indicates a mean depth of approximately 40 m.

7.1.3 Cluster III (lagoon assemblage) Group B

The second biofacies is identified by Q-mode cluster III and in R-mode Group A (Figs 7-1, 7-2). Group A is characterized species showing slightly similar ecological traits while R-mode consists of *A. tepida, H. depressula* and *E. granosum* foraminiferal species. *A. tepida*, which is the dominant species in Group A, is an opportunistic taxon that tolerates a wide range of salinity and temperature in nearshore, shallow marine, lagoonal and deltaic zones (e.g. Debenay et al., 2005; Frontalini et al., 2009; Goiran et al., 2011; Koukousioura et al., 2012). *H. depressula* is a species also tolerant of restricted conditions (e.g. Debenay and Guillou, 2002; Carboni et al., 2010). Furthermore, *E. granosum* has been reported from lagoonal and shallow-marine settings (e.g., Albani and Serandrei Barbero, 1990; Bellotti et al., 1994). Smaller and thin-walled tests thrive in low salinity conditions (e.g., Debenay et al., 1996; Melis and Violanti, 2006; Koukousioura et al., 2012); this is also evidenced in samples with high A-ratio values.

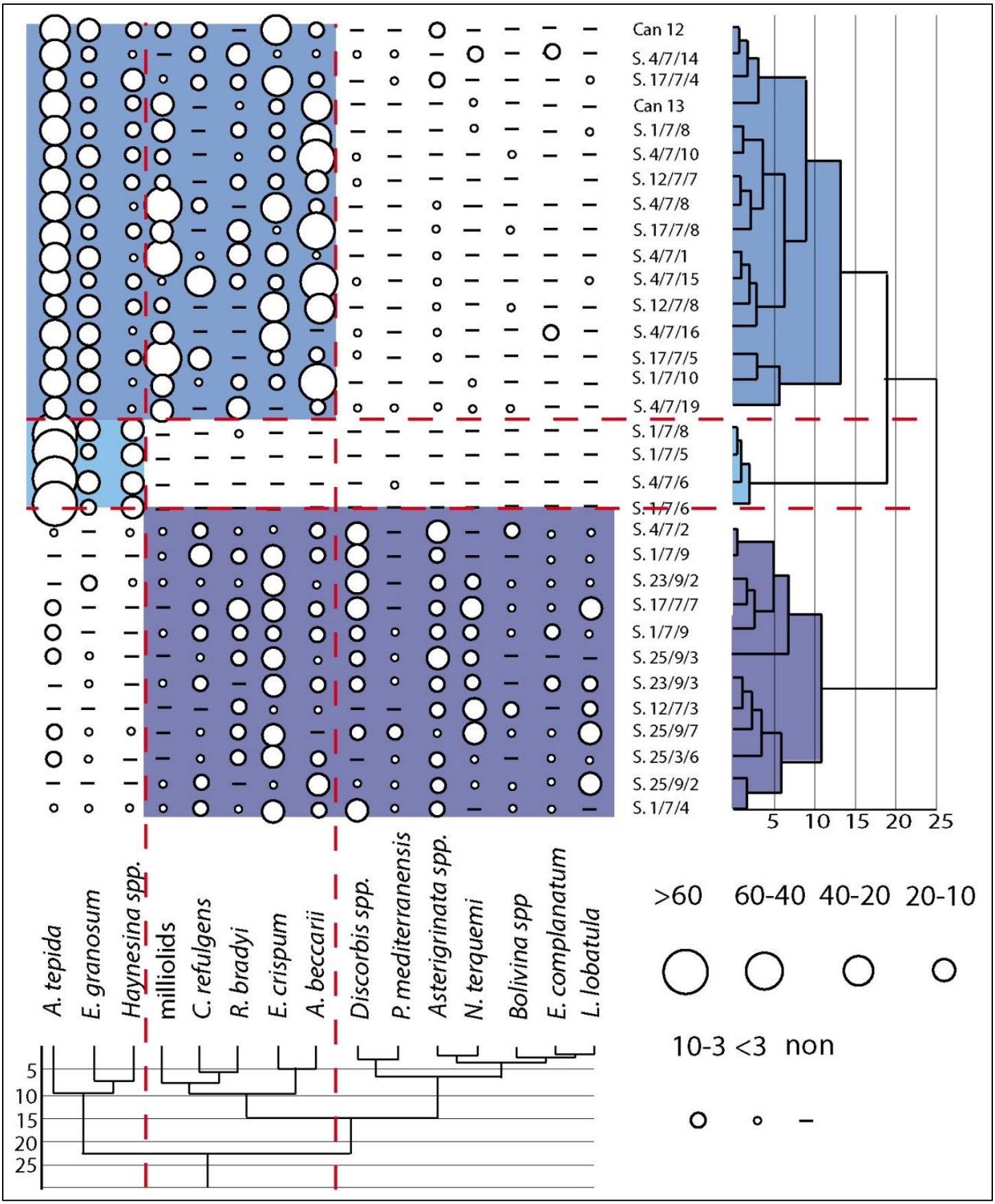
Can 12
S. 4/7/14
S. 17/7/4
Can 13
S. 1/7/8
S. 4/7/10
S. 12/7/7
S. 4/7/8
S. 17/7/8
S. 4/7/1
S. 4/7/15
S. 12/7/8
S. 4/7/16
S. 17/7/5
S. 1/7/10
S. 4/7/19
S. 1/7/8
S. 1/7/5
S. 4/7/6
S. 1/7/6
S. 4/7/2
S. 1/7/9
S. 23/9/2
S. 17/7/7
S. 1/7/9
S. 25/9/3
S. 23/9/3
S. 12/7/3
S. 25/9/7
S. 25/3/6
S. 25/9/2
S. 1/7/4
5 10 15 20 25
A. tepida
E. granosum
Haynesina spp.
milliolids
C. refulgens
R. bradyi
E. crispum
A. beccarii
Discorbis spp.
P. mediterranensis
Asterigrinata spp.
N. terquemi
Bolivina spp
E. complanatum
L. lobatula
5
10
15
20
25
>60 60-40 40-20 20-10
10-3 <3 non

Figure 7-1. *Two-way cluster analysis of foraminiferal species from surface samples based on Q- mode and R-mode (Ward's method and Euclidean distances as a similarity index) which was used to determine species associations and to assess the ecological affinity among different groups. Analyses were applied to 14 taxa that exceeded 3% of the assemblage in at least one sample. Species were grouped into Groups A, B and C and three clusters are highlighted and identified.*
Εικόνα 7-1*. Παρουσίαση της δι-παραμετρικής στατιστικής ανάλυσης των επιφανειακών δειγμάτων, με βάση την οποία έγινε και ο οικολογικός προσδιορισμός των δειγμάτων. Η ανάλυση έγινε σε 14 είδη που υπερέβαιναν το 3% του συνόλου σε τουλάχιστον ένα δείγμα. Τα είδη ομαδοποιήθηκαν στις ομάδες A, B και C και στις ομάδες I, II,, III*

Morigi et al. (2005) based on Jorissen (1988) suggested a 0-20 m with a mean depth at 10 m bathymetrical range for *A. tepida* in lagoonal sites from the Adriatic Sea, whereas Di Bella et al. (2008) indicated that *E. granosum* is an inhabitant of the nearshore zone (7.5–25 m water depth), where it reaches its maximum abundance at about 25 m water depth. Therefore, Cluster III/Group A foraminiferal assemblage points to a mean depositional depth shallower than 20 m. Furthermore, in samples where the presence of *A. tepida* was dominant, even shallower (~10 m depth) and less saline conditions are implied.

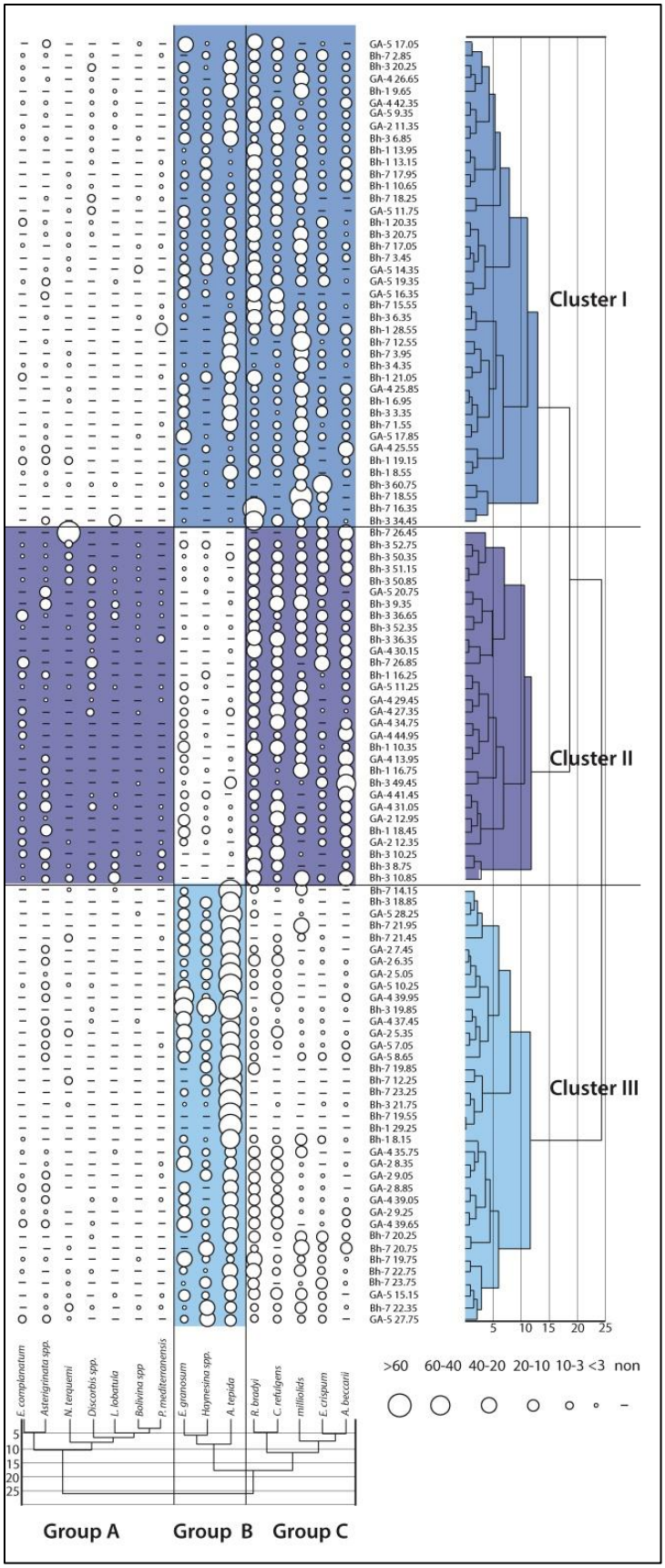

***Figure 7-2**. Two-way cluster analysis of foraminiferal species in boreholes based on Q- mode and R-mode (Ward's method and Euclidean distances as a similarity index) which was used to determine species associations and to assess the ecological affinity among different groups. Analyses were applied to 14 taxa that exceeded 3% of the assemblage in at least one sample. Species were grouped into Groups A, B and C and three clusters are highlighted and identified.*

***Εικόνα 7-2.** Παρουσίαση της δι-παραμετρικής στατιστικής ανάλυσης των δειγμάτων από τις γεωτρήσεις, με βάση τν οποία έγινε και ο οικολογικός προσδιορισμός των δειγμάτων. Η ανάλυση έγινε σε 14 είδη που υπερέβαιναν το 3% του συνόλου σε τουλάχιστον ένα δείγμα. Τα είδη ομαδοποιήθηκαν στις ομάδες A, B και C και στις ομάδες I, II,, III*

Non-Metric Multidimensional analysis performed based on same similarity matrix of the hierarchical clustering described before, also indicates a separation into three groups (Clusters I, II, III). Low 2D stress value suggests a valid separation among the separated groups (Fig. 7-3).

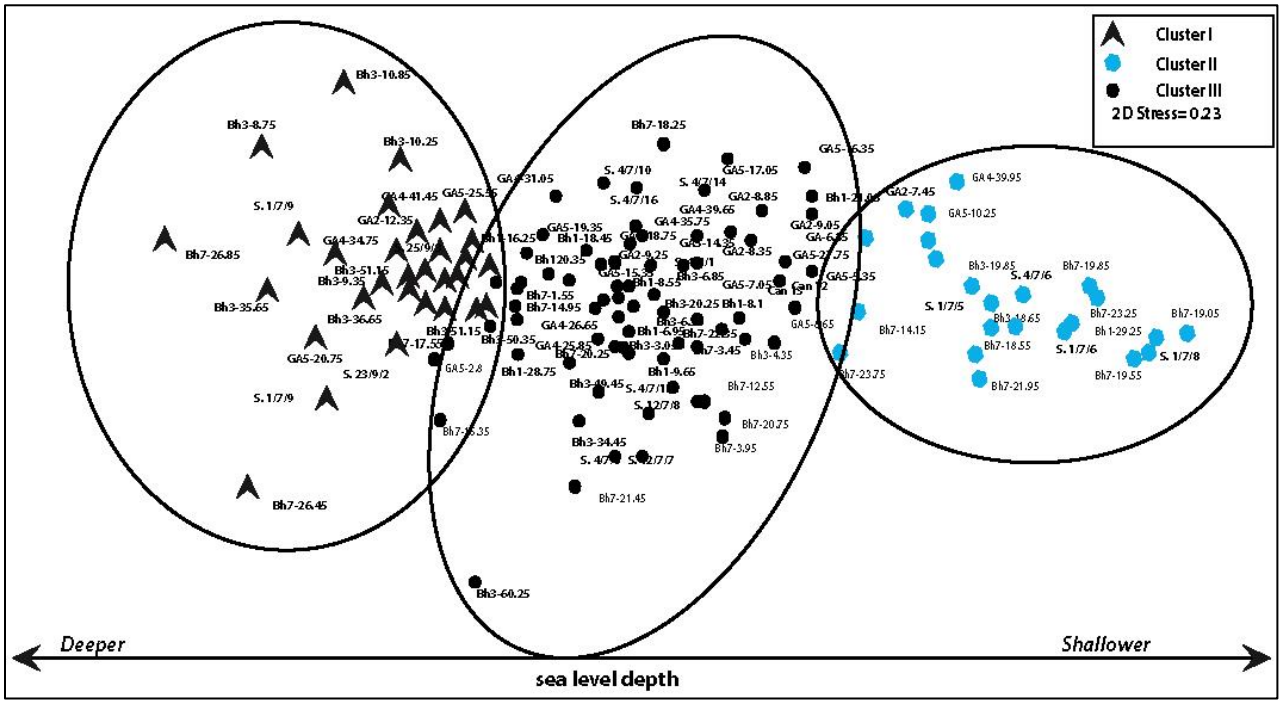

Figure 7-3. *Non-metric multi-dimensional scaling (MDS) illustration in two dimensions computed using the Wards similarity matrix of the hierarchical clustering, showing relatively good separation of the three assemblages. A partial overlap between the assemblages is notable, a logical outcome considering that Cluster III is described as a transition between shallow marine (Cluster I) to lagoonal environment (Cluster III).* ***Εικόνα 7-3.*** *Μη παραμετρική ανάλυση (MDS) των δειγμάτων που αναλύθηκαν που δείχνει σχετικά καλή ομαδοποίηση των δειγμάτων.*

7.2 Magnetic Susceptibility Analysis

MS measurements show a clear difference between fine marine sediments and coarse terrestrial sediments (Table 14, Fig. 7-4). Higher values are measured at gravely layers (mean value 233.3×10^{-5} (SI units)), while clayey and sandy layers demonstrated significantly lower (11.3×10^{-5} (SI units) and 40.8×10^{-5} (SI units) respectively. Marine sediments demonstrated low mean values, shallow marine sediments at ~22.6×10^{-5} (SI units) (Cluster II), lagoonal sediments 12.8×10^{-5} (SI units) (Cluster III and the sediments indicating a transitional from lagoonal to shallow marine paleoenvironment (Cluster I) demonstrate a mean value 26.2×10^{-5} (SI units). Sediments described as fluvial/upper shoreface demonstrate higher values (201.8×10^{-5} (SI units)) as was expected.

Based on the One-Sample Kolmogorov-Smirnov Test results (normal distribution (e.g. Hülle et. al., 2010)), the Pearson correlation test is considered as the most appropriate for examining the correlation of the MS values among the different lithologies and paleoenvironments which were described.

Table 14. The mean values of the measured magnetic susceptibility. The One-Sample Kolmogorov-Smirnov Test values are less than 0.05 suggesting a normal distribution of the MS values. Πίνακας 14. Οι μέσες τιμές της μαγνητικής επιδεκτικότητας. Μέσω στατιστικής ανάλυσης προσδιορίστηκε η κανονική κατανομή των μετρήσεων.

	clay	sand	gravels	Shallow marine	Lagoon	Transitional zone	Coastal/ upper shoreface/ fluvial
Mean value×10^{-5} (SI units)	11.3	40.8	233.3	22.6	12.8	26.2	201.8
One-Sample Kolmogorov-Smirnov Test	.000	.000	.003	.000	.000	.000	.000

The significance of Pearson analysis correlation is also displayed in table 15, marked as one* ($p<.0.05$) or two** ($p<0.01$) asterisks. The significance level (or p-value, where the lower values indicate higher significance) is the probability of obtaining results which are strongly correlated. If the significance level value is less than 0.05 then the correlation is significant and the two variables are linearly related. If the significance level value is relatively higher (for example 0.30) then the correlation is not significant and the two variables are not strongly related.

Pearson analysis indicates a positive and significant correlation between the low MS values in clay sediments and shallow marine sediments; and a positive correlation between non-marine sediments with gravels (two asterisks**) (Table 15). A positive correlation between the MS values of sandy layers and the transitional sediments is also indicated. Finally, there is a negative correlation between the MS values of gravels with the marine sediments, as well as a negative correlation of the MS values between fine sediments and terrestrial sediments.

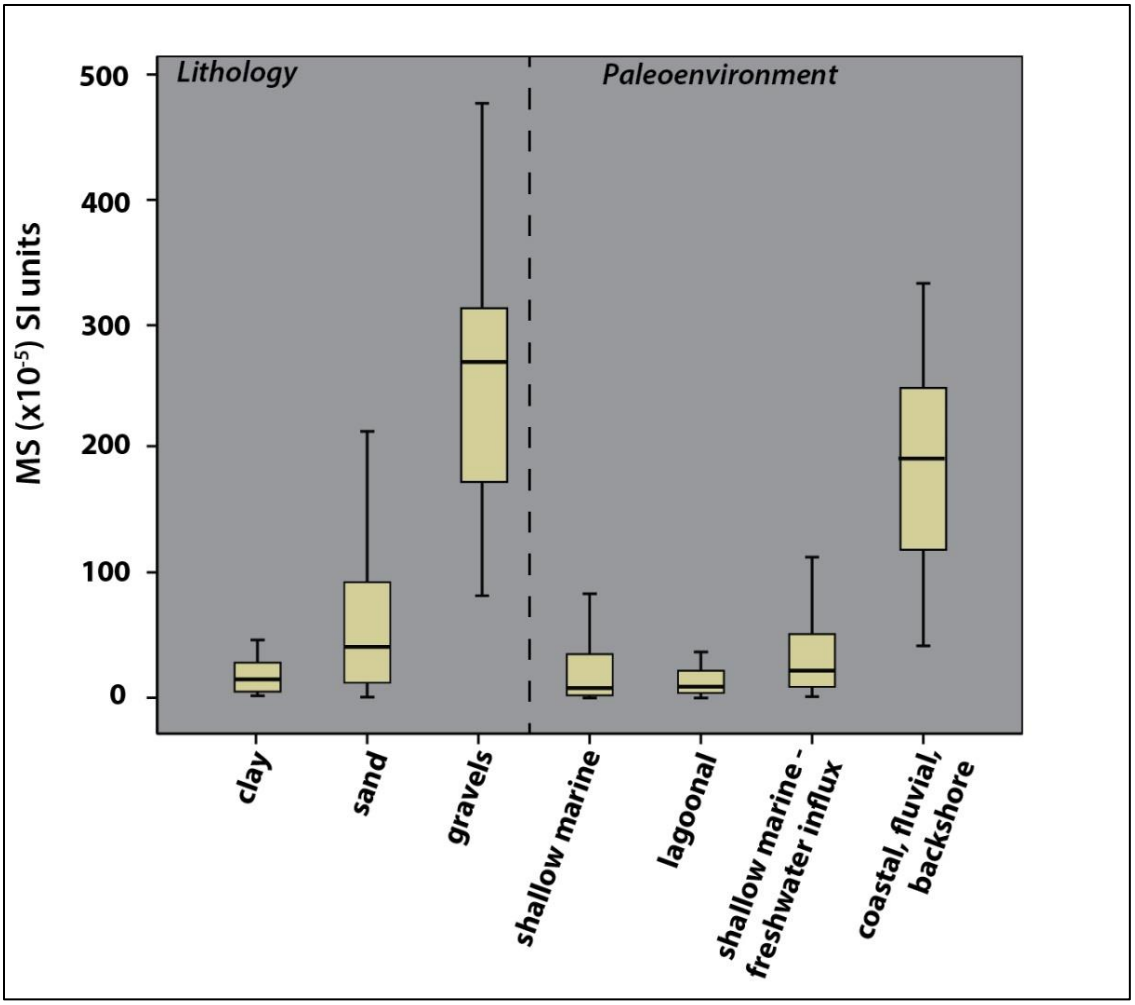

Figure 7-4. *The mean values of the MS signal based on the different lithologies and the paleoenvironmental alternations described within the boreholes.*
Εικόνα 7-4. *Οι μέσες τιμές της μαγνητικής επιδεκτικότητας σε σχέση με το παλαιοπεριβάλλον και τις λιθολογίες μέσα στις γεωτρήσεις.*

Table 15. The correlation (from -1 for negative to +1 for positive correlation) of the described MS values based on different lithologies and paleoenvironments within the borehole cores (Pearson analysis). Πίνακας 15. Η συσχέτιση (από -1 για αρνητική έως +1 για θετική) των τιμών μαγνητικής επιδεκτικότητας με τις λιθολογίες και το παλαιοπεριβάλλον.

	Clay	Sand	Gravels	Shallow marine	Lagoon	Transitional zone	Coastal/ upper shoreface/ fluvial
Clay	1	-.064	-.084	.278*	-.061	-.010	-.185*
Sand	-.064	1	-.190	-.167	-.069	.260**	-.113
Gravels	-.084	-.190	1	-.246*	-.080	-.133	.251**
Shallow marine	.278*	-.167	-.246*	1	-.056	-.139	.142
Lagoon	-.061	-.069	-.080	-.056	1	-.215	-.133
Transitional zone	-.010	.260**	-.133	-.139	-.215	1	-.162
Coastal/ upper shoreface	-.185*	-.113	.251**	.142	-.133	-.162	1

Statistical analysis has revealed a correlation between relatively low MS values with low energy environments and relatively high MS values with high energy environments. The latter proved to be a significant factor during the detailed paleoenvironmental description of the borehole cores, acting as an independent physical parameter of the sediments. Furthermore, in samples where foraminifera were relative scarce, the MS

values assisted to the safer description of the paleoenvironment (e.g. the lower part of borehole Bh-7 which was eventually described as lagoonal)

8 *Paleoenvironmental interpretation*

8.1 Surface samples

Based on the described sedimentary facies and the micropaleontological analysis in samples extracted from surface outcrops, the paleoenvironmetal description of the study area was feasible (Fig. 8-1). Samples with no or few specimens extracted from coarse grained sediments were indicative for high-energy environments (fluvial/backshore conditions). Layers with fine grained sands and clays indicate low-energy lagoonal to shallow marine paleoenvironments, based on the hierarchical cluster and MDS analysis (Figs 7-1, 7-3). Furthermore, ostracods specimens described in fine grained marls indicate brackish-oligohaline conditions partially influenced by marine waters (lagoonal paleoenvironment).

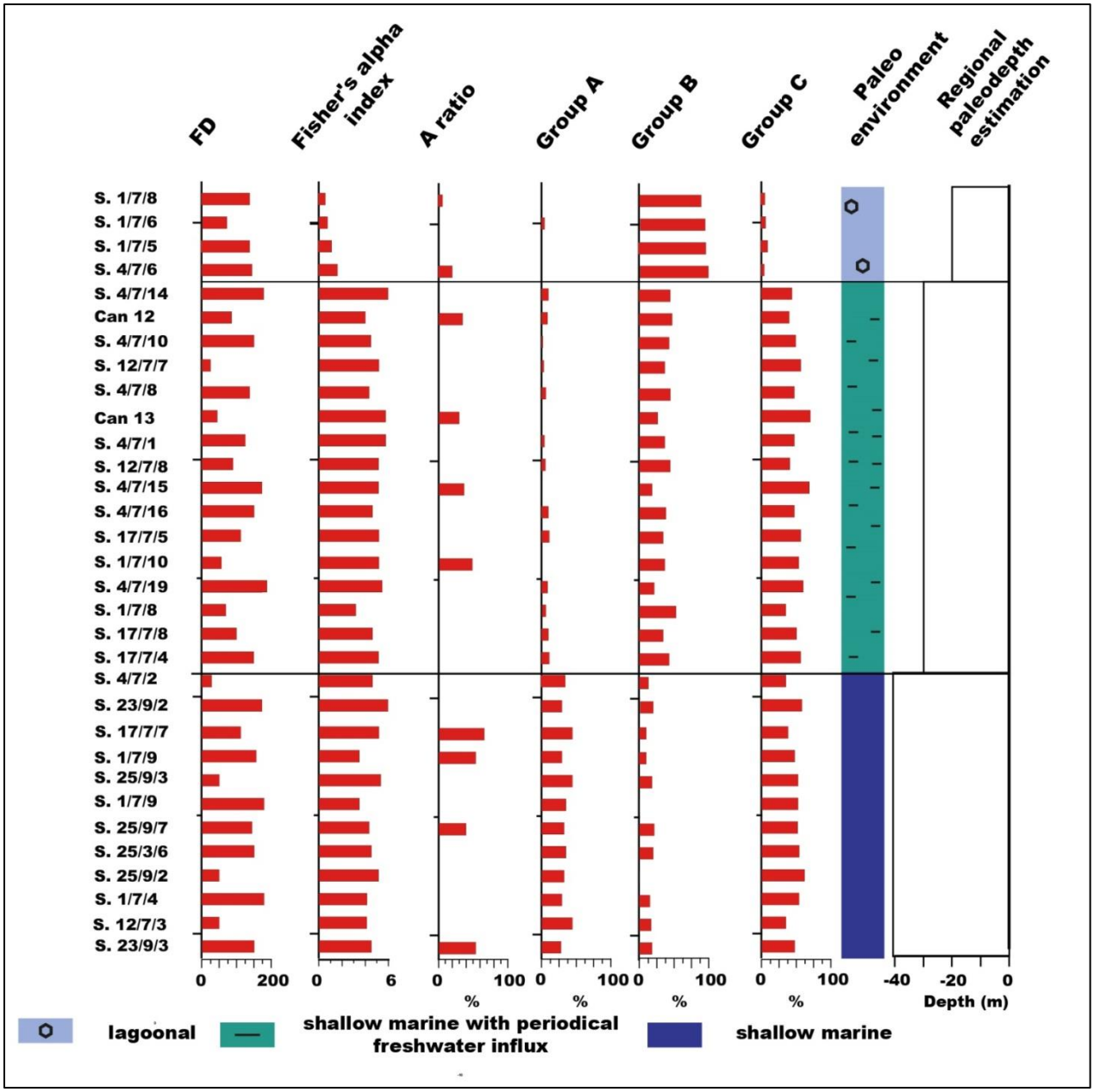

Figure 8-1. *Diagram showing the paleoenvironmetal estimation in samples extracted from surface outcrops based on the counted foraminifera per gram (FD), BR-ratio, Fisher's alpha index, A-ratio, Group A, B and C relative abundances the regional paleodepth estimation based on foraminiferal assemblages.*
Εικόνα 8-1. *Σχεδιάγραμμα που απεικονίζει το παλαιοπεριβάλλον και το εκτιμώμενο παλαιοβάθος στα επιφανειακά δείγματα, με βάση την ανάλυση των δειγμάτων και τους δείκτες FD, BR-ratio, Fisher's alpha index, A-ratio, Group A, B and C.*

8.2 Borehole Bh-1

In Bh-1 from 31.00 to 29.70 m depth gravels and coarse sands indicate a high-energy depositional environment (Fig. 8-2). Considering as well the absence of micro fauna and the high MS values (>200x10^{-5}) (e.g. Ghilardi et al., 2008) this layer is ascribed to a nearshore coastal to upper shoreface paleoenvironment. From 29.70 to 29.10 m depth fine sediments are correlated with low-energy lagoonal paleoenvironment based as well on the presence of lagoonal foraminiferal assemblages (Cluster III/Group B) and the low MS values. The dominance of *A. tepida* (Fisher's alpha index ~ 0.3) indicates a regional paleodepth < 10 m. From 29.10 to 27.20 m combined presence of both Groups B and C (Cluster I) suggests transitional conditions between lagoonal and shallow marine environments. The gravely interval 27.20–22.60 m depth is characterized by high MS values, high BR-ratio (~40%) and low FD–index (2< forams/gram) indicating a nearshore to fluvial/upper shoreface paleoenvironment. Fine sediments from 22.60–12.50m depth with the combined presence of both Groups A and C (Cluster II) foraminiferal assemblages suggest shallow marine paleoenvironment (~40 paleodepth).

The lower and upper part of this interval is characterized by transitional conditions between lagoonal and shallow marine paleoenvironment (regional paleodepth estimation ~30 m). These layers are also characterized by lower BR-ratio and relatively low MS values. From 12.50 to 11.20 m depth coarse layers indicate high-energy depositional environment even though that MS values are relatively low. The relatively low FD- index (2< forams/gram) with high BR-ratio values (~35%) indicate nearshore to upper shoreface paleoenvironment. The interval 11.20–6.50 m depth is characterized by the combined presence of both Groups B and C (Cluster I) foraminiferal assemblages, with low BR-ratio (<5%), MS values (~20x10^{-5}) and A-Fisher index, indicating transitional paleoenvironmental conditions (regional paleodepth ~30 m); interrupted by the interval 8.20-7.50 m depth where the dominance of Group B/Cluster III foraminiferal assemblages indicate shallower paleodepth (<20 m) and lagoonal paleoenvironmental conditions. The upper 6.50 m of the borehole are characterized by

higher MS values (~90x10^{-5}), high BR-ratio (~40%) and low FD (2< forams/gram) indicating a nearshore to fluvial/upper shoreface paleoenvironment.

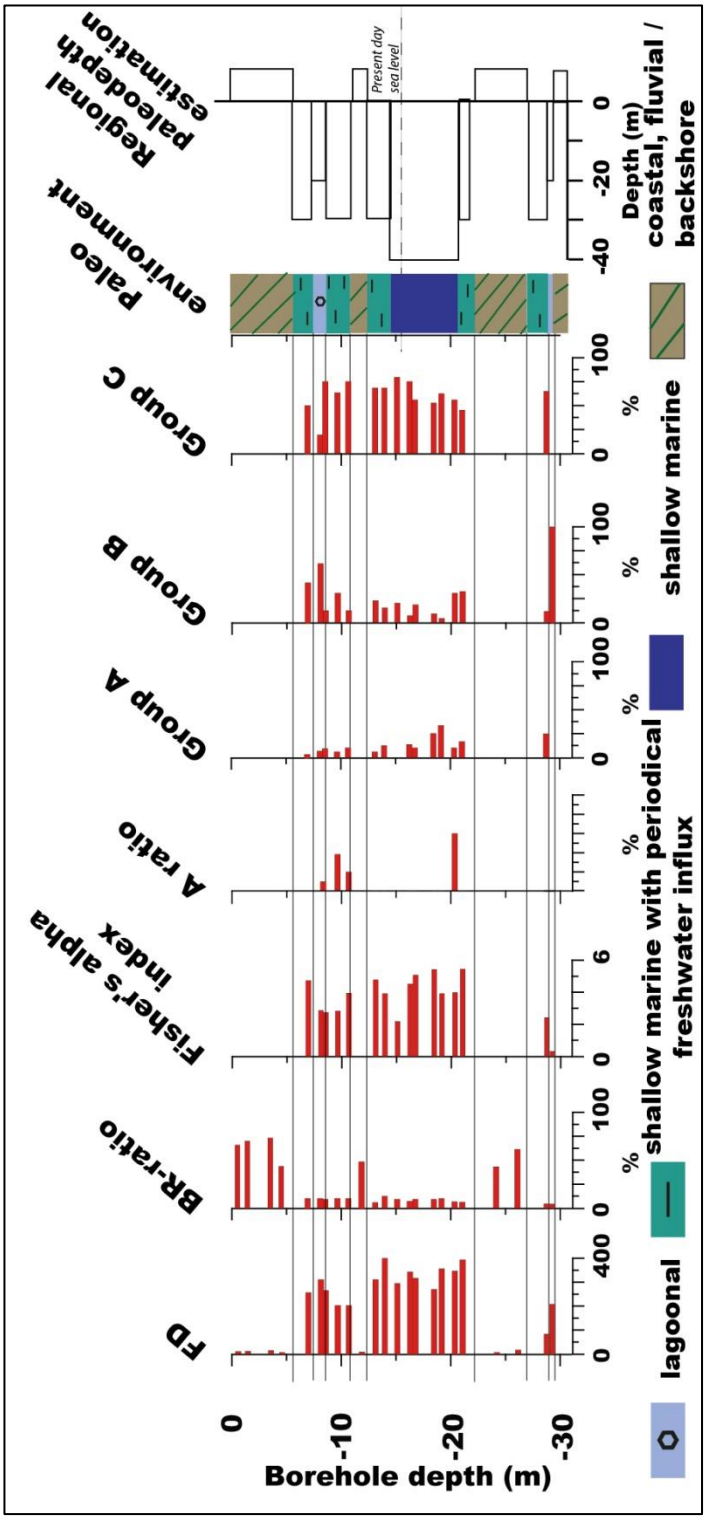

Figure 8-2. *Diagram showing the counted foraminifera per gram (FD), % P, Group A, B and C relative abundance, Fisher's alpha index, A-ratio, BR-ratio, the paleoenvironmetal interpretation in Bh-1 and the regional paleodepth estimation based on foraminiferal assemblages.*

Εικόνα 8-2. *Σχεδιάγραμμα που απεικονίζει το παλαιοπεριβάλλον και το εκτιμώμενο παλαιοβάθος στην γεώτρηση Bh-1, με βάση την ανάλυση των δειγμάτων και τους δείκτες FD, BR-ratio, Fisher's alpha index, A-ratio, Group A, B and C.*

8.3 Borehole Bh-3

In Bh-3 from the 70.20‑66.50 m core depth, gravels and coarse sands indicate a high energy depositional environment. Considering the absence of microfauna as well, this layer is described as coastal nearshore paleoenvironment. From the 66.50–60.00 m core depth, clayey to sandy layers indicate shoreface low-energy environments. The presence of numerous ostracod *Cyprideis* spp. values from the 66.50–61.50 m core depth is indicative of an oligohaline lagoonal paleoenvironment (*e.g.*, Ben Rouina *et al.,* 2016), whereas from the 61.50–60.00 m core depth, the presence of foraminiferal groups B and C (cluster I) suggests transitional settings between lagoonal and shallow marine paleoenvironments. These layers are also characterized by lower BR-ratio and relatively low MS values. *Cladocora caespitosa* specimens found in the 60.00–61.50 m core depth interval support depositional depths between 0 and 20 m and rarely below 30 m depth (*e.g*., Peirano *et al*., 1994).

From the 60.00–54.50 m core depth, coarse sand layers indicate a high-energy depositional environment. Even though MS values are relatively low, the relatively low FD-ratio (<2 forams/g) with the high BR-ratio values (~35%), point toward a nearshore coastal to upper shoreface paleoenvironment. From the 54.50‑49.60 m core depth, sandy layers indicate a low-energy depositional environment, also supported by the low BR-ratio, the relatively high A - ratio and Fisher’ s alpha index, and the relatively low MS. The micropaleontological analysis suggests transitional settings between lagoonal and shallow marine paleoenvironments (Fig. 8-3) based on the combined presence of foraminifer groups B and C (cluster I), even though the key foraminifer species indicate fully marine conditions (*N. terquemi, Asterigerinata* spp.).

The 49.60‑39.60 m core depth interval of gravelly layers with relatively high MS values with high BR-ratio and low FD are also indicative of nearshore to fluvial/upper shoreface paleoenvironments. From the 39.60‑37.00 m core depth, fine sediments are correlated with low energy lagoonal paleoenvironments because of the monotaxic association of *Cyprideis* spp., a key taxon of oligohaline lagoonal settings (*e.g.,* Ben Rouina *et al.*,

2016). Shallow marine paleoenvironments are documented at the 35.00-37.00 m core depth, featured by the group A/C foraminiferal assemblage (cluster II) and the presence of planktonic foraminifera that indicates a depositional depth of approximately 40 m, whereas at the 34.00-35.00 m core depth, the group B/C foraminiferal assemblage (cluster I) suggests transitional settings between lagoonal and shallow marine environments (Fig. 8-3).

From the 34.00-22.40 m core depth, the described coarse sand and gravel layers with ophiolite fragments and relatively high MS values (up to 200 × 10−5 SI units) (*e.g*., Ghilardi et al., 2008), and the high BR-ratio/low FD-ratio values, indicate a nearshore to fluvial/upper shoreface paleoenvironment. From the 22.40-21.00 and 20.00-16.50 m core depths, a lagoon paleoenvironment is described, as evidenced by the dominance of the group B assemblage (cluster III) in relation to the low Fisher's alpha index and A-ratio foraminifer values, indicating water depths of <20 m. In sample Bh-3, 21.75 m, the high abundance of *A. tepida* (~92%) indicates even shallower conditions (<10 m depth) (Morigi *et al*., 2005). Within the 20.00-21.00 m core depth interval, microfossil inferences (cluster I, regional paleodepth 20–40 m) coupled with the relatively high Fisher's alpha index and A-ratio values and the presence of *C. caespitosa* (considering that corals live from 0 to 20 m water depth and rarely till 30 m water depth (*e.g*., Peirano et al., 1994); a shallow marine setting of between 20 and 30 m water depth is described. Since corals prefer not muddy but harder substratum to grow, the presence of in situ Cladocora corals and lagoonal sediments indicates relatively rapid changes to the paleoenvironmetal conditions, where the identified corals could be described as a thanatocoenosis. From the 16.50-11.00 m core depth, reddish clay, coarse-grained deposits with rootlets, high-BR-ratio values (75 at the 13.00-16.50 m core depth), relatively high MS values (up to 180 × 10^{-5}), and low FD-ratio indicate predominantly subaerial to nearshore coastal conditions. Furthermore, the Corinth Canal offers a unique opportunity to observe the continuation of these exposed strata (Fig. 6-2), where subaerial conditions (paleosoil) marked by an erosional surface are observed. The described paleosoil horizons strongly indicate that between the lagoonal and the shallow marine sediments, the Corinth Isthmus area was emerged (terrestrial

paleoenvironment). The 11.00–3.30 m core depth interval, however, is characterized by fine sediments correlated with low-energy environments. Cluster II (combined presence of both groups A and C) suggests a shallow marine environment, also documented by a low BR ratio and MS values and a high FD-ratio, whereas cluster I (with a combined presence of both groups B and C), suggests transitional conditions between lagoonal and shallow marine environments, also documented by a low BR-ratio and MS values and a high FD-ratio. The upper part of the borehole (the 0–3.30 m core depth) is characterized by coarse material with higher MS values and BR-ratio, which is associated with a high-energy environment (nearshore coastal).

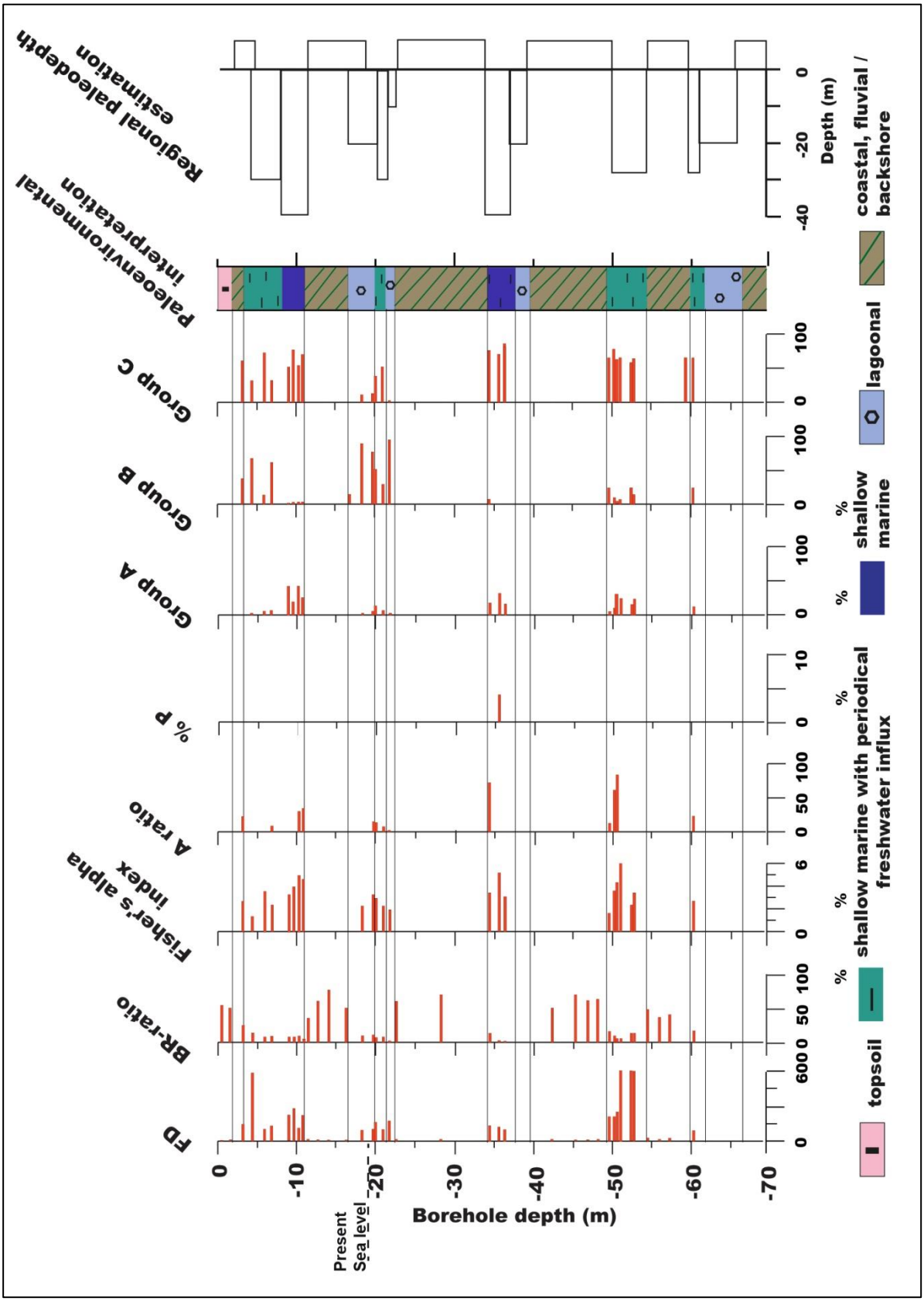
Regional paleodepth estimation
Depth (m)
0
-20
-40
Paleoenvironmental interpretation
coastal, fluvial / backshore
lagoonal
shallow marine
shallow marine with periodical freshwater influx
topsoil
Group C
Group B
Group A
% P
A ratio
Fisher's alpha index
BR-ratio
FD
0
100
600
50
6
10
%
Present Sea level
Borehole depth (m)
0
-10
-20
-30
-40
-50
-60
-70

Figure 8-3. *Counted foraminifera per gram (FD), % P, Group A, B and C relative abundance, Fisher's alpha index, A-ratio, BR-ratio, the paleoenvironmetal interpretation in Bh-3 and the regional paleodepth estimation based on foraminiferal assemblages.* ***Εικόνα 8-3.*** *Σχεδιάγραμμα που απεικονίζει το παλαιοπεριβάλλον και το εκτιμώμενο παλαιοβάθος στην γεώτρηση Bh-3 με βάση την ανάλυση των δειγμάτων και τους δείκτες FD, BR-ratio, Fisher's alpha index, A-ratio, Group A, B and C.*

8.4 Borehole Bh-7

In borehole Bh-7 (Fig. 8-4) the interval 56.00–49.00 m depth clayey to sandy layer indicates low energy environments. The presence of numerous ostracods Cyprideis spp. valves is indicative for oligohaline lagoonal paleoenvironment (e.g. Ben Rouina et al., 2016). From 49.00 to 45.00 m depth coarse sediments indicate high-energy depositional environment. Considering as well the absence of micro fauna this layer is correlated with nearshore coastal or upper shoreface paleoenvironment. The deformation zone of the Kalamaki-Isthmia fault is described from 45.00 to 33.00 m depth. At the interval from 33.00 to 27.00 the gravely layers characterized by relatively high MS values, high BR-ratio and low FD also indicates nearshore to fluvial/upper shoreface paleoenvironments. The interval from 27.00 to 26.00 m depth on the contrary is characterized by sediments correlated to low-energy environments. Cluster II (combined presence of both Groups A and C) suggests shallow marine environment also documented by low BR-ratio, MS values and high FD-index (estimated regional paleodepth ~40 m).The interval from 26.00 to 24.00 the gravely layers characterized by relatively high MS values, high BR-ratio and low FD also indicates nearshore to fluvial/upper shoreface paleoenvironments. The interval from 24.00 to 19.00 m depth lagoon paleoenvironment is described evidenced by the dominance of Group B assemblage (Cluster III) in relation with the low Fisher's alpha index and A-ratio values, indicating depositional depths shallower than 20 m. The interval 19.00 m to 16.00 m depth the combined presence of both Groups B and C (Cluster I) suggests transitional conditions between lagoonal and shallow marine environments while relatively high

Fisher's alpha index values and A-ratio values are documented. Furthermore considering that *Cladocora caespitosa* corals live from 0 to 20 m water depth and rarely till 30 m water depth (e.g., Peirano et al., 1994); a shallow marine setting of between 20 and 30 m water depth is described. Since corals prefer not muddy but harder substratum to grow, the presence of in situ *Cladocora* corals and lagoonal sediments indicates relatively rapid changes to the paleoenvironmetal conditions, where the identified corals could be described as a thanatocoenosis. From 16.00 to 12.00 m depth the paleoenvironment is also described as lagoonal evidenced by the dominance of Group B assemblage (Cluster III) in relation with the low Fisher's alpha index and A-ratio values, indicating depositional depths shallower than 20 m.

From 12.00 m to 5.50 m depth reddish clay, coarse sand with rootlets and few gravels indicate almost subaerial conditions. High BR-ratio values (73% at sample Bh-7 8.15 m depth), relatively high MS values (up to $190x10^{-5}$) and low FD-index reinsure that these layers are correlated with high-energy (nearshore to upper shoreface) paleoenvironments. Furthermore, the Corinth Canal offers a unique opportunity to observe the continuation of these strata exposed, where subaerial conditions (paleosoil) marked by erosional surface are observed (Fig. 6-2). This reinsures that during the transition from the lagoonal sediments to shallow marine the area was emerged (terrestrial paleoenvironment). The interval from 5.50 to 1.50 m depth on the contrary is characterized by fine sediments correlated to low-energy environments. Cluster I (combined presence of both Groups B and C) suggests transitional conditions between lagoonal and shallow marine environment (regional paleodepth ~30 m), also documented by low BR-ratio, MS values and high FD-index.

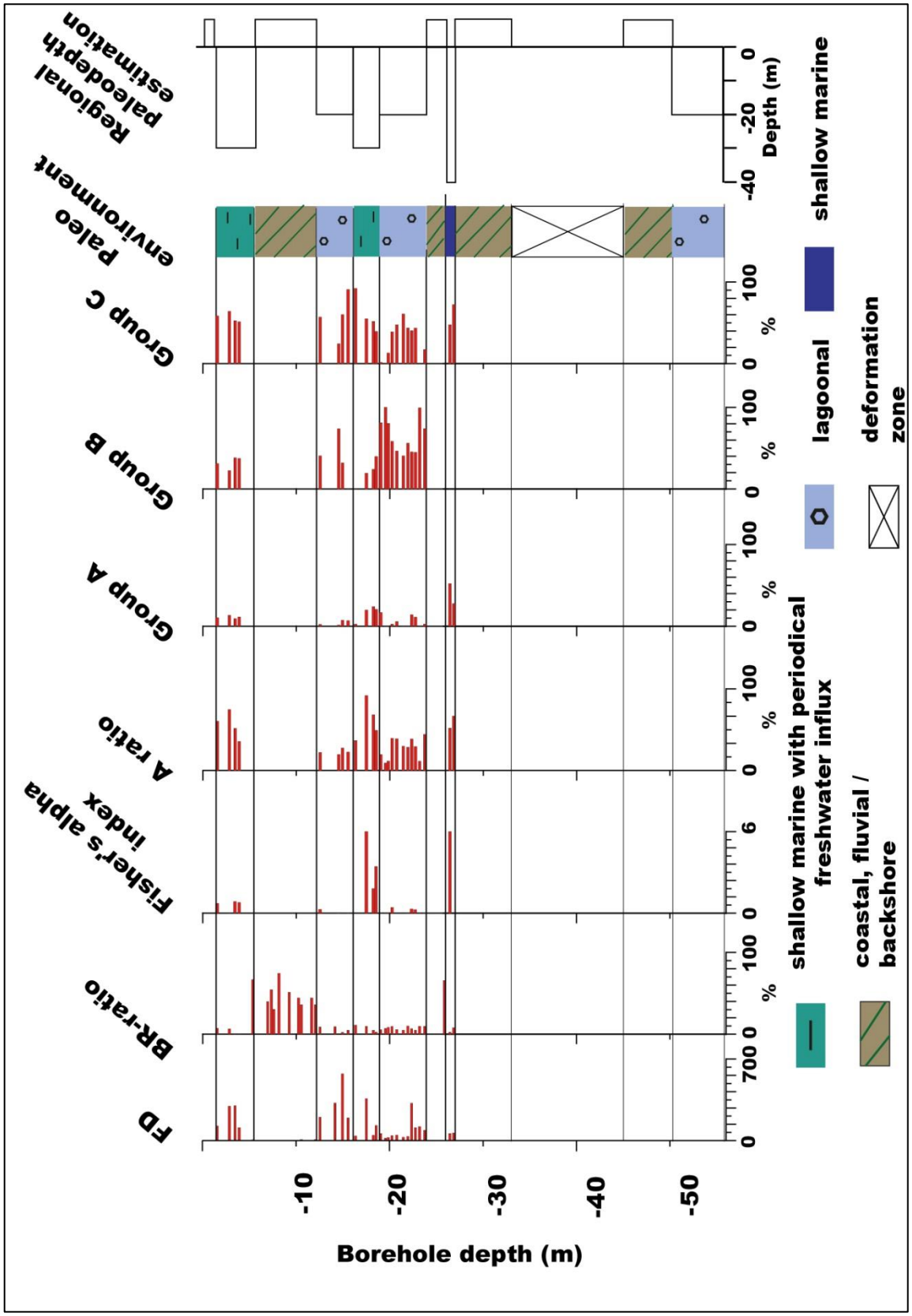
Regional paleodepth estimation
Depth (m)
0
-20
-40
Paleo environment
shallow marine
lagoonal
deformation zone
Group C
Group B
Group A
A ratio
Fisher's alpha index
BR-ratio
FD
%
0
100
6
700
shallow marine with periodical freshwater influx
coastal, fluvial / backshore
-10
-20
-30
-40
-50
Borehole depth (m)

Figure 8-4*. Diagram showing the counted foraminifera per gram (FD), % P, Group A, B and C relative abundance, Fisher's alpha index, A-ratio, BR-ratio, the paleoenvironmetal interpretation in Bh-7 and the regional paleodepth estimation based on foraminiferal assemblages.*

Εικόνα 8-4*. Σχεδιάγραμμα που απεικονίζει το παλαιοπεριβάλλον και το εκτιμώμενο παλαιοβάθος στην γεώτρηση Bh-7 με βάση την ανάλυση των δειγμάτων και τους δείκτες FD, BR-ratio, Fisher's alpha index, A-ratio, Group A, B and C.*

8.5 Borehole GA-2

In borehole GA-2 (Fig. 8-5) the interval from 14.00 to 12.30 m depth is characterized by fine sediments correlated to low-energy environments. The foraminiferal assemblages are dominated by Cluster II (combined presence of both Groups A and C) suggesting a shallow marine environment also documented by low BR-ratio, MS values and high FD-index (estimated regional paleodepth ~40 m). The interval 12.30–9.90 m depth is characterized by Cluster I (combined presence of both Groups Band C) suggesting transitional conditions between lagoonal and shallow marine environment (regional paleodepth ~30 m); also supported by the documented low BR-ratio (<5%), MS values (1–70x 10^{-5} SI units) and the high FD-index. A-ratio varied from ~5 to 22 also indicates a shallow marine with lagoonal features paleoenvironment. The interval 9.90 to 3.80 m depth is dominated by Group B/Cluster III assemblages indicates lagoonal paleoenvironments (regional paleodepth <20 m), also supported by the significant lower A-ratio (1–4). The interval 3.80 to 0.00 m depth is characterized by coarse sands indicating a high-energy depositional environment. Considering as well the absence of micro fauna, this layer is correlated with nearshore paleoenvironment coastal or upper shoreface.

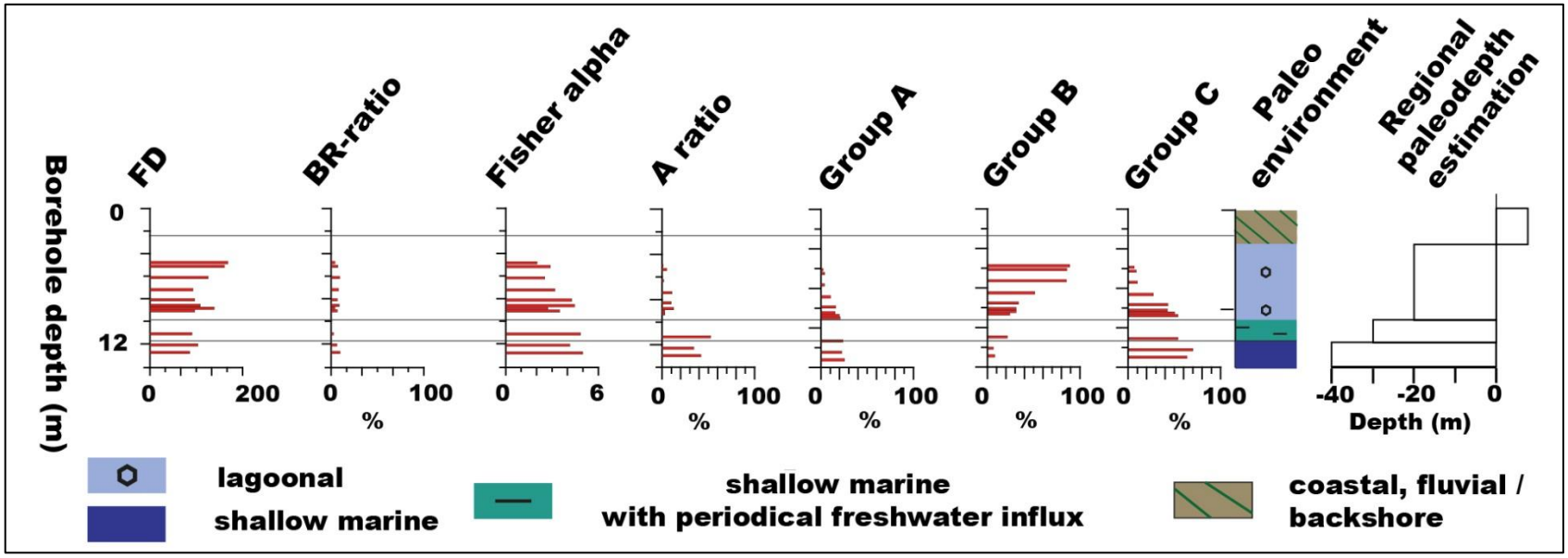

***Figure 8-5**. Diagram showing the counted foraminifera per gram (FD), % P, Group A, B and C relative abundance, Fisher's alpha index, A-ratio, BR-ratio, the paleoenvironmetal interpretation in GA-2 and the regional paleodepth estimation based on foraminiferal assemblages.*

***Εικόνα 8-5.** Σχεδιάγραμμα που απεικονίζει το παλαιοπεριβάλλον και το εκτιμώμενο παλαιοβάθος στην γεώτρηση GA-2, με βάση την ανάλυση των δειγμάτων και τους δείκτες FD, BR-ratio, Fisher's alpha index, A-ratio, Group A, B and C.*

8.6 Borehole GA-4

In borehole GA-4 the interval from 45.50 to 39.00 m depth is characterized by fine sediments correlated to low-energy environments (Fig. 8-6). Till 40.00 m depth Cluster II (combined presence of both Groups A and C) suggests shallow marine environment also documented by the circumstantial presence of full marine species (*Textularia* spp., *Conurbella* spp.) the low BR-ratio (<5%), MS values (1–20 x 10^{-5} SI units) and high FD-index (estimated regional paleodepth ~40 m).From 40.00 to 39.00 m depth the foraminiferal assemblages indicated lagoonal conditions and estimated regional paleodepth ~20 m (Cluster III, Group B). From 39.00 to 38.50 m depth the described coarse sand and gravels layers with the relatively high MS values (173 x 10^{-5} SI units) (e.g. Ghilardi et al., 2008), and the high BR-ratio values / low FD-index indicate a nearshore to fluvial/upper shoreface paleoenvironment. On the contrary the interval 38.50–34.20m depth is characterized by fine sediments correlated to low-energy environments. From 38.50 to 37.00 the dominance of group B/Cluster III assemblages indicates lagoonal paleoenvironments (regional paleodepth <20 m) also documented by low BR-ratio, MS values and high FD-index; while till ~35.00 m depth Cluster I (combined presence of both Groups B and C) suggests transitional conditions between lagoonal and shallow marine environment (regional paleodepth ~30 m). Till 34.20 m depth Cluster II (combined presence of both Groups A and C) suggests shallow marine environment also documented by low BR-ratio, MS values and high FD-index (estimated regional paleodepth ~40 m).

On the contrary the interval 34.20 – 31.20 m core depth is characterized by coarse sand and gravels with the relatively high MS values (up to 260 x 10^{-5} SI units) and the high BR-ratio values (~60%) / low FD-index (3< forams/gram) indicating a nearshore to fluvial/upper shoreface paleoenvironment. The dominance of Cluster III, combined presence of both Groups A and B) also documented by the low BR-ratio (<7%), MS values (4–50 x 10^{-5} SI units) and high FD-index suggests transitional conditions between lagoonal and shallow marine environment (estimated regional paleodepth ~30 m). Approximately at 30.00 m depth the foraminiferal assemblages indicate shallow

marine environment estimated regional paleodepth ~40 m. On the contrary the interval 34.20–31.20 m depth is characterized by coarse sand and gravels with the relatively high MS values (up to 310 x 10^{-5} SI units) and the high BR-ratio values (~40%) / low FD-index (5 < forams/gram) indicate a nearshore to fluvial/upper shoreface paleoenvironment. The interval from 31.20 m to 25.50 m core depth is characterized by fine sediments where Cluster II foraminiferal assemblages (combined presence of both Groups A and C) suggests shallow marine environment also documented by low BR-ratio, MS values and high FD- index (estimated regional paleodepth ~40 m). From 25.50 m to 8.80 m core depth the interval is characterized by coarse sand and gravels with the relatively high MS values (up to 220 x 10^{-5} SI units) and the high BR-ratio values (~45%) / low FD-index (3 < forams/gram) indicate a nearshore to fluvial/upper shoreface paleoenvironment. The upper 8.80 m of the borehole core represent man-made Canal debris and therefore have not been examined at all.

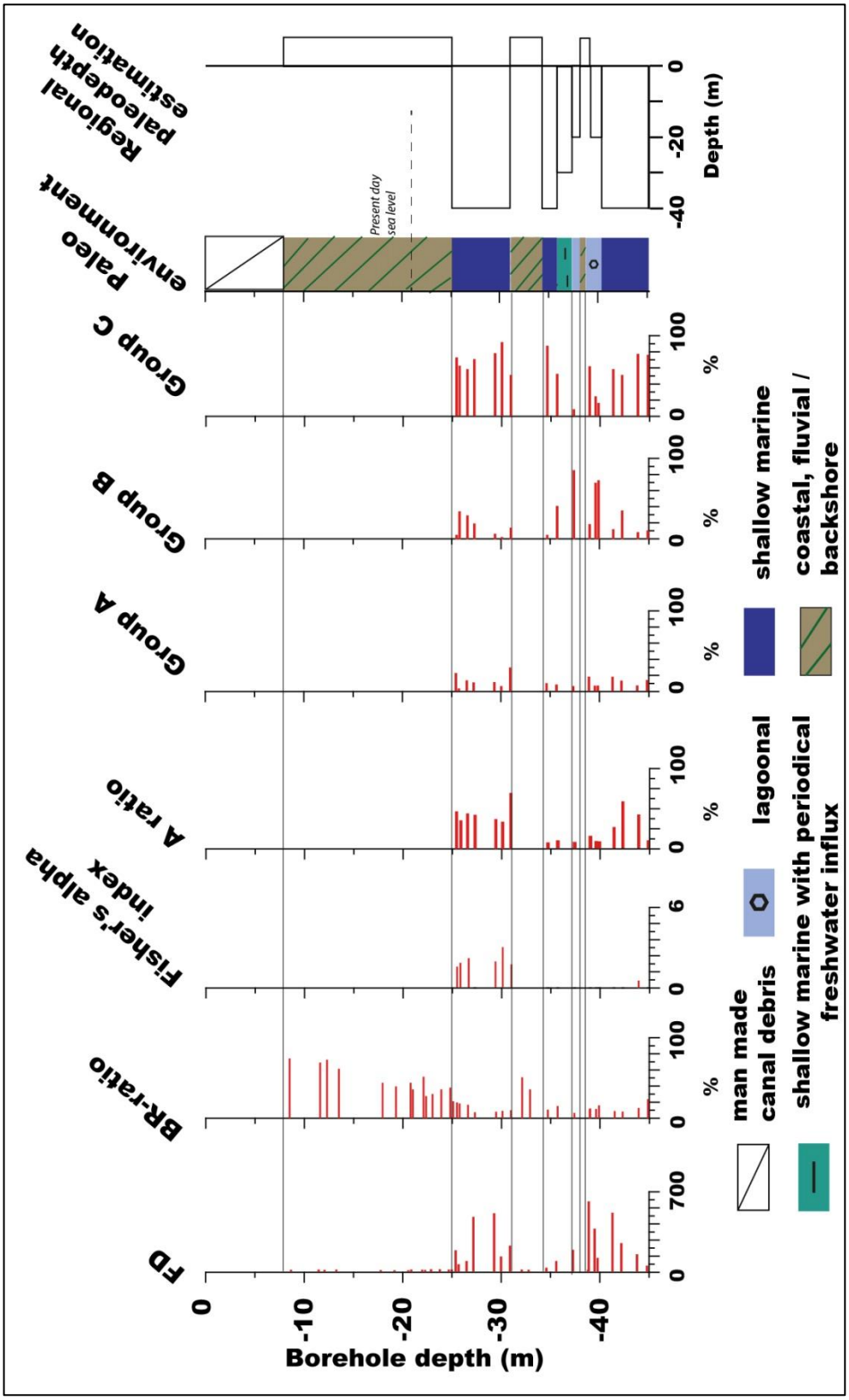

Figure 8-6. *Diagram showing the counted foraminifera per gram (FD), % P, Group A, B and C relative abundance, Fisher's alpha index, A-ratio, BR-ratio and the paleoenvironmetal interpretation in GA-4.*

Εικόνα 8-6. *Σχεδιάγραμμα που απεικονίζει το παλαιοπεριβάλλον και το εκτιμώμενο παλαιοβάθος στην γεώτρηση GA-4, με βάση την ανάλυση των δειγμάτων και τους δείκτες FD, BR-ratio, Fisher's alpha index, A-ratio, Group A, B and C.*

8.7 Borehole GA-5

In borehole GA-5 (Fig. 8-7) the interval 30.0–29.30 m core depth is characterized by coarse sediments indicating high-energy depositional environment. Considering the absence of micro fauna and the relatively high MS value (~400 x 10^{-5} SI units) this layer is correlated with nearshore coastal or upper shoreface paleoenvironment. From 29.30 to 26.60 m core depth, fine sediments indicate low-energy environments. Lagoonal paleoenvironment (estimated regional paleodepth <20 m) is described from 29.30 to 26.60 m depth, also documented by the low MS value (~ 22 x 10^{-5} SI units), the high FD-index and the BR-index (<5%) of the clayey sediments.

On the contrary the interval 26.60–20.80 m depth is characterized by coarse sediments indicating high-energy depositional environment. Considering the absence of micro fauna and the relatively high MS value (~185 x 10^{-5} SI units) this layer is correlated with nearshore coastal or upper shoreface paleoenvironment. From 20.80 to 13.80 m depth fine sediments indicates low-energy environments. The interval 20.80–20.60 m depth is characterized by Cluster II (combined presence of both Groups A and C) suggesting shallow marine environment also documented the low BR-ratio (<7%), MS values (1–40 x 10^{-5} SI units) and high FD- index (estimated regional paleodepth ~40 m). Till 13.80 m depth the foraminiferal assemblages are dominated by Cluster I (combined presence of both Groups Band C) suggesting transitional conditions between lagoonal and shallow marine environment (regional paleodepth ~30 m); also supported by the documented low BR-ratio (<5%), MS values (~10 x 10^{-5} SI units) and the A-ratio (15–25). High energy environment is also documented at the interval 13.80–1.70 m depth. Considering as well the high BR-ratio (>35%) with high MS values (up to 296 x 10^{-5} SI units) this layer is described as nearshore- upper shoreface.

From 11.70 to 6.80 m depth fine sediments indicate low-energy environments. The interval 11.70– 11.20 m depth is characterized by Cluster I (combined presence of both Groups B and C) suggesting transitional conditions between lagoonal and shallow marine environment (regional paleodepth ~30 m); also documented the low BR-ratio (<7%), MS values (1–80 x 10^{-5} SI units) and high FD- index (estimated regional

paleodepth ~40 m). Till 10.20 m depth Cluster III / Group B assemblages suggests lagoonal environment (regional paleodepth ~20 m); also supported by the documented low BR-ratio (<7%), MS values (~65 x 10^{-5} SI units) and the A-ratio (~15). Till 6.80 m depth the foraminiferal assemblages are characterized by Cluster I (combined presence of both Groups B and C) suggesting transitional conditions between lagoonal and shallow marine environment (regional paleodepth ~30 m) also documented by low BR-ratio (<4%), MS values (~25 x 10^{-5} SI units) and low A-ratio (<5).

High energy environment is also documented at the interval 6.80 – 0.00 m core depth. Considering as well the high BR-ratio (~35%) with high MS values (up to 204 x 10^{-5} SI units) this layer is described as nearshore- upper shoreface.

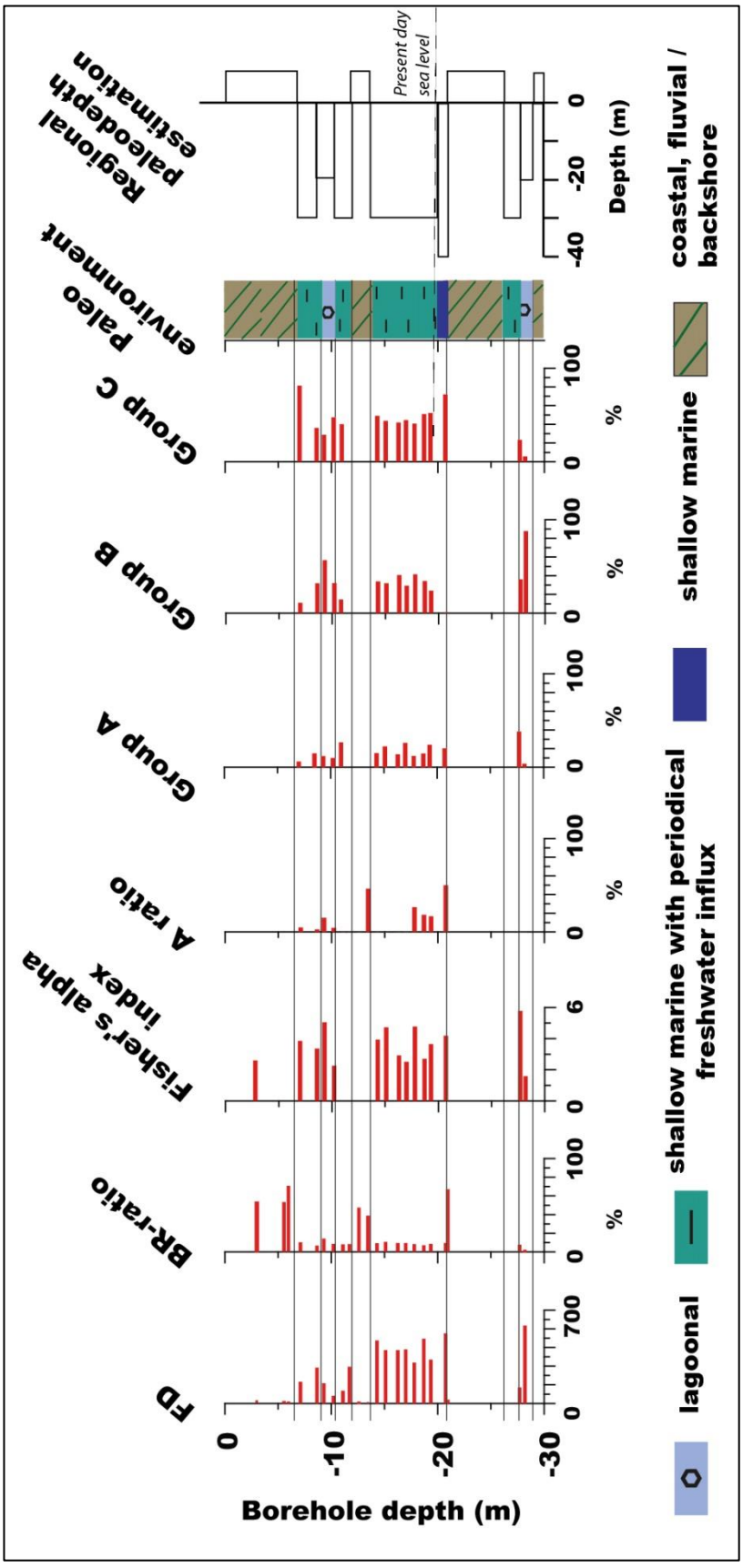

Figure 8-7*. Diagram showing the counted foraminifera per gram (FD), % P, Group A, B and C relative abundance, Fisher's alpha index, A-ratio, BR-ratio and the paleoenvironmetal interpretation in GA-5.*

Εικόνα 8-7*. Σχεδιάγραμμα που απεικονίζει το παλαιοπεριβάλλον και το εκτιμώμενο παλαιοβάθος στην γεώτρηση GA-5, με βάση την ανάλυση των δειγμάτων και τους δείκτες FD, BR-ratio, Fisher's alpha index, A-ratio, Group A, B and C.*

9 Age constraints and dating results

Three independent methods were used for constraining the age of the sediments. Two methodologies concerned absolute dating (OSL and IRSL luminescence and corals dating) and one (Calcareous nannofossils biozonation) concerned relevant dating. Unfortunately the results from luminescence techniques were of limited significant value, while the corals dating have not indicated a certain age, but have only narrowed the possible range of the sediments' age. On the other hand, the results from the nannofossils biozonation proved more valuable, since they provided significant age constraints.

9.1 Luminescence

Initially, this methodology was chosen since it offers the advantage of dating not fossils, but the sediments grains. Six samples which were analyzed for OSL and IRSL in the laboratory of Archaeometry / Paleoenvironment & Archaeometallurgy of N.C.S.R. Demokritos, while a small fragment of them was send for detailed chemical analysis in Bureau Veritas Commodities in Canada. Based on Tsakalos et al. (2016) and the Dose Rate calculator (DRc)" software and the results of the analysis the total dose rate of each sample has been estimated (table 16).

Among the six examined samples only four contained a sufficient proportion of Quartz for further examination (Bh-1 6.05 m, Bh-3 20.45 m, Bh-7 20.65 m, Bh7-33.45). As was described before the 'double-SAR' ('post-IR blue') protocol was followed where 12 aliquots of each sample[12] have been examined. Unfortunately, quartz was highly

[12] *Quartz grains mounted on stainless steel discs of 10 mm diameter using silicone oil as an adhesive. The grains quartz and feldspar grains covered the central 5 mm diameter portion of each disc, corresponding to several hundred grains per aliquot.*

saturated, meaning that the energy traps of the quartz crystal lattice were fully occupied and were not suitable for further analysis (Fig. 9-1). When measuring quartz samples it revealed that OSL signals were saturated, greatly deviating from the expected paleoenvironmental framework, and highly scattered[13]. Circumstantial aliquots in which quartz was not saturated indicated an age older than 600 ka. It is well established though that the age of the sediments at the canal ranges from Holocene sediments to maximum MIS 11 (~400 ka). Ages implied by these aliquots are rather unlikely and most probably due to insufficient bleaching of the grains from previous exposure. Furthermore, considering that most of the examined samples were saturated and were unsuitable for further analysis, feldspar grains were also used to obtain D_e values.

Unfortunately feldspar analysis (IRSL) was also of limited value. The emitted signal was weaker than the expected resulting into anomalous fading (Fig. 9-2). The latter means this signal was also highly scattered and therefore without any useful scientific result.

[13] The measured emitted signal from the aliquots has been analyzed based on the standard procedures (e.g. Thiel et al., 2011; Tsakalos et al., 2016) in the laboratory of Archaeometry / Paleoenvironment & Archaeometallurgy of N.C.S.R. Demokritos. This analysis has shown that the results varied from relative low to relative high signal and therefore it was not safe to proceed into further examination, even if the average value has been taken as a possible result.

Table 16 U and Th concentrations of the analyzed samples. Πίνακας 16. Οι συγκεντρώσεις U και Th στα δείγματα που αναλύθηκαν.

Samples	*U(ppm)*	*Th(ppm)*	*K(wt%)*	*Cosmic rays*	*depth (cm)*	*water (%)*	*elevation (m)*	*total dose rate*	*error*
Bh-1, 5.25	1.7	0.2	0.03	0.087	525	1.1	16	0.511	0.021
Bh-1, 6.05	1	0.3	0.05	2.872	605	1.8	16	0.34	0.022
Bh-3, 20.45	1.7	0.7	0.11	0.018	2045	1.9	19.1	0.579	0.081
Bh-3, 21.25	3.1	1	0.19	0.017	2125	2.1	19.1	1.007	0.165
Bh-7, 20.65	0.9	0.4	0.06	0.018	2065	1.1	16	0.321	0.006
Bh-7, 33.45	1.1	0.5	0.09	0.008	3345	2.2	16	0.391	0.008

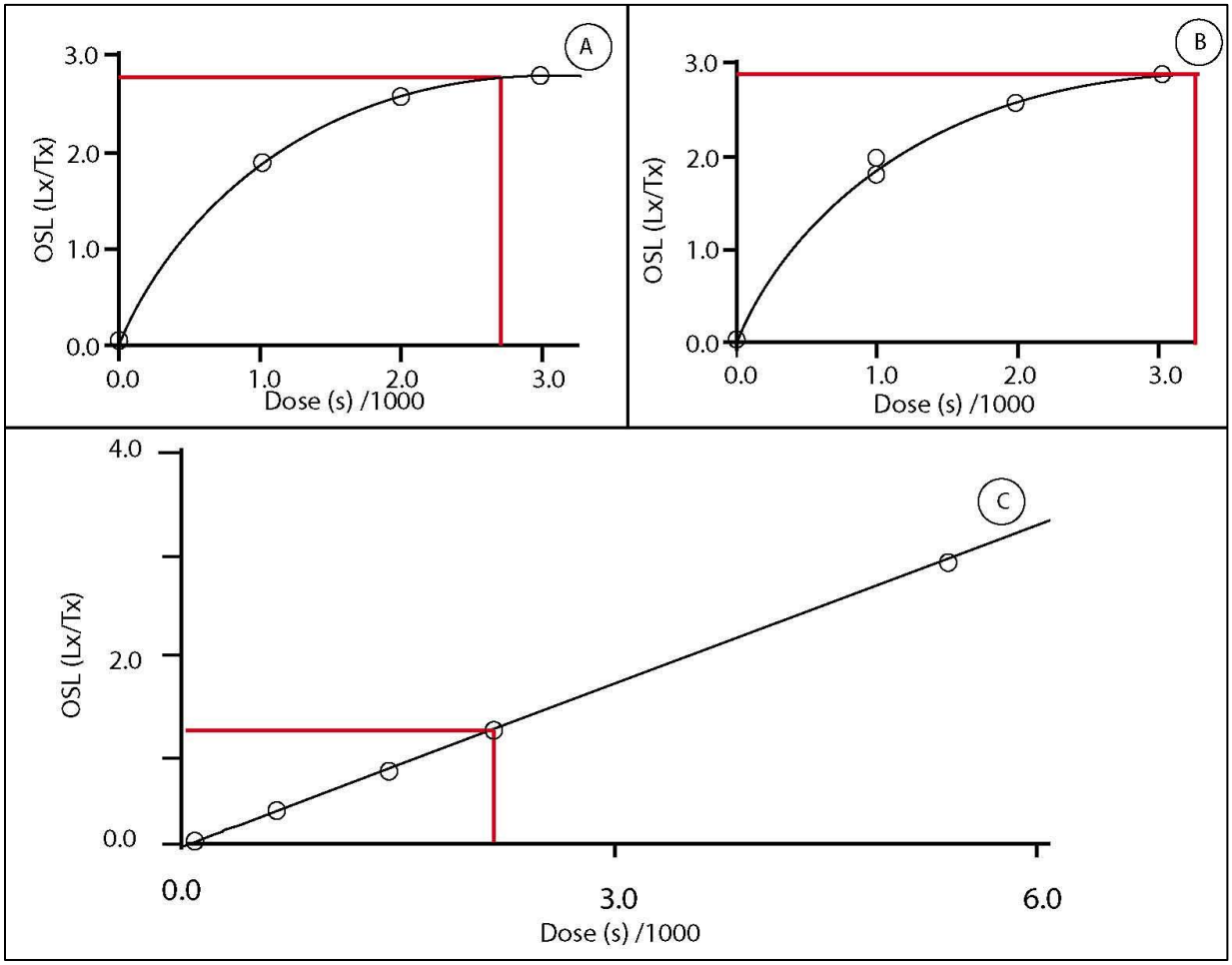

Figure 9-1. *The OSL dose–response curve for aliquots of two samples (A) Bh7-20.65m and (B) Bh-7 33.45 m depth) showing saturation. (C) A typical dose–response curve modified from Duller (2008), where for comparison reasons the scale is similar in both figures.* ***Εικόνα 9-1.*** *Η καμπύλη απόκρισης οπτικής φωταύγειας δύο δειγμάτων (A) Bh7-20,65m και (B) Bh-7 33,45m) που δείχνουν κορεσμό. (C) Μια τυπική καμπύλη απόκρισης ενός δείγματος τροποποιημένη από Duller (2008), με την κλίμακα να είναι σταθερή σε όλες τις εικόνες για λόγους συσχέτισης.*

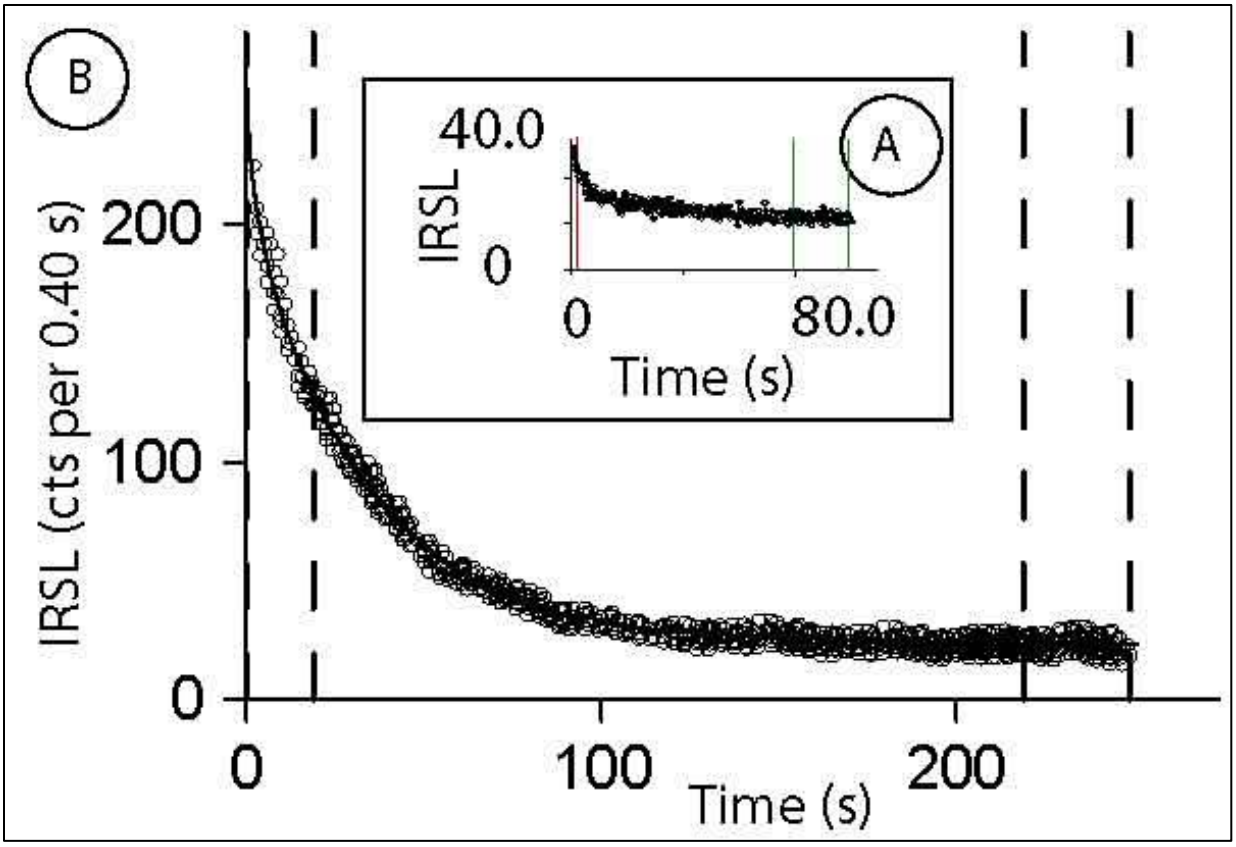

***Figure 9-2**. (A) Decay curve for an aliquot of sample Bh-1, 6.05 m, showing the pIRIR290 signals from coarse grain (80-125μm) feldspars. (B) Decay curve for an aliquot analyzed by Porat et al. (2009) showing the difference between them (scattered values and lower IRSL signal). For comparison reason the scale is similar in both figures.*

***Εικόνα 9-2**. (A) Η καμπύλη απόσβεσης για το δείγμα Bh-1, 6,05 m, που δείχνει το σήμα μέσω της υπέρυθρης φωταύγειας σε κόκκο αστρίου διαμέτρου (80-125 μm). (Β) Μια τυπική καμπύλη ενός δείγματος από Porat et al. (2009), με την κλίμακα να είναι σταθερή και στις δύο εικόνες για λόγους συσχέτισης.*

9.2 Fossil corals

Seven coral stems of *Cladocora caespitosa* corals found in growth position (sample Bh-7, 18.25 m) have been dated with the ^{230}Th/U-method. The results are displayed in

Table *17*, where the ages range from 241 to 358 ka with relatively large uncertainties between ± 20 and ± 80 ka. Since all coral stems are from the same borehole sample and, thus, should have a similar age, the large differences between the individual ages suggest that the corals are possibly affected by post depositional diagenetic processes.

Although fossil reef corals are among the best suited material for ^{230}Th/U-dating, it is well established that the majority of fossil reef corals are affected by post-depositional diagenetic alteration, which results in apparently wrong ages (Edwards et al., 2003; Scholz and Hoffmann, 2008; Scholz and Mangini, 2007; Stirling and Andersen, 2009). For this reason, several criteria were developed in order to identify reliable ages. These include (i) initial (^{234}U/^{238}U) activity ratios in agreement with the (^{234}U/^{238}U) activity ratio of modern seawater (i.e., 1.1468 ± 0.004, Andersen et al., 2010); (ii) ^{232}Th content <1 ng g^{-1}; ^{238}U concentration in the range of the respective modern coral species; calcite content ≤2% and primary aragonitic textures (Obert et al., 2016; Stirling et al., 1998). The latter two criteria cannot be applied to our corals since calcite content and textures were not studied. The average U content of the samples is *2.5 µg.*g^{-1} and, thus, relatively low. This may indicate post-depositional U loss (Obert et al., 2016; Scholz et al., 2007), as has previously been observed for other fossil corals from the Corinth Isthmus (Collier et al., 1992). The mean ^{232}Th content is 44 ng g^{-1} and thus elevated for all coral samples. This suggests post-depositional addition of detrital Th to all corals. Both processes, U loss and contamination by detrital Th, would result in ages that are apparently too old. Finally, only three corals have initial (^{234}U/^{238}U) activity ratios in agreement with the modern seawater value, whereas the other samples have significantly elevated initial (^{234}U/^{238}U) activity ratios (Table 17). Elevated initial (^{234}U/^{238}U) activity ratios are generally interpreted as resulting in apparently too old ^{230}Th/U-ages. (Fig. 9-3) shows the coral data on a (^{234}U/^{238}U) vs. (^{230}Th/^{238}U) activity ratio diagram in comparison to the seawater evolution curve.

Table 17 U/Th data form the coral analysis and the estimated age. Πίνακας 17. Τα αποτελέσματα από τα κοράλλια που αναλύθηκαν και η εκτιμώμενη ηλικία.

Sample	*^{238}U(μg/g)*	*^{232}Th(ng/g)*	*$(^{234}U/^{238}U)$*	*$(^{234}U/^{238}U)_{INIT}$*	*$(^{230}Th/^{238}U)$*	*$(^{230}Th/^{232}Th)$*	*$\delta^{234}U$ (‰)*	*Age (ka)*	*Error*
1	2.62 ±0.03	48.9± 0.6	1.077 ±0.012	1.190 ±0.021	1.044 ±0.014	170.9 ±2.4	76.5± 1.1	**321.9**	+ 42,8 - 30,9
2	2.47 ±0.03	34.7 ±0.4	1.070 ±0.011	1.189 ±0.020	1.050 ±0.012	227.7 ±2.9	70.3± 1.1	**350.0**	+ 50,6 - 35,2
3	2.49 ±0.04	36.9 ±0.6	1.071 ±0.015	1.140 ±0.025	0.969 ±0.018	200.2 ±3.6	70.7± 1.5	**240.5**	+ 24,9 - 19,5
4	2.64 ±0.04	22.0 ±0.3	1.063 ±0.014	1.151 ±0.024	1.018 ±0.016	374.1 ±5.0	63.2± 1.4	**307.3**	+ 46,4 - 31,1
5	2.38 ±0.03	69.8 ±0.8	1.069 ±0.014	1.190 ±0.025	1.052 ±0.015	109.4 ±1.2	69.0± 1.4	**357.8**	+ 82,6 - 44,1
6	2.58 ±0.04	30.5 ±0.3	1.081 ±0.014	1.191 ±0.023	1.037 ±0.014	268.2 ±2.7	81.4± 1.4	**301.0**	+ 38,9 - 28,1
7	2.42±0. 04	63.7 ±0.8	1.072 ±0.017	1.165 ±0.028	1.019 ±0.018	118.5 ±1.5	72.0± 1.7	**292.6**	+ 47,5 - 31,5

The coral data describe a trend to the right on the diagram (i.e., increasing ($^{230}Th/^{238}U$) activity ratios with relatively constant ($^{234}U/^{238}U$) activity ratios). This may indicate post-depositional U loss. Due to the high particle reactivity of Th, this process results in elevated ($^{230}Th/^{238}U$) activity ratios, but has a minor effect on ($^{234}U/^{238}U$). Post-depositional U loss results in apparently too old ages and may – depending on the timing of U loss – result in large age biases (Obert et al., 2016; Scholz et al., 2007; Tomiak et al., 2016). In addition, this effect cannot be corrected by the available models aiming to correct the effects of post-depositional diagenesis on fossil coral $^{230}Th/U$-ages, which are all based on elevated ($^{234}U/^{238}U$) activity ratios (Scholz et al., 2004; Thompson et al., 2003; Villemant and Feuillet, 2003).

In summary, all coral $^{230}Th/U$-ages were probably affected by post-depositional U loss and/or contamination with detrital Th. Based on the $^{230}Th/U$-ages described before, ages approximately at 175 ka can also be a possibility and not be excluded since the post depositional digenesis has affected the original concentrations. An age younger than 125 ka though, also a marine highstand which was a possible candidate for the coral's age, is clearly excluded since the measured ages are significant older, even if diagenetic processes have affected the original chemistry of the corals.

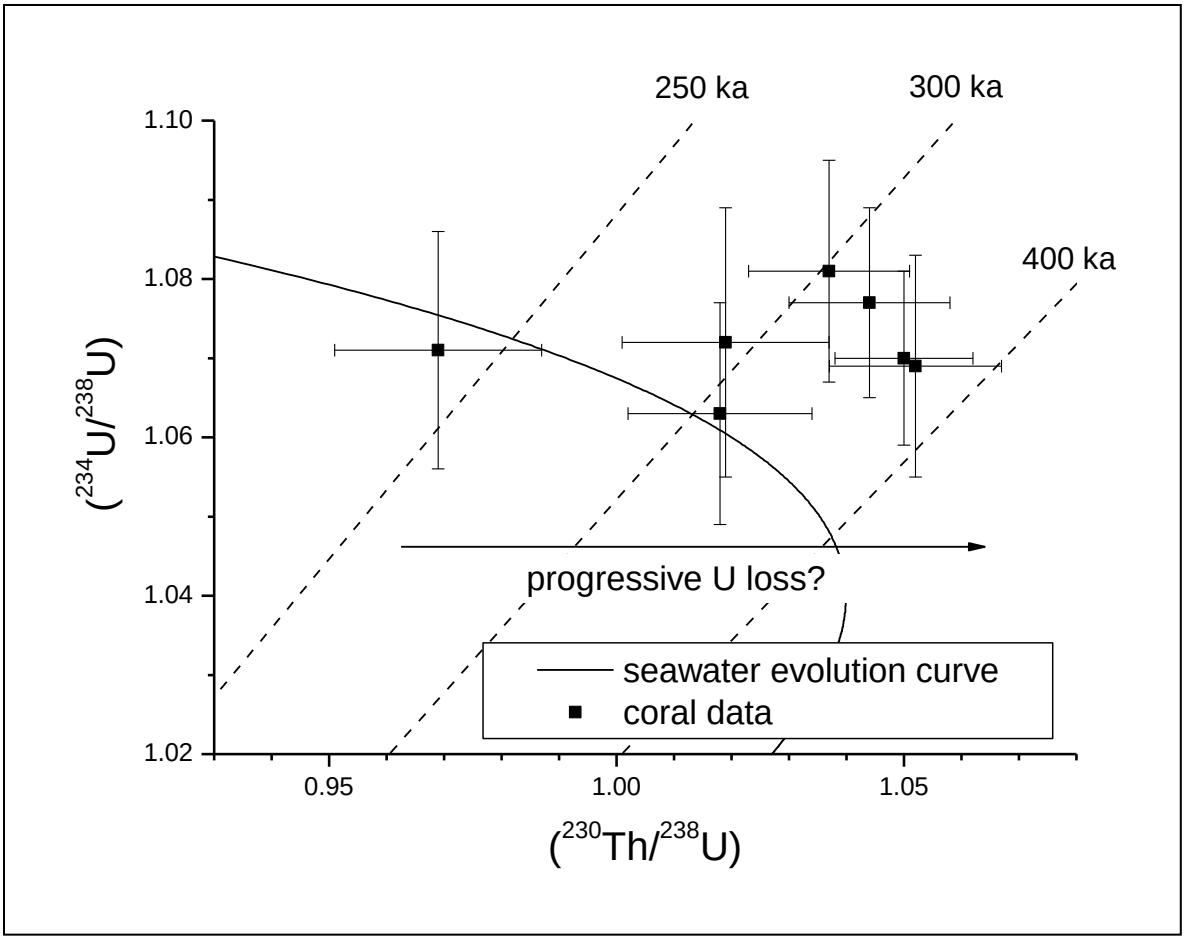

Figure 9-3. ($^{234}U/^{238}U$) vs. ($^{230}Th/^{238}U$) activity ratio diagram showing the coral data in comparison with the seawater evolution curve (solid line). The dashed lines are isochrones (i.e., lines highlighting combinations of activity ratios resulting in a specific $^{230}Th/U$-age) for 250, 300 and 400 ka, respectively.

Εικόνα 9-3. Το διάγραμμα ($^{234}U/^{238}U$) προς ($^{230}Th/^{238}U$) που δείχνει τα δεδομένα κοραλλιών σε σύγκριση με την καμπύλη του θαλασσινού νερού (συνεχής γραμμή). Οι διακεκομμένες γραμμές είναι ισόχρονες καμπύλες (δηλ. γραμμές που επισημαίνουν συγκεκριμένες ηλικίες ^{230}Th / U) για 250, 300 και 400 ka αντίστοιχα.

9.3 Nannoplankton analysis.

Following the inconclusive data from OSL and the variable ages extracted from corals that however, provide a lower threshold age of older than 175 ka is possible, more dating data are needed. In order to achieve this nannofossils have been used offering not only some valuable dating constraints but also a high spatial resolution since they have been collected both from different borehole depths and from several surface localities. As has been described before in samples from surface outcrops small *Reticulofenestra* spp. (~45%), small *Gephyrocapsa* spp (~33%) and in few samples *E. huxleyi* specimens (5-8%) have been identified.

Calcareous nannoplankton specimens have also been identified through SEM analysis, in certain levels of the examined boreholes where samples were dominated by the presence of small *Reticulofenestra* spp. (~40%) and small *Gephyrocapsa* spp. (~30%) coccoliths, while *Emiliania huxleyi* specimens were relatively scarce (5-8% of the total assemblage), but consistently present.

Even though calcareous nannoplankton is mostly preserved in pelagic marine sediments (e.g. Perch-Nielsen, 1985; Young, 1994), numerous relatively well preserved coccoliths, have been identified in the clayey and sandy layers of the shallow marine paleoenvironments identified in boreholes cores; featured by low BR-ratio values and depositional depths ranging between ~20 and 40 m. Because certain nannoplankton species (e.g. *E*. *huxleyi*, *Gephyrocapsa* spp.) are taphonomically resistant to the highly energetic and aggressive conditions between the estuaries and the shelf (e.g., Guerreiro et al., 2005), they can be useful for age determinations (e.g., Palyvos et al., 2010; Triantaphyllou, 2015). Thus, the presence or the absence of *E*. *huxleyi* in the studied samples indicates an age of the examined sediments before or after the first occurrence of the species (base of nannofossil biozone NN21a; Martini, 1971); namely within marine isotopic stage MIS 8, at ~265 ka in the eastern Mediterranean (e.g. Raffi et al., 2006).

Consequently, the age of the sediments described in the examined boreholes have to be constrained between ~240 ka and 175 ka for corals horizons (boreholes Bh-3 and Bh-7) and up to 125 ka for the horizons right above them (Fig. 9-4) (e.g. the interval from 11.00 m to 3.30 m core depth in borehole Bh-3 and the interval from 5.50 m to 1.50 m core depth in borehole Bh-7).

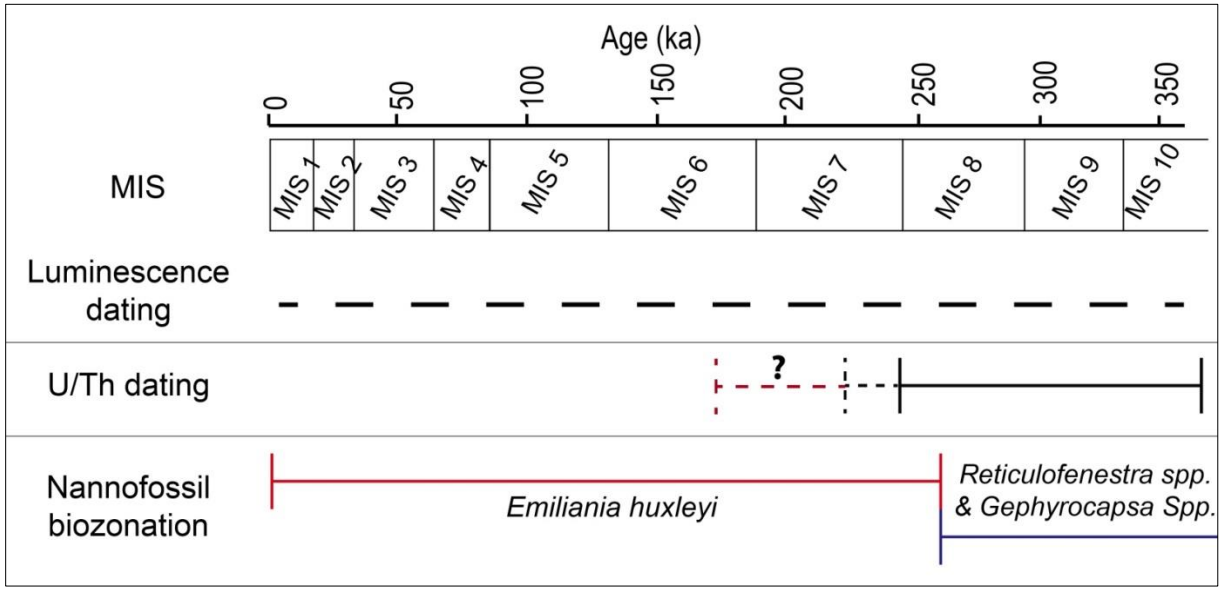

Figure 9-4. *The estimated ages based on the results of both absolute and relevant dating methodologies. There is no significant outcome based on the luminescence signal, based on the U/Th dating on coral samples an age ranging from ~240 to ~358 ka (±~30 ka), is estimated, while based on the nannofossils biozonation a threshold younger or older than 265 ka is established based on the presence or absence of the Emiliania huxleyi specimens. At the U/Th dating the black dotted line indicates the error of the analysis, while the red dotted line indicates the MIS 6.5 and MIS 7 periods that cannot be excluded as potential ages of corals.*

Εικόνα 9-4. *Οι εκτιμώμενες ηλικίες των μεθοδολογιών που ακολουθήθηκαν. Δεν προέκυψαν αξιόλογα αποτελέσματα μέσω της φωταύγειας λόγω κορεσμού και ασθενούς σήματος, μέσω της χρονολόγησης των κοραλλιών με U/Th οι ηλικίες που προκύπτουν κυμαίνονται από ~240 σε ~358 ka (±~30 ka), ενώ μέσω τις βιοστρωματογραφίας προκύπτει το όριο των 265 ka, ανάλογα εάν εντοπίζεται ή όχι η Emiliania huxleyi. Με μαύρη διακεκομμένη γραμμή επισημαίνεται το όριο σφάλματος της χρονολόγησης μέσω*

U/Th ενώ με κόκκινη οι πιθανές ηλικίες των κοραλλιών από το MIS 6.5 και MIS 7 που δεν μπορούν να αποκλειστούν.

10 Saronic Gulf (boreholes P-2, P-4, P-5)

10.1 Introduction

The sediments from boreholes cores and surface outcrops described in previous chapters are from MIS 5 (Upper Pleistocene) or older. In a completely different tectonic and sedimentological environment, the coastal plain of Piraeus at the western part of the Saronic gulf, three boreholes (P-2, P-4, P-5) have also been examined for their contend in foraminifera assemblages (Fig. 10-1). Apart from the different environmental conditions, the sediments in Piraeus are significantly younger and have been deposited during Holocene (Goiran et al., 2011, Triantaphyllou et al., 2016). Therefore it is possible to compare the paleoenvironmental conditions from two different marine highstands, with similar paleoclimate conditions, correlating the relatively young sediments from Piraeus coastal plain, with the sediments described before (older sediments). Furthermore, the Corinth Isthmus and Piraeus coastal plain have completely different geological conditions. The main factors that influence the Piraeus coastal landscape is the relative sea level rise in the Holocene, the tectonic stability since no significant earthquakes have been documented during the last few thousand years, the low tidal range (±0.25-0.30m) and the progradation of the deltaic fan of the Kephissos River (Triantaphyllou et al., 2016). On the contrary, the Corinth Isthmus area is mostly influenced by significant glacioeustatic sea level changes and tectonic activity, while the fluvial systems which influence this area are less significant (a few km^2) compared with the Kephissos River.

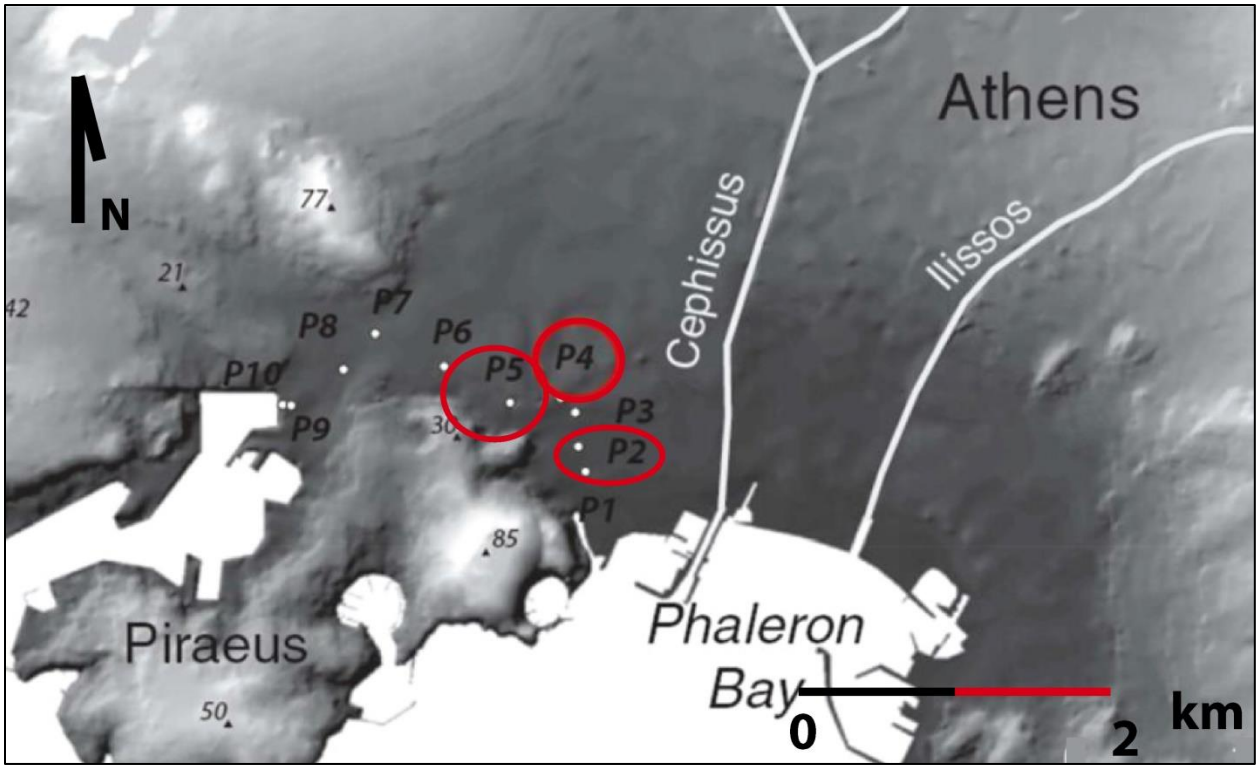

Figure 10-1*. Location map of boreholes P-2, P-4 and P-5 in Piraeus coastal plain, Attica (modified from Goiran et al., 2011, Triantaphyllou et al., 2016).* ***Εικόνα 10-****1. Ο χάρτης που απεικονίζει τις γεωτρήσεις P-2, P-4 και P-5 στον Πειραιά (από Goiran et al., 2011, Triantaphyllou et al., 2016).*

10.2 Borehole analysis

In the examined boreholes, alternations of fine to coarse sediments have been described (Goiran et al., 2011, Triantaphyllou et al., 2016) corresponding to different depositional environments (Fig. 10-2, Tables 18, 19 and 20). In general finest sediments, from clay to sandy clay have been described at the deepest part of the boreholes, while more coarse sediments from sand to coarse sand at the upper part.

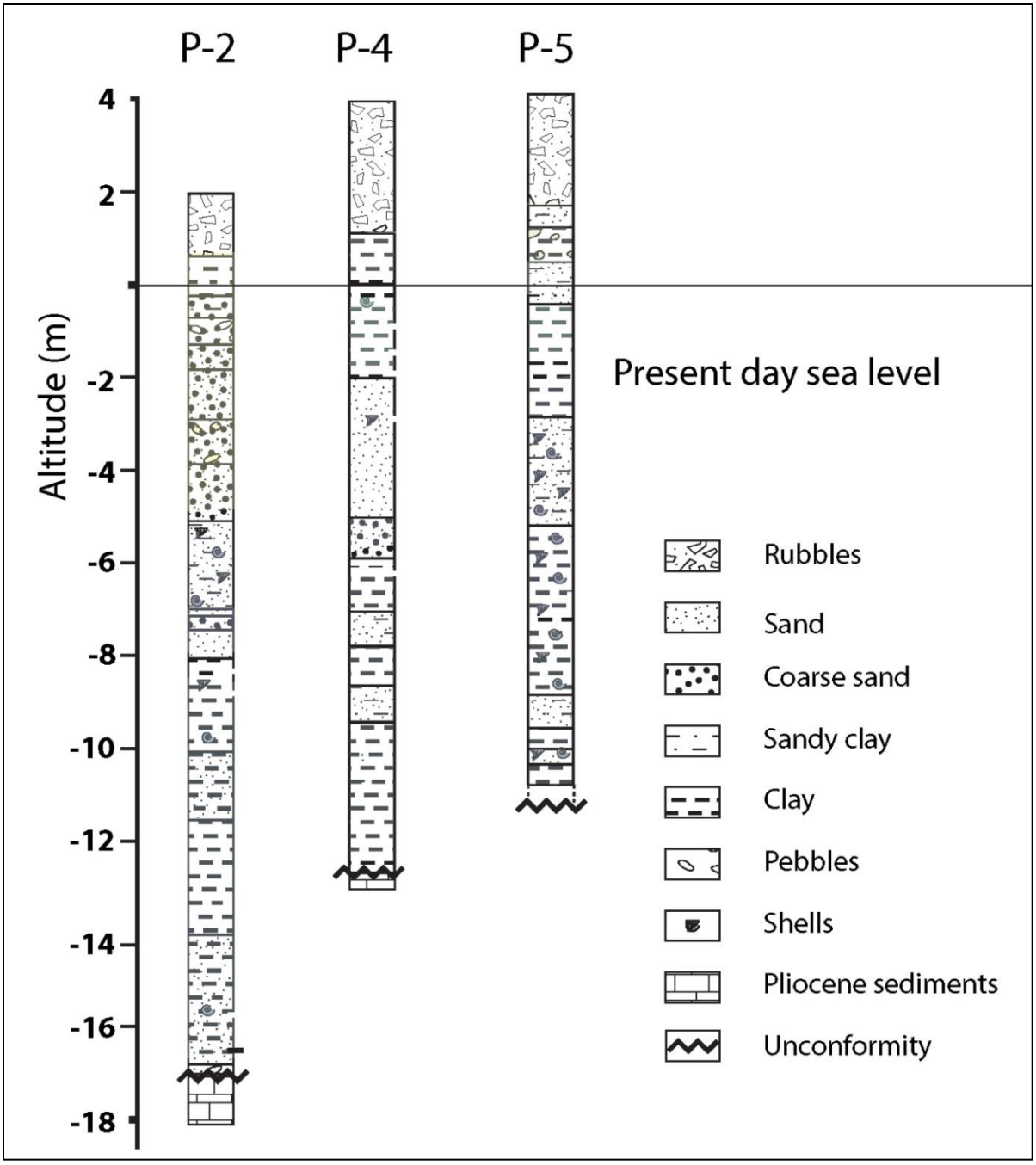

Figure 10-2*. The lithological description of the examined boreholes (modified from Goiran et al. (2011)).*

Εικόνα 10-2. *Η λιθολογία των γεωτρήσεων από την περιοχή του Πειραιά (από Goiran et al., 2011).*

Table 18. The lithological description of borehole P-2. Πίνακας 18. Η λιθολογία της P-2.

Depth (m)	Lithology
0.00–1.50	Rubbles
1.50–2.50	Clay
2.50–7.00	Coarse sand
7.00–10.00	Sand
10.00-19.00	Clay to sandy clay
19.00–20.00	Pliocene bedrock

Table 19. The lithological description of boreholes P-4. Πίνακας 19. Η λιθολογία της P-4.

Depth (m)	Lithology
0.00–3.00	Rubbles
3.00–6.00	Clay
6.00–9.00	Sand
9.00–10.00	Coarse sand
10.00–17.00	Clay to sandy clay
17.00–17.20	Pliocene bedrock

Table 20. The lithological description of borehole P-5. Πίνακας 20. Η λιθολογία της P-5.

Depth (m)	Lithology
0.00–2.20	Rubbles
2.20–3.00	Sandy clay
3.00–3.80	Clay with pebbles
3.80–4.20	Sandy cay
4.20–7.00	Clay
7.00–9.00	Sandy cay
9.00–13.00	Clay
13.00–13.50	Sandy clay
13.50–15.00	Pliocene bedrock

To analyze the foraminiferal assemblages in boreholes P-2, P-4 and P-5 the standard procedure has been followed as has been described for the micropaleontological analysis before.

Apart from foraminifera, borehole P-4 has been analyzed for its molluscan and pollen content and the magnetic susceptibility of sediments has been measured (Triantaphyllou et al., 2016).

For pollen analysis the standard procedure has been followed[14] (e.g. Kouli et al., 2009; Kouli, 2012) on 52 samples from core P4, even though only in 28 of them the pollen concentration was sufficient to be included in their study (Triantaphyllou et al., 2016). Furthermore, Molluscan analysis performed on 113 selected samples, which have been washed into 125 μm sieve and dried at 70^{o} C. All molluscs and fragments were identified and counted in a semi-quantitative approach (Triantaphyllou et al., 2016).

A total of 128 samples P4 have been used for magnetic susceptibility analysis. The MS signal of borehole P-a has been performed in the laboratory of department of Geology in Aristotle University of Thessaloniki and therefore, a different procedure has been followed for measuring the MS signal (compared with the MS analysis performed in boreholes from the Corinth Canal). *All samples were sieved in order to remove all the impurities and packed in cylindrical plastic boxes (2x2x2 cm). The laboratory measurements of the volume-specific magnetic susceptibility (k, SI units) have been performed using the Bartington MS2B sensor at low frequency (0.465 kHz). The examined samples were weighed before the measurements therefore all the results are expressed as mass-specific magnetic susceptibility (x, 10^{-8} m^3/kg). Every sample was measured at least 3 times and the average value considered as the final one for the sample. Two air measurements before and after the sample's measurement have been performed in all samples* (Triantaphyllou et al., 2016).

[14] *All samples were spiked with known quantity of Lycopodium spores, chemically treated with HCl (37%), HF (40%), acetolysed and finally sieved over a 10 μm sieve, while residues were mounted in silicon oil.*

10.3 Results

10.3.1 Borehole P-2

Based on foraminiferal assemblages the borehole sequence is divided to four subdivisions. The first division is described as Unit Aa (lagoonal environment with mesohaline-oligohaline conditions (Goiran et al., 2011; Triantaphyllou et al., 2016). In particular, in between 17.00 13.50 m core depth (Unit Aa), benthic foraminiferal analysis revealed the dominance of *Haynesina germanica* (reaching occasionally 60%); and partly the presence *Ammonia tepida* sometimes up to almost ~50% of the assemblage, Fig. 10-3), together with presence of *Ammonia beccarii* (almost ~20% of the total assemblage, Fig. 10-3). This assemblage is featuring lagoonal environment with mesohaline- oligohaline conditions (e.g., Koukousioura *et al*., 2012; Dimiza *et al*., 2016).

The interval from 13.50 to 7.00 m core depth (Unit B) is featured by the high abundance of *A. tepida* (even higher than ~80%) and A. beccarii (up to even ~ 50% of the total assemblage), accompanied by the presence of *Elphidium* spp. (*gunteri* and *complanatum), Aubignyna perlucida* (up to 8%), miliolids (Quinqueloculina spp. up to ~ 30% of the total assemblage), Bolivina spp. (up to ~50% of the total assemblage) a typical species of Shallow-marine environment with freshwater influences (e.g., Carboni *et al*., 2010; Evelpidou *et al*., 2010). In the upper part even though several foraminiferal representatives have been identified, specimens were scarce and not included for the paleoenvironmental analysis. This part has been described as coastal and/or paralic (Goiran et al., 2011).

10.3.2 Borehole P-4

Based on foraminiferal assemblages the borehole sequence is divided to four subdivisions. The first division is described as Unit A (lagoonal environment with mesohaline-oligohaline conditions; ~8700- 7800 yrs. BP, (Goiran et al., 2011;

Triantaphyllou et al., 2016) and can be also divided into two subunits (Unit Aa and Unit Ab, Fig. 10-4). In particular, in between 17-12 m core depth (Unit Aa), benthic foraminiferal analysis revealed the dominance of *Ammonia tepida* (>50%, sometimes up to almost 100% of the assemblage; Fig. 10-4), together with increased presence of *Haynesina germanica* (reaching occasionally 60%; Fig. 10-4). This assemblage is featuring mesohaline to oligohaline biofacies in modern closed lagoons of the Aegean area (e.g., Koukousioura *et al*., 2012; Dimiza *et al*., 2016).

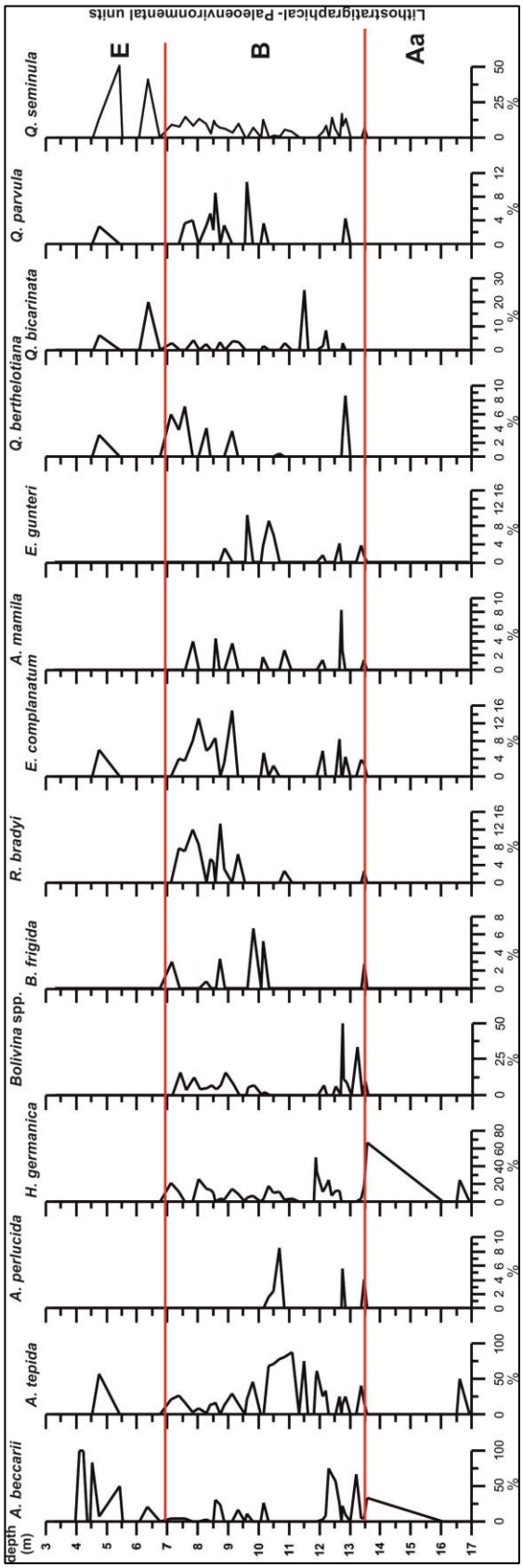

Figure 10-3. *Foraminiferal abundances in borehole P-2.*

Εικόνα 10-3*. Οι συγκεντρώσεις των τρηματοφόρων στην γεώτρηση P-2.*

The interval from 12 to 11 m core depth (Unit Ab) is featured by the high abundance of *A. tepida* (generally higher than 70%), accompanied by the presence of *Elphidium gunteri* and *Aubignyna perlucida* (up to 20%), a typical species of estuarine and shallow marine environments (e.g., Carboni *et al*., 2010; Evelpidou *et al*., 2010). Overall similar foraminiferal assemblages have been characterized as open lagoon environments (e.g., Carboni *et al*., 2010; Koukousioura *et al*., 2012).

Benthic foraminiferal assemblages of Unit B (9.5-6.5 m core depth) consist mainly of marine foraminiferal species (e.g., *Rosalina bradyi*, *Bolivina dilatata*, *Peneroplis pertusus*, *Elphidium complanatum*; Fig. 10-4). In addition, miliolids (*Quinqueloculina berthelotiana*, *Q. seminula*) featuring the infralittoral and upper circalittoral zones (e.g., Sgarrella and Moncharmont Zei, 1993), consist an important fraction of the assemblage together with specimens of planktonic foraminiferal species (Fig. 10-4). However, the presence of euryhaline species such as *H. depressula*, *A. tepida* suggests a shallow marine paleoenvironment which also exhibits lagoonal features.

The microfaunal content of Unit C (6.5-4 m core depth) reveals the relative increase of *A. tepida* and *H. depressula*, along with *Q. seminula* (Fig. 10-4), suggesting closed lagoon paleoenvironmental conditions. Within Unit D (the upper 4m of the core P4; younger than 2800 yr cal BP, Goiran *et al*., 2011), the microfauna is characterized by the slight presence of *Ammonia* and *Haynesina* and mollusks are totally absent, indicating a marshy oligohaline paleoenvironment.

Apart from benthic foraminifera, borehole P-4 has also been examined for pollen and mollusks, while the magnetic susceptibility of the sediments was measured (Triantaphyllou et al., 2016). The described molluscan assemblages consist mainly of *Cerastoderma glaucum* (small sized and juvenile forms), *Abra* spp. and few Hydrobiidae, revealing a typical lagoonal environment (Nicolaidou *et al.,* 1988; Kevrekidis *et al*., 1996), at the interval from 17.00 ~ 10.00 m core depth (Unit A) to Similar assemblages feature meso-ologohaline conditions in several Aegean coastal plains (e.g., Triantaphyllou *et al*., 2003; Evelpidou *et al*., 2010; Goiran *et al*., 2011; Syrides, 2008) and define inner lagoon environment (e.g., Carboni *et al*., 2010; Koukousioura *et al*., 2012). Mollusc fauna in Unit B is characterized mainly of

Cerithiidae, *Bittium* sp., *Alvania*/ *Rissoa* spp. and *Tricolia* sp. indicates a shallow marine environment (Syrides, 2008), but the intense presence of *C. glaucum* suggests lagoonal features, confirming the foraminiferal findings. In Unit C (6.50-4.00 m core depth) molluscan fauna consists of *C. glaucum*, *Abra* spp. and numerous Hydrobiidae, suggesting closed lagoon paleoenvironmental conditions. In unit D mollusks were absent.

The palynological evidence of unit A in borehole P-4 consists of *Pseudoschizaea,* indicators of soil erosion and increased riverine runoff (Triantaphyllou et al., 2016); implying increased fresh water input in the depositional environment, thus supporting the closed lagoon paleoenvironmental conditions. Arboreal vegetation (AP), being in general ~30% of the pollen content, with *Pinus* being the most common tree taxa, followed by deciduous *Quercus*, exhibits significantly increased abundances during the middle part of Unit A, in-between 14 and 13 m.

Nevertheless the increase of *Cerealia*-type towards the upper part of the Unit A may be the signal of first farming communities in the area. Unit B is characterized by the absence of pollen. The upper part is characterized by the presence of *Chenopodiaceae* halophytes, *Sordaria* and parasites. *Asteraceae*, *Poaceae* and *Chenopodiaceae* are the most common non arboreal taxa, with the latter being the dominant feature of this unit. The human presence is inevitably detected since Unit C (Early Bronze Age) by the increase of cultivars like *Cerealia* type and *Olea*

In the interval from 17.00 m to 12.00 m core depth the Magnetic susceptibility has a mean value ~40 $x10^{-8}$ m^3/kg (Triantaphyllou et al., 2016). In unit B the Magnetic susceptibility values are relatively (~1 $x10^{-8}$ m^3/kg). In the upper part of the borehole core, the measured Magnetic susceptibility shows relatively higher values reaching the maximum of 100 x10-^{8} m^3/kg, thus implying the intense impact of fresh water input (Ghilardi *et al.,* 2008).

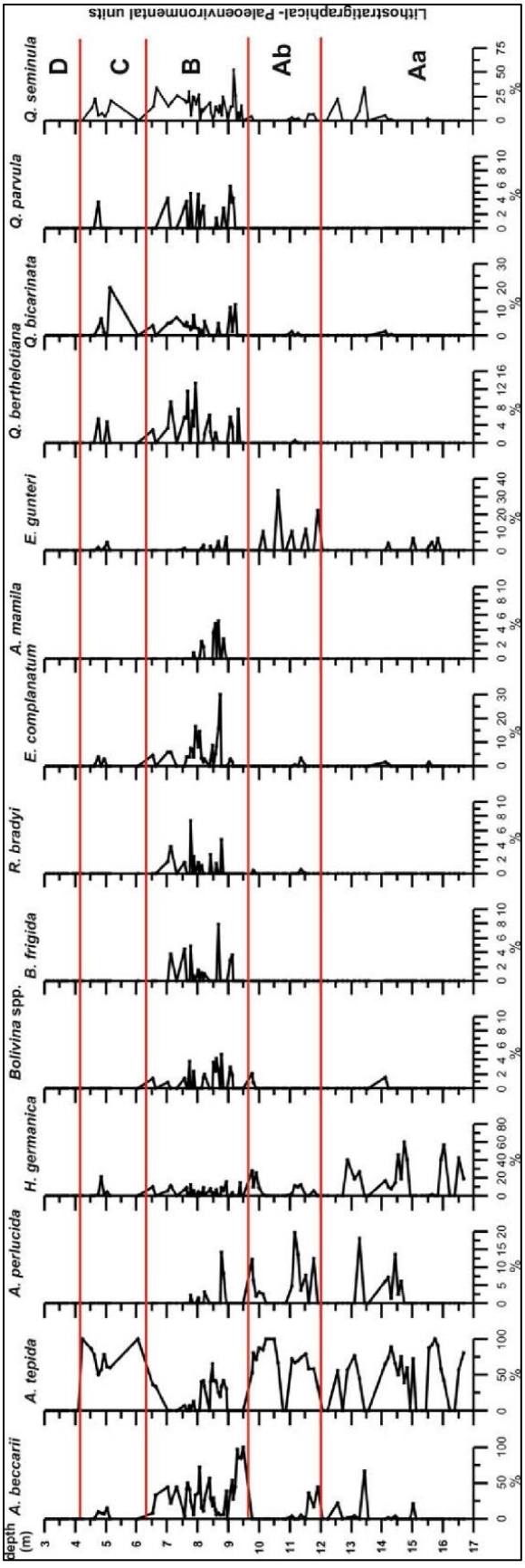

Figure 10-4. *Foraminiferal abundances in borehole P-4.*

Εικόνα 10-4*. Οι συγκεντρώσεις των τρηματοφόρων στην γεώτρηση P-4.*

10.3.3 Borehole P-5

In borehole P-5 the interval from 15.00 to 9.00 m core depth (Unit Ab) is featured by the high abundance of *A. tepida* (generally higher than 70%), accompanied by the presence of *Elphidium gunteri* and *Aubignyna perlucida* (up to ~ 12%), *Haynesina germanica* (up to ~ 20%), *Rossalina bradyi* (up to ~ 8%), *Quinqueloculina* spp. (up to ~ 30%), a typical species of estuarine and shallow marine environments (e.g., Carboni *et al*., 2010; Evelpidou *et al*., 2010). Overall similar foraminiferal assemblages have been characterized as open lagoon environments (e.g., Carboni *et al*., 2010; Koukousioura *et al*., 2012).

The interval from 9.00 to 5.50 m core depth (Unit C) consists mainly of marine foraminiferal species (e.g., *Rosalina bradyi*, *Bolivina dilatata*, *Peneroplis pertusus*, *Elphidium complanatum*; Fig. 10-5). In addition, miliolids (*Quinqueloculina berthelotiana*, *Q. seminula*) featuring the infralittoral and upper circalittoral zones (e.g., Sgarrella and Moncharmont Zei, 1993), consist an important fraction of the assemblage together with specimens of planktonic foraminiferal species (Fig. 10-5). However, the presence of euryhaline species such as *H. depressula*, *A. tepida* suggests a shallow marine paleoenvironment which also exhibits lagoonal features.

The microfaunal content of Unit C (5.50 to 0.00 m core depth) reveals the relative increase of *A. tepida* and *H. depressula*, along with *Q. seminula* (Fig. 10-5), suggesting closed lagoon paleoenvironmental conditions.

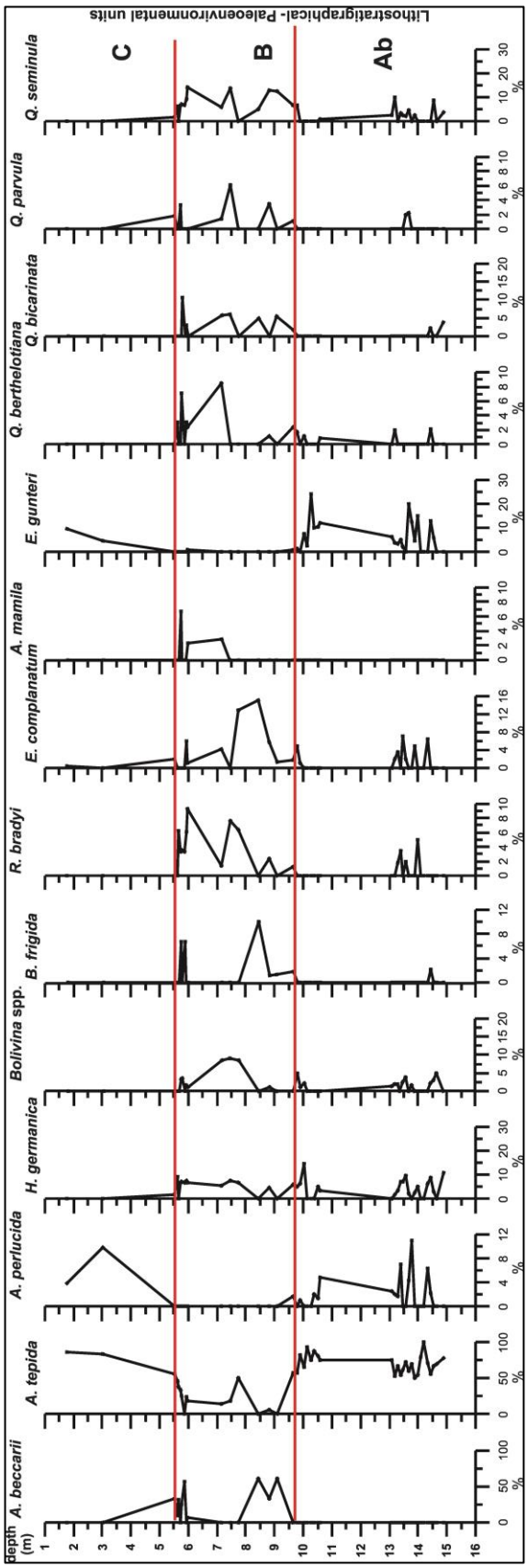

Figure 10-5*. Foraminiferal abundances in borehole P-5.*

Εικόνα 10-5. *Οι συγκεντρώσεις των τρηματοφόρων στην γεώτρηση P-5.*

10.4 Correlation of the Pleistocene – Holocene facies

Through foraminiferal analyses of boreholes P-2, P-4 and P-5 in western Saronic Gulf (Piraeus coastal plain), four different paleoenvironmental facies have been identified. Unit A (divided into categories Aa and Ab) is characterized as a lagoonal environment with mesohaline-oligohaline conditions (subunit Aa as a closed lagoon and subunit Ab as an open lagoon environment). Unit B is characterized as shallow-marine environment with freshwater influences. Unit C is characterized as lagoonal environment with oligohaline conditions (also closed lagoon), while Unit D as coastal, paralic and/or freshwater marsh environment. Definitely though Unit D is not considered a marine environment, but it exhibits more subaerial/ terrestrial features.

In boreholes from the Corinth area also four environments have been described. The first is lagoonal (mesohaline to oligohaline conditions) where regional paleodepth ≤ 20 m depth is proposed (Cluster II/ Group B). The second is shallow marine environment with no influence from freshwater input, where regional paleodepth ≥ 40 m depth is proposed (Cluster II / Group A/C). The third is a transitional situation between lagoonal and shallow marine environment, where regional paleodepth between 20 m and 40 m depth is proposed (Cluster I / Group B/C). The forth is a coastal/ fluvial backshore environment.

A significant correlation among the environment described in these boreholes and the environment described in boreholes from the Corinth Canal is identified.

Unit D shows high resemblance with the forth environment, the coastal/ fluvial backshore environment. Both these facies are characterized the likewise based on the few or broken foraminifera specimens described within (Goiran et al., 2011; Triantaphyllou et al., 2016).

A correlation is also suggested between Unit B and the transitional environment in Corinth boreholes (Cluster I / Group B/C). In both cases full marine species (miliolids, *Rossalina bradyi*) are described, accompanied by *Ammonia tepida* and *Haynesina* spp.. Despite similarities some differences have been traced. In particular the presence of

Bolivina dilatata, *Peneroplis pertusus*, *Elphidium complanatum*, have been found only in Unit B from Piraeus.

Unit A is significantly correlated with the (Cluster II/ Group B) lagoonal assemblages. In both cases the dominance of *Ammonia tepida* in the examined samples is prominent. Even though that minor differences are described (in P-2, P-4 and P-5 boreholes the presence of *Aubignina perlucida* and *E. gunteri* is described, while in samples extracted from the Corinth area the presence of E. granosum is mentioned), the high percentage of the *A. tepida* in the samples (in some cases even 100% of the total sample), is undeniable.

A significant difference between these two case studies is the absence of deeper marine environment in the Piraeus samples. In the examined samples from the Corinth area, deeper marine facies are described (with regional paleodepth ≥ 40 m depth). The main reason is the different tectonic regime of these areas. The area of Piraeus is not influenced by major active faults and is more stable than the Corinth Isthmus area. Therefore, the absence of subsidence and /or uplift procedures resulted into a less complicated sedimentological pattern. During an equivalent time period (~ 10 ka, Goiran et al., 2011) the boreholes from the Corinth area exhibited significant alternations where the paleoenvironment in Corinth changed from fluvial- backshore to shallow marine, then to shallow marine with lagoonal features and the into fluvial again (e.g. Bh-3 interval from 12.00 m to 5.50 m core depth, associated with the MIS5 highstand, ~125 ka).

Furthermore, the significance of the Kephissos river input is significant, documented not only to foraminiferal assemblages, but to the examined mollusks and pollen as well (Triantaphyllou et al., 2016).

In conclusion, the presence of *Ammonia tepida* is indeed the most significant indicator to describe lagoonal (mesohaline-oligohaline) environments. In both cases the dominance of the *A. tepida* was prominent. Furthermore, in Piraeus coastal plain the palynological and molluscan analysis (borehole P-4, Triantaphyllou et al., 2016), also indicates deposition in shallow environments. Therefore, the ≤20 m regional estimated

paleodepth proposed for (Cluster II/ Group B), is now a more valid hypothesis, based on the findings from Piraeus area.

Another interesting conclusion is the relationship between the measured magnetic susceptibility measurements extracted form borehole P-4 (Triantaphyllou et al., 2016) and the described paleoenvironment in the borehole sequence. There is a clear correlation between higher MS values and coastal – paralic environment (also proposed in Ghilardi et al., 2008) and MS values with marine conditions. The latter also confirms the correlation between MS values and paleoenvironmental analysis where high values are documented for fluvial terrestrial coarser sediments.

11 3D visualization and paleoenvironmental interpretation

The paleoenvironmental units in the boreholes are described through hierarchical cluster analysis of the foraminiferal assemblages (two way cluster analysis, non-metric multi-dimensional scaling (MDS)), correlated with the described lithologies and with the measured MS values. Lagoonal environment is associated with Group B-Cluster III assemblages (dominated by small sized *A. tepida*, followed by *E. granosum* and *Haynesina* spp.) (Fig. 7-2, chapter 7.1*)*. Shallow marine environments are associated with Group A/C-Cluster II assemblages (dominated by full marine species (e.g. *N. terquemi, Asterigerinata* spp., *Discorbis* spp.). Transitional environmental conditions (from shallow marine to lagoonal) are associated with Group B/C-Cluster I (dominated by *A. beccarii*, *E. crispum*). Based on these divisions different depositional paleoenvironments can be differentiated and therefore a temporal reconstruction of the paleoenvironment is feasible. This analysis clearly demonstrates and confirms that not only lithology but also the depositional environment display significant spatial and temporal variations over short distances.

Micropaleontological analysis has shown successions of lagoonal to shallow marine deposits (sea level rise/highstand) with terrestrial deposits (sea level fall/lowstand). The latter indicates that glacioeustatic sea level changes and the tectonic uplift of the area caused constant shifts of the coastline seaward (forced regression sequences) or landward (transgression sequences) (e.g. Emery and Myers, 1994; Nichols, 1999; Nagendra et al., 2011) and their imprint is documented within the paleoenvironmental alternations described before. Landward shifting of the coastline and the upwards deepening sequence pattern reflects transgression (Transgressive Systems Tract, TST), whereas seawards shifting of the coastline and the upward shallowing sequence pattern reflects forced regression (forced Regressive System Track, FRST) (e.g. Nagendra et al., 2011; Avnaim et al., 2012; Amorosi et al., 2014a; Farouk, et al., 2016).

The vertical stacking of the borehole cores mark five distinct successive sedimentary sequences, indicating an onset of transgressive-regressive (T-R) conditions (Figs 11-1,

11-2, 11-3) which are better manifested in the deepest borehole (Bh-3). In boreholes Bh-1 and GA-5 (Figs 11-1, 11-2) three successive transgressive-regressive (T-R) sequences can be described. Notable, the described sediments and the estimated palaeobathymetry in these boreholes can be significantly correlated. In borehole GA-4 (Figs 11-1, 11-2) three successive transgressive-regressive (T-R) sequences can be described as well. The shallow marine paleoenvironment (~40 m water depth) described at the interval 25.50 – 31.00 m core depth can be correlated with the equivalent regional estimated palaeobathymetry in Bh-3 (37.00–39.60 m core depth) and in Bh-7 (Figs 11-1, 11-2) (26.00–27.00 m core depth) horizons. Furthermore, even though no paleoenvironmental description of boreholes Bh-6 and Bh-4 exists, this horizon can possible be correlated with fine sediments in boreholes Bh-6 (20.70–24.30 m core depth) and Bh-4 (17.50–20.00 m core depth). In cross section Bh-6 / GA-4 (Fig. 11-2) a clayey horizon is correlated between boreholes Bh-6 and Bh-4. Notable, this horizon is displaced from the Kalamaki-Isthmia fault's activity ~5 m. The latter is in agreement with the ~ 5 m offset described in Papanikolaou et al. (2015) between lagoonal horizons in boreholes Bh-3 and Bh-7. This reinsures the Kalamaki-Isthmia fault's activity, considering as well the proximity of these boreholes (Figs 3-2, 11-1).

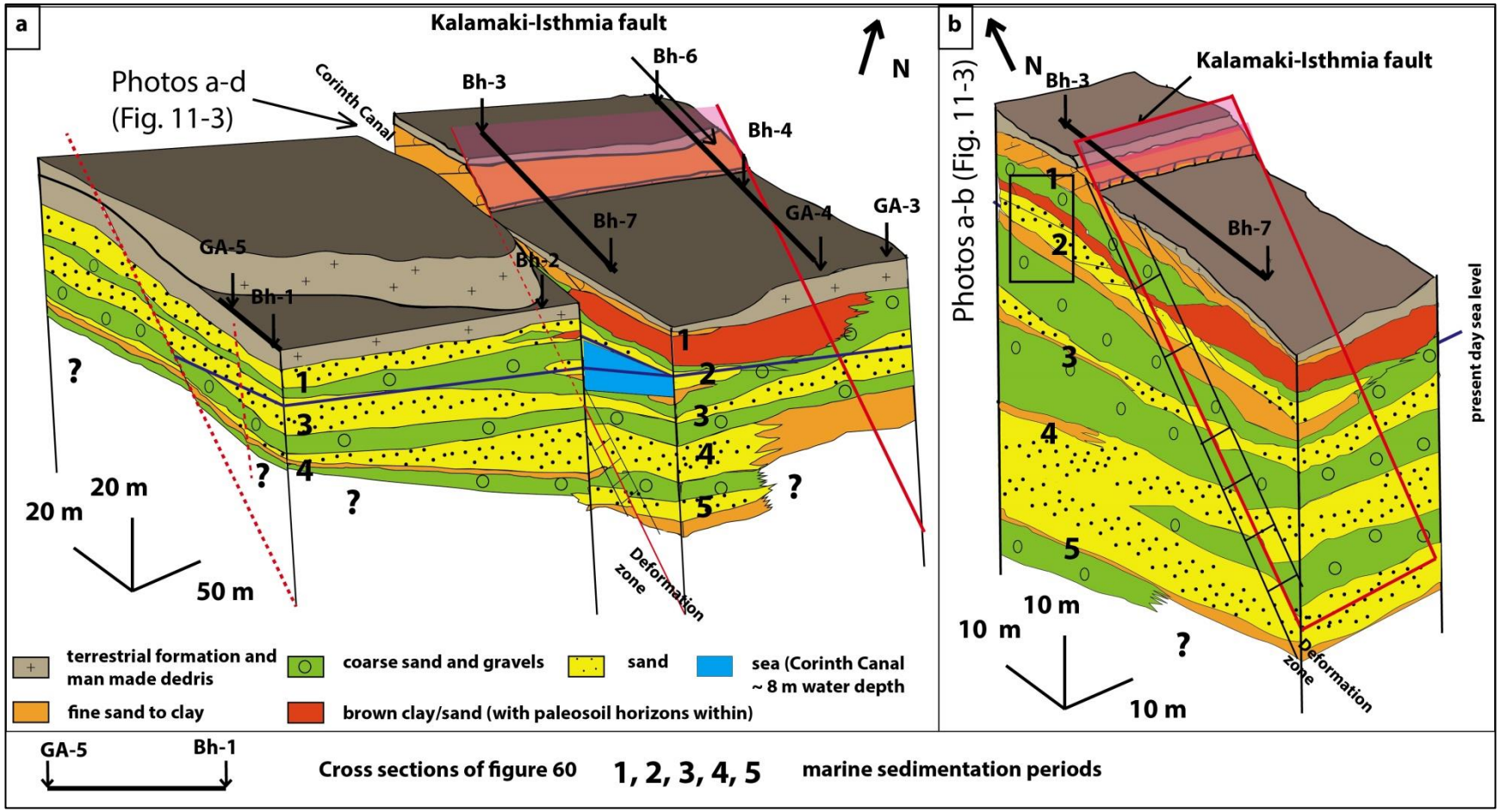

Figure 11-1. *a-b) 3D sketch of the study area based on the boreholes description. Numbers 1-5 show the correlation among the sediments described at the 3-D sketch with the borehole Bh-3 and in photos in figures 11-2, 11-3.*
Εικόνα 11-1. *a-b) Τρισδιάστατο σκίτσο της περιοχής μελέτης με βάση την περιγραφή των γεωτρήσεων και τα επιφανειακά στρώματα. Οι αριθμοί 1-5 υποδεικνύουν την συσχέτιση των στρωμάτων μεταξύ του σκίτσου, της γεώτρησης Bh-3 και των φωτογραφιών στις εικόνες 11-2, 11-3*

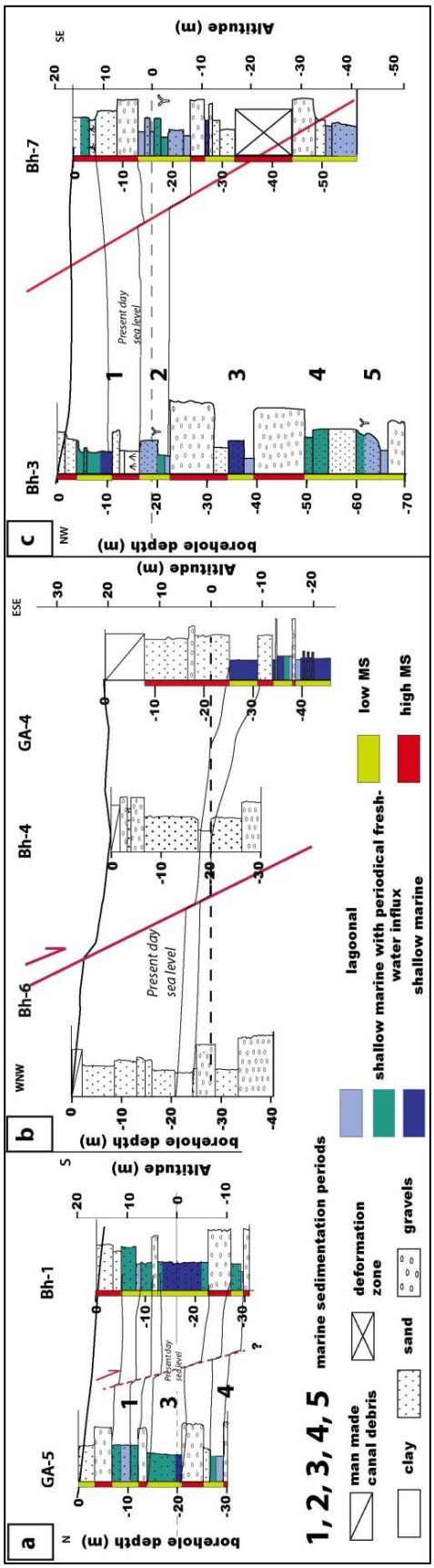

Figure 11-2. *a-d) Cross sections showing the correlation of the stratigraphy and the paleoenvironment between neighbouring boreholes.*

Εικόνα 11-2. *a-d) Τομές που δείχνουν τη συσχέτιση της στρωματογραφίας καθως και του παλαιοπεριβάλλοντος στις γεωτρήσεις.*

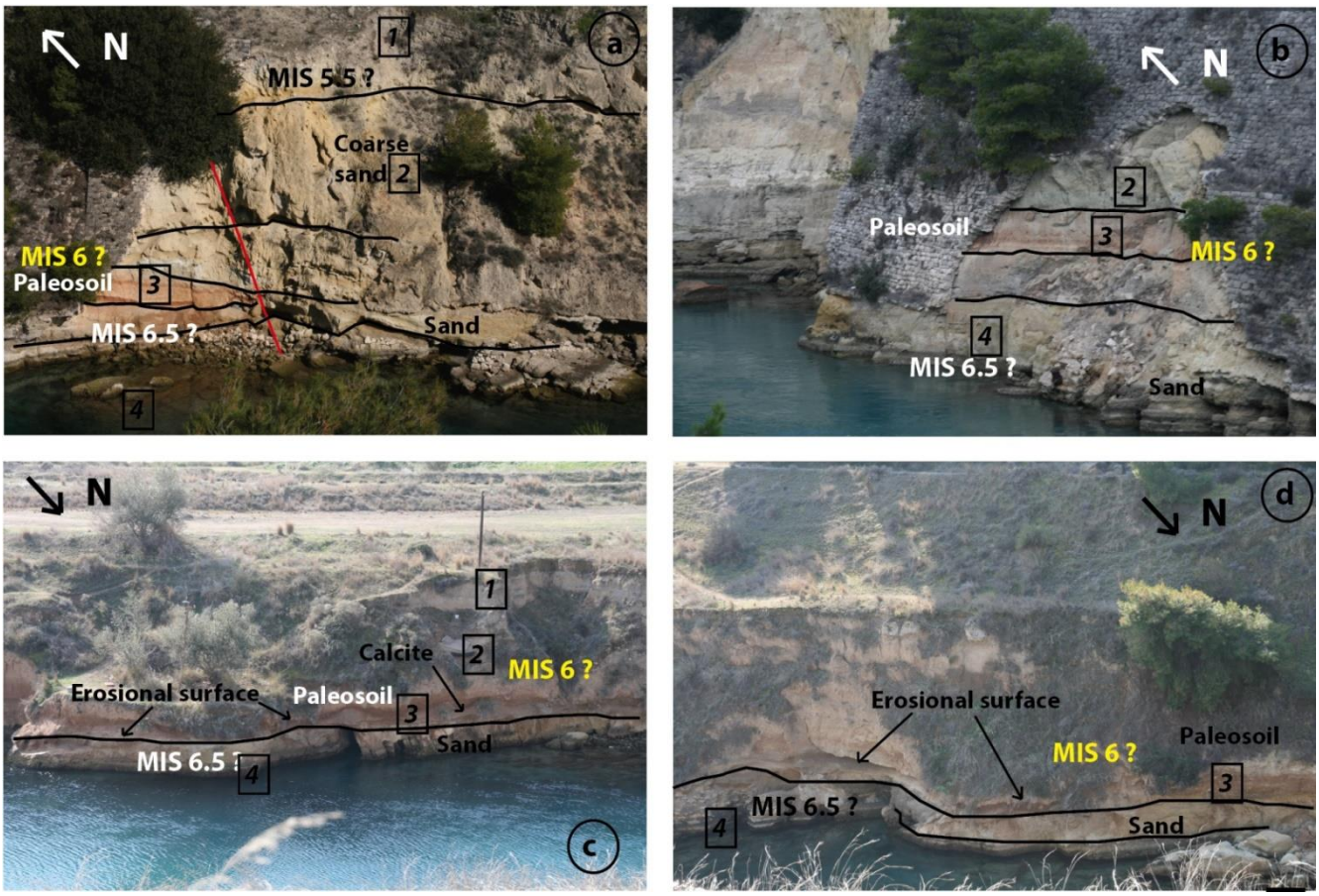

Figure 11-3. *a-d) Strata observed in (a, b) the northern part; (c, d)) southern part of the Corinth Canal (for locality see green box in figure 3-2). Paleosoil horizons and sands are observed approximately at the same altitude with those described in the borehole core. Furthermore, erosional surfaces are observed, and calcite surfaces strongly indicate subaerial exposure. The observed outcrops are correlated with the upper part of the Bh-3 borehole sequence.*

Εικόνα 11-3. *Στρώματα που παρατηρούνται στο κανάλι (a, b) στο βόρειο τμήμα. (c, d) νότιο τμήμα (πράσινο πλαίσιο στην εικόνα 3-2). Οι ορίζοντες του παλαιοεδάφους και οι άμμοι παρατηρούνται περίπου στο ίδιο υψόμετρο με αυτές που περιγράφονται στον πυρήνα της γεώτρησης Bh-3. Επιπρόσθετα, παρατηρούνται επιφάνειας ασυνέχειας με ασβεστοποίηση υποδεικνύοντας επιφανειακές συνθήκες. Τα στρώματα αυτά συσχετίζονται με το ανώτερο τμήμα της γεώτρησης Bh-3.*

12 Discussion

12.1 Age constraints

Even though that the data from OSL/IrSL were inconclusive and the corals can only indicate a possible age of 175 ka and older, the nannofossils assemblages offer more valuable insights regarding age constraints and proved helpful in determining the age of the sediments.

12.1.1 Surface samples

Nanno fossils were sparse in the examined samples extracted from surface outcrops where, from 32 samples examined only 8 contained nannofossils (Fig. 6-8). The presence of *E. huxleyi* in samples S.23.9/2, S.25.9./3, S.25.9/2 and S.12/7/3 indicates that sediments have been deposited at least after the first occurrence of the species (base of nannofossil biozone NN21a; Martini, 1971); namely within marine isotopic stage MIS 8, at ~265 ka in the eastern Mediterranean (e.g. Raffi et al., 2006). On the contrary, the absence of *E. huxleyi* in samples S.17.7/5, S.17.7/6, 4/7/17 and Can.12 indicates an age older than ~260 ka (older than MIS 9). Furthermore the absence of Large *Gephyrocapsa* (>4 μm) and *Pseudoemiliania lacunose* indicates an age younger than 430 ka (Backman et al., 2012). It is important to mention that sample Can.12 was extracted from the Corinth Canal approximately at the same area where Collier et al. (1992), estimated the age of the corals at ~311 ka (MIS 9). The latter also confirms both absolute and relative ages.

12.1.2 Boreholes

By correlating the glacioeustatic sea level change curve of Siddall et al. (2003) with the uplift rate 0.3 mm/yr for the Corinth Isthmus area as it is estimated by Collier et al. (1992), Dia et al. (1997) and Pierini et al. (2016) dating results, it appears that marine deposits would have been expected to be preserved during the high stands within MIS 5.5, 6.5, MIS 7 and MIS 9 with maximum depths ranging between ~20 and 80 m (e.g., Siddall et al., 2003; Thompson and Goldstein, 2006) (Fig. 12-1). In the same line, the study area is expected to be emerged ~120 m above sea level (cold MIS 2.21 at 23.7 ka) and ~70 m and ~30 m during the cold MIS 6.0 (129.3 ka) and MIS 7.0 (179.2 ka) respectively (e.g. Thompson and Goldstein, 2006). Transgressive stacking patterns therefore, would have been expected to be deposited during the high stands where the coastline had shifted landwards and the area was emerged. Consequently, transgressions phases correspond to MIS 5.5, 6.5, 7, 9 (Fig. 12-1e).

The continuous existence of *E. huxleyi* throughout the borehole sediments indicates depositional ages younger than 265 ka, limiting the marine sedimentation to MIS 5.5, MIS 6.5 and MIS 7 high stands. The lack of accurate radiometric data though does not allow determining the exact ages of the sediments. The latter can be described only through different scenarios involving marine sedimentation in all /or some of the MIS 5, MIS 6 and MIS 7. The estimated regional paleodepths of the present study can also be correlated with the expected paleodepths during MIS 5.5, MIS 6.5 and MIS 7, based on sea level curve and the tectonic uplift of the area. Papanikolaou et al. (2015) suggested that the MIS 5.5 paleoshoreline is expected ~40 m above present sea level, whereas MIS 6.5 and MIS 7 paleoshorelines are expected at ~5 m and ~ (60–70) m above present sea level respectively. The estimated regional paleodepths, in correlation with the modeled shoreline elevations (Papanikolaou et al., 2015) through the uplift rate of the area and the glacioeustatic sea level curve can significantly help to constrain the possible scenarios describing the sedimentation processes of the area.

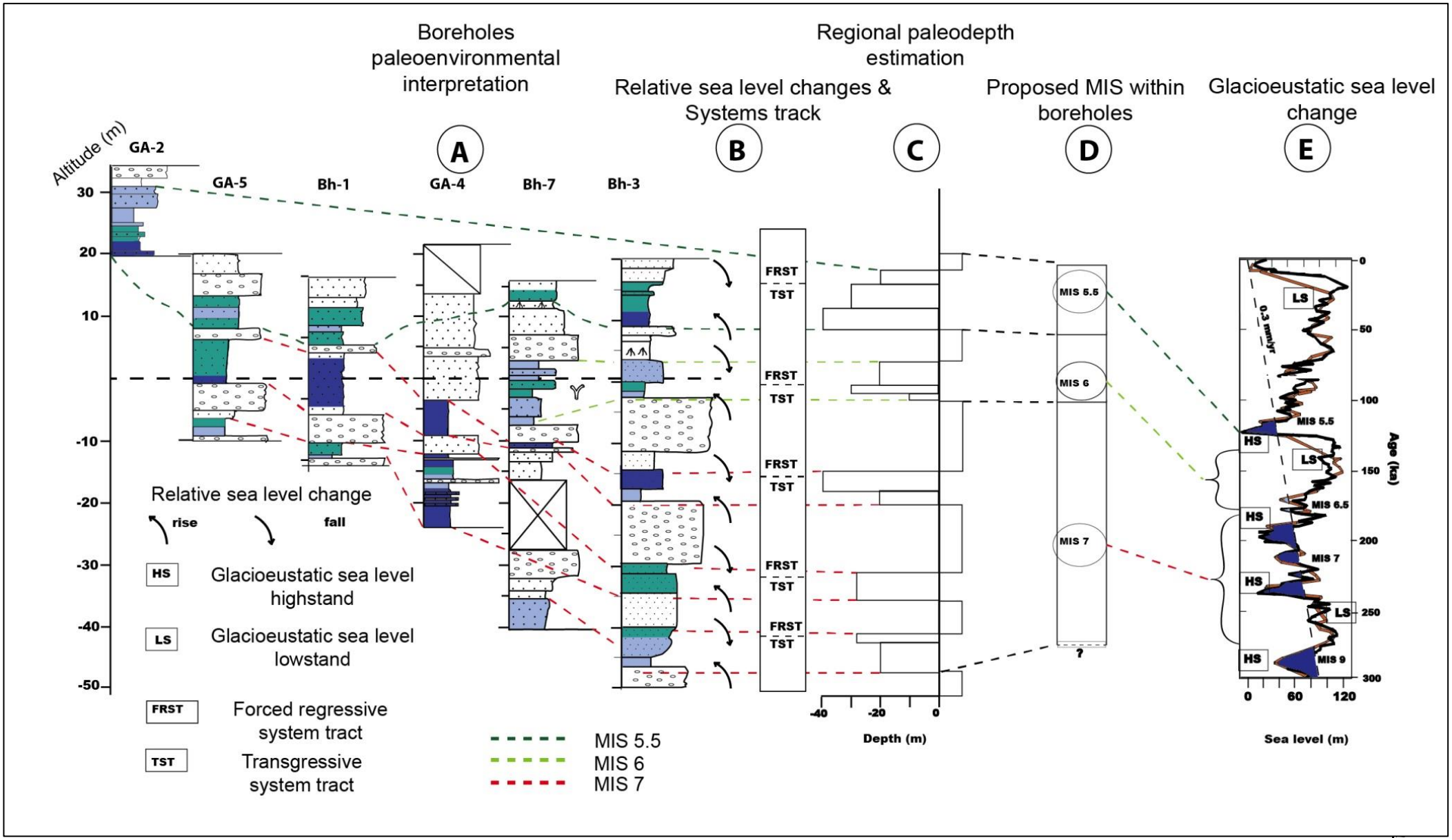
Boreholes paleoenvironmental interpretation
Regional paleodepth estimation
Relative sea level changes & Systems track
Proposed MIS within boreholes
Glacioeustatic sea level change
A
B
C
D
E
Altitude (m)
GA-2
GA-5
Bh-1
GA-4
Bh-7
Bh-3
30
20
10
-10
-20
-30
-40
-50
FRST
TST
MIS 5.5
MIS 6
MIS 7
?
LS
HS
0.3 mm/yr
Age (ka)
0
50
100
150
200
250
300
-40
-20
0
Depth (m)
0
60
120
Sea level (m)
Relative sea level change
rise
fall
HS
Glacioeustatic sea level highstand
LS
Glacioeustatic sea level lowstand
FRST
Forced regressive system tract
TST
Transgressive system tract
MIS 5.5
MIS 6
MIS 7

Figure 12-1*. Synthetic sketch showing the sedimentation processes model of the examined boreholes (GA-2, GA-4, GA-5, Bhi-1, Bh-3, Bh-7) where marine sediments are associated with MIS 5 to 7. (A) Sedimentary patterns within boreholes, where the depositional paleoenvironment is shown (dark blue- shallow marine, light blue- lagoonal, emerald- partially influenced by lagoonal features). (B) Sketch illustrating relatively sea rise or fall based on the paleoenvironmental description of the boreholes, in respect with sequence stratigraphic interpretation. (C) Sketch illustrating regional paleodepth estimation based on foraminiferal assemblages. (D) Expected isotopic stages successions, within boreholes which develops in response to glacioeustatic highstands of sea-level and tectonic uplift. According to the most probable scenario sediments were deposited during MIS 5.5, MIS 6.5 and MIS 7. (E) Based on the glacioeustatic sea level curve from Siddall et al. (2003) and the 0.3 mm/yr uplift rate from Collier et al. (1992), the expected depositional environment is described. The timetable where the study area is expected to be submerged are highlighted, in comparison with the periods that it is expected to be emerged (modified from Papanikolaou et al., 2015).*
Εικόνα 12-1*. Σχηματική απεικόνιση του μοντέλου ιζηματογένεσης των γεωτρήσεων (GA-2, GA-4, GA-5, Bhi-1, Bh-3, Bh-7) όπου τα θαλάσσια ιζήματα συνδέονται με τα μεσοπαγετώδη διαστήματα MIS 5 έως 7 (A). Το παλαιοπεριβάλλον μέσα στις γεωτρήσεις (σκούρο μπλε, ρηχό θαλάσσιο, γαλαζοπράσινο ρηχό θαλάσσιο μερικώς επηρεασμένο από λιμνοθάλασσες, γαλάζιο, λιμνοθαλάσσιο περιβάλλον). (Β) Σχηματική απεικόνιση της ανόδου και πτώσης της θάλασσας με βάση την παλαιοπεριβαλλοντική περιγραφή των γεωτρήσεων. (C) Σχηματική απεικόνιση του εκτιμώμενου παλαιοβάθους, (D) Τα αναμενόμενα στάδια κατά τα οποία έγινε η απόθεση των ιζημάτων. (E) Με βάση την καμπύλη μεταβολής της θαλάσσιας στάθμης και του ρυθμού ανόδου της περιοχής περιγράφεται το αναμενόμενο περιβάλλον απόθεσης των ιζημάτων. Επισημαίνονται οι περίοδοι που στην περιοχή αναμένεται να επικρατεί θαλάσσια ιζηματογένεση (από Papanikolaou et al., 2015).*

Pallikarakis et al. (Cor. Proof.) based on the regional estimated paleodepths, suggested a scenario involving marine sedimentation in all three MIS 5, MIS 6 and MIS 7 as the

most favorable to describe the sedimentation processes within borehole Bh-3. The scenario involving marine sedimentation in all three MIS 5, MIS 6 and MIS 7 is the most favorable to describe the sedimentation processes within borehole Bh-7 as well, considering the proximity and the similar described paleoenvironments and paleodepths with borehole Bh-3 (Fig. 8-3). The presence of in situ *Cladocora* corals and lagoonal sediments approximately at the sea level in both boreholes indicates that this horizon, identified in both boreholes, s associated with MIS 6.5 highstand (Pallikarakis et al., Cor. Proof). Considering that corals prefer not muddy but harder substratum to grow, the presence of in situ *Cladocora corals* and lagoonal sediments indicates relatively rapid changes to the paleoenvironmetal conditions. Shallow marine sediments above this layer area associated with MIS 5.5 highstand, while shallow marine sediments beneath this horizon are associated with MIS 7 highstand.

On the contrary, in boreholes Bh-1, GA-5 and GA-4 neither lagoonal sediments nor in situ corals were traced. Furthermore, the relatively deeper marine conditions described in GA-5 (14.30–20.80 m core depth), in Bh-1 (12.00–21.00 m core depth) and in GA-4 (25.50–31.00 m core depth) are not in agreement with the expected paleodepth during MIS 6.5. Based on the sea level curve and the tectonic uplift of the area the paleoshoreline is estimated at ~5 m above the present sea level and therefore shallower conditions are expected. Therefore the presence of MIS 6.5 sediments in these boreholes is excluded and were either eroded or not deposited at all. Consequently, the most favorable scenario describing the sedimentation processes in Bh-1 and GA-5 involves marine deposits during MIS 5.5 and MIS 7 highstands (Fig. 12-1). The scenario suggesting that the entire borehole sequences can be associated with the MIS 7 highstand is based on the assumption that major erosion processes removed marine sediments from MIS 5.5 and although this hypothesis cannot be excluded, it is less probable, considering that this require major erosional processes.

In GA-4, the presence of coarse sand with gravels associated with terrestrial environment (8.80–25.50 m core depth) and the deeper marine conditions at the interval (25.50–31.00 m core depth), indicates that the most favorable scenario describing the sedimentation processes is that the remaining sediments are from MIS 7 (Fig. 12-1).

Considering the altitude where borehole GA-2 was drilled and the paleoenvironmental description of the core sequence, sedimentation during MIS 6.5 is clearly excluded. The paleoenvironmetal interpretation indicates a shallowing upwards paleogeography, in agreement with the expected paleoshoreline at ~40 m. Therefore the most favorable scenario is that the sedimentation sequence occurred during MIS 5.5.

12.2 Tectonic activity

12.2.1 Uplift rate

The 0.3 mm/yr since MIS 7.3 (205 ka) uplift rate of the Corinth Canal is well documented by Collier et al. (1992), Dia et al. (1997) and Pierini et al. (2016). Nannofossils though, can also provide an independent methodology for estimating the age and consequently the uplift of the area. In sample GA-2, at 12.95 m depth the presence of *E. huxleyi* indicates an age younger than 265 ka. Based on the glacioeustatic sea level curve and the estimated palaeobathymetry (maximum ~40 m water depth), an age between ~125 ka (MIS 5.5) and 265 ka (MIS 7) is suggested and an uplift rate ~0.34 ± 0.12 mm/yr is estimated (Fig. 12-2). Ages younger than 125 ka (MIS 5.5) are excluded since the area was constantly emerged and no marine sedimentation was occurring. If sediments were younger than 125 ka, then based on the sea level curve and the palaeobathymetry, a minimum uplift rate ~0.5 mm/yr is proposed. In this scenario though, the paleoenvironment within the boreholes could not be correlated with the borehole data excluding as well such probability. For example instead of alternations of lagoonal and shallow marine facies, relatively deep marine sediments would have been described.

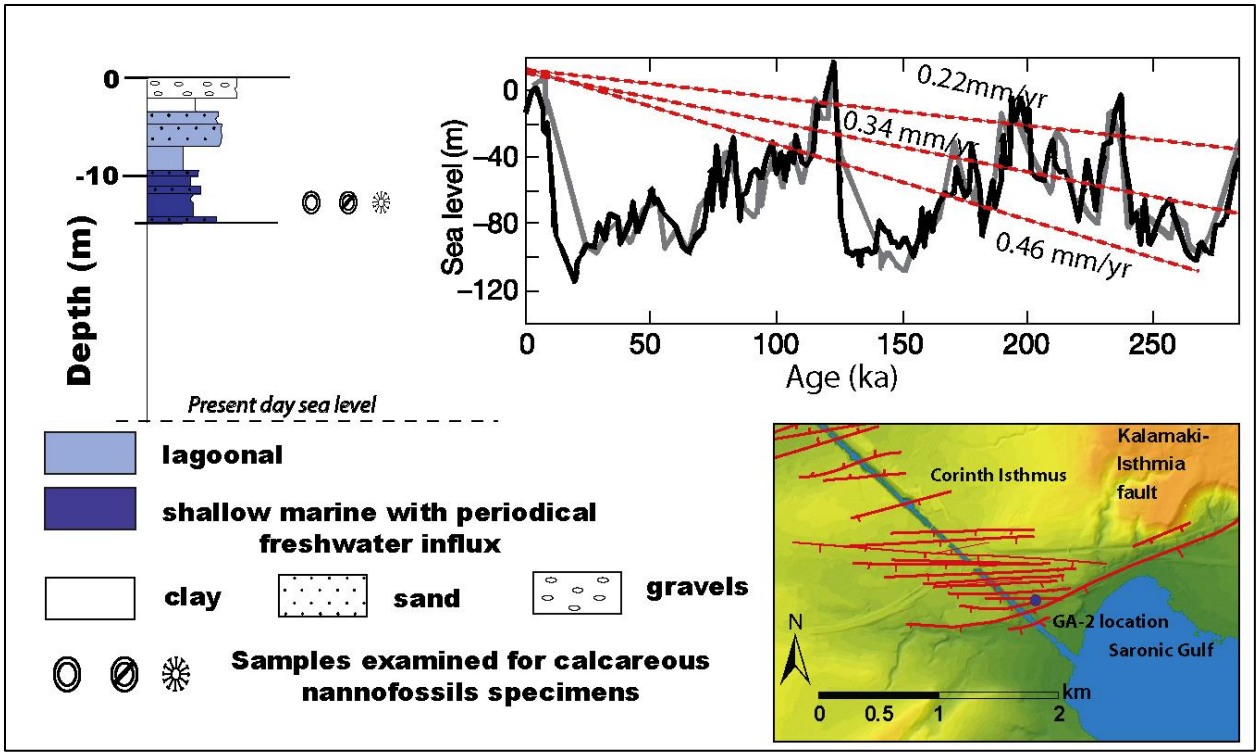

Figure 12-2. *The paleoenvironmental interpretation of borehole GA-2 and the possible range of the estimated uplift rate based on the described calcareous nannofossils from sample GA-2 12.95 m.*

Εικόνα 12-2. *Το παλαιοπεριβάλλον στην γεώτρηση GA-2 και το πιθανό εύρος του εκτιμώμενου ρυθμού ανύψωσης με βάση τα νανοαπολιθώματα του δείγματος GA-2 12.95 m.*

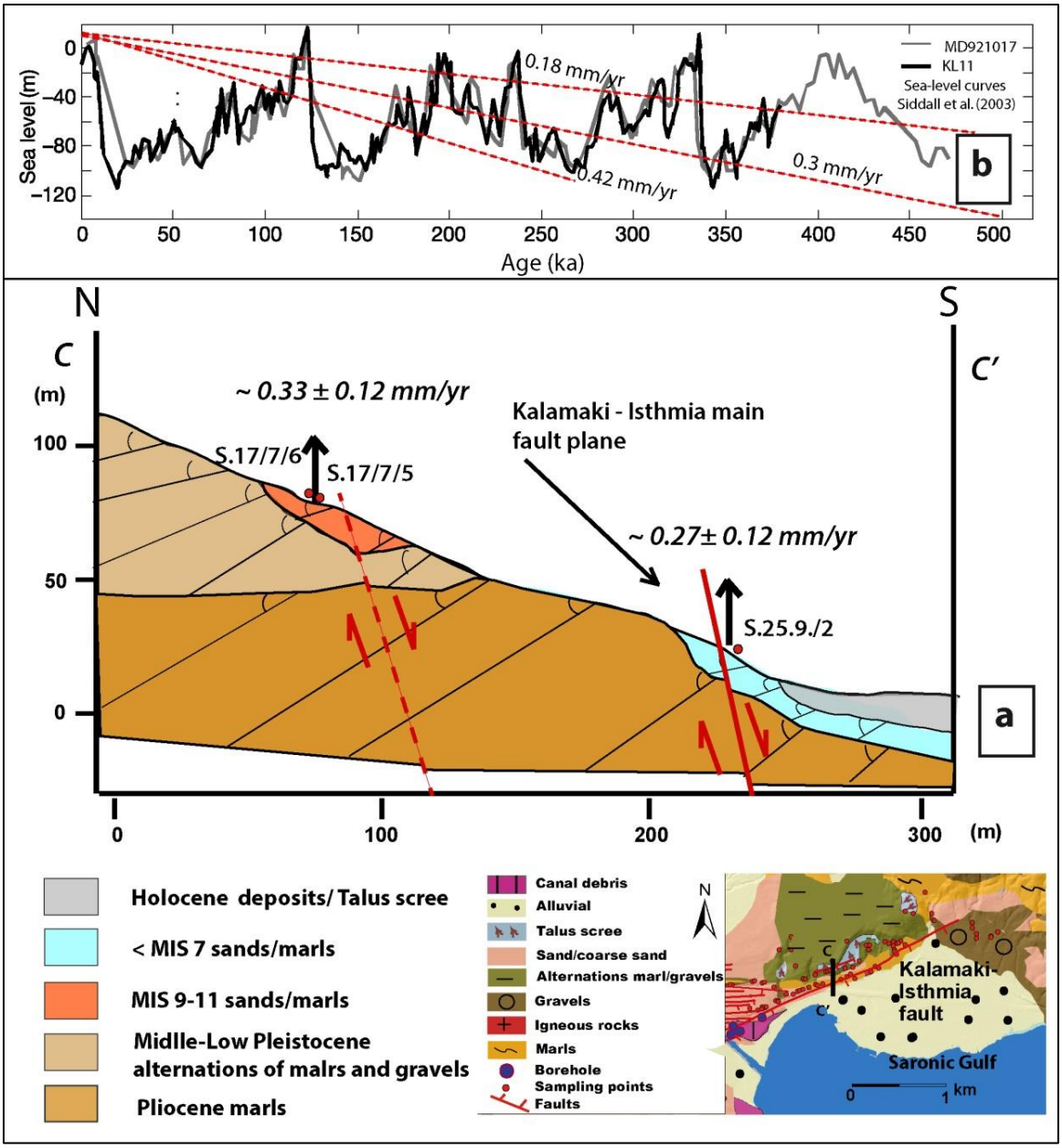

Figure 12-3. *a) The paleoenvironmental interpretation in cross section C-C' almost perpendicular to the Kalamaki-Isthmia fault trace, showing the estimated uplift rate based on calcareous nannofossils assemblages. b) The possible range of the estimated uplift rate based on the described calcareous nannofossils from surface outcrops.* ***Εικόνα 12-3.*** *a) Το παλαιοπεριβάλλον στην τομή C-C' που δείχνει τον εκτιμώμενο ρυθμό ανύψωσης με βάση τα νανοαπολιθώματα. β) Το πιθανό εύρος του εκτιμώμενου ρυθμού ανύψωσης με βάση τα νανοαπολιθώματα τόσο από τα επιφανειακά δείγματα όσο και από την γεώτρηση GA-2.*

Furthermore, in surface samples (S.23.9/2, S.25.9./3, S.25.9/2 and S.12/7/3) (Fig. 6-8) where nannofossils were traced, the presence of *E. huxleyi* also suggests an age between ~125 ka (MIS 5.5) and 265 ka (MIS 7). Nannofossils in samples S.17/7/5 and S.17/7/6 indicate an age in-between MIS 9 to MIS 11. Based on the regional estimated paleodepth (~30 m water depth) in both cases and the altitude in which the samples were extracted, an 0.27 ± 0.12 mm/yr uplift rate on the hangingwall and 0.33 ± 0.12 mm/yr uplift rate on the footwall of the fault is estimated (cross section C-C') (Fig. 12-3). Therefore following all the above constraints an average 0.30 ± 0.12 mm/yr uplift rate for the cross section C-C' is suggested and based also on the results from borehole GA-2 (Fig. 12-2, ~0.34 ± 0.12 mm/yr), an average 0.32 ± 0.14 mm/yr uplift rate for the eastern part of the Corinth Isthmus is extracted.

The error of the estimated rates incorporates the uncertainties of the paleodepth and the different highstands where the sedimentation was possible. However, the extracted rates are in agreement with the rates extracted through absolute dating techniques by Collier et al. (1992), Dia et al. (1997) and Pierini et al. (2016) adding confidence to the reported rates.

12.2.2 The Kalamaki - Isthmia fault activity

The ~0.3 mm/yr uplift rate of the area is the aftermath of all the combined factors which subside or uplift the Corinth Isthmus. Collier (1990), Collier et al. (1992), though mentioned a relatively lower uplift rate at the western part (~0.2 mm/yr) than the eastern part (~0.3 mm/yr). Furthermore, the morphology of the western part of the Isthmus is relatively smoother than the eastern part where the Kalamaki- Isthmia fault is the dominant structure (e.g. Papanikolaou et al., 2015), also indicating higher tectonic activity. The cross section of the Canal (e.g. Collier, 1990; Collier et al., 1992; McMurray and Gawthorpe, 2000 and this study) shows significantly more faults at the eastern part (Kalamaki- Isthmia fault zone) than the western (Fig. 12-4).

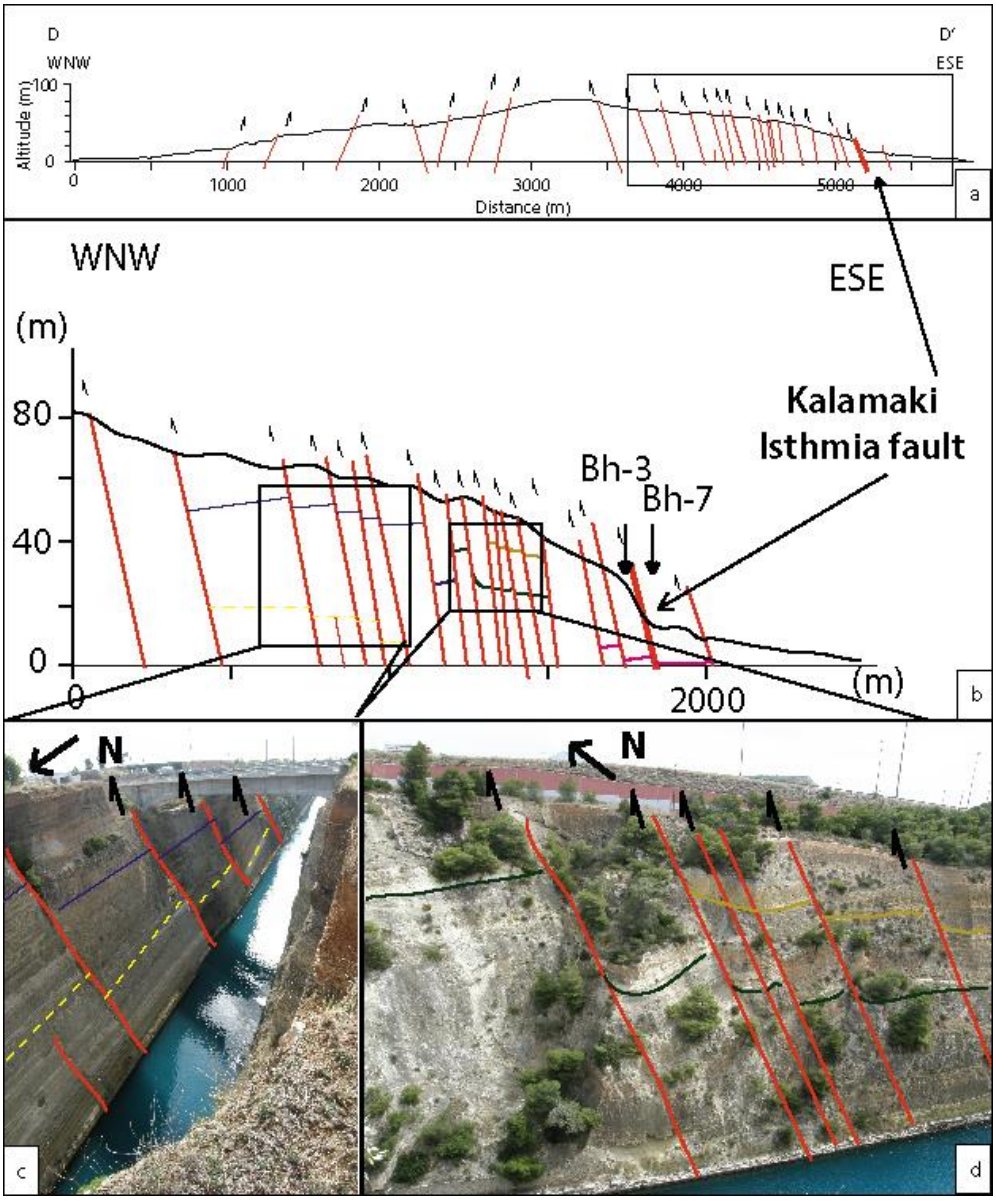

Figure 12-4. *a-b) Cross section of the Corinth Canal (based on Collier (1990) and this study), showing significantly more faults intersecting the eastern than the western part of the Canal. c-d) Photos from the northern part of the canal showing how the faults have displaced characteristic horizons.*

Εικόνα 12-4. a-b) Η διατομή της Διώρυγας, όπου τα περισσότερα ρήγματα βρίσκονται στο ανατολικότερο τμήμα. c-d) Φωτογραφίες από το βόρειο τμήμα της Διώρυγας που δείχνουν μετατοπισμένους ορίζοντες από τη δράση των ρηγμάτων.

Mapping of the area has also revealed several faults displacing the exposed strata at the Corinth Canal (Fig. 12-4c, d). It is questionable though whether these displacements

were caused only from their activity and/or have been passively ruptured during another earthquake triggered by distal faults, like possible the Kalamaki-Isthmia fault during the 1981 earthquake sequence (e.g. South Alkyonides fault system, Papanikolaou et al. (2015)).

Papanikolaou et al. (2015) suggested a ~0.04 mm/yr maximum slip rate since MIS 6.5 for the main trace of the Kalamaki-Isthmia fault, based on displaced lagoonal horizons in boreholes Bh-3 (footwall) and Bh-7 (hangingwall). In cross section C-C' (Fig. 12-3a) between surface outcrops samples S.17/7/5, S.17/7/6 at the footwall and S.23/9/2 at the hangingwall of the fault, a ~0.06 mm/yr difference between the estimated uplift rates is noticed. Considering of course the error mentioned before, this difference can be interpreted as the offset caused by the Kalamaki-Isthmia fault zone activity (Fig. 12-3). Furthermore, since cross section C-C' is located approximately at the center of the fault, the difference of the uplift from the footwall and the hangingwall extracts the maximum fault's throw rate at least during MIS 7. Based on the geometry of the fault (~65^{o} dip), a maximum slip rate ~0.07 ± 0.02 mm/yr for the Kalamaki-Isthmia fault zone since MIS 7 is extracted.

12.3 Uplift / Subsidence model at the Kenchreai – Loutraki graben

The major faults influencing the area of Corinth Isthmus are the SAFS (South Alkyonides Fault System) which uplift the area (e.g. Mariolakos and Stiros, 1987; Roberts et al., 2009) and the Agios Vassileios, the Kenchreai and the Loutraki faults that subside the area (e.g. Roberts et al., 2011; Koukouvelas et al., 2017). The last two faults form the Kenchreai - Loutraki tectonic graben (Fig. 12-5)

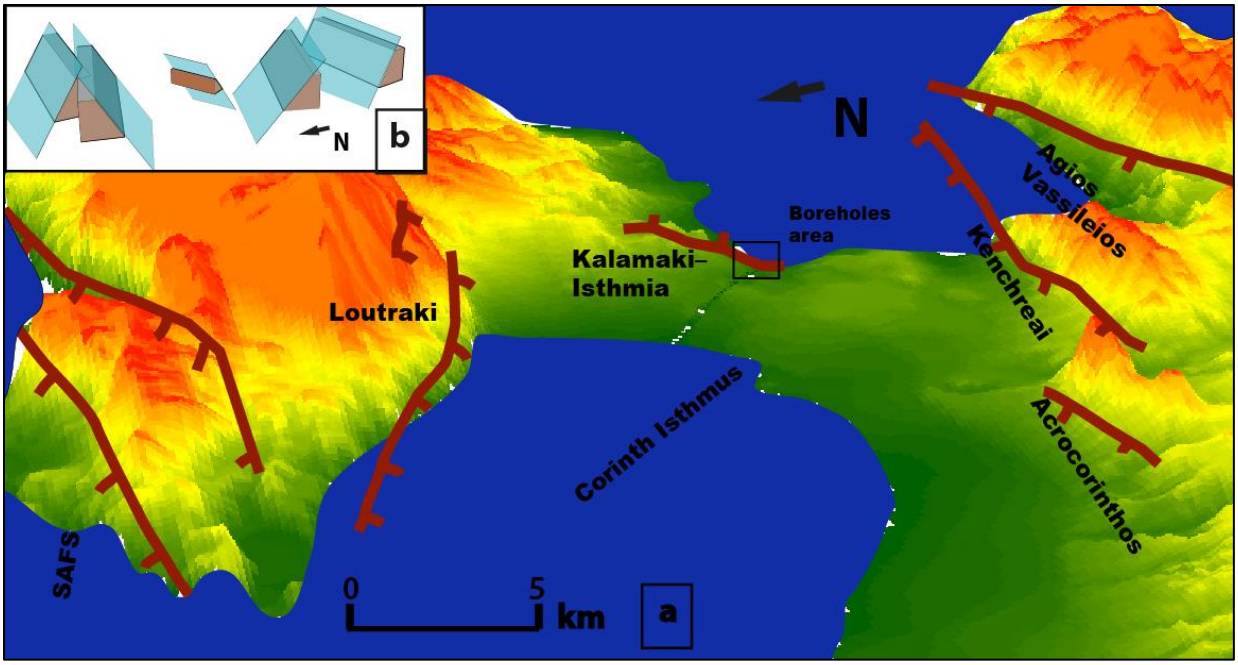

Figure 12-5. *a) 3-D DEM of the area, showing the major active faults and their influence to the topography (vertical exaggeration x3)) b) Simplified 3-D model of the faults, based on their geometry.*

Εικόνα 12-5. *a) Τρισδιάστατο DEM της περιοχή που διακρίνονται τα ρήγματα που επηρεάζουν την περιοχή (ο κατακόρυφος άξονας είναι μεγεθυμένος x3) b) Απλοποιημένο τρισδιάστατο μοντέλο των ρηγμάτων.*

The Kenchreai fault consists both of offshore and onshore fault segments (Papanikolaou et al., 1988, 1989), comprising a ~ 24 km long fault structure (Fig. 12-6). Koukouvelas et al. (2017) thoroughly studied the E-W-trending Kenchreai fault and more specific the onshore segments. They described two segments approximately 3.8 and 6.5 km long where *the morphology of the segment's footwall differs in a change of maximum elevation, from east to west, from 40 m to 300 m. The maximum scarp height is in the order of 275 m in the west fault segment and much less in the east fault segment* (In Koukouvelas et al., (2017)). The western tip of the fault is located at the main stem of the Solomos River. It is interesting to mention the presence of the Acrocorinthos fault (Fig. 12-5).

Figure 12-6. *View of the onshore segment of the* Kenchreai *fault.*
Εικόνα 12-6. *Το χερσαίο τμήμα του ρήγματος των Κεχριών.*

The Kenchreai fault has subsided the area southwards the Canal and has contributed to the submersion of the ancient harbor of Kenchreai (e.g. Mourtzas et al., 2014; Mourtzas and Kolaiti, 2014; Kolaiti and Mourtzas, 2016). For the Kenchreai fault a slip rate approximately 0.15 – 0.20 mm/yr has been proposed (Koukouvelas et al., 2017; Deligiannakis et al., in press),

The Loutraki fault consists of two parallel segments approximately 1.5 km apart, the southern segment that bounds the Loutraki basin, also traced offshore (e.g. Sakellariou et al., 2001) and the northern segment at about 500 m altitude near to Osios Potapios (Fig.12-7). *"The northern segment exhibits a clear postglacial scarp close to the Osios Patapios Monastery). The Loutraki Fault is active as it offsets a slope formed during periglacial activity in the last glacial maximum (~15 ± 3 ka). It deforms sediments from*

the last glacial maximum exposed in a small quarry on the roadside. Slip in the Quaternary was ongoing, but intense erosion and sedimentation during glacial episodes would have outpaced scarp growth. Holocene slip and low sedimentation rates have produced a bedrock fault scarp that based on detailed scarp profiles is 8-9 m high, implying it has a throw-rate of approximately 0.50 mm/yr" (Roberts et al., 2011).

The Agios Vassileios fault is a more distant fault located at the southern margin of the Proto-Corinth Gulf (Fig. 12-5). This ~38 km long E-W structure consists both of onshore and offshore segments, dipping northwards. Agios Vassileios fault was significantly more active during Pliocene since it was the south margin of the Proto-Corinth gulf (e.g. Leeder et al., 2002). In the present day though, its slip rate does not exceed ~0.10 to 0.20 mm/yr (Roberts et al., 2011).

Figure 12-7*. View of the northern segment of the Loutraki fault plane (near to Osios Patapios) and the deformed sediments.*

Εικόνα 12-7. *Το βορειότερο τμήμα του ρήγματος του Λουτρακίου, κοντά στον Όσιο Πατάπιο).*

The last 10 years the co-seismic uplift and/or subsidence of earthquake events is been well documented based on satellite images. One of these events is the L'Aquila earthquake on April 6th 2009 in central Italy. This (Mw 6.3) earthquake occurred on the Paganica fault. Several field surveys were conducted during the weeks following the main-shock, with the aim to characterize the pattern of surface faulting (e.g. EMERGEO Working Group, 2009, 2010; Papanikolaou et al., 2010; Goudarzi et al., 2011; Cheloni et al., 2014; Livio et al., 2017). Primary faulting was clearly recognized along the Paganica fault, for a 6 km in length while a maximum displacement of ca. 15 cm has been traced (e.g. Livio et al., 2017). In Papanikolaou et al. (2010) a ~ 25 cm maximum subsidence is described (~ 3 to 4 km from the fault trace), while in Goudarzi et al. (2011), several profiles executed both along and across the Paganica fault revealing an approximately 27 cm subsidence towards the center of the fault structure, also approximately 3 to 4 km distance from the fault trace (Fig. 12-8).

Undoubtedly each earthquake has a unique influence to the environment but it is assumed that an earthquake caused by these faults will have a similar impact in the Corinth region as the L'Aquila event has. The main reason for choosing the L'Aquila earthquake is that in both cases similar lithologies have been described (e.g. Goudarzi et al., 2011). Furthermore, both areas experience a similar tectonic regime (normal faults). Therefore, the described subsidence caused by L'Aquila earthquake can be the base of a simple model to examine the uplift and the subsidence caused by the faults influencing the Canal (SAFS, the Loutraki, the Kenchreai, the Agios Vassileios and the Kalamaki – Isthmia faults).

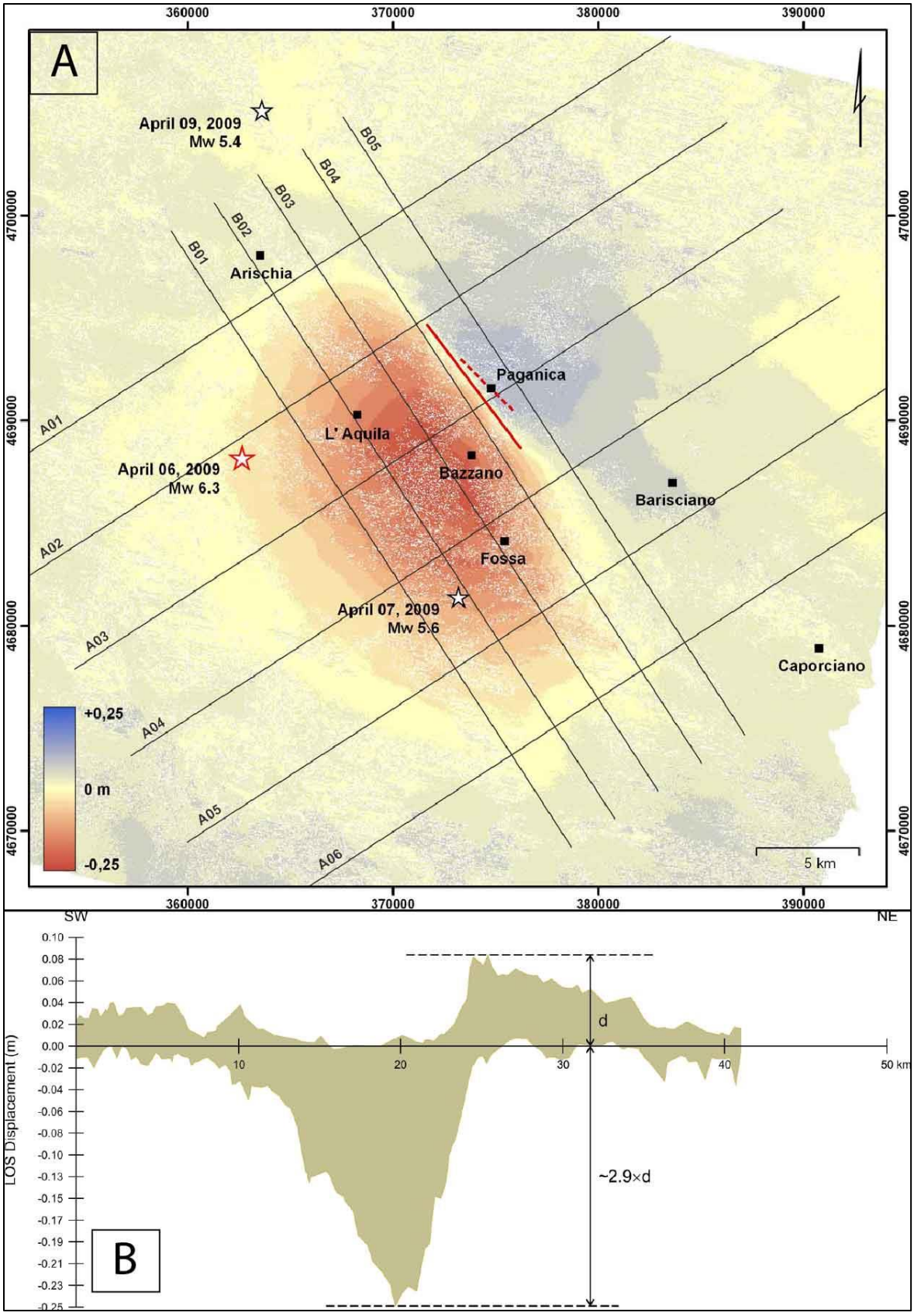
A
360000
370000
380000
390000
4700000
4690000
4680000
4670000
April 09, 2009
Mw 5.4
April 06, 2009
Mw 6.3
April 07, 2009
Mw 5.6
B01
B02
B03
B04
B05
A01
A02
A03
A04
A05
A06
Arischia
Paganica
L' Aquila
Bazzano
Barisciano
Fossa
Caporciano
+0,25
0 m
-0,25
5 km
SW
NE
LOS Displacement (m)
0.10
0.08
0.06
0.04
0.02
0.00
-0.02
-0.04
-0.06
-0.08
-0.10
-0.13
-0.15
-0.17
-0.19
-0.21
-0.23
-0.25
10
20
30
40
50 km
d
~2.9×d
B

Figure 12-8. *(A) Displacement field of the 6 and 7 of April 2009 L'Aquila earthquakes and (B) the diagram showing the range of the observed ground deformation in the epicentral area as appears from all profiles perpendicular to the activated fault plane. A footwall uplift/hangingwall subsidence ratio of about 1/3 with is extracted (Papanikolaou et al., 2010).*

Εικόνα 12-8*. (Α) Οι μετατοπίσεις στις περιοχή της L'Aquila, έπειτα από τους σεισμούς στις 6 και 7 Απριλίου (2009) και (Β) Το διάγραμμα που απεικονίζει την εδαφική μετατόπιση βασισμένοι στα προφίλ κάθετα στο ρήγμα, όπου εκτιμάται και ο λόγος ανύψωσης/ταπείνωσης περίπου 1/3 (Papanikolaou et al., 2010).*

The subsidence/uplift distribution depends on:

a) The subsidence/uplift ratio

b) The fault's dip

In L'Aquila earthquake, a coseismic subsidence/uplift ratio ~1/2.9 is proposed (Papanikolaou et al., 2010, Fig. 12-8), while for the Eliki fault a ratio 1/2 is proposed (e.g. Koukouvelas, 1998). The dip of a fault varies from relatively high angles (e.g. ~65^{o} for the Loutraki fault, Roberts et al., 2011) to relatively low angles (e.g. ~45^{o} for the SAFS, Jackson et al., 1982). Therefore, different scenarios have to been considered involving all different variables (Table 21). Based on the average values of ratio and fault's dip (55^{o} dip and 1/2.5 subsidence/uplift ratio) a model is proposed, describing the excepted uplift and subsidence rate for the SAFS, the Loutraki, the Kenchreai, the Agios Vassileios and the Kalamaki – Isthmia faults (Figs 12-9 to 12-13).

Consequently, according to the average scenario described in table 21 and considering the ~0.20 mm/yr slip rate of the Kenchreai and the Agios Vassileios faults (e.g. Roberts et al., 2011), a maximum subsidence ~ 0.12 mm/yr is estimated for these two faults. Likewise, based on the ~0.50 mm/yr slip rate of the Loutraki fault (e.g. Deligiannakis et al., in press) a maximum subsidence rate ~0.29 mm/yr is estimated and a maximum uplift ~ 0.53 mm/yr for the SAFS fault (e.g. Deligiannakis et al., in press). Finally, a

maximum uplift ~ 0.02 mm/yr and 0.04 mm/yr subsidence rates are estimated for the Kalamaki-Isthmia fault.

Table 21. The different scenarios of the subsidence and the uplift rates of the examined faults. The first two scenarios consider that the subsidence/uplift ratio is 1/3 (while the faults dip ranges from 45^o to 65^o), while the third and the forth scenarios consider that the subsidence/uplift ratio is 1/2 (while the faults dip ranges from 45^o to 65^o). Finally the average scenario (55^o dip and 1/2.5 subsidence/uplift ratio) is presented. The examined pointe which is mentioned at the table the immediate footwall of the Kalamaki-Isthmia fault. Πίνακας 21. Τα διαφορετικά σενάρια της κατανομής των ρυθμών ανύψωσης και ταπείνωσης στην περιοχή. Στα δυο πρώτα ο λόγος ταπείνωσης/ανύψωσης είναι 1/3 (με την κλίση των ρηγμάτων να μεταβάλλεται από 45^o σε 65^o), ενώ στο τρίτο κι τέταρτο είναι1/2 (με την κλίση των ρηγμάτων να μεταβάλλεται από 45^o σε 65^o). Το σενάριο με τις μέσες τιμές παρατίθεται στο τέλος του πίνακα. Το σημείο αναφοράς είναι το ανερχόμενο τέμαχος του ρήγματος Καλαμακίου-Ισθμίων.

1st scenario (Fault dip 65^o subsidence/uplift ratio ~1/3)							
65^o fault dip	slip rate (mm /yr)	Throw rate (mm/yr) (1/3 ratio)	Max uplift rate (+) (mm/yr)	Max subsidence rate (-) (mm/yr)	Subsidence or uplift at the examined point (mm/yr)	Cumulative movements since MIS5 at examined point (in m)	Cumulative movements since MIS7 at examined point (in m)
SAFS	2.30	2.08	0.52	-1.56	+0.115	+14.4	+23
Loutraki	0.50	0.45	0.11	-0.34	-0.11	-14	-22
Kenchreai	0.20	0.18	0.04	-0.14	-0.09	-11.2	-18
Ag. Vass.	0.20	0.18	0.04	-0.14	-0.01	-1.75	-2.8
Kalamaki	0.07	0.06	0.02	-0.04	+0.02	+2.5	+4
Total					**-0.08**	**-10.1**	**-16**
2nd scenario (Fault dip 45^o subsidence/uplift ratio ~1/3)							

45° fault dip	slip rate (mm /yr)	Throw rate (mm/yr) (1/3 ratio)	Max uplift rate (+) (mm/yr)	Max subsidence rate (-) (mm/yr)	Subsidence or uplift at the examined point (mm/yr)	Cumulative movements since MIS5 at examined point (in m)	Cumulative movements since MIS7 at examined point (in m)
SAFS	2.30	1.62	0.41	-1.21	+0.09	+11.25	+18
Loutraki	0.50	0.35	0.09	-0.26	-0.08	-10	-16
Kenchreai	0.20	0.15	0.04	-0.11	-0.07	-8.7	-12
Ag. Vass.	0.20	0.15	0.04	-0.11	-0.01	-1.75	-4
Kalamaki	0.07	0.06	0.02	-0.04	+0.02	+2.5	+4
Total					**-0.05**	**-6.5**	**-10**

3rd scenario (Fault dip 65° subsidence/uplift ratio ~1/2)

65° fault dip	slip rate (mm /yr)	Throw rate (mm/yr) (1/2 ratio)	Max uplift rate (+) (mm/yr)	Max subsidence rate (-) (mm/yr)	Subsidence or uplift at the examined point (mm/yr)	Cumulative movements since MIS5 at examined point (in m)	Cumulative movements since MIS7 at examined point (in m)
SAFS	2.3	2.08	0.69	1.39	+0.15	+18.75	+30
Loutraki	0.5	0.45	0.15	0.30	-0.09	-11.25	-18
Kenchreai	0.2	0.18	0.06	0.12	-0.07	-8.75	-14
Ag. Vass.	0.2	0.18	0.06	0.12	-0.01	-2.5	-4
Kalamaki	0.07	0.06	0.02	0.04	+0.02	+2.5	+4
Total					**-0.01**	**-1.25**	**-2**

4th scenario (Fault dip 45° subsidence/uplift ratio ~1/2)

45° fault dip	slip rate (mm /yr)	Throw rate (mm/yr) (1/2 ratio)	Max uplift rate (+) (mm/yr)	Max subsidence rate (-) (mm/yr)	Subsidence or uplift at the examined point (mm/yr)	Cumulative movements since MIS5 at examined point (in m)	Cumulative movements since MIS7 at examined point (in m)
SAFS	2.3	1.62	0.54	1.08	+0.12	+15	+24
Loutraki	0.5	0.35	0.12	0.23	-0.07	-10	-16

Kenchreai	0.2	0.14	0.05	0.09	-0.06	-6.25	-10
Ag. Vass.	0.2	0.14	0.05	0.09	-0.01	-1.25	-2
Kalamaki	0.07	0.06	0.02	0.04	+0.02	+2.5	+4
Total					**0.00**	**0**	**0**

Average scenario (Fault dip 55° subsidence/uplift ratio ~1/2.5)

Average 55° fault dip	slip rate (mm/yr)	Throw rate (mm/yr) (Average 1/2.5 ratio)	Max uplift rate (+) (mm/yr)	Max subsidence rate (-) (mm/yr)	Subsidence or uplift at the examined point (mm/yr)	Cumulative movements since MIS5 at examined point (in m)	Cumulative movements since MIS7 at examined point (in m)
SAFS	2.3	1.86	0.53	1.33	+0.12	+15	+24
Loutraki	0.5	0.41	0.12	0.29	-0.09	-12.5	-20
Kenchreai	0.2	0.16	0.04	0.12	-0.07	-7.5	-12
Ag. Vass.	0.2	0.16	0.04	0.12	-0.02	-2.5	-4
Kalamaki	0.07	0.06	0.02	0.04	+0.02	+2.5	+4
Total					**-0.04**	**-5**	**-8**

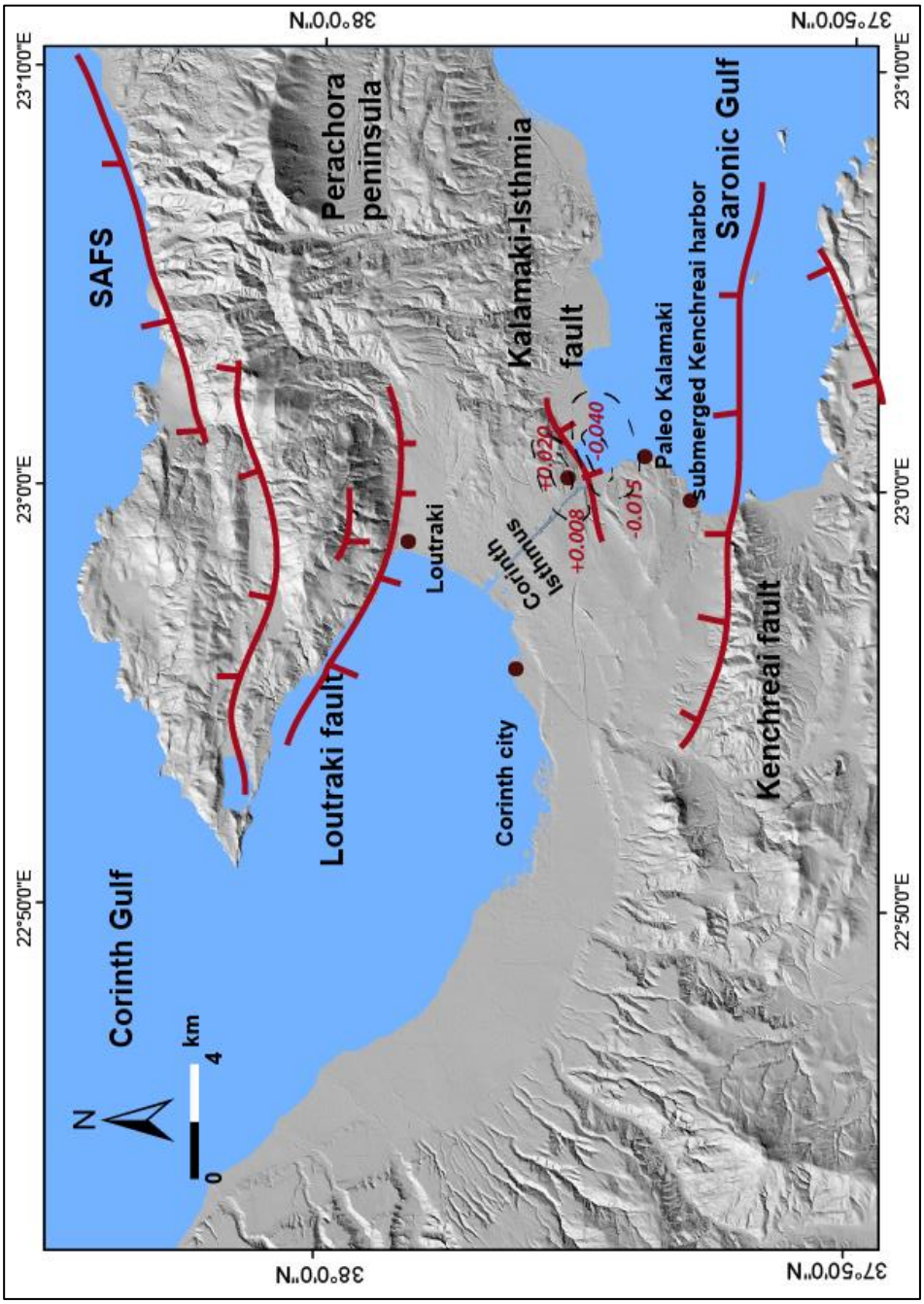

Figure 12-9*. The estimated uplift and subsidence rate in mm/yr due to the activity of the Kalamaki – Isthmia fault based on the average values (55^{o} dip and 1/2.5 subsidence/uplift ratio, Table 21).*

Εικόνα 12-9*. Ο εκτιμώμενος ρυθμός ανύψωσης και ταπείνωσης από την δράση του ρήγματος του Καλαμακίου-Ισθμίων, με βάση τις μέσες τιμές του λόγου ταπείνωσης/ανύψωσης και κλίσης του ρήγματος.*

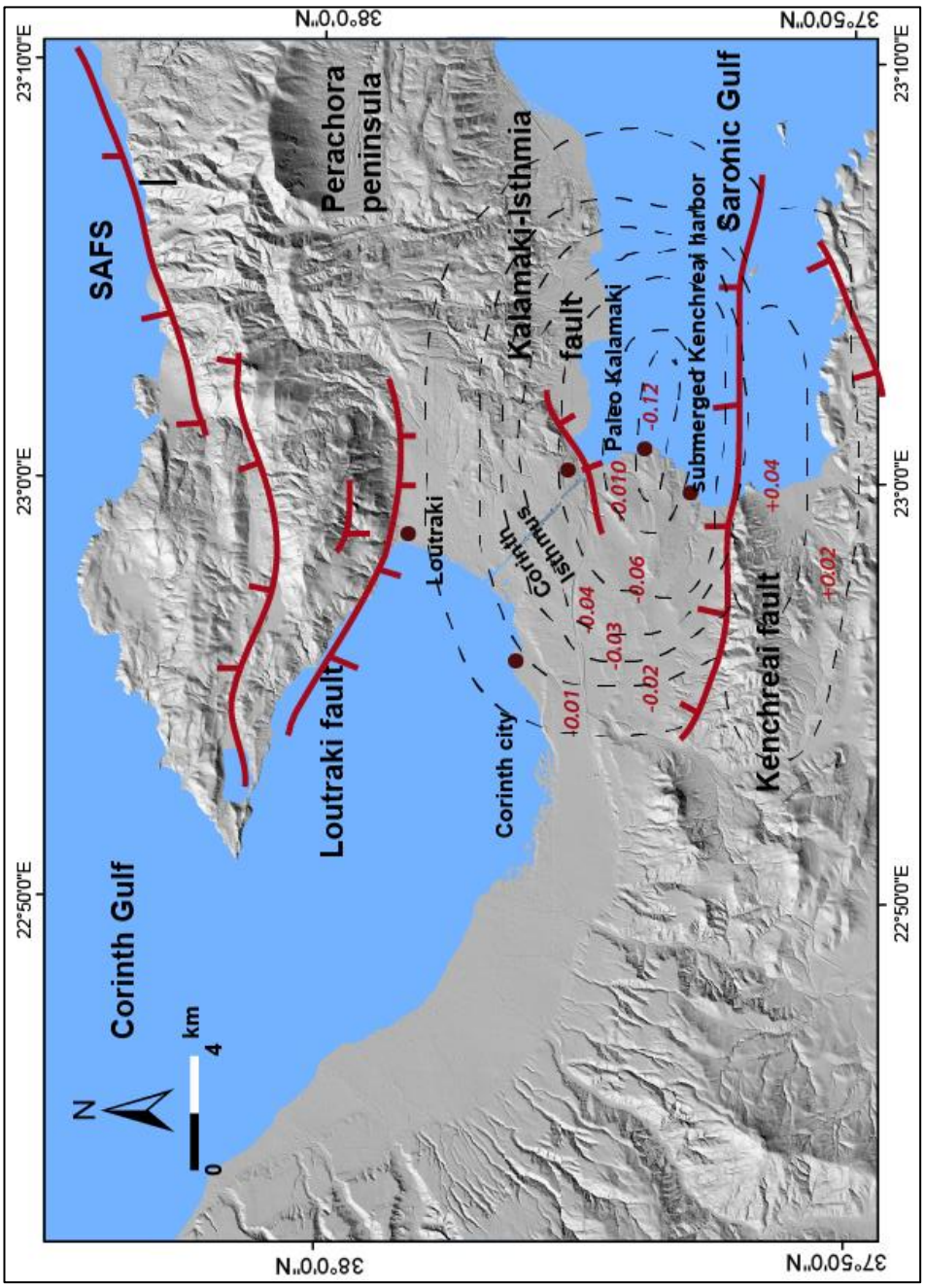

Figure 12-10*. The estimated uplift and subsidence rate in mm/yr due to the activity of the* Kenchreai *fault based on the average values (55^{o} dip and 1/2.5 subsidence/uplift ratio, Table 21).*

Εικόνα 12-10. *Ο εκτιμώμενος ρυθμός ανύψωσης και ταπείνωσης από την δράση του ρήγματος των Κεχριών, με βάση τις μέσες τιμές του λόγου ταπείνωσης/ανύψωσης και κλίσης του ρήγματος.*

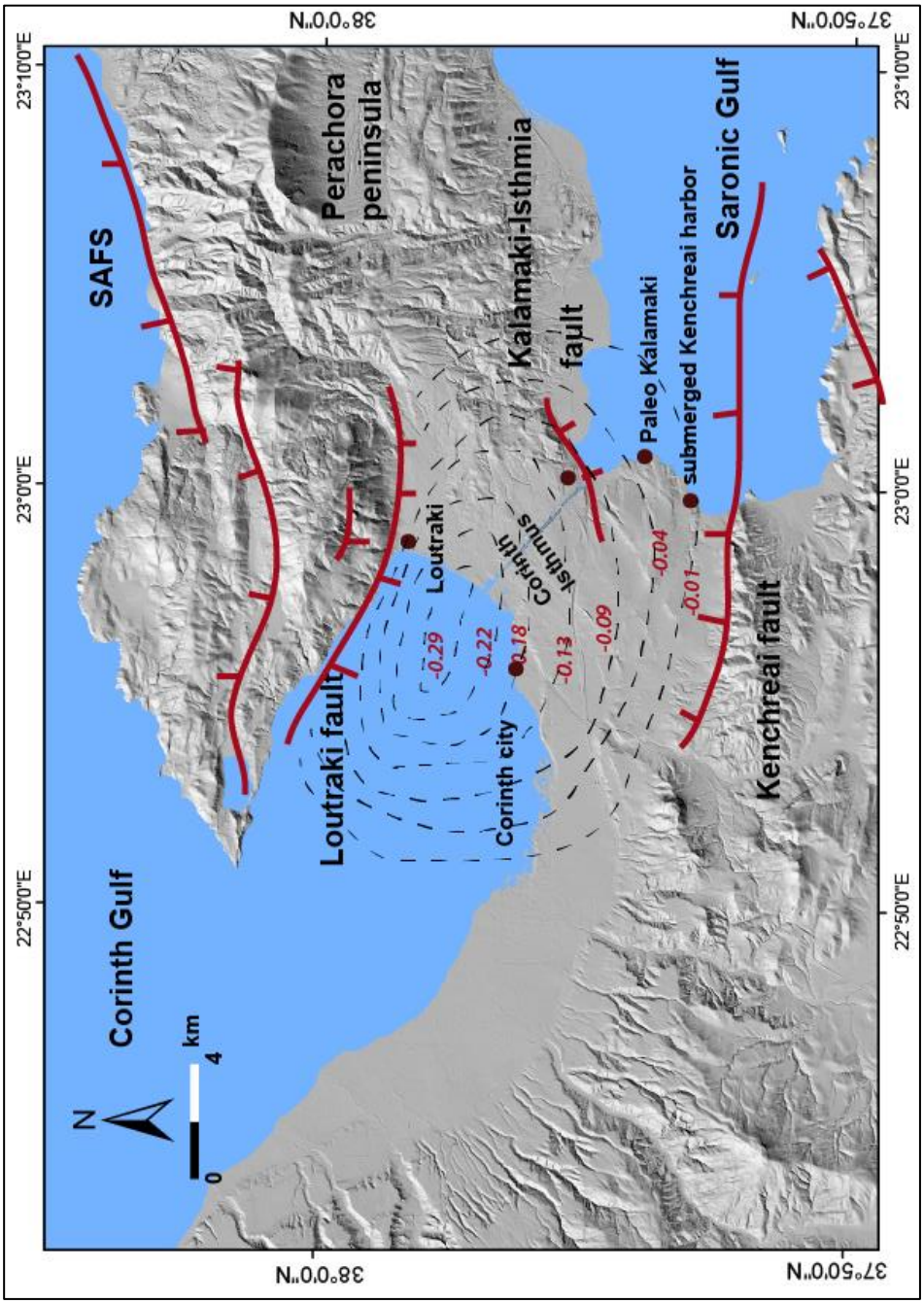

Figure 12-11. *The estimated subsidence rate in mm/yr due to the activity of the Loutraki fault based on the average values (55^{o} dip and 1/2.5 subsidence/uplift ratio, Table 21).*
Εικόνα 12-11. *Ο εκτιμώμενος ρυθμός ανύψωσης και ταπείνωσης από την δράση του ρήγματος του Λουτρακίου, με βάση τις μέσες τιμές του λόγου ταπείνωσης/ανύψωσης και κλίσης του ρήγματος.*

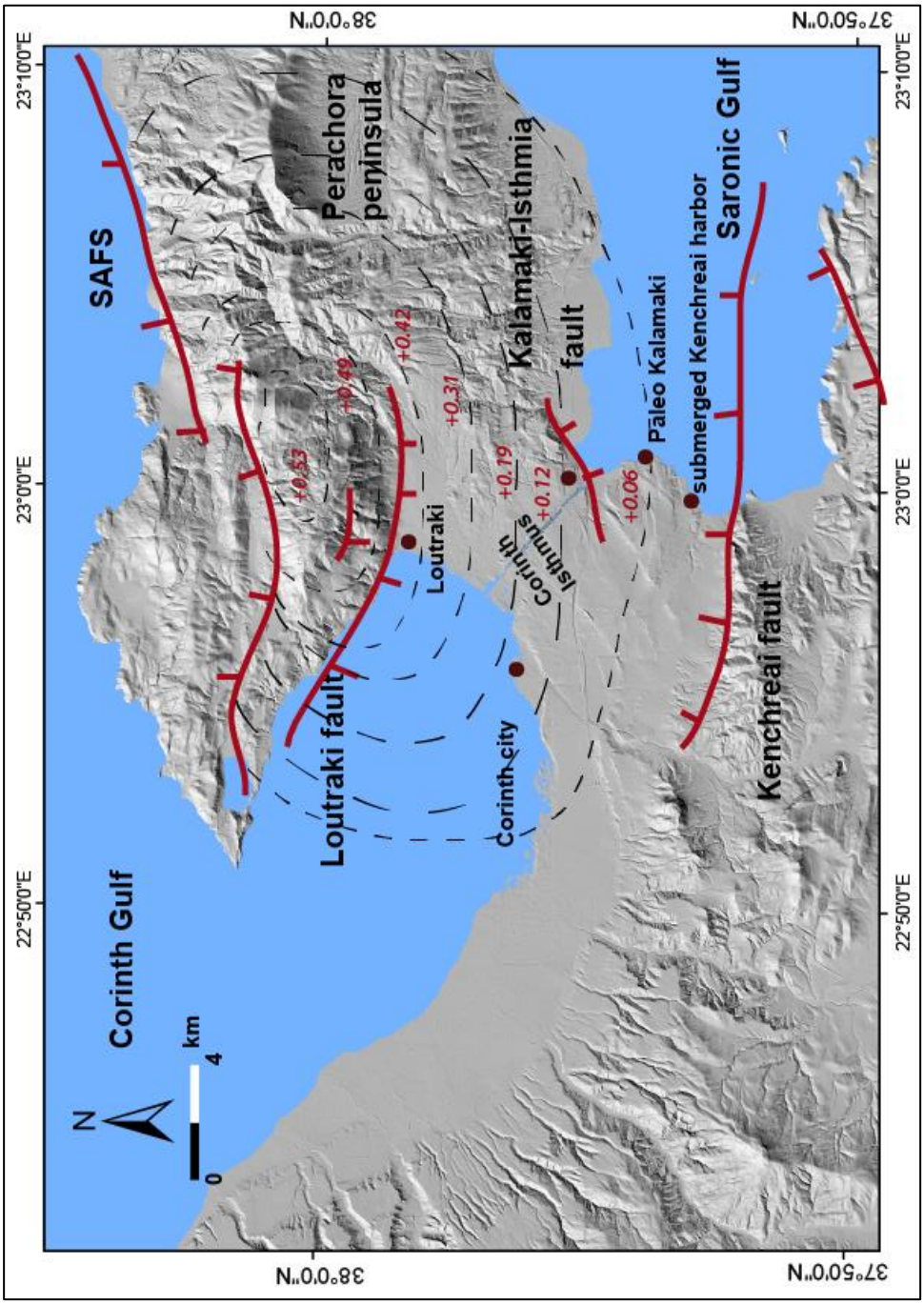

Figure 12-12*. The estimated uplift rate in mm/yr due to the activity of the SAFS based on the average values (55^{o} dip and 1/2.5 subsidence/uplift ratio, Table 21).* ***Εικόνα 12-12****. Ο εκτιμώμενος ρυθμός ανύψωσης από την δράση των ρηγμάτων των Αλκυονίδων, με βάση τις μέσες τιμές του λόγου ταπείνωσης/ανύψωσης και κλίσης των ρηγμάτων.*

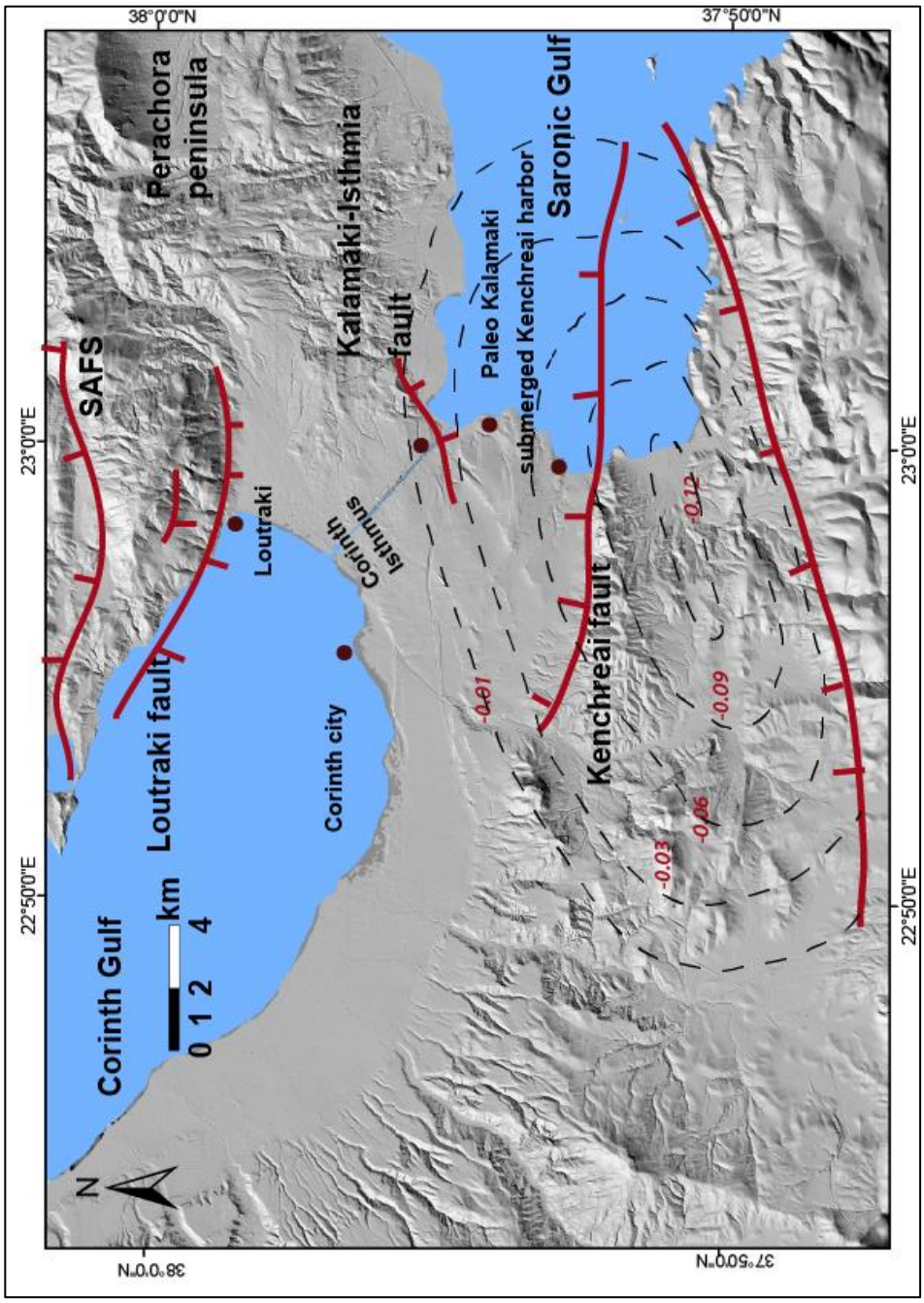

Figure 12-13. *The estimated subsidence rate in mm/yr due to the activity of the Agios Vassileios fault based on the average values (55^{o} dip and 1/2.5 subsidence/uplift ratio, Table21).*

Εικόνα 12-13. *Ο εκτιμώμενος ρυθμός ταπείνωσης από την δράση του ρήγματος του Αγίου Βασιλείου, με βάση τις μέσες τιμές του λόγου ταπείνωσης/ανύψωσης και κλίσης του ρήγματος.*

All previous researchers concluded that the uplift rate of the eastern part of the Corinth Canal is 0.3 mm/yr (e.g. Collier et al., 1992; Dia et al., 1997; Pierini et al., 2016). This 0.3 mm/yr rate is the result of all factors which uplift or subside the Canal, including the regional uplift of the area. Based on the described scenarios the examined faults the influence at the immediate footwall of the Kalamaki-Isthmia fault; ranges from 0.0 to ~0.08 mm/yr subsidence and while the average rate is -0.04±0.04 mm/yr. Even though that the equilibrium among these four faults for the examined scenario is approximately -0.04 mm/yr subsidence the area is undeniably uplifted. The latter can be explained if the influence of the regional uplift is estimated approximately at ~0.34±0.04 mm/yr (Fig. 12-14).

The significance of the regional uplift is highlighted in figure 12-15, where a hypothetical paleogeographical model of the area is shown, based only on the influence of the faults described before. Instead of the uplift of the area (as it is expected based on the findings from the borehole cores and the surface mapping described before, as well as the results from previous researchers), the final outcome from the interplay of these faults cause the subsidence of the area. The latter resulted into a completely different paleogeography during MIS 5.5 (125 ka) and MIS 7 (~200 –240 ka) (Fig. 12-15 a, b).

Based on the subsidence rates mentioned, the cumulative impact of the faults can be estimated based on this model. Therefore, an approximately 12.5 ± 3 m subsidence is caused by the Loutraki fault at the eastern part of the Corinth canal since MIS 5 (125 ka) is expected. The Kenchreai fault subside the area of Corinth Canal ~ 7.5 ± 3 m since MIS 5 (125 ka). The SAFS uplift the Canal ~ 15 ± 3 m while a ~ 2.5 ± 2 m cumulative uplift is caused by the Kalamaki – Isthmia fault the last 125 ka. The Agios Vassileios fault is expected to subside the Canal ~ 2.5 m for the same period. Therefore, at the eastern part of the canal a ~ 5 m subsidence is expected. On the contrary based on the estimated uplift rate of the area, uplift ~ 37 m above the present day sea level is expected. Furthermore, marine deposits (e.g. the interval in Bh-3 from 12.00 m to 5.50 m core depth) associated with the MIS 5 highstand, also implies uplifting procedures.

Figure 12-14. *a) The estimated uplift rate based on Collier et al. (1992), Dia et al. (1997), Pierini et al. (2016). b) The subsidence rate of the study area based only on the combined influence of the faults (average values, 55^{o} dip and 1/2.5 subsidence/uplift ratio, Table 21). c) The required regional uplift, to preserve the total uplift rates described in (a).*

Εικόνα 12-14. *a) Ο ρυθμός ανύψωσης της περιοχής με βάση τους Collier et al. (1992), Dia et al. (1997), Pierini et al. (2016). β) Η ταπείνωση της περιοχής με βάση μόνο τα κύρια ρήγματα που την επηρεάζουν και τις μέσες τιμές του λόγου ταπείνωσης/ανύψωσης και κλίσης των ρηγμάτων. c) Η απαιτουμένη γενικότερη τεκτονική ανύψωση της περιοχής ώστε να ισχύει ο ρυθμός ανύψωσης στην εικόνα (a).*

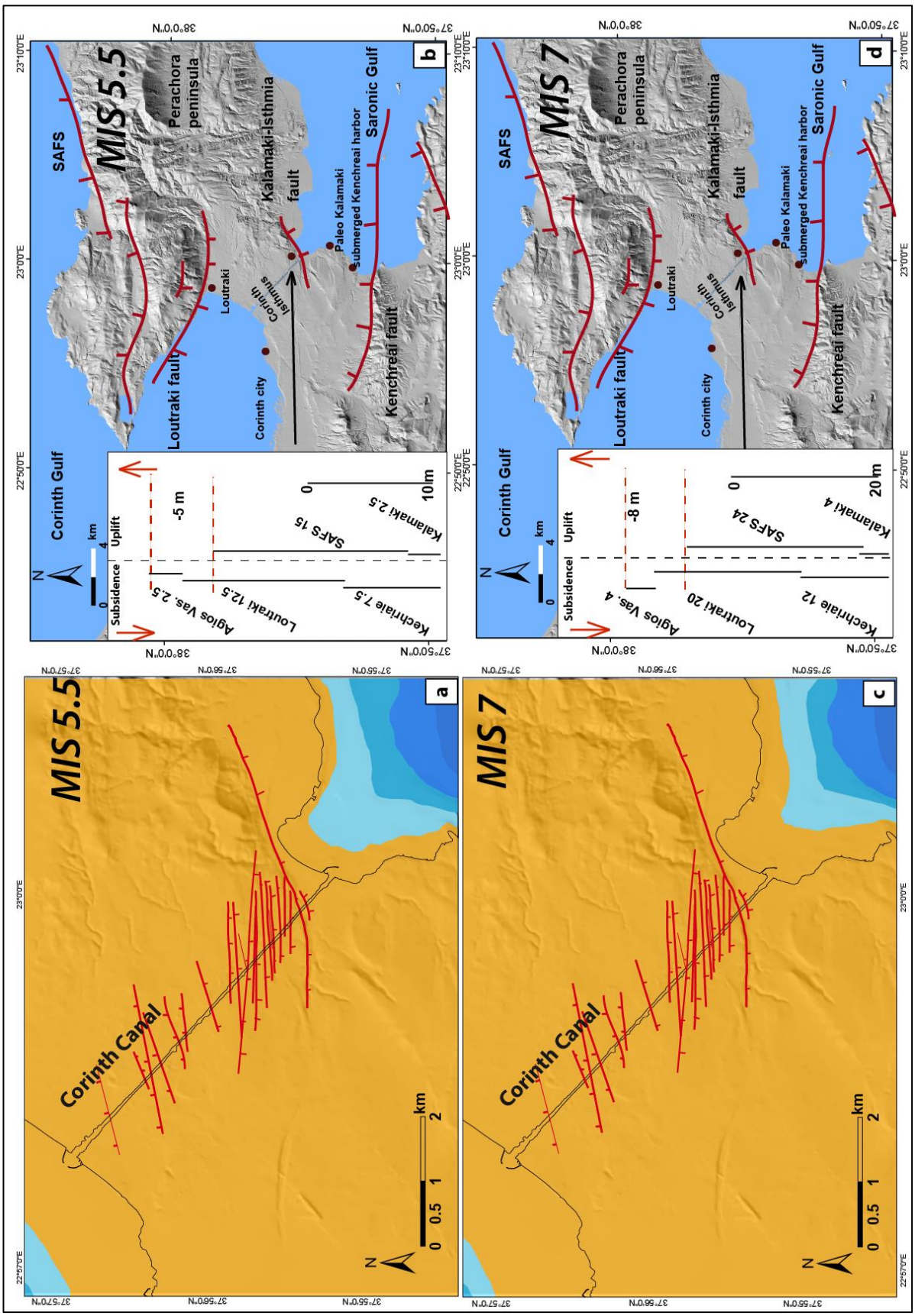
MIS 5.5
MIS 7
SAFS
Perachora peninsula
Kalamaki-Isthmia fault
Paleo Kalamaki
Submerged Kenchreai harbor
Saronic Gulf
Loutraki fault
Loutraki
Corinth Isthmus
Corinth city
Kenchreai fault
Corinth Gulf
Uplift
Subsidence
-5 m
-8 m
Agios Vas. 2.5
Loutraki 12.5
Kechriaie 7.5
SAFS 15
Kalamaki 2.5
Agios Vas. 4
Loutraki 20
Kechriaie 12
SAFS 24
Kalamaki 4
Corinth Canal
a
b
c
d
km

Figure 12-15*. The hypothetically paleogeography of the Corinth Isthmus during the MIS 5.5 (125 ka) (a and b) and MIS 7 (~200–240 ka) (c and d) highstands based only on the influence of the active faults of the area (average values 55^{o} dip and 1/2.5 subsidence/uplift ratio, Table 21). It is notable that the entire area is constantly emerged since MIS 7, which is not compatible with the findings of this study and with the previous researches as well. Figures b and d illustrate the cumulative subsidence and uplift in meters caused by the examined faults at the Eastern part of the Corinth Canal (see text for description).*

Εικόνα 12-15. *Η υποθετική παλαιογεωγραφία της περιοχής με βάση μόνο την επίδραση των ρηγμάτων πριν από 125 και 200 χιλιάδες χρόνια και με βάση τις μέσες τιμές του λόγου ταπείνωσης/ανύψωσης και κλίσης των ρηγμάτων. Είναι εμφανές πως η περιοχή ήταν μονίμως αναδυμένη, κάτι που δεν συμφωνεί τόσο με την βιβλιογραφία όσο και τα αποτελέσματα τις παρούσας εργασίας. Στις εικόνες b και d απεικονίζεται η τεκτονική ανύψωση και ταπείνωση τις περιοχής, στο ανατολικό τμήμα του Καναλιού με βάση το μοντέλο αλληλεπίδρασης των ρηγμάτων.*

An approximately 20 ± 3 m subsidence is caused by the Loutraki fault at the eastern part of the Corinth canal since MIS 7 (200 ka). The Kenchreai fault subside the area of Corinth Canal ~ 12 ± 3 m. The SAFS uplift the Canal ~ 24 ± 3 m and a ~ 4 ± 2 m cumulative uplift is caused by the Kalamaki – Isthmia fault the last 200 ka. The Agios Vassileios fault is expected to subside the Canal ~ 4 m for the same period. Therefore, at the eastern part of the canal a ~ 8 m subsidence is expected, while based on the already estimated uplift rate of the area, the eastern part of the Corinth Canal has been uplifted ~ 60 m above the present day sea level the last 200 ka. The described paleoenvironment within the boreholes, as well as the detailed description of the marine facies at the Corinth Canal (e.g. Collier, 1990), strongly indicate different paleogeographical conditions during these highstands.

12.4 Paleogeography

Tectonic movements along with the glacioeustatic sea level changes have resulted into the complicated paleogeography of the Corinth area. Glacioeustatic sea level changes at least since MIS 11 are described by several researchers (e.g. Siddall et al., 2003; Thomson and Goldstein, 2006), mentioning a 100 ka cyclicity of highstands/lowstands. During lowstand periods the sea level falls even ~125 m beneath the present sea level (MIS 2, Siddall et al. (2003)), while during highstands the sea level rises even in ~5 m above the present level (MIS 5.5, Siddall et al. (2003)). The paleogeography of the isthmus has been reconstructed since MIS 9, based on:

I. The glacioeustatic sea level changes (e.g. Siddall et al., 2003; Thomson and Goldstein, 2006),
II. The measured uplift rate (~0.3 mm/yr for the Corinth Canal),
III. The paleoenvironmetal description and the palaeobathymetry as it was studied and interpreted in borehole cores,
IV. The detailed morphology of the Isthmus based on a 5 m resolution DEM of the area.

One of the questions rising concerns the paleogeography of the Saronic Gulf and its potential influence to the area of Corinth Isthmus (Fig. 12-6 a). The bathymetry of the Saronic Gulf strongly indicates that during glacioeustatic lowstands the sea level falls only to ~90 m depth, where a barrier forms a paleolake at the western part of the Saronic Gulf (Fig. 12-6 b, c). The paleolake of Saronic is also mentioned by Lykousis (2009) only during the last lowstand though. The major offshore faults which influence the Gulf have relatively low slip rate (~0.25 mm/yr) (e.g. Papanikolaou et al., 1989; Deligiannakis et al., in press) and are not capable to significantly influence this barrier. Based on their geometry and their slip rate it appears that can either subside the barrier (and consequently the barrier was even higher during previous lowstands), or uplift it at such a low rate that at least during the last 300 ka, no significant changes are expected (<10 m) (Deligiannakis et al., in press). Considering as well that the deepest point of the western part of the Gulf is ~400 m deep, it is most likely that a paleolake was formed

during MIS 2, 4, 6, 8 lowstands. The exact shape of the lake or its water salinity properties remains uncertain.

During MIS 9 based on the glacioeustatic sea level change curve (Siddall et al., 2003) and the estimated uplift rate, constant marine conditions are expected. Therefore, a connection between the Corinth Gulf and the Aegean Sea is suggested (Fig. 12-17 a).

During MIS 8 lowstand sea level falls approximately 80m below the present sea level. Considering the uplift of the area and the glacioeustatic sea level curve (Siddall et al., 2003), the Isthmus area was emerged leading to regressive stacking patterns while the area was subjected to subaerial conditions, based on the sediments and the paleoenvironment described within the examined boreholes. It is unknown though if there was a connection of the Saronic Gulf with the Aegean Sea, or if there was a paleolake like the one during MIS 2.21 (~27 ka).

During MIS 7 the glacioeustatic sea level rise resulted into a connection between Saronic and Corinth Gulfs based also on Collier and Thomson (1991) (Fig. 12-17 b). Collier et al. (1992), Dia et al. (1997) and Pierini et al. (2016) through corals and Pecten dating confirmed the presence of MIS 7.3 (~205 ka) at the eastern part of the Isthmus (~45 m height). The presence of E. huxleyi described both in borehole cores and in samples extracted from surface outcrops, also strongly indicates a post 240 ka age or younger (≤MIS 7). Collier and Thomson (1991) have also described the connection of Corinth Gulf with the Aegean Sea during 205 ka based on the sedimentological processes of the subaqueous dunes, as well as on coral dates from the Canal.

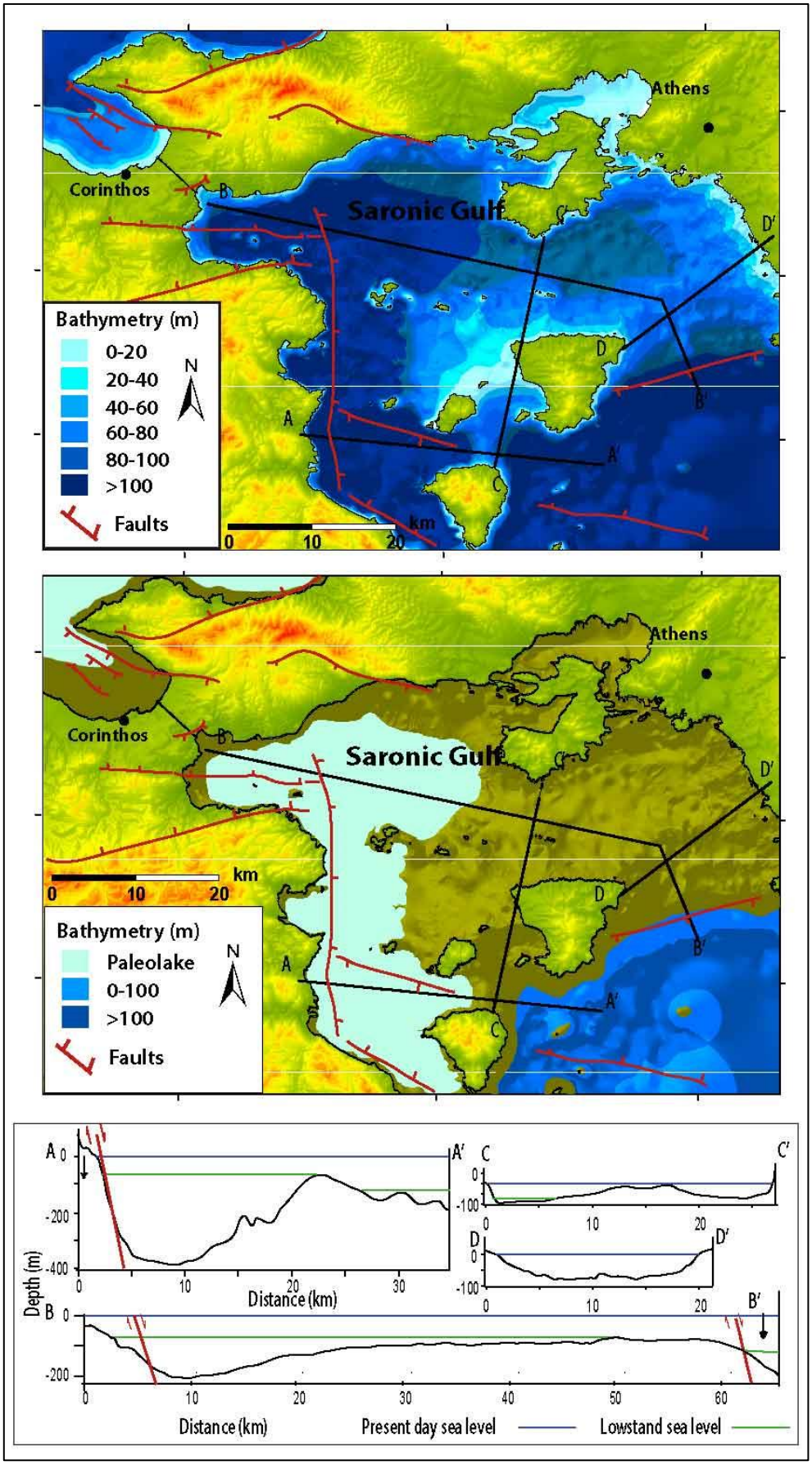

Figure 12-16. *Based on the detailed bathymetry of the Saronic Gulf and the tectonic movements during glacioeustatic lowstand periods a paleolake was formed.*

Εικόνα 12-6. *Με βάση την λεπτομερής βυθομετρία του Σαρωνικού και τις τεκτονικές κινήσεις σχηματίζεται μια παλαιολίμνη κατά τα παγετώδη διαστήματα.*

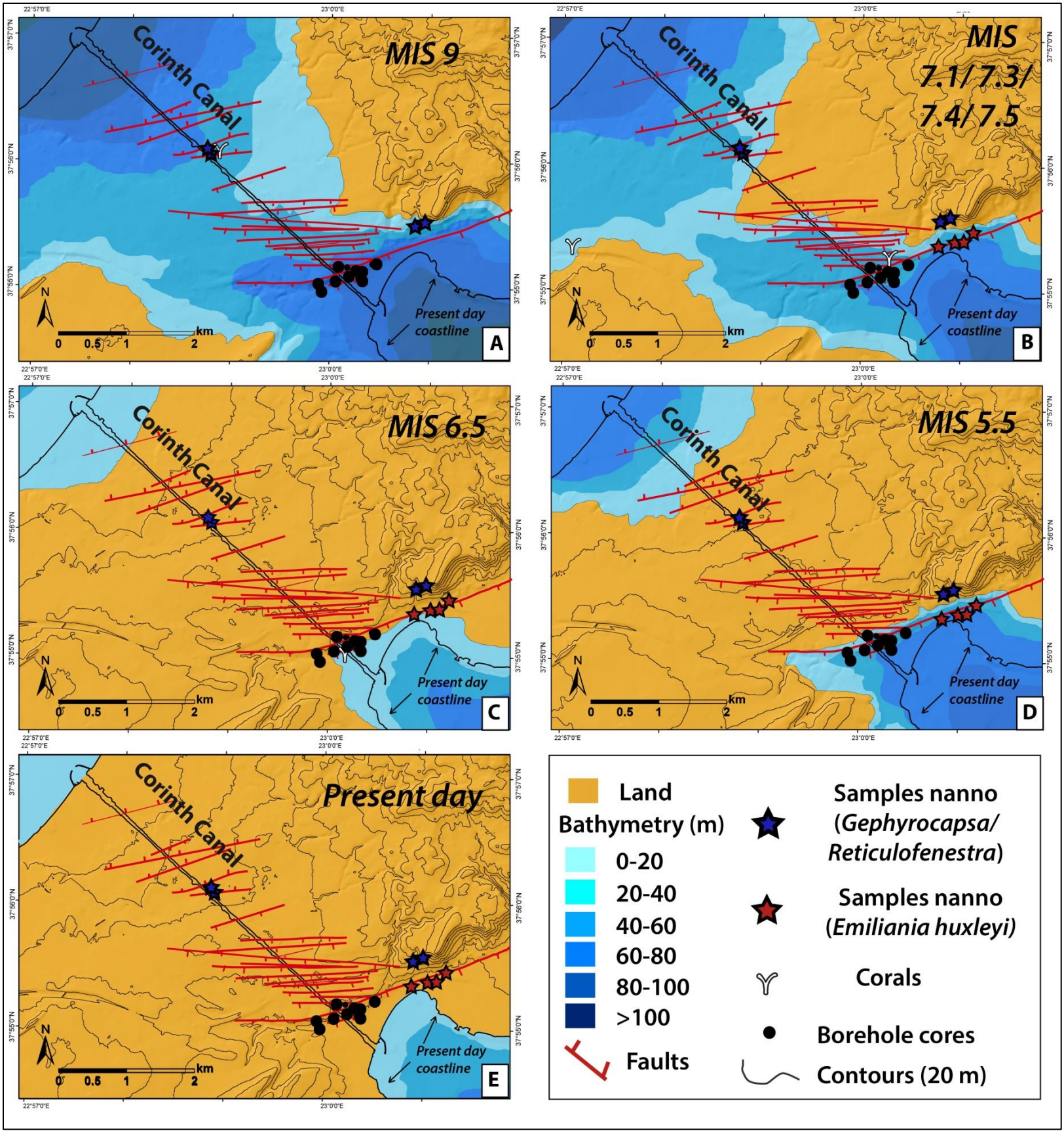
MIS 9
Corinth Canal
Present day coastline
A
MIS 7.1/7.3/ 7.4/7.5
Corinth Canal
Present day coastline
B
MIS 6.5
Corinth Canal
Present day coastline
C
MIS 5.5
Corinth Canal
Present day coastline
D
Present day
Corinth Canal
Present day coastline
E
22°57'0"E
23°0'0"E
37°57'0"N
37°56'0"N
37°55'0"N
N
km
0 0.5 1 2
Land
Bathymetry (m)
0-20
20-40
40-60
60-80
80-100
>100
Faults
Samples nanno (*Gephyrocapsa/ Reticulofenestra*)
Samples nanno (*Emiliania huxleyi*)
Corals
Borehole cores
Contours (20 m)

Figure 12-17. *Based on the glacioeustatic sea level changes, the 5 high resolution DEM of the area, the uplift rate of the area and data obtained from borehole cores and surface outcrops, the paleogeography of the Corinth Isthmus from MIS 9 till today is estimated.*

Εικόνα 12-17. *Με βάση την μεταβολή της στάθμης της θάλασσας, το υψηλής χωρικής ανάλυσης ψηφιακό μοντέλο του ανάγλυφου, τον ρυθμό ανύψωσης και τα δεδομένα από την παρούσα εργασία, δημιουργήθηκε η παλαιογεωγραφία της περιοχής του Ισθμού σε επιλεγμένες στιγμές κατά τα τελευταία 350 χιλιάδες χρόνια.*

During MIS 7 interstadials (MIS 7.1, 7.3, 7.4) the maximum sea level surface at the Isthmus ranged from ~65 m to ~80 m above the present sea level. Even though that the glacioeustatic sea level curve correlated with the tectonic uplift can barely resulted into a strait, based also on Collier and Thomson (1991), the most probable scenario is that there was a connection between the Saronic Gulf and the Corinth Gulf. Notably, the expected paleodepths during MIS 7 based on sea level curve and the tectonic uplift of the area, are in consistence with the estimated regional paleodepths through the foraminiferal analysis of the present study (ranging from 30 to 40 m depth).

Glacioeustatic sea level fall during MIS 7.0 (~189.6 ka e.g. Thomson and Goldstein, 2006) resulted into seawards movement of the coastline, regressive sequence staking patterns and exposure of the area to subaerial conditions, based on the sediments and the paleoenvironment described within the examined boreholes. Based on the glacioeustatic sea level changes (Siddall et al., 2003) the sea level fell ~90 beneath the present level, resulting into the paleolake of Saronic (Fig. 12-6) considering as well the palaeobathymetry of the Saronic Gulf and the barrier approximately at ~90 m beneath the sea surface.

During MIS 6.5 sea level was approximately 30 m below the present level (Siddall et al., 2003; Thomson and Goldstein, 2006). Considering the estimated uplift rate of the area (0.3 mm/yr), the maximum sea level surface at the Isthmus was ~5 m above the present sea level (Fig. 12-7 c). Shallow marine sediments possibly associated with MIS 6.5

were described in boreholes Bh-3 and Bh-7. Notably, the expected paleodepths during MIS 6.5 based on sea level curve and the tectonic uplift of the area, are in agreement with the estimated regional paleodepths based on foraminiferal analysis and *Cladocora* corals (e.g. Peirano et al., 1994) ranging from 0 to ~20 m depth.

Considering the systematic error of the sea level curves, the uncertainties of the estimated uplift and the uncertainties of the 5 m resolution DEM of the area, the maximum sea level could not be higher than ~30 m above present sea level, and still not enough to overcome the ~70 m barrier of the Isthmus (Fig. 12-7 c). Therefore, during MIS 6.5 a narrow isthmus separated the Corinth Gulf and the Aegean Sea. Roberts et al. (2009) described corals at Perachora peninsula in growth position from MIS 6.5 (~178 ka), while Armijo et al. (1996) and Westaway (1996) have ascribed marine terraces from the Corinth Gulf to MIS 6.5 as well. Therefore, marine conditions can be implied in the Corinth Gulf during MIS 6.5 (e.g. Perissoratis et al., 2000; Lykousis et al., 2007). Roberts et al. (2009) based on the influence of the active faults (Rio) to the morphology of the Strait suggested that a connection of Corinth Gulf with the Ionian Sea was not possible then and marine conditions can be explained only through a connection of the Gulf with the Aegean Sea in Isthmus. Since borehole data also imply that a connection was not possible through Corinth Isthmus, it is possible that the Corinth Gulf was a closed sea with marine characteristics and freshwater input (Kershaw & Guo, 2001) at least for a short period during MIS 6.5.

Glacioeustatic sea level fall during MIS 6 resulted into seawards movement of the coastline, regressive sequence staking patterns and exposure of the area to surface conditions, described in boreholes Bh-3 and Bh-7. Sea level fall beneath ~90 m has probably resulted into the formation of the paleolake of Saronic. Paleosoils described both in boreholes Bh-3, Bh-7 and in the Canal are attributed to this stage (Fig. 8-3) (Pallikarakis et al., Cor. Proof).

Questions also emerge concerning on whether there was a connection between the Aegean and the Corinth Gulf during MIS 5.5. Siddall et al. (2003) mentioned that the sea level was approximately 5 m above the present sea. Based on the uplift rate of the Canal (~0.3 mm/yr) (e.g. Collier et al., 1992) and the high resolution DEM the maximum

flooding surface of the area was approximately 60 m above the present sea level and a narrow Isthmus was formed during MIS 5.5. Considering though the systematic error of the sea level curve, the uncertainties of the estimated uplift and the uncertainties of the 5m resolution DEM of the area, a connection between Aegean and Corinth Gulf is not unlikely. Nonetheless sea level rise during MIS 5 resulting into transgressive sequences stacking pattern at the eastern part of the Isthmus, described in boreholes Bh-1, Bh-3, Bh-7, GA-2, GA-4, GA-5.

Based on the glacioeustatic sea level curve and the estimated uplift of the area post MIS 5.5 marine sediments are not expected since the area was constantly emerged (Fig. 12-7 d), since sea level fall up to ~125 m below the present level. As has been described before a paleolake, the paleolake of Saronic Gulf has been formed (Lykousis, 2009).

Global ice melting resulted in a rapid sea level rise over the last 19 ka (e.g. Lambeck et al., 2002). Notable, borehole G-1 located at the Kalamaki alluvial fan is described as fluvial-terrestrial environment based on the microfauna analysis, the described lithology and the high MS values, indicating no marine influence. Therefore, the Kalamaki alluvial fan was formed during relatively stable sea level the last thousand years and more probably over the last 6 ka where sea level has been relatively stable (Pirazzoli, 2005), where sediment influx caused the coastline to move seawards (regression).

It has to be acknowledged that there is a systematic error of the sea level curve (~12 m), as well as there are uncertainties of the estimated uplift (considering the ±10 m water depth in which the analyzed corals grow) and a smaller error due to the 5 m resolution of the area. Therefore, even though that the paleogeographical reconstruction of the Corinth Isthmus area is feasible there are uncertainties of several meters to the described paleoenvironments.

12.5 The significance of the followed methodology and its limitations

An interesting outcome of this study is this multi – proxy analysis and the combination of different methodologies which proved to be a very useful approach (quantitative benthic foraminiferal analysis, with nanno fossils assemblages and magnetic susceptibility data). The combination of all three methods can be established as a very promising paleoenvironmental tool box for the study of the paleoenvironment and paleogeography in a complicated active tectonically environment.

Studies focused on the paleoenvironment and/or the paleogeography of an area are generally more common in tectonically stable areas, in order to avoid any disturbance and turbulence of the examined sediments (e.g. Keller et al., 2002 (Egypt); Melis, and Violanti, 2006 (Thailand Gulf); Kouli et al., 2009 (Marathon coastal plain); Evelpidou et al., 2010 (Naxos island); Goiran et al., 2011 (Piraeus coastal plain); Triantaphyllou et al., 2010 (Vravron, Attica); Woodroffe and Webster, 2014 (Great Barrier Reef)). These studies are focused on the description of the foraminifera and how can they be used for the paleoenvironmental analysis, without examined the tectonic influence since their sites are characterized by low or neglectable tectonic movements.

On the contrary, paleoenvironmental studies performed in tectonically active areas are relatively rare and do not equally examine both the paleoenvironment and the tectonics of the area (e.g. Yasuhara et al., 2005 (Japan); Ferranti et al., 2011 (Southern Italy) Avnaim – Katav et al., 2012, 2013 (Israel coast); Yeager et al., 2012 (Louisiana, USA): Feagin et al., 2013 (Texas)).

This study has equally examined how an active fault interacted with the paleoenvironment / paleogeography of an area (Corinth Canal), through different paleontological techniques and the active tectonics of this area. Active tectonics have determine the uplift rate of the area, resulting to the described transgression / forced regression sedimentary patterns, while through the meticulous examination of the paleoenvironment, the tectonic movements of the study area (uplift rate, regional uplift rate and the Kalamaki-Isthmia fault's slip rate) has been estimated.

The combination of the indexes which have been used to refine the analyzed foraminiferal assemblages with the lithological formations and the MS values can form a reliable scientific tool to distinguish in situ marine and undisturbed strata, from fluvial-terrestrial backshore sediment formations.

Furthermore, biozonation of the nannofossils combined with the glacioeustatic sea level changes and the estimated uplift rate of the area proved to be a reliable methodology relatively age constraints of the sediments, considering of course the absence of accurate radiometric data.

The followed methodologies are bounded by significant limitations. The estimation of the paleodepth is based on the depth where foraminifera thrive. There is a significant depth range for the described specimens varying from a few meters (e.g. *Ammonia tepida* ± 10 m depth), to several tens of meters (e.g*. Asterigerinata mammilla* ± 100 m depth).

Even though that the relative age of the sediments can be estimated, the absence of specific dates which other methodologies offer, inevitable leads to different proposed scenarios to include all possible alternatives. Furthermore, the uplift and slip rates described in this thesis, lack the accuracy which other methodologies can offer (e.g. ^{230}Th/U absolute dating).

Furthermore, the model describing the relationship of the subsidence/uplift of the area is based on the subsidence/uplift described after the L'Aquila earthquake in Italy. Despite the similarities of these two regions it is questionable whether the response to an earthquake event at the Corinth area will be exactly the same as in L'Aquila. the later has been evaluated by a sensitivity analysis that considers: a) different fault dips and b) different subsidence/uplift ratios.

Finally, even though that the paleogeographical reconstruction of the Corinth Isthmus area is feasible, it has to be acknowledged that there is a systematic error of the sea level curve (~12 m), as well as there are uncertainties of the estimated uplift and an error to the 5 m resolution DEM of the area.

13 Conclusions

This thesis has reconstructed the paleoenvironment and the paleogeography of the eastern part of the Corinth Isthmus and has studied the interaction between the glacioeustatic and tectonic rates. This was achieved based on a multi-proxy analysis of data obtained both from 11 borecole cores and surface outcrops. In total 355 samples extracted from long borehole cores and from surface outcrops, 986 measurements of the Magnetic Susceptibility (MS) and 63 samples analysed for their nanno fossils contend, are described for analyzing the paleoenvironment, the paleogeography and the tectonic rates.

The results of the foraminifer's analysis are refined by three different indexes (FD, Br, and A-ratio). In correlation with the MS values, the lithological description of the boreholes, the surface outcrops and the two-way clusters analyses of the results, three different facies have been described (lagoonal, shallow marine and a transitional zone between them). Through these results the regional paleodepth has been estimated ranging from shallow lagoonal environments (even lower than ~5 m water depth), to more than 40 m water depth).

The analysis of the boreholes and the surface mapping revealed a complicated sedimentological pattern and only through the detail quantitative foraminiferal, magnetic susceptibility and lithological analysis, the described sedimentary sequences (both from the borehole cores and the exposed outcrops) have been safely correlated. These results have been visualized in a 3D model focused on the eastern part of the Corinth Canal.

Furthermore, the age of the sediments has been estimated in the basis of calcareous nannofossils assemblages, limitations deprived from ^{234}U/Th corals dating, the glacioeustatic sea level changes and the independent radiometric data at the eastern part of the Corinth Canal extracted from the literature. Five T-R sequences have been identified within borehole cores associated with the MIS 7 to MIS 5.5.

Detailed mapping of the area revealed parallel/subparallel fault segments, striking at ~ 060^{o} – 110^{o} and dipping towards SSE at ~ 55^{o} – 70^{o}, while the main fault trace strikes at 075^{o} and dips towards SSE at ~65^{o}. A maximum 0.07±0.2 mm/yr slip rate has been implied for the Kalamaki-Isthmia fault since MIS 7 while 0.32 ± 0.12 mm/yr uplift rate is proposed for the eastern part of the Corinth Isthmus during the same period. Furthermore, the influence of the regional uplift is described after modeling the influence of the surrounding faults based on the described uplift/subsidence from the L'Aquila earthquake.

Furthermore, based on the glacioeustatic sea level changes, the estimated uplift rate, the paleoenvironmetal description and the palaeobathymetry as was interpreted from the examined borehole cores and high resolution DEM of the area, the paleogeography of the Corinth Isthmus has been reconstructed during Pleistocene.

Finally the multi – proxy analysis and combination of different methodologies proved to be a very useful approach, resulting into a promising paleoenvironmental tool box for studying the paleoenvironment and paleogeography in a highly complicated and tectonically active environment.

References

Aitken, M.J., 1985. Thermoluminescence Dating. *Academic Press*, London, 359pp.

Albani, A.D., Serandrei Barbero, R., 1990. I Foraminiferi de lla Laguna e del Golfo di Venezia. *Memorie de lla Società Geologica,* Padova 42, 271– 341.

Amorosi, A., Antonioli, F., Bertini, A., Marabini, S., Mastronuzzi, G., Montagna, P., Negri, A., Rossi, V., Scarpone, D., Taviani, M., Angeletti, L., Piva, A., Vai, G.B., 2014a.The Middle-Upper Pleistocene Fronte Section (Taranto, Italy): an exceptionally preserved marine record of the Last Interglacial. *Glob. Planet. Chang.* 119, 23-38.

Amorosi, A., Rossi, V., Scarponi, D., Vaiani, S., Ghosh, A., 2014b. Bio-sedimentary record of post-glacial coastal dynamics: high-resolution sequence stratigraphy from the northern Tuscan coast (Italy). Boreas. http://dx.doi.org/10.1111/bor.12077

Alexandris, S., Stricevic, R., Petkovic, S. 2008. Comparative analysis of reference evapotranspiration from the surface of rainfed grass in central Serbia, calculated by six empirical methods against Penman–Monteith formula. *Eur. Water* 21–22, 17–28.

Andersen, M.B., Stirling, C.H., Zimmermann, B., Halliday, A.N., 2010. Precise determination of the open ocean $^{234}U/^{238}U$ composition. *Geochemist., Geophysics., Geosystems.* 11, Q12003

Arai, K., Machiyama, H., Chiyonobu, S., Matsuda, H., Sasaki, K., Humblet, M., Iryu, Y., 2014. Subsidence of the Miyako-Sone submarine carbonate platform, east of Miyako-jima Island, northwestern Pacific Ocean. *Island Arc,* 23,1–15

Armijo, R., Meyer, B., King, G.C.P., Rigo, A., Papanastassiou, D., 1996. Quaternary evolution of the Corinth Rift and its implications for the Late Cenozoic evolution of the Aegean. *Geophys. J. Int,* 126(1), 11– 53.

Athanasiou, M., Triantaphyllou, M., Dimiza, M., Gogou, A., Theodorou, G., 2015. Zanclean/Piacenzian transition on Cyprus (SE Mediterranean): calcareous nannofossil evidence of sapropel formation. *Geo-Marine Letters*, 35, 367–385.

Avallone, A., Briole, P., Agatza-Balodimou, A.M., Billiris, H., Charade, O., Mitsakaki, C., Nercessian, A., Papazissi, K., Paradissis, P., Veis, G., 2004. Analysis of eleven years of deformation measured by GPS in the Corinth Rift Laboratory area. *C. R. Geoscience* 336, 301–311.

Avnaim-Katav, S., Almogi-Labin, A., Sandler, A., Sivan, D., Porat, N. Matmon, A., 2012. The chronostratigraphy of a Quaternary sequence at the distal part of the Nile Littoral cell, Haifa Bay, Israel. J. *Quat. Sci.* 27(7), 675–686.

Avnaim-Katav, S., Almogi-Labin, A., Sandler, A., Sivan, D.; 2013.Benthic foraminifera as paleoenvironmental indicators during the last million years in the eastern Mediterranean inner shelf. *Palaeogeography, Palaeoclimatology, Palaeoecology..* 386, 512–530.

Avnaim-Katav, S., Hyams-Kaphzan, O., Milker, Y., Almogi-Labin, A., 2015. Bathymetric zonation of modern shelf benthic foraminifera in the Levantine Basin, eastern Mediterranean Sea. *J. of Sea Research* 99, 97–106.

Backert, N., Ford, M., Malarte, F., 2010. Architecture and sedimentology of the kerinitis Gilbert-type fan delta. Corinth rift, Greece. Sedimentology 57, 543–586.

Backman, J., Raffi, I., Rio, D., Fornaciari, E., Pälike, H., 2012. Biozonation and biochronology of Miocene through Pleistocene calcareous nannofossils from low and middle latitudes: *Newslett. on Stratigr*. 45, 221–244. doi: 10 .1127 /0078 -0421 /2012 /0022.

Banerjee, D., Murray, A.S., Botter-Jensen, L., Lang, A., 2001.Equivalent dose estimation using a single aliquot of polymineral 7ne grains. *Radiat. Meas*. 33, 73–94.

Bell, R., McNeill, L., Bull, J., Henstock, J., Collier, R., Leeder, M., 2009. Fault architecture and evolution of the Gulf of Corinth Rift, Central Greece. *Basin Res.* 21, 824–855.

Bellotti, P., Carboni, M.G., Di Bella, L., Palagi, I., Valeri, P., 1994. Benthic foraminiferal assemblages in the depositional sequence of the Tiber Delta. In: Matteucci, R.; Carboni, M.G., Pignatti, J.S. (eds.), Studies on Ecology and Paleoecology of Benthic Communities. *Bollettin o della Società Paleontologica Italiana,* special vol. 2, Modena, pp. 29–40.

Ben Rouina, S., Bassetti, M.A., Touir, J., Rabelsi, K., Berne, S., 2016. Sedimentary and microfaunal evolution in the Quaternary deposits in El Akarit river mouth (Gulf of Gabes, Tunisia): Paleo-environments and extreme events. *J. of Afric. Earth Sci.* 121, 30–41.

Benson, R.H., 1976. Changes in the ostracodes of the Mediterranean with the Messinian Salinity Crisis. *Palaeogeography, Palaeoclimatology, Palaeoecology.* 20, 147–170.

Beug, H.J., 2004. Leitfaden der Pollenbestimmung für Mitteleuropa und angrenzende Gebiete, 17 Verlag Dr. Friedrich Pfeil, München, Germany.

Billiris, H., Paradissis, D., Veis, G., England, P., Featherstone, W., Parsons, B., Cross, P., Rands,P., Rayson, M., Sellers, P., Ashkenazi, V., Davison, M., Jackson, J., Ambraseys, N., 1991. Geodetic determination of tectonic deformation in central Greece from 1900 to 1988. *Nature* 350, 124–129.

Bornovas, J., Lalechos, N., Filipakis, N., 1972. Korinthos geological map. Athens, Greece: Institute of Geology and Mineral Exploration, scale 1:50,000, 1 sheet

Bornovas, J., Gaitanakis, P., Spiridopoulos, A., 1984. Perachora geological map. Athens, Greece: Institute of Geology and Mineral Exploration, scale 1:50,000, 1 sheet.

Braun J, Voisin C, Gourlan A.T, Chauvel C., 2015. Erosional response of an actively uplifting mountain belt to cyclic rainfall variations. *Earth Surf. Dynam.* 3, 1–14.

Briole, P., Rigo, A., Lyon-Caen, H., Ruegg, J.C., Papazissi, K., Mitsakaki, C., Balodimou, A., Veis, A., Hatzfeld, D., Deschamps, A., 2000. Active deformation of the Corinth rift, Greece: results from repeated Global Positioning System surveys between 1990 and 1995. *J. Geophys. Res. Solid Earth* 21, 25,605–25,625.

Broecker, W. S., and J. van Donk. 1970. Insolation changes, ice volumes and the •80 record in deep-sea cores. *Rev. Geophys,* 8, 169–197.

Brooks,M., Ferentinos,G., 1984. Tectonics and sedimentation in the Gulf of Corinth and the Zakynthos and Kefallinia channels, western Greece. *Tectonophysics* 101 (1–2), 25–54.

Bouchet, V.M.P.,Alve, E.,Rygg, B., Telford, R.J., 2012. Benthic foraminifera provide a promising tool for ecological quality assessment of marine waters. *Ecol. Indicat.* 23, 66–75.

Campeau, S., Pienitz, R., Héquette, A.,1999. Diatoms as quantitative paleodepth indicatorsin coastal areas of the southeastern Beaufort Sea, Arctic Ocean. *Palaeogeography, Palaeoclimatology, Palaeoecology.* 146, 67–97.

Carboni, G.M., Bergamin, L., Di Bella, L., Esu, D., PisegnaCerone, E., Antonioli, F. and Verrubbi, V., 2010. Palaeoenvironmental reconstruction of late Quaternary foraminifera and mollusks from the ENEA borehole (Versilian plain, Tuscany, Italy).Quat. Research 74, 2, 265–276.

Charalampakis, M., Lykousis, V., Sakellariou, D., Papatheodorou, G., Ferentinos, G., 2014. Thetectono-sedimentary evolution of the Lechaion Gulf, the south eastern branch of the Corinthgraben, Greece. *Mar. Geol.* 351, 58–75.

Cheloni, D., Giuliani, R., D'Anastasio, E., Atzori, S., Walters, R.J., Bonci, L., D'Agostino, N., Mattone, M., Calcaterra, S., Gambino, P., Deninno, F., Maseroli, R., Stefanelli, G., 2014. Coseismic and post-seismic slip of the 2009 L'Aquila (central Italy) MW 6.3 earthquake and implications for seismic potential along the Campotosto fault from joint inversion of high-precision levelling, InSAR and GPS data. *Tectonophysics* 622,168–185.

Chen, R., Mckeever, S.W.S., 1997. Theory of Thermoluminescence and related phenomena. Singapore (World Scientific Singapore). 576 pp.

Chen, Y.W., Chen, Y.G., Murray, A.S., Watanuki, T., Chen, W.S., Yang, C.C.B., Liu, T.K., Lin, C.W., 2009. Long-term crustal movement caused by the Chiuchiung keng Fault in south western Taiwan: Constraints from luminescence dating. *Quat. Inter.* 199.

Chen, Y.W., Huang, Y.G., Lin, C.W., Zhao, Q., Yan, Y., Chen, D., Zhang. X., Lan, Q., Yu, M., 2015. Depleted deep South China Sea δ13C paleoceanographic events in response to tectonic evolution in Taiwan–Luzon Strait since Middle Miocene. *Deep Sea Research Part II: Topical Studies in Oceanography,* 122, 195-225.

Cheng, H., Edwards, R.L., Hoff, J., Gallup, C.D., Richards, D.A., Asmerom, Y., 2000. The half-lives of uranium-234 and thorium-230. *Chem. Geol.* 169, 17–33.

Chousianitis, K., Ganas, A., Gianniou, M., 2013. Kinematic interpretation of present-day crustal deformation in central Greece from continuous GPS measurements. *J. Geodyn.* 71, 1–13.

Clark, P.J., Davies, R.R., England, P.C., Parsons, B.E., Billiris, H., Paradissis, D., Veis, G., Denys, P.H., Cross, P.A., Askenazi, V., Bingley, R., 1997.Geodetic estimate of seismic hazard in the Gulf of Korinthos. *Geophys. Res. Lett.* 24, 1303–1306.

Clauzon, G., Le Strat, P., Duvail, C., Do Couto, D., Suc, J.-P., Molliex, S., Bache, F., Besson, D., Lindsay, E.H., Opdyke, N.D., Rubino, J.-L., Popescu, S.-M., Haq, B.U., Gorini, C., 2015. The Roussillon Basin (S. France): a case-study to distinguish local and regional events between 6 and 3 Ma. *Mar. Pet. Geol*. 66, 18-40

Collier, R.E.L., 1990. Eustatic and tectonic controls upon Quaternary coastal sedimentation in the Corinth Basin, Greece. *J. Geol. Soc,* 147, 301–314.

Collier, R.E.L. and Dart, C.J., 1991. Neogene to Quaternary rifting, sedimentation and uplift in the Corinth Basin, Greece. *J. Geol. Soc.* 148, 1049–1065.

Collier, R.E.L. and Thompson, J., 1991. Transverse and linear dunes in an upper Pleistocene marine sequence, Corinth Basin, Greece. *Sedimentology* 38(6), 1021–1040.

Collier, R.E.L., Leeder, R.M., Rowe, P., Atkinson, T., 1992. Rates of tectonic uplift in the Corinth and Megara basins, Central Greece. *Tectonics* 11(6), 1159–1167.

Collier, R. and Jones, G., 2003. Rift sequences of the southern margin of the Gulf of Corinth (Greece) as exploration/production analogs. Extended Abstract, In: AAPG International Conference, Barcelona, Spain.

Collier, R.E.L., Pantosti, D., D' Addezio, G., De Martini, P.M., Masana, E. Sakellariou, D., 1998. Paleoseismicity of the 1981 Corinth earthquake fault: seismic contribution to extensional strain in central Greece and implications for seismic hazard. *J. Geophys. Res.* 103(B12), 30001–30019.

Cosentino, C., Molisso, F., Scopelliti, G., Caruso, A., Insinga, D.D., Lubritto, C., Pepe, F., Sacchi, M., 2017. Benthic foraminifera as indicators of relative sea-level fluctuations: Paleoenvironmental and paleoclimatic reconstruction of a Holocene marine succession (Calabria, south-eastern Tyrrhenian Sea). Quat. Inter. 1–23.

Cooper, F.J., Roberts, G.P., Underwood, C.J., 2007. A comparison of 10^3-10^5year uplift rates on the South Alkyonides Fault, central Greece: Holocene climate stability and the formation of coastal notches. *Geophysic. Research Lett.* 34, 1–6.

Cundy, A.B., Kortekaas, S., Dewez, T., Stewart, I.S., Collins, P.E.F., Croudace, I.W., Maroukian, H., Papanastassiou, D., Gaki-Papanastassiou, P., Pavlopoulos, K., Dawson, A., 2000. Coastal wetlands as recorders of earthquake subsidence in the Aegean: a case study of the 1894 Gulf of Atalanti earthquakes, central Greece. *Mar. Geol.* 170, 3–26.

Da Silva, A.C., Potma, K., Weissenberger, J.A.W., Whalen, M.T., Humblet, M., Mabille, C., Boulvain, F., 2009. Magnetic susceptibility evolution and sedimentary environments on carbonate platform sediments and atolls, comparison of the Frasnian from Belgium and Alberta, Canada. *Sed. Geol.* 214(1–4), 3–18.

Danelian, T., Zambetakis, Lekkas, A., Galoyan, G., Sosson, M., Asatryan, G., Hubert, B., Grigoryan, A., 2014. Reconstructing Upper Cretaceous (Cenomanian) paleoenvironments in Armenia based on Radiolaria and benthic Foraminifera; implications for the geodynamic evolution of the Tethyan realm in the Lesser Caucasus, *Palaeogeography, Palaeoclimatology, Palaeoecology.*. 413, 123–132.

Dart, C., Collier, R., Gawthorpe, R., Keller, J., Nichols, G., 1994. Sequence stratigraphy of (?) Pliocene ± Quaternary syn-rift, Gilbert-type fan deltas, northern Peloponnesos, Greece. Mar. Petrol.Geol.11, 545–560.

Davies, R.R., England, P.C., Parson, B.E., Billiris, H., Paradissis, D., Veis, G., 1997. Geodetic strain of Greece in the interval 1892–1992. *J. Geophys. Res.* 102, 24, 571–588.

De Blasio, F. V., Liow, L. H., Schweder, T., De Blasio, B.F., 2015. A model for global diversity in response to temperature change over geological time scales, with reference to planktic organisms. *J. of Theoretic. Biol.* 365, 445–456.

de Boer B, Stocchi P, Whitehouse PL, van de Wal RSW., 2017. Current state and future perspectives on coupled ice-sheet sea-level modelling. *Quat. Sci. Rev.* 169, 13–28.

De Martini, P.M., Pantosti, D., Palyvos, N., Lemeille, F., McNeill, L., Collier, R., 2004. Slip rates of the Aigion and Eliki Faults from uplifted marine terraces, Corinth Gulf, Greece. *CR Acad. Sci. Paris* 336, 325–334.

Debenay, J.P., Guillou, J.J., 2002. Ecological transitions indicated by foraminiferal assemblages in paralic environments. *Estuaries* 25 (6A), 1107–1120.

Debenay, J.P., Guillou, J.J., Lesourd, M., 1996. The texture of the foraminiferal tests in relation with the crystallogenesisod colloidal calcite. Comptes Rendues de l' Academie de Sciences-SerieIIa: Sciences de la Terre des Planetes 323 (2), 171–178.

Debenay, J.P.; Millet, B., Angelidis, M.O., 2005.Relationships between foraminiferal assemblages and hydrodynamics in the gulf of Kalloni, Greece. *J. of Foraminif. Research,* 35 (4), 327–343.

Deligiannakis, G., Papanikolaou, I., Roberts, G. (in press). Fault specific GIS based seismic hazard maps for the Attica region, Greece. *Geomorphology*, doi.org/10.1016/j.geomorph.2016.12.005

Demoulin, A., Beckers, A., Hubert-Ferrari, A., 2015. Patterns of quaternary uplift of the Corinth rift southern border (N. Peloponnese, Greece) revealed by fluvial landscape morphometry. *Geomorphology* 246,188–204.

Depéret, G., 1913. Observations surl' histoire géologique pliocène et quaternaired u golfe et de l' isthme de Corinthe: Comptes Rendus de l' Academiedes Sciences, Paris, v. 156, p. 1048–1052.

Dewey, J.F., Sengor, A.M.C., 1979. Aegean and surrounding regions: Complex multiplate and continuum tectonics in a convergent zone. *Geol. Soc. Am. Bull.* 90, 84 – 92.

Di Bella, L., Casieri, S., Carboni, G.M., 2008. Late Quaternary paleoenvironmental reconstruction of the Tremiti structural high (Central Adriatic Sea) from benthic foraminiferal assemblages. *Geobios* 41(6), 729–742.

Dia, A.N., Cohen, A.S., O' Nions, R.K., Jackson, J.A., 1997. Rates of uplift investigated through ^{230}Th dating in the Gulf of Corinth (Greece). *Chem. Geol.* 138(3-4), 171–184.

Dimiza, M.D.; Triantaphyllou, M.V., and Krasakopoulou, E., 2011. Coccolithophores (calcareous nannoplankton) distribution in the surface waters of the western Cretan Straits (South Aegean Sea): Productivity and relation with the circulation pattern. *Hellenic Journal of Geosciences*, 45, 55–63.

Dimiza, M.D., Triantaphyllou, M.V., Koukousioura, O., Hallock, P., Simboura, N., Karageorgis, A.P., Papathanasiou, E., 2016. The Foram Stress Index: a new tool for environmental assessment of soft-bottom environments using benthic foraminifera. A case study from the Saronikos Gulf, Greece, Eastern Mediterranean. *Ecol. Indic.* 60, 611–621.

Doutsos, T., Piper, D.J.W., 1990.Listric faulting, sedimentation, and morphological evolution of the Quaternary eastern Corinth rift, Greece: first stages of continental rifting. *Geologic. Societ. of America Bull.* 102, 812–829.

Doutsos, T., Kontopoulos, N., Populimenos, G., 1988.The Corinth– Patras rift as the initial stage of the continental fragmentation behind an active island arc [Greece]. *Basin Res.* 1, 177–190.

Duermeijer, C.E., Nyst, M., Meijer, P.Th.,Langereis, C.G., Spakman, W., 2000. Neogene evolution of the Aegean arc: palaeomagnetic and geodetic evidence for a rapid and young rotation phase. *Earth Planet. Sci. Lett.* 176, 509–525.

Duller, G A T 2008 Luminescence Dating: guidelines on using luminescence dating in archaeology. Swindon: English Heritage

Drahor, M.G., Berge, M.A., 2017. Integrated geophysical investigations in a fault zone located on southwestern part of Izmir city, Western Anatolia. *Turk. J. Appl. Geophys.* 136, 114–33.

Drakatos, G., Karastathis, V., Makris, J., Papoulia, J., Stavrakakis, G., 2005. 3D crustal structure in the neotectonic basin of the Gulf of Saronikos (Greece). *Tectonophysics* 400 (1–4), 55–65.

Edwards, R.L., Gallup, C.D., Cheng, H., 2003. Uranium-series dating of marine and lacustrine carbonates. In: Uranium-series Geochemistry (eds. B. Bourdon, G.M. Henderson, C.C. Lundstrom S.P. Turner) Mineralogic. *Societ. of America, Washington, DC*, p. 656.

Eldevik, T. et al., 2014. A brief history of climate—the northern seas from the Last Glacial Maximum to global warming. *Quat. Sci. Rev.* 106, 225–246

EMERGEO Working Group, 2009. Rilievi geologici nell' area epicentrale della sequenza sismica dell' aquilano del 6 Aprile 2009. *Quaderni Geofisica* 70, 1–53.

EMERGEO Working Group, 2010. Evidence for surface rupture associated with the Mw 6.3 L'Aquila earthquake sequence of April 2009 (central Italy). *Terra Nova* 22 (1), 43–51.

Emery, D. and Myers, K.J., 1996.Sequence Stratigraphy. Oxford: Blackwell Science, 305pp.

Emiliani, C., 1955. Pleistocene temperatures. *J. Geol.* 63, 538–578.

Emiliani, C., 1961. Cenozoic climate changes as indicated by the stratigraphy and chronology of deep-sea cores of Globigerina-ooze facies. Ann. N. Y. *Acad. Sci.* 95, 521–536.

Ershova, V.B., Prokopiev, A.V., Khudoley, A.K., 2016. Devonian-Permian sedimentary basins and paleogeography of the eastern Russian Arctic: an overview. *Tectonophysics* 619, 234–255.

Evans, D., Brierley, C., Raymo, M.E., Erez, J., Müller, W., 2016. Planktic foraminifera shell chemistry response to seawater chemistry: Pliocene- Pleistocene seawater Mg/Ca, temperature and sea level change. *Earth Planet. Sci. Lett.* 438, 139–148.

Evelpidou, N., Pavlopoulos, K., Vassilopoulos, A., Triantaphyllou, M., Vouvalidis, K. Syrides, G., 2010. Sea level changes in Upper Holocene and palaeogeographical reconstruction. *Geodinamica Acta*, 23(5-6), 233–240.

Fahrmeir, L., Hamerle, A., 1984. Multivariate statistische Methoden. Berlin, New York: de Gruyter.

Farouk, S., Elamri, Z., El-Sorogy, A., 2016. Thanetian transgressive-regressive sequences based on foraminiferal paleobathymetry at Gebel Matulla, west-central Sinai, Egypt. *J. of Afric. Earth Sciences* 121, 210–218.

Feagin, R.A., Yeager, K.M., Brunner, C.A., Paine, J.G., 2013.Active fault motion in a coastal wetland: Matagorda, Texas. *Geomorphology* 199, 150–159.

Ferranti, L., Pagliarulo, R., Antonioli, F., Randisi, A., 2011. Punishment for the Sinner‖: Holocene episodic subsidence and steady tectonic motion at ancient Sybaris (Calabria, southern Italy). *Quat. Int.* 232, 56–70.

Flotte, N., Sorel, D., Móller, C., Tensi, J., 2005. Along strike changes in the structural evolution over a brittle detachment fault: example of the Pleistocene Corinth– Patras rift (Greece). *Tectonophysics* 403 (1–4), 77–94.

Folz, E., Bodu, P., Bonte, P., Joron, J. L., Mercier, N. Reyss, J.L., 2001: OSL dating of fluvial quartz from Le Closeau, a Late Paleolithic site near Paris – comparison with 14C chronology. *Quat. Sci. Rev.* 20, 927–933.

Ford, M., Williams, E.A., Malartre, F., Popescu, S.P., 2007. Stratigraphic architecture, sedimentology and structure of the Vouraikos Gilbert-type delats, Gulf of Corinth, Greece. In: Paola, C., Nichols, G.J., Williams, E.A., (Eds.), I.A.S. Special Publication.

Ford, M., Rohais, S.,Williams, E., Bourlange, S., Jousselin, D., Backert, N., Malartre, F., 2012. Tectono-sedimentary evolution of the western Corinth rift (Central Greece). *Basin Res.* 25, 3–25.

Foroughi, F., Gardin, S., Lotfali Kani, A., Vahidinia, M., Calcareous nannofossil biostratigraphy of Campanian strata (Abtalkh Formation) from the eastern Koppeh-Dagh Basin, NE Iran. *Cretaceous Research,* DOI: 10.1016/j.cretres.2016.10.002

Freyberg, V., 1973.Geologie des Isthmus von Korinth, Erlangen Geologische Ablhandlungen, Heft 95. Junge und Sohn, Universitats Buchdruckerei Erlangen,183 pp.

Frontalini, F., Buosi, C., Da Pelo, S., Coccioni, R., Cherchi, A., Bucci, C., 2009. Benthic foraminifera as bio-indicators of trace element pollution in the heavily contaminated Santa Gilla lagoon (Cagliari, Italy). *Mar. Pollution Bull.* 58(6), 858–877.

Fytikas, M., Innocenti, F., Manetti, Mazzuoli, R., Percerillo, A., Villari, L. 1984. Tertiary to Quaternary evolution of volcanism in the Aegean region. In: Dixon,J .E., Robertsoan, H.F., (eds) The Geological Evolution of the Eastern Mediterranean. *Geologic.l Society, London, Special Publication* 17,687–699.

Gaitanakis, P., Mettos, A., Fytikas, M., 1985. Sofikon geological map. Athens, Greece: Institute of Geology and Mineral Exploration, scale 1:50,000, 1 sheet.

Gawthorpe, R.L, Fraser, A. J., Collier, R., 1994. Sequence stratigraphy in active extensional basins: implications for the interpretation of ancient basin fills. *Mar. Petrol. Geology,* 11(6), 642–658.

Geslin, E., Debenay, J.P., Duleba, W., Bonetti, C., 2002. Morphological abnormalities of foraminiferal tests in Brazilian environments: a comparison between polluted and non-polluted areas. *Mar. Micropaleontol.* 45(2), 151–168.

Ghilardi, M., Kunesch, S., Styllas, M., Fouache, E., 2008. Reconstruction of Mid-Holocene sedimentary environments in the central part of the Thessaloniki Plain (Greece), based on

microfaunal identification, magnetic susceptibility and grain-size analyses. *Geomorphology*, 97(3-4), 617–630.

Gibert, L., Scott, G. R., Scholz, D., Budsky, A., Ferrandez, C., Martin, R. A., Ribot, F., and Leria, M., 2016. Chronology for the Cueva Victoria fossil site (SE Spain): Evidence for Early Pleistocene Afro-Iberian dispersals. *Journal of Human Evolution*, 90, 183-197.

Gobo, K., Ghinassi, M., Nemec, W., Sjursen, E., 2014.Development of an incised valley-fill at an evolving rift margin: Pleistocene eustasy and tectonics on the southern side of the Gulf of Corinth. *Sedimentology* 61,1086–1119.

Goiran, J.P., Pavlopoulos, K.P., Fouache, E., Triantaphyllou, M., Etienne, R., 2011. Piraeus, the ancient island of Athens: evidence from Holocene sediments and historical archives. *Geology* 39(6), 531–534.

Goldsworthy, M., Jackson, J., 2001. Migration of activity within normal fault systems: examples from the Quaternary of mainland Greece. *J. Struct. Geol* 23(2–3), 489–506.

Goldsworthy, M., Jackson, J., Haines, J., 2002. The continuity of active fault systems in Greece. *Geophys. J. Int,* 148, 596–618.

Goff, J., Chagué-Goff, C., Nichol, S., Jaffe, B., Dominey-Howes, D., 2012.Progress in paleotsunami research. *Sediment.Geol.* 243–244, 70–88.

Goudarzi, A.M., Woldai, T., Tolpekin, V. A ., 2011. Surface deformation caused by April 6th 2009 earthquake in L'Aquila (Italy): a comparative analysis from ENVISAT ASAR, ALOS PALSAR and ASTER". *Inter. J. of Applied Earth Observ. and Geoinform.,* vol. 13, no. 5, pp. 801–811.

Guérin, G., Discamps, E., Lahaye, C., Mercier, N., Guibert, P., Turq, A., Dibble, H.L.,Mc Pherron, S.P., Sandgathe, D., Goldberg, P., Jain, M., Thomsen, K., Patou-Mathis, M., Castel, J.C., Soulier, M.C., 2012. Multi-method (TL and OSL), multi material (quartz and flint) dating of the Mousterian site of Roc de Marsa l(Dordogne, France): correlating Neanderthal occupations with the climatic variability of MIS 5-3. *J. Archaeol. Sci.* 39, 3071–3084.

Guerreiro, C., Cachão, M., Drago, T., 2005.Calcareous nannoplankton as a tracer of the marine influence on the NW coast of Portugal over the last 14000 years. *J.of Nannoplankton Res.* 27(2), 159–172.

Hemelsdaël, R., Ford, M., 2015. Relay zone evolution: a history of repeated fault propagation and linkage, central Corinth rift, Greece. *Basin Res.* 1–23.

Hammer, O., Harper, D.A.T,. Ryan, P.D., 2001. Past Paleontological statistics software. Package for education and data analysis. *Paleontologia Electronica*.

Hoffman, J.S., Clark, P.U., Parnell, A.C., He, F., 2017. Regional and global sea-surface temperatures during the last interglaciation. *Science* 355, 276–279.

Hollenstein, C., Geiger, A., Kahle, H.G., Veis, G., 2006. CGPS time-series and trajectories of crustal motion along the West Hellenic Arc. *Geophys. J. Int*. 164 (1), 182–191.

Houghton, S.L., Roberts, G.P., Papanikolaou, I.D., McArthur, J.M., Gilmour, M.A., 2003. New 234U-230Th coral dates from the western Gulf of Corinth: implications for extensional tectonics. *Geophys. Res. Lett*. 30, 2013.

Howell, M.W., Rio, D., Thunell, R.C., 1990. Laminated sediments from the Vrica Section (Calabria, S. Italy): evidence for Plio-Pleistocene climatic change in the Mediterranean region. *Palaeogeography, Palaeoclimatology, Palaeoecology*, 78,195-216.

Hülle, D., Hilgers, A., Radtke, U., Stolz, C., Hempelmann, N., Grunert, J., Felauer, T., Lehmkuhl, F., 2010.OSL dating of sediments from the Gobi Desert, Southern Mongolia. *Quat. Geochronol.* 5, 107–113.

Hubert, A., King, G.C.P., Armijo, R., Meyer, B., Papanastassiou, D., 1996. Fault reactivation, stress interaction and rupture propagation in the 1981 Corinth earthquake sequence. Earth Planet. Sci. Lett. 142, 573–585. http://dx.doi.org/10.1016/0012-821X(96)00108-2.

Imbrie, J., et al., 1993. On the structure and origin of major glaciation cycles, 2, The 100,000 year cycle. *Paleoceanography* 8, 699–735.

Imbrie, J., Imbrie, J.Z., 1980. Modeling the climatic response to orbital variations, *Science* 207, 943–953

Ivanova, E.V., Murdmaa, I.O., Karpuk, M.S., Schornikov, E.I., Marret, F., Cronin, T.M.,Buynevich, I.V., Platonova, E.A., 2012. Paleoenvironmental changes on the northeastern and southwestern Black Sea shelves during the Holocene. *Quat. Int.* 261, 91–104.

Jackson, J.A., 1999. Fault death: a perspective from actively deforming regions. *J. Struct. Geol.* 21, 1003–1010.

Jackson, J.A., Gagnepain, J., Houseman, G., King, G.C.P., Papadimitriou, P., Soufleris, C., Virieux, J., 1982. Seismicity, normal faulting, and the geomorphological development of the Gulf of Corinth (Greece): the Corinth earthquakes of February and March 1981. *Earth Planet. Sci. Lett.* 57, 377–397.

Jalut, G., Amat, A.E., Riera i Mora, S., Fontugne, M., Mook, R., Bonnet, L., Gauquelin, T. 1997. Holocene climatic changes in the western Mediterranean: installation of the Mediterranean climate. *Earth and Planetary Sciences,* 325, 327–334.

Jolivet, L., 2001. A comparison of geodetic and finite strain pattern in the Aegean, geodynamic implications. *Earth Planet. Sci. Lett.* 187, 95–104.

Jolivet, L., Facenna, C., Goffé, B., Burov, E., Agard, P.,2003. Subduction tectonics and exhumation of high-pressure metamorphic rocks in the Mediterranean orogeny. American J. of Sci. 303, 353–409.

Jolivet, L., Labrousse, L., Agard, P., Lacombe, O., Bailly, V., Lecomte, E., Mouthereau, F., Mehl, C., 2010. Rifting and shallow-dipping detachments, clues from the Corinth Rift and the Aegean. *Tectonophysics*, 483, 287–304.

Jorissen, F.J., 1988. Benthic foraminifera from the Adriatic Sea: principles of phenotypic variation. *Utrecht Micropaleontol. Bull* 37, 1–174.

Kahle, H.G., Muller, M.V., 1993. The Kephalonia Transform Fault and the rotation of the Apulian platform: Evidence from satellite geodesy. *Geophys. Res. Lett.* 20, 651–654.

Kahle, H.G., Muller, M., Geiger, A., Danuser, G., Mueller, S., Veis, H., Billiris, G., Paradissis, D., 1995. The strain field in northwestern Greece and the Ionian Islands: Results inferred from GPS measurements, *Tectonophysics* 249, 41–52.

Kahle, H.G., Cocard, M., Peter, Y., Geiger, A.R., Reilinger, E., Barka, A.A., Veis, G., 2000. GPS derived strain rate field within the boundary zones of the Eurasian, African and Arabian plates. *J. Geophys. Res.* 105, 23,353–23, 370.

Karavitis, C.A., Vasilakou, C.G., Tsesmelis, D.E., Oikonomou, P.D., Skondras, N.A., Stamatakos, D., Fassouli, V., Alexandris, S. 2015. Short-term drought forecasting combining stochastic and geo-statistical approaches. *Eur. Water* 49,43–63.

Keller, G., Adatte, T., Burns, S., Tantawy, A.A., 2002. High-stress paleoenvironment during the late Maastrichtian to early Paleocene in Central Egypt. *Palaeogeography, Palaeoclimatology, Palaeoecology.*187, 35–60.

Keraudren, B., 1970–72. Les formations quaternairesmarines de la Grace. *Bull. Mus. Anthrop. Prehist.* Monaco, 16, 5 153, 17, 87–169, 18, 245–279.

Kemp, A.C., Horton, B.P., Vann, D.R., 2012. Quantitative vertical zonation of salt-marsh foraminifera for reconstructing former sea level, an example from New Jersey, USA. *Quaternary Science Reviews*, 54, 26–39.

Keraudren, B., Sorel, D., 1987. The terraces of Corinth(Greece) a detailed record of eustatic sea-level variations during the last 500,000 years *Mar. Geol.* 77, 99–107.

Keraudren, B., Falguères, C., Bahain, J.J., Sorel, D., Yokoyama, Y., 1995. Nouvelles datations radiométriques des terrasses marines de Corinthie (Péloponnèses eptentrional Grèce), *C. R. Acad. Sci.* Paris, 320 (II a), 483–489.

Kershaw, S., Guo, L., 2001. Marine notches in coastal cliffs: indicators of relative sea-level change, Perachora Peninsula, central Greece. *Mar. Geol.* 179, 213–228.

Kershaw, S., Guo, L., Braga, J.C., 2005.A Holocene coral–algal reef at Mavra Litharia, Gulf of Corinth, Greece. Structure, history, and applications in relative sea-level change. *Mar. Geol.* 215, 171–192.

Kevrekidis, T., Gouvis, N., Koukouras, A., 1996.Bionomy of Macrobenthic Molluscs in Evros Delta (North Aegean Sea). *Int. Revue ges. Hydrobiol.* 81(3), 455–468.

Kolaiti, E., Mourtzas, N.D., 2016. Upper Holocene sea level changes in the west Saronic gulf, Greece. *Quat. Int.* 401, 71–90.

Koukousioura, O., Triantaphyllou, M.V., Dimiza, M.D., Pavlopoulos, K., Syrides, G., Vouvalidis, K., 2012. Benthic foraminiferal evidence and paleoenvironmental evolution of Holocene coastal plains in the Aegean Sea (Greece). *Quat. Int.* 261, 105–117.

Koukouvelas, I.K., 1998. The Egion fault, earthquake – related and long – term deformation, Gulf of Corinth, Greece. *Journal of Geodynamics* ,26, 501 – 513.

Koukouvelas, I.K., Katsonopoulou, D., Soter, S., Xypolias, P., 2005. Slip rates on the Helike Fault, Gulf of Corinth, Greece: new evidence from geoarchaeology. *Terra Nova*. 17, 158–164.

Koukouvelas, I., Zygouri, V., Papadopoulos, G., Verroios, S., 2017.Holocene record of slip-predictable earthquakes on the Kenchreai Fault, Gulf of Corinth, Greece. *J. Struct. Geol.* 94, 258–274.

Kouli, K., 2012. Vegetation development and human activities in Attiki (SE Greece) during the last 5000 years. *Veget. Hist. Archaeobot,* 21, 267–278.

Kouli, K., Triantaphyllou, M., Pavlopoulos, K., Tsourou, T., Karkanas, P., Dermitzakis, M.D., 2009. Palynological investigation of the Holocene palaeoenvironmental changes in the coastal plain of Marathon (Attica, Greece). *Geobios* 42, 43–51.

Krbetschek, M.R., Götze, J., Dietrich, A., Trautmann, T., 1997. Spectral information from minerals relevant for luminescence dating. *Radiation Measurements*, 27, 695-748.

Lambeck, K., Esat, T. M. & Potter, E., 2002. Links between climate and sea levels for the past three million years. *Nature* 419, 199–206.

Lang, A., Wagner, G.A., 1996. Infrared stimulated luminescence dating of archaeo sediments. *Archaeometry* 38, 129–141.

Le Pichon, X., Angelier, J., 1979.The Hellenic arc and trench system: a key to the neotectonic evolution of the Eastern Mediterranean area, *Tectonophysics* 60, 1–42.

Le Pourhiet, L., Burov, E., Moretti, I., 2003. Initial crustal thickness geometry controls on the extension in a back arc domain: case of the Gulf of Corinth, *Tectonics* 22, 1032.

Leeder, M.R., Collier, R.E.Ll., Azis, L.H.A., Trout, M., Ferentinos, G., Papatheodorou, G., Lyberis, E., 2002.Tectono-sedimentaryprocesses along an active marine/lacustrine half-graben margin: Alkyonides Gulf, E. Gulf of Corinth, Greece. *Basin Res.* 14, 25–41.

Leeder, M.R., Mack, G.H., 2007. Basin- fill incision, Rio Grande and Gulf of Corinth rifts: convergent response to climatic and tectonic drivers. In: Nichols, G., Williams, E., Paola, E. (eds.), Sedimentary Processes, Environments and Basins: a Tribute to Peter Friend. Int. Assoc. *Sedimentologists Spec. Publ*. 38, 9–28.

Leeder, M.R., Mack, G.H., Brasier, A.T., Parish, R.R., McIntosh, W.C., Andrews, J.E. Durmeijer, C.E., 2008. Late-Pliocene timing of Corinth (Greece) rift-margin fault migration. *Earth planet. Sci.* 274, 132–141.

Leeder, M.R., McNeill, L.C., Collier, R.E.Ll., Portman, P., Rowe, P.J., Andrews, J.E., Gawthorpe, R.L., 2003. Corinth rift margin uplift: new evidence from late quaternary marine shorelines. *Geophys. Res. Lett*. 30, 1611.

Lézin, C., Caetano, P.S., Gonçalves, P., Rey, J., Rocha, F., Rocha, R.B., 2012.Biosedimentarydisturbances in shallow-water carbonate environments: an example from the Upper Hauterivian in the Lusitanian Basin. *Palaeogeography, Palaeoclimatology, Palaeoecology.* 315–316, 24–37.

Livio, F., Serva, L., Gürpinar, A., 2017. Locating distributed faulting: contributions from InSAR imaging to probabilistic fault displacement hazard analysis (PFDHA). *Quatern. Int.* http://dx.doi.org/10.1016/j.quaint.2016.09.034

Lombard, F., Labeyrie, L., Michel, E., Spero, H.J., Lea, D.W., 2009. Modelling the temperature dependent growth rates of planktic foraminifera. *Mar. Micropaleontol.* 70, 1–7.

Lykousis, V., 2009. Sea-level changes and shelf break prograding sequences during the last 400 ka in the Aegean margins: Subsidence rates and palaeogeographic implications. *Contin. Shelf Research* 29, 2037–2044.

Lykousis, V., Sakellariou, D., Moretti, I., Kaberi, H., 2007. Late Quaternary basin evolution of the Gulf of Corinth: sequence stratigraphy, sedimentation, fault-slip and subsidence rates. *Tectonophysics* 440, 29–51.

Malartre, F., Ford, M., Williams, E.A., 2004. Preliminary biostratigraphy and 3d geometry of the Vouraikos Gilber-type fan delta, Gulf of Corinth, Greece. *Comp. Ren., Geoscience* 336, 269–280.

Marinos, P., Tsiambaos, G., 2008. The geotechnics of Corinth Canal: a review. *Bull. Geol. Soc. Greece* 41, 400–420.

Mariolakos, I., Papanikolaou, D., Symeonidis, N., Lekkas, S., Karotsieris, Z., Sideris, Ch., 1982. The deformation of the area around the eastern Korinthian gulf, affected by the earthquakes of February–March 1981. *Proc. Inter. Symp.* On the Hellenic Arc and Trench (H.E.A.T.) 1, pp. 400–420.

Mariolakos, I., Stiros, S.C., 1987. Quaternary deformation of the Isthmus and Gulf of Corinth (Greece). *Geology* 15, 225–228.

Martin, P.A., Lea, D.W., Rosenthal, Y., Shackleton, N.J., Sarnthein, M., Papenfuss, T., 2002. Quaternary deep sea temperature histories derived from benthic foraminiferal Mg/Ca. *Earth Planet. Sci. Lett.* 198 (1–2), 193–209.

Martini, E., 1971. Standard Tertiary and Quaternary calcareous nannoplankton zonation. In: Farinacci, A. (ed.), Proceedings of the Second Planktonic Conference. (Roma). *Technoscienza*, pp. 739–785.

Maselli, V., Trincardi, F., Asioli, A., Ceregato, A., Rizzetto, F. Taviani, M., 2014. Delta growth and river valleys: the influence of climate and sea level changes on the South Adriatic shelf (Mediterranean Sea). *Quat. Sci. Rev*. 99, 146–163.

Mayo, A.L., Bruthans, J., Tingey, D., Kadlec, J., Nelson, S., 2009, Insights into Wasatch fault vertical slip rates using the age of sediments in Timpanogos Cave: Utah: *Quat.Res.* 72, 275–283.

McClusky, S., et al., 2000. Global Positioning System constraints on plate kinematics and Dynamics in the eastern Mediterranean and Caucasus. *J. Geophys.Res*.105, 5695–5719.

McKenzie, D., 1972. Active tectonics of the Mediterranean region. *Geophys. J. R. Astron. Soc.* 30,109–185.

McKenzie, D., 1978. Active tectonics of the Alpine-Himalayan belt: The Aegean Sea and surrounding regions. *Geophys. J. R. Astron. Soc,* 55, 217–254.

McMurray, L.S., Gawthorpe, R.L., 2000. Along-strike variability of forced regressive deposits: late Quaternary, northern Peloponnesos, Greece. In: Hunt, D., Gawthorpe R.L., (eds.), Sedimentary Responses to Forced Regressions. *Geol. Soc. Spec.* Publ., 172, pp. 363–377.

McNeill, L.C., Collier, R.E.L., Pantosti, D., De Martini, P.M., DAddezio, G., 2005. Recenthistory of the Eastern Eliki Fault, Gulf of Corinth: geomorphology, palaeoseismologyand impact on palaeoenvironments. *Geophys. J. Int.* 161, 154–166.

Melis, R., Violanti, D., 2006. Foraminiferal biodiversity and Holocene evolution of the Phetchaburi coastal area (Thailand Gulf). *Mar. Micropaleontol.* 61(1–3), 94–115.

Milankovitch, M., 1941.Kanon der Erdbestrahlung und seine Anwendung auf das Eiszeitenproblem (Royal Serbian Academy).

Mine, A.H, Waldeck, A., Olack, G., Hoerner,M..E., Alex, S., Colman A.S., 2017. Microprecipitation and $\delta^{18}O$ analysis of phosphate for paleoclimate and biogeochemistry research. *Chem. Geol.* 460, 1–14.

Mischke, S., Schudack, U., Bertrand, S., Leroy, S.A.G., 2012. Ostracods from a Marmara Sea lagoon (Turkey) as tsunami indicators. *Quat Int* 261,156–161

Moretti, I., Sakellariou, D., Lykousis, V., Micarelli, L., 2003. The Gulf of Corinth: a half graben? J*. Geodyn.* 36, 323–340.

Morewood, N.C., Roberts, G.P., 1997. The geometry, kinematics and rates of deformation in a normal fault segment boundary, central Greece, *Geophys. Res. Lett*., 24, 3081– 3084, doi:10.1029/97GL03100.

Morewood, N.C. Roberts, G.P., 1999. Lateral propagation of the surface trace of the South Alkyonides normal fault segment, central Greece: its impact on models of fault growth and displacement–length relationships. *J. Struct. Geol.* 21(6), 635–652.

Morigi, C., Jorissen, F.J., Fraticelli, S., Horton, B.P., Principi, M., Sabbatini, A., Capotondi, L., Curzi, P.V., Negri, A., 2005. Benthic foraminiferal evidence for the formatiom of the Holocene mud-belt and bathymetrical evolution in the cental Adriatic Sea. *Mar. Micropaleontol.* 57(1–2), 25–49.

Moulfi-El-Houari, L., Ambroise, D., Mathieu, R., 1999. Distribution des foraminifères bentiques actuelssur la marge continent aleargeroise (Baie de Bou-Ismaıl). *Revue de Micropaleontol.* 42(4), 315–327.

Mullins, C.E., 1977. Magnetic susceptibility of the soil and its significance in soil science–a review. *J. Soil Sci.* 28(2), 223–246.

Murray, J.W., 1991. Ecology and Palaeoecology of Benthic Foraminifera. Harlow/Essex, New York: Longman, Wiley, p.397.

Murray, J.W., 2007. Ecology and Applications of Benthic Foraminifera. Cambridge: Cambridge University Press, p.426.

Mourtzas N.D., Kissas, C., Kolaiti, E., 2014. Archaeological and geomorphological indicators of the historical sea level changes and the related palaeogeographical reconstruction of the ancient fore harbour of Lechaion, East Corinth Gulf (Greece). *Quat. Intern.* 332, 151–171.

Mourtzas, D.N., Kolaiti, E., 2013. Historical coastal evolution of the ancient harbor of Aegina in relation to the Upper Holocene relative sea level changes in the Saronic Gulf, Greece. *Palaeogeography, Palaeoclimatology, Palaeoecology.*. 392, 411–425.

Myrianthis, M., 1982. Geophysical study of the epicentral area of Alkyonides Islands earthquakes, central Greece. *Geophys. Transact.,* vol. 28/2. Eotvos Lorand Geophysical Institute of Hungary, pp. 5–17.

Nathan, R.P., Mauz, B., 2008. On the dose-rate estimate of carbonate-rich sediments for trapped charge dating. *Radiat. Measur*.43, 14–25.

Nagendra, R., Kamalak Kannan, B.V., Sen, G., Gilbert, H., Bakkiaraj, D., Nallapa Reddy A., Jaiprakash, B.C., 2011.Sequence surfaces and paleobathymetric trends in Albian to Maastrichtian sediments of Ariyalur area, Cauvery Basin, India. *Mari. Petrol. Geol.* 28, 895–905.

Nichols, G., 1999. Sedimentology and Stratigraphy. Oxford: Blackwell, 355 pp.

Nicolaidou, A., Bourgoutzani, F., Zenetos, A., Guelorget, O., Perthuisot, J.P., 1988. Distribution of Molluscs and Polychaetes in coastal lagoons in Greece. *Estuar. Coast. Shelf S.* 26, 33–350.

Nigam, R., Kurtarkar, S.R., Saraswat, R., Linshy, V.N., Rana, S.S., 2008. Response of benthic foraminifera Rosalina leei to different temperature and salinity, under laboratory culture experiment. *J. Mar. Biol. Assoc.* 88, 699–704.

Noller, J.S., Wells, L.E., Reinhardt, E., Rothaus, R.M., 1997. Subsidence of the harbor at Kenchreai, saronic gulf, Greece, during the earthquakes of AD 400 and AD 1928. *Am. Geophys. Union Trans.* 78, 636.

Nomikou, P., Papanikolaou, D., Alexandri, M., Sakellariou, D., Rousakis, G., 2013. Submarine volcanoes along the Aegean Volcanic Arc. *Tectonophysics.* 597, 123–146

Nurnberg, D., Bijma, J., Hemleben, C., 1996. Assessing the reliability of magnesium in foraminiferal calcite as a proxy for water mass temperature. *Geochim. et Cosmochim.* Acta 60, 803–814.

Nyst, M., Thatcher, W., 2004. New constraints on the active tectonic deformation of the Aegean. *Journal of Geophysical Research* 109. http://dx.doi.org/10.1029/2003JB002830.

Obert, J.C., Scholz, D., Felis, T., Brocas, W. M., Jochum, K.P., Andreae, M.O., 2016. ^{230}Th/U dating of Last Interglacial brain corals from Bonaire (southern Caribbean) using bulk and theca wall material. *Geochim. et Cosmochim.* Acta 178, 20–40.

Oldfield, F., 1991.Environmental magnetism—a personal perspective. *Quat. Sci. Rev.* 10(1), 73–85.

Ori, G., 1989. Geologic history of the extensional basin of the Gulf of Corinth (?Miocene – Pleistocene),Greece. *Geology* 17, 918–921.

Ozturk, M.Z., Erginal, A.E., Kiyak, N.G., Ozturk, T., 2016. Cement Fabrics and Optical Luminescence Ages of Beachrock, North Cyprus: Implications for Holocene Sea-level Changes .*Quat. Inter.* 401, 132–140.

Pantosti, D., De Martini, P., Koukouvelas, I., Stamatopoulos, L., Palyvos, N., Pucci, S.,Lemeille, F., Pavlides, S., 2004. Palaeoseismological investigations of the Aigion fault (gulf of Corinth, Greece). *Comptes Rendus Geosci.* 336, 335–342.

Pallikarakis, A., Grützner, C., Mason, J., Schneiderwind, S., Papanikolaou, I., Triantaphyllou, M., Migiros, G., 2015. Correlating magnetic susceptibility with facies changes within borehole cores on either sides of an active fault in Corinth Canal. *Proceedings of the 6th International INQUA Meeting on Paleoseismology, Active Tectonics and Archaeoseismology,* (Pescina, Fucino Basin, Italy), pp.332–336.

Pallikarakis, A., Triantaphyllou, V.M., Papanikolaou, I., Dimiza, D.M., Reicherter, K., Migiros, G., Cor. Proof. Age Constraints and Paleoenvironmental Interpretation of a Borehole Sedimentary

Sequence at the Eastern Part of Corinth Isthmus, Greece. *Journal of Coastal Research*. DOI: 10.2112/JCOASTRES-D-16-00191.1

Palyvos, N., Mancini, M., Sorel, D., Lemeille, F., Pantosti, D., Julia, R., Triantaphyllou, M., De Martini, P.M., 2010. Geomorphological, stratigraphic and geochronological evidence of fast Pleistocene coastal uplift in the westernmost part of the Corinth Gulf Rift (Greece).*Geol. J.* 45(1), 78–104.

Papantoniou, L., Rozos, D., Migiros, G., 2008. Engineering geological conditions and slope failures along the Corinth Canal. Bull. *Geol. Soc. Greece* 36, 17–24.

Papatheodorou, G., Stefatos, A., Christodoulou, D., Ferentinos, G., 2003. Small scale present day turbidity currents in a tectonically active submarine graben, the Gulf of Corinth (Greece): Their significance in dispersing mine tailings and their relevance to basin filling. In: Locat, J., Mienert, J. (Eds.), *Submarine Mass Movements and their Consequences. Kluwer Academic Publishers,* pp. 459–468.

Papanastassiou, D., Gaki-Papanastassiou, K., 1994.Geomorphological observations in the Kechries – Ancient Corinth region and correlation with seismological data. *Proceedings of the 3rd Panellenic Geographical Congress,* pp. 210–223.

Papanikolaou, D.J., Royden, L.H., 2007. Disruption of the Hellenic arc: Late Miocene extensional detachment faults and steep Pliocene–Quaternary normal faults Orwhat happened at Corinth? *Tectonics* 26, TC5003.

Papanikolaou, D., Lykousis, V., Chronis, G., Pavlakis, P., 1988. A comparative study of neotectonic basins across the Hellenic Arc: the Messiniakos, Argolikos, Saronikos and Southern Evoikos Gulfs. *Basin Res* 1(3), 167–176.

Papanikolaou, D., Chronis, G., Lykousis, V., Pavlakis, P., Roussakis, G., Syskakis, D., 1989. Offshore Neotectonic Map the Saronic Gulf. Athens, Greece: Earthquake Planning and Protection Organization, National Centre for Marine Research, University of Athens, scale 1: 100,000, 1 sheet.

Papanikolaou, D., Logos, E., Lozios, S., Sideris, Ch., 1996.Neotectonic Map of Korinthos, Athens, Greece: Earthquake Planning and Protection Organization, scale 1:100,000, 1 Sheet.

Papanikolaou, I., Foumelis, M., Parcharidis, I., Lekkas, E.L. and Fountoulis, I. (2010). Deformation pattern of the 6 and 7 April 2009, Mw=6.3 and Mw=5.6 earthquakes in L' Aquila (central Italy) revealed by ground and space based observations. *Natural Hazards and Earth System Sciences* 10, 73-87.

Papanikolaou I.D., Van Balen, R., Silva, P.G., Reicherter, K., 2015. Geomorphology of Active Faulting and seismic hazard assessment: New tools and future challenges. *Geomorphology* 237, 1-13.

Papanikolaou I.D., Triantaphyllou, M., Pallikarakis A., Migiros, G., 2015. Active faulting at the Corinth Canal based on surface observations, borehole data and paleoenvironmental interpretations. Passive rupture during the 1981 earthquake sequence?. *Geomorphology* 237, 65-7–8.

Papazachos, B., Papazachou, C., 1997. The Earthquakes of Greece. P. Ziti and Co, Thessaloniki, Greece. 304 pp.

Pavlakis, P., Lykoussis, V., Papanikolaou, D., Chronis, G., 1990. Discovery of a new submarine volcano in the western Saronic Gulf: the Paphsanias Volcano. *Bull. of the Geol. Soc. Greece* 24, 59–70.

Pavlopoulos, K., Theodorakopoulou, K., Bassiakos, Y., Hayden, B., Tsourou, T., Triantaphyllou, M., Kouli, K., Vandarakis, D., 2007. Paleoenvironmental evolution of Istron (N.E. Crete), during the last 6000 years: depositional environment, climate and sea level changes. *Geodinamica Acta,* 20(4), 219–229.

Pawley, S.M., Toms, P., Armitage, S.J., Rose, J., 2010. Quartz luminescence dating of Anglian Stage (MIS 12)fluvial sediments: comparison of SAR age estimates to the terrace chronology of the Middle Thames valley, UK. *Quat. Geochronol*. 5, 569–582.

Pe-Piper, G., Piper, D., 2002. The igneous rocks of Greece. Beitrage zur perionalen geologie der erde, vol. 30. *Gebruder Borntraeger* (573 pp).

Peirano, A., Morri, C., Mastronuzzi, G., Nike Bianchi, C.N., 1994. The coral Cladocora caespitosa (Anthozoa, Scleractinia) as a bioherm builder in the the Mediterranean Sea . *Mem. Descr. Carta Geol. Ital.* 59–74.

Perch-Nielsen, K., 1985.Cenozoic calcareous nannofossils. In: Bolli, H.M.; Saunders, J.B. and Perch-Nielsen, K. (eds.), Plankton Stratigraphy. Cambridge University Press, Cambridge, pp. 427–554.

Perissoratis, C., Piper, D.J.W., Lykousis, V., 2000. Alternating marine and lacustrine sedimentation during late Quaternary in the Gulf of Corinth rift basin, Central Greece. *Mar. Geol.* 167, 391–411.

Pierini, F., Demarchi, B., Turner, J., Penkman, K., 2016. Pecten as a new substrate for IcPD dating: The quaternary raised beaches in the Gulf of Corinth, Greece. *Quat. Geochron.* 31, 40–52.

Pirazzoli, P.A., 2005. A review of possible eustatic, isostatic and tectonic contributions in eight late-Holocene relative sea-level histories from the Mediterranean area, *Quaternary Science* Reviews 24,1989-2001.

Pirazzoli, P., Stiros, S., Fontugne, M., Arnold, M., 2004. Holocene and quaternary uplift in the central part of the southern coast of the Corinth Gulf (Greece), *Mar. Geol.* 212, 35–44.

Place, J., Géraud, Y., Diraison, M., Warr, L., 2007.North–south transfer zonesand paleo-morphological reconstruction of the Xylokastro area (Corinth Gulf, Greece). *Tectonophysics* 440, 121–139.

Pope, R., Wilkinson, K., Skourtsos, E., Triantaphyllou, M., Ferrier, G., 2008. Clarifying stages of alluvial fan evolution along the Sfakian piedmont, southern Crete: new evidence from analysis of post-incisive soils and OSL dating. *Geomorphology* 94,206–225.

Porat, N., Amit, R., Zilberman, E., Enzel, Y., 1997. Luminescence dating of fault-related alluvial fan sediments in the southern Arava valley, Israel. *Quat. Geochronol.(Quat. Sci. Rev.)* 16, 397–402.

Porat, N., Duller, G.A.T., Amit, R., Zilberman, E., Enzel, Y., 2009. Recent faulting in the southern Arava, Dead Sea Transform: Evidence from single grain luminescence dating. *Quat. Inter*. 199, 34–44.

Prazeres, M., Uthicke, S., Pandolfi, J.M., Influence of local habitat on the physiological responses of large benthic foraminifera to temperature and nutrient stress. *Sci Rep*. 6

Prescott, R.J., Stephan, L.G., 1982. The contribution of cosmic radiation to the environmental dose for thermoluminescence dating, latitude, attitude and depth dependences. *Counc. Europ. J. PACT* 6, 17–25.

Prescott, J.R., Hutton, J.T., 1988. Cosmic ray and gamma ray dosimetry for TL and ESR. *Nuclear Tracks Rad. Measur.* 14, 223–227.

Prescott, J.R., Hutton, J.T., 1994. Cosmic ray contribution to dose rates for luminescence and ESR dating: large depths and long-term variations. Radiation Measurements 23, 497-500.

Preusser, F., Degering, D., Fuchs, M., Hilgers, A., Kadereit, A., Klasen, N., Krbetschek, M., Richter, D., Spencer, J.Q.G., 2008. Luminescent dating: basics, methods and applications. *Eiszeitalter und Gegenwart* 57, 95–149.

Raffi, I., Backman, J., Fornaciari, E., Palike, H., Rio, D., Lourens, L., Hilgen, F., 2006. A review of calcareous nannofossil astrobiochronology encompassing the past 25 million years. *Quat. Sci. Rev.* 25(23), 3113–3137.

Reicherter, K., Vonberg, D., Koster B., Fernández-Steeger, T., Grützner, C., Mathes-Schmidt, M., 2010. The sedimentary inventory of tsunamis along the southern Gulf of Cádiz (southwestern Spain). *Zeitschrift für Geomorphologie*, 54, 3, 147–173.

Reimann, T., Tsukamoto, S., Harff, J., Osadczuk, K., Frechen, M., 2011. Reconstruction of Holocene coastal foredune progradation using luminescence dating-An example from the Swina barrier (southern Baltic Sea, NW Poland). *Geomorphology* 132, 1–16.

Regenberg, M., Steph, S., Nürnberg, D., Tiedemann, R., Garbe-Schönberg, D., 2009. Calibrating Mg/Ca ratios of multiple planktonic foraminiferal species with delta O^{-18} calcification temperatures: palaeothermometry for the upper water column. *Earth Planet. Sci. Lett.* 278, 324–336.

Rio, D., Raffi, I., Villa, G., 1990. Pliocene Pleistocene calcareous nannofossil distribution patterns in the western Mediterranean. *Proceedings of the Ocean Drilling Program. Sci. Results* 107, 513–533.

Rizza, M., Mahan, S., Ritz, J-F., Nazari, H., Hollingsworth, J., Salamati, R. 2011.Usingluminescence dating of coarse matrix material to estimate the slip rate of the Astaneh fault, Iran. *Quat. Geochronol.* 6, 3–4, 390–406.

Ruiz, F., Abad, M., Olias, M., Galan, E., Gonzalez, I., Aguila, E., Hamoumi, N., Pulidod, I., Cantano, M., 2006.The present environmental scenario of the Nador Lagoon (Morocco). Environm. Res., 102(2), 215–229.

Roberts, G.P., 1996. Variation in fault-slip directions along active and segmented normal fault systems. *J. Struct. Geol.* 18(6), 835–845.

Roberts, G.P., Houghton, S.L., Underwood, C., Papanikolaou, I., Cowie, P.A., van Calsteren, P., Wigley, T., Cooper, F.J., McArthur, J.M., 2009. Localization of Quaternary slip rates in an active rift in 10^5 years: an example from central Greece constrained by ^{234}U-^{230}Th coral dates from uplifted paleoshorelines. *J. Geophys. Res.* 114 (B104), http://dx.doi.org/10.1029/2008JB0058.

Roberts, G.P., Koukouvelas, I.K., 1996. Structural and seismological segmentation of the Gulf of Corinth fault system: implication for models of fault growth. *Ann. Geophys*. 39, 619–646.

Roberts, G., Papanikolaou, I., Vött, A., Pantosti, D., Hadler, H., 2011. Active tectonics and earthquake geology of the Perachora Peninsula and the area of the Isthmus, Corinth Gulf, Greece. In: Roberts, G., Papanikolaou, I., Vött, A., Pantosti, D., Hadler, H. (Eds.), INQUA - TERPRO Focurs Area on Paleoseismology and Active Tectonics & IGCP-567. *Earthq. Archaeol. Athens* (40 pp.).

Roberts, H.M., Wintle, A.G., 2001. Equivalent dose determinations for poly mineralic 7ne-grains using the SAR protocol: application to a Holocene sequence of the Chinese Loess Plateau. Quat. Sci. Rev. 20, 859–863.

Rohais, S., Eschard, R., Guillocheau, F., 2008. Depositional model and stratigraphic architecture of rift climax Gilbert-type fan deltas (Gulf of Corinth, Greece). *Sedim. Geol.* 210, 132–145.

Rondoyanni, Th., Livaditi, A. and Mettos, A., 2008. Eastern Corinthia: structure and characteristics of an active geological environment. Bull. *Geol. Soc. Greece* 41, 35–42 (In Greek).

Rossi, V., Horton, B.P., 2009. The application of subtidal foraminifera-based transfer function to reconstruct Holocene paleobathymetry of the Po Delta, northern Adriatic Sea. *J. Foraminif. Res.* 39, 180–190.

Sakellariou, D., Lykousis, V., Papanikolaou, D., 2001. Active faulting in the Gulf of Corinth, Greece. In: Briand, F. (Ed.), 36th CIESM Congress Proceedings 36, p. 43.

Sakellariou, D., Lykousis, V., Alexandri, S., Kaberi, H., Rousakis, G., Nomikou, P., Georgiou, P., Ballas, D., 2007.Faulting, seismic stratigraphic architecture and late Quaternary evolution of the Gulf of Alkyonides Basin — east Gulf of Corinth, central Greece. *Basin Res.* 19(2), 273–295.

Scarponi, D., Huntley, J.W., Capraro, L. Raffi, S., 2014. Stratigraphic paleoecology of the Valle di Manche section (Crotone Basin, Italy): A candidate GSSP of the Middle Pleistocene. *Palaeogeography, Palaeoclimatology, Palaeoecology,* 402, 30–43.

Sachpazi, M., Hirn, A., Clement, C., Laigle, M., Roussos, N., 2003. Evolution to fastest opening of the Gulf of Corinth continental rift from deep seismic profiles, *Earth Planet. Sci. Lett.*, 216, 243 – 257.

Scholz, D. Hoffmann, D.L., 2008. $^{230}Th/U$-dating of fossil reef corals and speleothems. *E&G Quat. Sci. J.* 57, 52–77.

Scholz, D., Mangini, A., 2007. How precise are U-series coral ages? *Geochim. Cosmochim. Acta* 71, 1935–1948.

Scholz, D., Mangini, A., Felis, T., 2004. U-series dating of diagenetically altered fossil reef corals. *Earth Planet. Sci. Lett.* 218, 163–178.

Scholz, D., Mangini, A., Meischner, D., 2007. U-redistribution in fossil reef corals from Barbados, West Indies, and sea level reconstruction for MIS 6.5. In: Sirocko, F., Claussen, M., Litt, T., and Sanchez- Goni, M. F. Eds.), The climate of past Interglacials. Elsevier, Amsterdam.

Scott, D.S., Medioli, F.S., 1980. Quantitative studies of marsh foraminiferal distributions in Nova Scotia and comparison with those in other parts of the world: implications for sea level studies. *A Special Publication of the Cushman Foundation for Foraminif. Res.,* 17, 58.

Scranton, R.L., 1957. Mediaeval Architecture: in the Central Area of Corinth*. Corinth, vol. 16. Princeton, New Jersey* 1–147 pp.

Shackleton, N.J., 1967. Oxygen isotope analyses and Pleistocene temperatures re-assessed. *Nature* 215, 15–17.

Shackleton, N.J., 2000. The 100,000-year Ice-Age cycle identified and found to lag temperature, carbon dioxide, and orbital eccentricity. Science 289, 1897–1902.

Shackleton, N.J., Opdyke, N.D., 1973. Oxygen isotope and palaeomagnetic stratigraphy of equatorial Pacific core V28-238: oxygen isotope temperatures and ice volumes on a 105 and 106 year scale. *Quat. Res*. 3, 39–55.

Siddall, M., Rohling, E.J., Almogi-Labin, A., Hemleben, Ch., Meischner, D., Schmelzer, I., Smeed, D.A., 2003. Sea-level fluctuations during the last glacial cycle. *Nature*, 423, 853–858.

Sgarrella, F., Moncharmont Zei, M., 1993. Benthic foraminifera of the Gulf of Naples (Italy): systematics and autoecology. *Bollettin o dellaSocietà Paleontologica Italiana*, 32, 145–264.

Skirbekk, K., Hald, M., Marchitto, T.M., Junttila, J., litgaard Kristensen, D., Aaagaard Sørensen, S., 2016. Benthic foraminiferal growth seasons implied from Mg/Ca-temperature correlations for three Arctic species. Arctic species. *Geochemist., Geophysics., Geosystems.* 17, 11, 4684–4704.

Sonnenburg , E.P., Boyce, J.I., Reinhardt, E.G., 2013. Multi-proxy lake sediment record of prehistoric (Paleoindian–Archaic) archaeological paleoenvironments at Rice Lake, Ontario *Canada. Quat.Sci. Rev.* 73, 77–92.

Sorel, D., 2000. A Pleistocene and still-active detachment fault and the origin of the Corinth-Patras Rift, Greece. *Geology* 28, 83–86.

Stefatos, A., Papatheodorou, G., Ferentinos, G., Leeder, M., Collier, R., 2002. Seismic reflection imaging of active offshore faults in the Gulf of Corinth: their seismotectonic significance. *Basin Res.* 14, 487–502.

Stirling, C.H., Andersen, M.B., 2009. Uranium-series dating of fossil coral reefs: Extending the sea-level record beyond the last glacial cycle. *Earth Planet. Sci. Lett.* 284, 269–283.

Stirling, C. H., Esat, T. M., Lambeck, K., McCulloch, M. T., 1998. Timing and duration of the Last Interglacial: evidence for a restricted interval of widespread coral reef growth *Earth Planet. Sci. Lett* 160, 745–762.

Syrides, G., 2008. Marine mollusk fauna and Holocene stratigraphy of the marsh of Agia Paraskevi, (Lamia, Fthiotida) Greece. *Bull. Geol. Soc. Greece* XLII/I, 1–14.

Taylor, B., Weiss, J.R., Goodliffe, A., Sachpazi, M., Laigle, M., Hirn, A., 2011. The structures ,stratigraphy and evolution of the Gulf of Corinth rift, Greece. *Geophys. J. Inter.* 185, 1189–1219.

Taymaz, T., Jackson, J. and McKenzie., D. 1991. Active tectonics of the north and central Aegean. *Geophys. J. Int.,* 106, 433‑490.

Thiel, C., Buylaert, J. P., Murray, A., Terhorst, B., Hofer, I., Tsukamoto, S., Frechen, M. 2011. Luminescence dating of the Stratzing loess profile (Austria) – Testing the potential of an elevated temperature post-IR IRSL protocol. *Quat. Inter.* 234, 23–31.

Thierstein, H.R., Geitzenauer, K.R., Molfino, B., Shackleton, N.J., 1977. Global synchroneity of Late Quaternary coccolith datum levels validation by oxygen isotopes. *Geology* 5(7), 400–404.

Thompson, W.G., Goldstein, S.L., 2006. A radiometric calibration of the SPECMAP timescale. *Quat. Sci. Rev.* 25(23-24), 3207–3215.

Thompson, W.G., Spiegelmann, M.W., Goldstein, S.L., Speed, R.C., 2003. An open-system model for U-series age determinations of fossil corals. *Earth Planet. Sci. Lett.* 210, 365–381.

Tomiak, P.J., Andersen, M.B., Hendy, E.J., Potter, E.K., Johnson, K.G., Penkman, K. E.H., 2016. The role of skeletal micro-architecture in diagenesis and dating of Acropora palmata. Geochimica et Cosmochimica Acta 183, 153–175.

Triantaphyllou, M., 2015. Calcareous nannoplankton dating of the Late Quaternary deposits in Greece and the eastern Mediterranean: Case studies from terrestrial and marine sites. *J. Paleogeography*. 4(4), 1–9.

Triantaphyllou, M.V., Pavlopoulos, K., Tsourou, Th., Dermitzakis, M.D., 2003. Brackish marsh benthic microfauna and paleoenvironmental changes during the last 6000 years on the coastal plain of Marathon (SE Greece). *Riv. Ital. Paleontol. Stratigr.* 109(3), 539–547.

Triantaphyllou, M.V., Kouli, K., Tsourou, T., Koukousioura, O., Pavlopoulos, K., Dermitzakis, M.D., 2010. Paleoenvironmental changes since 3000 BC in the coastal marsh of Vravron (Attica, SE Greece). *Quat. Inter.* 216(1-2), 14–22.

Triantaphyllou, M., Pavlopoulos, K.P., Kouli, K., Koukousioura, O., Dimiza, M.D., Aidona, E. Syrides, G. Pallikarakis, A. Goiran, J.P., Fouache, E. 2016. Multiproxy Paleoenvironmental Reconstruction: The Piraeus Coastal Plain Case Study. Bull. Geol. Soc. Greece, 50, 478–488.

Tsakalos, E., Christodoulakis, J., Charalambous, L., 2016. The dose rate calculator (DRc) for luminescence and ESR dating-a Java application for dose rate and age determination. *Archaeometry.*

Tsodoulos, I.M., Stamoulis, K., Caputo, R., Koukouvelas, I., Chatzipetros, A.,Pavlides, S., Gallousi, C., Papachristodoulou, Ch., Ioannides, K., 2016. Middle-Late Holocene earthquake history of the Gyrtoni Fault, Central Greece: insight from optically stimulated luminescence (OSL) dating and paleoseismology. *Tectonophysics* 687, 14–27.

Turner, J.A., Leeder, M.R., Andrews, J.E., Rowe, P.J., Van Calsteren, P., Thomas, L., 2010. Testing rival tectonic upliftmodels for the Lechaion Gulf in the Gulf of Corinth. *J. Geol. Soc.,* 167, 1237–1250.

Tzedakis, P.C., Crucifix, M., Mitsui, T., Wolff, E. W. 2017. A simple rule to determine which insolation cycles lead to interglacials *Nature* 542, 427–432.

Urey, H.C. 1947. The thermodynamic properties of isotopic substances. *J. Chem. Soc.* 562–581

van Hinsbergen, D.J.J.; Kouwenhoven, T.J., van der Zwaan, G.J., 2005. Palaeobathymetry in the backstripping procedure: Correction for oxygenation effects on depth estimates. *Palaeogeography, Palaeoclimatology, Palaeoecology*. 221(3–4), 245–265.

van Hinsbergen, D.J.J., Schmid, S.M., 2012. Map-view restoration of Aegean–westAnatolian accretion and extension since the Eocene. *Tectonics* 31, TC5005.

van Voorthuysen, J.H., 1973. Foraminiferal ecology in the Ria de Arosa, Galicia, Spain. *Zoolog. Verhandelingen* 123, 3–82.

van der Zwaan, G.J.; Jorissen, F.J., de Stigter, H.C., 1990. The depth dependency of planktonic/benthic foraminiferal ratios: Constraints and applications. Mar. Geol. 95, (1), 1–16.

Vaughn, D.R., Caissie, B.E., 2017. Effects of sea-level, sea-ice extent, and nutrient availability on primary production at the Umnak Plateau, Bering Sea (IODP Site U1339) during Marine Isotope Stage (MIS) 5. *Palaeogeography, Palaeoclimatology, Palaeoecology*. 485, 283–292.

Vassilakis, E., Royden, L., Papanikolaou, D., 2011. Kinematic links between subduction along the Hellenic trench and extension in the Gulf of Corinth, Greece: a multidisciplinary analysis. *Earth Planet. Sci. Lett.* 303, 108–120.

Vilela, C.G., Koutsoukos, E.A.M., 1992. Miliolina (Foraminiferida) em sedimentos recentes da foz do Amazonas: uma resposta comportamentala um ambiented inâmico. In: *37th Congresso Brasileiro de Geologia—SBG/SP.* (São Paulo, SP, Brasil), 92–93.

Villemant, B., Feuillet, N., 2003. Dating open systems by the ^{238}U-^{234}U-^{230}Th method: application to Quaternary reef terraces. *Earth Planet. Sci. Lett.* 210, 105–118.

Vita-Finzi, C., 1993. Evaluating late Quaternary uplift in Greece and Cyprus. In: Pritchard, H.M., Alabaster, T., Harris, N.B.W., Neary, C.R. (Eds.), Magmatic Processes and Plate Tectonics. *Geol. Soc. Special Publication* 76, 417–424.

Waelbroeck, C., Labeyrie, L., Michel, E., Duplessy, J.-C., McManus, J., Lambeck, K., Balbon, E., Labracherie, M., 2002. Sea-level and deep water temperature changes derived from benthic foraminifera isotopic records. Quat. Sci. Rev. 21, 295–305.

Waldmann, N., Borromei, A.M., Recasens, C., Olivera, D., Martinez, M.A., Maidana, N.I., Ariztegui, D., Austin Jr., J.A., Anselmetti, F., Moy, C.M., 2014.Integrated reconstruction of Holocene millennial-scale environmental changes in Tierra del Fuego, southern-most South America. *Palaeogeography, Palaeoclimatology, Palaeoecology..* 399, 294–309.

Walker, S.E., Parsons-Hubbard, K., Richardson-White, S., Brett, C., Powell, E., 2011. Alpha and beta diversity of encrusting foraminifera that recruit to long-term experiments along a carbonate platform-to-slope gradient: paleoecological and paleoenvironmental implications. *Palaeogeography, Palaeoclimatology, Palaeoecology.* 312, 325–349.

Westaway, R.W.C., 1996. Quaternary elevation change of the Gulf of Corinth in central Greece. *Philosoph. Transact. Royal Society of London*. A 354,1125–1164.

Westaway, R., 2002. The Quaternary evolution of the Gulf of Corinth, central Greece: coupling between surface processes and flow in the lower continental crust. *Tectonophysics* 348, 269–318.

Woodroffe, C.D., Webster, J.M., 2014. Coral reefs and sea-level change*. Mar. Geol.* 352, 248–267.

Yang, Q., Scholz, D., Jochum, K. P., Hoffmann, D. L., Stoll, B., Weis, U., Schwager, B., and Andreae, M. O., 2015. Lead isotope variability in speleothems - A promising new proxy for hydrological change? First results from a stalagmite from western Germany. *Chemical Geology*, 396, 143-151.

Yasuhara, M., Yoshikawa, S., Nanayama, F., 2005. Reconstruction of the Holocene seismic history of a seabed fault using relative sea-level curves reconstructed by ostracode assemblages: case study on the Median Tectonic Line in Iyo-nada Bay, western Japan. *Palaeogeography, Palaeoclimatology, Palaeoecology..* 222, 285–312.

Yeager, K.M., Brunner, C.A., Kulp, M.A., Fischer, D., Feagin, R.A., Schindler, K.J., Prouhet, J., Bera, G., 2012. Significance of active growth faulting on marsh accretion processes in the Lower Pearl River, Louisiana. *Geomorphology* 153–154, 127–143.

Young, J.R., 1994. Functions of coccoliths. In: Winter, A. and Siesser, W.G. (eds.), Coccolithophores. *Cambridge University Press, Cambridge*, pp. 63–82.

Zachos, J., Pagani, M., Sloan, L., Thomas, E., Billups, K., 2001, Trends, rhythms, and aberrations in global climate 65 Ma to present. *Science*, 292, 686-693.

Zubakov, V.A., Borzenkova I.I., 1988. Pliocene palaeoclimates: Past climates as possible analogues of mid-twenty-first century climate, *Palaeogeography, Palaeoclimatology, Palaeoecology*, 65, 35–49.

Zygouri, V., Verroios, S., Kokkalas, S., Xypolias, P., Koukouvelas, I., Papadopoulos, G., 2008. Growth of faults within the gulf of Corinth. *Bull. Geol. Soc. Greece*, 41, 25–33 (In Greek).

List of Figures

List of Tables

Appendix A

Abbreviations within the text

BR-ratio	The percentage of the broken/weathered specimens in each sample
FD	Foraminifera Density
FRST	Forced Regressive System Track
IRSL	Infrared Stimulated Luminescence
MDS	Multi-Dimensional Scaling
MS	Magnetic Susceptibility
MIS	Marine Isotopic Stage
SAFS	South Alkyonides fault System
OSL	Optical Stimulated Luminescence
T-R	transgressive-regressive sequences
TST	Transgressive Systems Tract

Appendix B

Samples preparation and analyses

The first step was to describe in detail the lithologies within the boreholes. Samples were extracted from every different described lithology within the borehole cores, to make sure that the entire sequence will be adequate described, even if the described lithologies were not that promising (such as the gravely and coarser sediments). Before extracting any samples the external layer of the core has been removed, to reinsure that the sample will not be polluted from broken or weathered specimens. Using a high precision scale 10 gr of dry sediment has been extracted. Each sample remain in a beaker with H_2O_2 (~ 20%) for a whole day to remove any remnants of organic matter.

Subsequently, every beaker was treated for approximately 10 to 20 minutes with an ultrasonic cleaner to dissolve the coherence among the sediments' grains. Afterwards, each sample was washed through a 125 μm sieve and the remains dried at 60 °C, at least for one day. A subset containing approximately 200 benthic foraminifera for each sample when this was feasible was obtained using an Otto microsplitter. The microfauna have been identified under a Leica APO S8 stereoscope.

Appendix C

Foraminiferal description

The studied benthic foraminiferal assemblages are relatively abundant and moderately preserved. The detailed analysis of the examined borehole cores and the surface samples:

a) Borehole Bh-1

In borehole Bh-1 the interval from 31.00 to 29.70 m core depth (samples Bh-1 30.65, Bh-1 29.85 m) is characterized by the total absence of foraminiferal representatives. From 29.70 to 29.10 m core depth (sample 29.25 m) the interval is dominated by the presence of small – sized *Ammonia tepida* (~100% of the total assemblages). From 29.10 to 27.20 m core depth (sample Bh-1 28.55 m) the presence of both euryhaline species (*Ammonia* spp. ~ 15%) and full marine representatives (e.g. *Rossalina* spp. ~ 10%, *Cibicides* spp. ~10%, *Elphidium crispum ~10%*) has been described. Furthermore in sample Bh-1 28.55 m, nannofossils (*E*. *Huxleyi*, *Gephyrocapsa* spp. and *Reticulofenestra* spp.), have been described.

The interval from 27.20 m to 22.60 m core depth (samples Bh-1 26.75, Bh-1 25.95, Bh-1 25.35, Bh-1 24.75, Bh-1 23.95 m) is characterized by the absence of foraminiferal representatives, or few broken and weathered have been counted (high Br – ratio). The interval from 22.60 m to ~20.00 m core depth (samples Bh-1 21.05 and Bh-1 20.35 m)

is characterized by the combined presence of euryhaline specimens (*ammonia tepida ~10%, E. granosum ~15%)* and full marine species (Rossalina spp. and Cibicides spp. ~20%, miliolids ~10%). In sample Bh-1 20.35 m, nannofossils (*E*. *Huxleyi*, *Gephyrocapsa* spp. and *Reticulofenestra* spp.), have been described. From ~20.00 m to ~13.50 m core depth (samples Bh-1 19.15, Bh-1 18.45, Bh-1 16.75, Bh-1 16.25, Bh-1 15.15 m) the interval is characterized by the dominance of *Rossalina* spp. (up to ~35%), *Cibicides* spp. and miliolids (~30%). Furthermore in sample Bh-1 19.15 m, nannofossils (*E*. *Huxleyi*, *Gephyrocapsa* spp. and *Reticulofenestra* spp.), have been described. The interval from ~13.50 m to 12.50 m core depth (samples Bh-1 13.95 and Bh-1 13.15 m) is characterized both by the presence of full marine species (e.g. *Rossalina* spp. and miliolids) and euryhaline specimens (*Ammonia tepida*).

From 12.50 m to 11.20 m core depth (sample Bh-1 11.85 m) is characterized by the presence of few and broken foraminiferal representatives (high Br ratio). From 11.20 to 8.00 core depth (samples Bh-1 10.65, Bh-1 9.65, Bh-1 8.55, Bh-1 m), *Rosalina* spp. (~20%), miliolids (~30%) and *Ammonia beccarii* (~15%) is described, followed by *Ammonia tepida* (~10%). In sample Bh-1 9.65 m, nannofossils (*E*. *Huxleyi*, *Gephyrocapsa* spp. and *Reticulofenestra* spp.), have been described. In the interval from 8.20 to 7.50 m core depth (sample Bh-1 8.15 m), the presence of *Ammonia tepida* and *E. granosum* is also described (~40%). The interval from 7.50 m to 6.50 (sample Bh-1 6.95 m) *Rosalina* spp. (~25%), miliolids (~20%) and *Ammonia beccarii* (~15%) is described, followed by *Ammonia tepida* (~15%). From 6.50 m to 0.00 m core depth the identified foraminifera (mostly *Ammonia* spp. and *Elphidium* spp. representatives) were broken and weathered and therefore were not included to the paleoenvironmental interpretation.

b) Borehole Bh-2

Borehole core Bh-2 has not been examined for tis micropaleontological content and only a description of the lithology is available.

c) Borehole Bh-3

In borehole Bh-3 from 70.20 m to 66.50 m core depth (samples Bh-3 66.55) no foraminiferal species have been found. The absence of foraminiferal representatives has been described to the interval 66.50 m – 61.50 m core depth as well (samples Bh-3 66.55, Bh-3 66.25, Bh-3 65.75, Bh-3 65.35, Bh-3 64.35, Bh-3 63.95 Bh-3 62.65, Bh-3 61.95); while in contrast, the samples are abundant in ostracod valves (*Cyprideis* spp.).

From 61.50 m to 60.00 m core depth (sample Bh-3 60.15) mostly miliolids (~20%) and *Ammonia* spp. (~20%) have been described, as well as fragments of *Cladocora caespitosa* corals. Furthermore in sample Bh-3 60.15 m, nannofossils (*E*. *Huxleyi*, *Gephyrocapsa* spp. and *Reticulofenestra* spp.), have been described. In the interval 60.00–54.50 m core depth few broken foraminifera have been described and most of them were broken (high BR-ratio) (samples Bh-3 56.05 and Bh-3 57.15 m). From 54.50 to 49.60 m core depth (samples Bh-3 52.75, Bh-3 52.35, Bh-3 51.15, Bh-3 50.35, Bh-3 49.65) full marine species have a considerable contribution (more than 36% of the total foraminiferal assemblage). Samples are dominated by *Elphidium* (*crispum* and *complanatum*), and *Rossalina* spp.– *Cibicides* spp. Few *Haynesina* spp. specimens have been found, while *Ammonia*, small and large, are less than 23% of the total assemblage at 52.30 m core depth. In samples Bh-3 51.75 and Bh-3 52.75 nannofossils (*E*. *Huxleyi*, *Gephyrocapsa* spp. and *Reticulofenestra* spp.), have been described. The interval 49.60 m to 39.60 m core depth (samples Bh-3 48.05, Bh-3 47.25, Bh-3 45.75, Bh-3 42.85 m) was characterized as barren. From 39.60 m to 37.00 m core depth (samples Bh-3 39.65, Bh-3 38.75, Bh-3 38.05, Bh-3 37.55) the analysed samples presented scarce foraminiferal specimens. In contrast, the samples are abundant in ostracod valves (*Cyprideis* spp.).

From 37.00 to 34.00 m core depth (samples Bh-3 36.35, Bh-3 35.65, Bh-3 34.45 m) the presence of full marine species (mostly *Rossalina* spp., miliolids and *Cibicides* spp., followed by *Elphidium* spp., with total concentration more than ~60% of the total sample) has been described. Euryhaline species as *Haynesina* spp., *Aubignyna*

perlucida and *Ammonia spp.* were scarce and circumstantial. Interestingly planktonic foraminifera have been identified (Globigerinoides ~ 4%) in sample Bh-3 36.35 m. In samples Bh-3 35.65 and Bh-3 36.35 calcareous nannofossils (*E*. *Huxleyi*, *Gephyrocapsa* spp. and *Reticulofenestra* spp.), have been described. From 34.00 to 22.40 (samples Bh-3 28.05 and Bh-3 22.45 m) core depth mostly barren and few broken specimens have been described (high BR-ratio). The interval 22.40 to 21.00 m core depth (sample Bh-3 21.75 m) ,has been dominated by the presence of small-sized *Ammonia tepida* (~93%), while from 21.00 m to 20.00 m core depth small- sized *Ammonia* and *Haynesina* spp. decrease and *Elphidium* spp. (~20%), miliolids (~10%) and other marine species (~25%) assemblages increase. Approximately at 20.40 m to 20.80 m depth, (sample Bh-3 20.75 m) a *Cladocora caespitosa* coral colony has been found *in situ*. This layer is 0.40 m thick and in growth position. Furthermore, calcareous nannofossils (*E*. *Huxleyi*, *Gephyrocapsa* spp. and *Reticulofenestra* spp.), have been described.

The interval 20.00 m to 16.50 m core depth (samples Bh-3 19.85, Bh-3 18.05 m), is also characterized by the presence of small- sized *Ammonia E. granosum* and *Haynesina* spp. (~70% of the total assemblages). The interval 16.50 m to 11.00 m core depth (samples Bh-3 16.35, Bh-3 15.75, Bh-3 15.25, Bh-3 14.45, Bh-3 12.75, Bh-3 11.45 m) is barren where most of the identified specimens were broken (high BR- ratio). From 11.00 m to 3.30 m depth (samples Bh-3 10.25, Bh-3 9.35, Bh-3 8.75, Bh-3 6.85, Bh-3 6.35, Bh-3 4.35 m) the presence of full marine species (*Rossalina* spp., *Cibicides* spp., miliolids, consisting more than the ~50% of the total assemblages) is described, while in the upmost samples (Bh-3 6.85, Bh-3 6.35, Bh-3 4.35 m) small- sized *Ammonia* spp. is dominant (more than ~50%). In samples Bh-3 10.25 and Bh-3 8.75 calcareous nannofossils (*E*. *Huxleyi*, *Gephyrocapsa* spp. and *Reticulofenestra* spp.), have been described. In the uppermost layer (interval 3.30 m to 0.00 m depth) (samples Bh-3 3.05, Bh-3 1.55, Bh-3 0.55 m) no or few foraminiferal species have been described.

d) Borehole Bh-4

Borehole core Bh-4 has not been examined for tis micropaleontological content and only a description of the lithology is available.

e) Borehole Bh-6

Borehole core Bh-6 has not been examined for tis micropaleontological content and only a description of the lithology is available.

f) Borehole Bh-7

In borehole Bh-7 the interval 56.00 – 49.00 m core depth is not characterized by the presence of foraminiferal representatives (samples Bh-7 55.55, Bh-7 55.05, Bh-7 54.75, Bh-7 54.25, Bh-7 53.45, Bh-7 52.35, Bh-7 51.75, Bh-7 51.35, Bh-7 50.55, Bh-7 49.15 m). Instead of them, the analysed samples are abundant in ostracod valves (*Cyprideis* spp.). From 49.00 m to 45.00 m core depth no foraminiferal representatives have been identified (samples Bh-7 47.65, Bh-7 46.85 m). From 45.00 m to 33.00 m core depth the deformation zone of the Kalamaki – Isthmus fault has been detected, also completely barren of microfauna (samples Bh-7 44.65, Bh-7 41.15, Bh-7 39.35, Bh-7 38.75, Bh-7 37.65, Bh-7 36.45, Bh-7 35.95, Bh-7 34.95, Bh-7 34.55, Bh-7 33.45 m). In the interval 33.00 m to 27.00 m core depth is also characterized by the absence of foraminifera (samples Bh-7 31.25, Bh-7 31.05, Bh-7 30.65, Bh-7 29.45, Bh-7 29.05, Bh-7 28.55, Bh-7 27.35 m). Full marine euryhaline species (e.g. *Rossalina spp., Cibicides* spp. miliolids, *Neoconorbina* spp.) comprise the 100% of the total samples described at the interval 27.00 to 26.00 m core depth (samples Bh-7 26.85, Bh-7 26.45 m). In sample Bh-7 26.85 m calcareous nannofossils (*E. Huxleyi, Gephyrocapsa* spp. and *Reticulofenestra* spp.), have been described.

The interval 26.50 m to 23.00 m core depth is characterized by the absence of foraminifera or few broken have been identified (high BR – ratio) (samples Bh-7 25.85, Bh-7 25.45, Bh-7 24.35, Bh-7 23.75, Bh-7 23.25 m). The interval from 23.00 m to 19.00 m core depth (samples Bh-7 22.75, Bh-7 22.35, Bh-7 21.95, Bh-7 21.45, Bh-7 20.75, Bh-7 20.25, Bh-7 19.85, Bh-7 19.75, Bh-7 19.55, Bh-7 19.05 m) is dominated by the presence of small - sized *Ammonia* spp. accompanied by *Haynesina* spp. and *E. granosum (*more than ~50% of the total sample). In sample Bh-7 22.35 m calcareous nannofossils (*E. Huxleyi, Gephyrocapsa* spp. and *Reticulofenestra* spp.), have been described. The interval from 19.00 m to 16.00 m core depth (samples Bh-7 18.55, Bh-7 18.25, Bh-7 17.95, Bh-7 17.05, Bh-7 16.35 m) is characterized by fewer *Ammonia* spp., *Elphidium granosum* and *Haynesina* species (in total less than ~30% of the total sample), while other marine species (e.g. *Rossalina* spp., *Cibicides* spp., *Neoconorbina* spp., *A. beccarii*) are dominant. At 18.40 m a *Cladocora caespitosa* coral colony has been found *in situ,* approximately 0.30 m thick.

The interval from 16.00 to 12.00 m core depth (samples Bh-7 15.55, Bh-7 14.15, Bh-7 12.55, Bh-7 12.25 m) is characterized by the presence of *Ammonia* spp. (≥ 20%). At sample Bh-7 15.55 the total foraminiferal assemblage also consists of miliolids (~20%) and other marine species (~25%) while at Bh-7 14.15 m euryhaline species have been described once again and there is balance between euryhaline and marine species. In sample Bh-7 12.25 m depth, *Ammonia spp.* and other euryhaline species prevail against marine species (more than ~50%).

The interval from 12.00 m to 5.50 m core depth (samples Bh-7 11.65, Bh-7 10.55, Bh-7 10.25, Bh-7 9.25, Bh-7 8.15, Bh-7 7.65, Bh-7 7.35, Bh-7 6.95), is characterized by foraminiferal assemblages (mostly *Ammonia* small- and large- sized and in a lesser degree miliolids*, Elphidium* spp.). However most of them were either broken or weathered (high BR – ratio) and therefore have not been considered as reliable data.

The interval from 5.50 to 1.50 m core depth (samples Bh-7 5.35, Bh-7 3.95, Bh-7 3.45, Bh-7 2.85, Bh-7 1.55 m) is characterized mostly by miliolids, small- sized *Ammonia* spp., *Elphidium* spp. and full marine species In Bh-7 the first 1.50 m was topsoil and was not examined for microfaunal assemblages.

g) Borehole G-1

In borehole G-1 even though that few foraminiferal specimens have been found (mostly *Ammonia* spp., *Elphidium* spp. and miliolids) they were broken and weathered (high BR – ratio) and have not been included to the paleoenvironmental identification (samples G-1 16.95, G-1 14.65, G-1 13.65, G-1 7.75 m). Since the entire borehole sequence has been described as sediments that have been transported, no samples have been examined for nanno fossils.

h) Borehole GA-2

In borehole GA-2 the interval from 14.00 m to 12.30 m core depth (samples GA-2 12.95 and GA-2 12.35 m), is characterized by the presence mostly of full marine specimens (*Rossalina* spp. ~20%, *Cibicides* spp. ~30%, miliolids ~15%), while euryhaline species are also well represented (*Ammonia tepida* ~20%). In sample GA-2 12.95 m calcareous nannofossils (*E. Huxleyi, Gephyrocapsa* spp. and *Reticulofenestra* spp.), have been described. The interval from 12.30 m to 9.90 m core depth (sample GA-2 11.15 m) is characterized by the presence full marine specimens (*Rossalina* spp. ~15%, *Cibicides* spp. ~20%, miliolids ~10%), while euryhaline species are also well represented (*Ammonia tepida* ~30%). From 9.90 m to 3.80 m core depth (samples GA-2 9.35, GA-2 9.05, GA-2 8.85, GA-2 8.25, GA-2 7.55, GA-2 6.35, GA-2 5.45, GA-2 5.05 m) is dominated by euryhaline species (*Ammonia tepida* ranges from ~30% to ~60%, *E. granosum* from ~10% to ~20% and *Haynesina* spp. from ~5% to ~15%). On the contrary full marine species are fewer (~30% of the total concentration) and mostly represented by *Rossalina* spp., *Cibicides* spp. and *Asterigerinata mammilla* and *planorbis*.

i) Borehole GA-3

In borehole GA-3 even though that few foraminiferal specimens have been found (mostly miliolids, *Cibicides* spp., *Rosalina* spp. and *Elphidium* spp.) they were broken and weathered (high BR – ratio) and have not been included to the paleoenvironmental identification (samples GA-3 15.05, GA-5 13.45, GA-3 12.65, GA-3 11.65, GA-3 9.65 m). Since the entire borehole sequence has been described as sediments that have been transported, no samples have been examined for nanno fossils.

j) Borehole GA-4

In borehole core GA-4 the interval from 45.50 m to 40.00 m depth (samples GA-4 45.05, GA-4 44.95, GA-4 43.95, GA-4 42.35, GA-4 41.45 m) is characterized by full marine species (*Cibicides* spp. ~20%, Rossalina spp. ~10%, *A.* bec*c*arii ~ 15% and in a lesser degree *Asterigerinata* spp. and *Bolivina* spp. ~5%). The circumstantial presence of *Textularia* spp. and *Conurbella* spp. is also documented. Euryhaline species (*Ammonia tepida*, *Haynesina* spp., and *E. granosum* are barely represented (~15% of the total assemblages). In sample GA-4 41.45 m calcareous nannofossils (*E. Huxleyi, Gephyrocapsa* spp. and *Reticulofenestra* spp.), have been described.

The interval from 40.00 m to 39.00 m core depth (samples GA-4 39.95, GA-4 39.65, GA-4 39.05 m) is characterized by E. granosum (~ 20–40%) and Ammonia tepida (~20%), accompanied by full marine species (mainly *Rossalina* spp. ~15% and *Cibicides* spp. ~15%). The interval from 39.00 m to 38.50 m core depth (samples GA-4 39.85 and GA-4 38.80 m) is characterized by the presence of a few broken identified specimens (mostly *Cibicides* spp. and *Ammonia* spp.) (high BR – ratio). From 38.50 m to 37.00 m core depth (samples GA-4 38.45, GA-4 38.35, GA-4 37.45 m), the dominance of euryhaline species (Ammonia tepida ~ 40%, E. granosum ~ 20% and Haynesina spp. ~ 8%) is described. Full marine species (e.g. *A. beccarii*, *E. crispum*,

Rosalina spp., miliolids), are also represented. From 37.00 m to ~35.00 m core depth (sample GA-4 35.75 m), a balance between full marine species and Ammonia tepida is described. From ~35.00 m to 34.20 m core depth (samples GA-4 34.75 and GA-4 34.25 m) the dominance of full marine species is described.

The interval 34.20 m to 31.20 m core depth (samples GA-4 33.85, GA-4 33.45, GA-4 32.95, GA-4 32.25 m) is characterized by the presence of a few broken identified specimens (mostly *Rossalina* spp. and *Ammonia* spp.) (high BR – ratio). The interval from 31.20 m to 25.50 m core depth (samples GA-4 31.05, GA-4 30.15, GA-4 29.45, GA-4 27.35, GA-4 26.65, GA-4 25.85, GA-4 25.55 m) is dominated by full marine species and more specific from the presence of *Cibicides* spp. (up to ~25%), *Rosalina* spp. (up to ~ 28%), miliolids (up to ~25%) and *Ammonia beccarii* (up to ~20%). In sample GA-4 31.05 m calcareous nannofossils (*E. Huxleyi, Gephyrocapsa* spp. and *Reticulofenestra* spp.), have been described. In the interval from 25.50 m to 8.80 m core depth (samples GA-4 25.15, GA-4 24.85, GA-4 23.95, GA-4 23.05, GA-4 22.25, GA-4 22.05, GA-4 21.05, GA-4 20.75, GA-4 19.35, GA-4 19.25, GA-4 18.35, GA-4 18.15, GA-4 17.95, GA-4 16.65, GA-4 15.55, GA-4 15.25, GA-4 13.95, GA-4 12.25, GA-4 11.65, GA-4 10.95, GA-4 8.85 m) even though that foraminiferal species have been identified (mostly *Ammonia* spp., *Rosalina* spp. *Elphidium* spp., miliolids and *Cibicides* spp.) most of them were broken or weathered and have not been included to the paleoenvironmental analysis (high BR – ratio). The upper 8.80 m of the borehole core have been described as man-made Canal debris and therefore have not been examined at all.

k) Borehole GA-5

In borehole GA-5 the interval from 30.00 m to 29.30 m core depth (sample GA-5 29.95 m) is characterized by the absence of micro fauna. From 29.30 m to 28.10 m core depth (samples GA-5 28.75, GA-5 28.25 m) the dominance of euryhaline species (*Ammonia tepida* ~ 65%, *E. granosum* ~ 20% and *Haynesina* spp. ~ 5%) is described. The

presence of full marine species (*Rossalina* spp., *Cibicides* spp. miliolids, *E. crispum* ~ 30% of the total assemblages), also with *Ammonia tepida* and *Haynesina* spp. is described in the interval from 28.10 m to 26.60 m core depth (sample GA-5 27.75 m). Furthermore, in sample GA-5 27.75 m calcareous nannofossils (*E. Huxleyi, Gephyrocapsa* spp. and *Reticulofenestra* spp.), have been described.

The interval from 26.60 m to 20.80 m core depth (samples GA-5 26.05, GA-5 25.35, GA-5 23.25, GA-5 22.15 m) is characterized by the absence of micro fauna, except sample GA-5 20.95 m where few, but broken full marine species (mostly miliolids and *Cibicides* spp.) have been described (high BR – ratio). The interval from 20.80 m to 20.60 m core depth (samples GA-5 20.75 m) is characterized by the dominance of full marine species (*Asterigerinata* spp. ~ 12%, *Cibicides* spp. ~ 20%, miliolids ~ 20%, *Rossalina* spp. ~ 20%, *E. crispum* ~ 10%) and the complete absence of shallower marine representatives (e.g. *A. tepida*).

From 20.60 m to 13.80 m core depth (samples GA-5 19.35, GA-5 18.75, GA-5 17.05, GA-5 16.35, GA-5 15.15, GA-5 14.35 m) full marine species have a considerable contribution (more than ~ 40% of the total foraminiferal assemblage), accompanied by the presence of *A. tepida* (~10%), *E. granosum* (~ 15%). Furthermore, in sample GA-5 19.35 m calcareous nannofossils (*E. Huxleyi, Gephyrocapsa* spp. and *Reticulofenestra* spp.), have been described. From 13.80 m to 11.70 m core depth (samples GA-5 13.35 and GA-5 11.75 m) few and mostly broken species have been described (mainly *Ammonia* spp. and *Elphidium* spp. representatives) (high BR – ratio).

The interval from 11.70 m to 11.20 m core depth (samples GA-5 11.65 and GA-5 11.25 m) is characterized both by euryhaline species (*A. tepida* ~ 10%, *E. granosum* ~ 15% and *Haynesina* spp. ~ 5%) and full marine species (mostly miliolids ~ 10%, *Rossalina* spp. ~ 20%, *Discorbis* ~ 15 % and *Cibicides* ~ 15%).

The interval from 11.20 m to 10.20 m core depth (sample GA-5 10.25 m) is dominated by the presence of euryhaline species (*A. tepida* ~ 55%, *E. granosum* ~ 10%, *Haynesina* spp. ~ 7%), while full marine species have been represented ~ 5 – 8% per species (mostly miliolids and *Cibicides* spp.). From 10.20 m to 6.80 m core depth

(samples GA-5 9.35, GA-5 8.65 and GA-5 7.05 m), once again a balance between euryhaline species (*A. tepida*, *E. granosum*) and full marine species (miliolids, *E. crispum*, *Rossalina* spp, *Cibicides* spp, *Asterigerinata* spp.) is described. The upper 6.80 m of the borehole core (samples GA-5 6.05, GA-5 5.65, GA-5 3.55 and GA-5 2.85 m), is characterized by the presence of a few broken identified specimens (mostly miliolids, *Rossalina* spp. and *Ammonia* spp.) (high BR – ratio).

l) Surface samples

In samples S.23.9/2, S.25.9./3, S.25.9/2 and S.12/7/3, apart from small *Reticulofenestra* spp. (~45%) and small *Gephyrocapsa* spp (~33%), *E. huxleyi* specimens were relatively scarce (5-8% of the total assemblage), but consistently present.

The dominance of euryhaline species, representative for shallow environments have been described in samples S. 1.7/8, S. 1.7/6, S. 1.7/5, S. 4.7/6. These samples are mostly characterized by small – size *Ammonia tepida* (more than ~70%), accompanied by *Elphidium granosum* (~ 10%) and *Haynesina* spp. (~ 10%). Full marine species have only circumstantial appearance (e.g. miliolids).

A balance between euryhaline species and full marine species is described in samples S. 4/7/14, Can 12, S. 4/7/10, S. 12/7/7, S. 4/7/8, Can 13, S. 4/7/1, S. 12/7/8, S. 4/7/15, S. 4/7/16, S. 17/7/5, S. 1/7/10, S. 4/7/19, S. 1/7/8, S. 17/7/8 and S. 17/7/4. Miliolids (up to ~ 44%, S.4/7/1), A. beccarri (up to ~ 41%, S.17/7/8), E. crispum (up to ~ 33%, S.4/7/16) and Cibicides refulgens (up to ~ 27%, S.4/7/15), have been described. *Ammonia tepida, E. granosum* and *Haynesina* spp. have been represented as well (~ 20%, ~ 10% and ~ 5% respectively). Furthermore, in samples S.17/7/8, 4/7/19, S.17/7/5 and Can.12 calcareous nannofossils small *Reticulofenestra* spp. and small *Gephyrocapsa* spp. coccoliths have been identified.

In samples S. 4/7/2, S. 1/7/9, S. 23/9/2, S. 17/7/7, S. 1/7/9, S. 25/9/3, S. 23/9/3, S. 12/7/3, S. 25/9/7, S. 25/3/6, S. 25/9/2, S. 1/7/4, the presence of euryhaline species (mostly Ammonia tepida) is only circumstantial described. These samples are dominated mostly by full marine species *Asterigerinata* spp. *E. crispum*, *Discorbis* spp. and *Neoconorbina terquemi*. In samples S.23.9/2, S.25.9./3, S.25.9/2 and S.12/7/3, calcareous nannofossils small *Reticulofenestra* spp., *E. huxleyi* and small *Gephyrocapsa* spp. coccoliths have been identified.

Appendix D

Magnetic susceptibility measurements

Magnetic Susceptibility within the core is measured with the Bartington MS2 system with the MS2K sensor. The MS measurements were taken in the laboratory every 2 cm along each core if that was possible and every sample was measured at least 2 times and the average value considered as the final one for the sample or by calculating the average value if the sample was in a sample bag. Air measurements before and after the sample's measurement have been performed in all samples. In total, 986 MS measurements were extracted.

All the extracted samples are presented in Tables 21 to 28 below. The described core depth is expressed in meters and the mean value in dimensional SI units

Table 21 The measured MS signal in borehole core Bh-1. Πίνακας 22. Η τιμές μαγνητικής επιδεκτικότητας στην γεώτρηση Bh-1.

Core depth	Mean value
-0.55	13
-1.45	32
-3.55	99.5
-4.55	95

-6.95	48.5
-8.1	16.5
-8.55	57
-9.65	73.5
-10.65	15
-11.85	61
-13.1	16.5
-13.95	51
-15.1	70
-16.25	22.5
-16.75	8.5
-18.45	6.5
-19.15	5
-20.35	5
-21.05	12
-23.95	188.5
-24.75	195
-25.35	212
-25.95	181
-28.75	8.5
-29.25	9
-29.85	267
-30.65	230.3

Table 22 The measured MS signal in borehole core Bh-3. Πίνακας 22. Η τιμές μαγνητικής επιδεκτικότητας στην γεώτρηση Bh-3.

Core depth	**Mean value**	***Core depth***	**Mean value**
-0.55	123	-35.65	51.5
-1.55	158.5	-36.35	41.5
-3.05	61	-36.95	46.5
-3.35	3	-37.55	8
-3.85	4.00	-38.25	10.5
-4.35	26	-45.75	101.50
-5.55	42.5	-47.15	69
-6.35	29	-48.55	5
-6.85	18	-50.35	1
-7.45	22.5	-51.15	1
-8.75	18	-51.85	3
-9.35	15	-52.35	2
-10.2	34.5	-52.75	4

-11.45	80.5	-54.05	3
-12.35	111.5	-55.05	3.5
-12.75	8.5	-55.65	2
-14.35	116	-56.25	6
-15.2	176	-56.55	6
-15.3	63.5	-56.75	2
-16.05	4	-57.15	4
-16.95	29	-60.15	3.5
-17.75	26.5	-60.85	18
-18.65	50	-61.95	2
-19.25	21.5	-62.35	1
-19.85	35.5	-63.95	7
-20.75	4	-64.45	10
-21.75	7	-65.25	3
-22.55	207	-66.25	2
-28.05	93.5	-66.45	9
-34.45	54	-67.25	31

Table 23 *The measured MS signal in borehole core Bh-7. Πίνακας 24. Η τιμές μαγνητικής επιδεκτικότητας στην γεώτρηση Bh-7.*

Core depth	Mean value	Core depth	Mean value
-1.55	23	-19.05	47.5
-2.85	215	-19.55	12
-3.15	163	-19.85	114.5
-3.45	3	-20.25	193.5
-3.9	44	-20.75	138.5
-4	250	-21.45	5
-4.85	104.5	-21.95	143
-5.35	36	-22.35	145
-5.6	14	-23.2	52
-5.7	1	-23.75	11.5
-6.45	19	-24.35	8
-6.95	53.5	-25.45	24.5
-7.35	3	-25.85	131.5
-7.6	12	-26.45	11
-7.95	227	-26.85	57
-8.15	125.5	-27.35	152
-9.25	125	-29.05	110

-9.75	28.5	-29.45	114.5
-9.85	3	-31.05	43
-10.25	73	-31.55	51.5
-10.45	81	-32.35	1
-10.55	191	-32.85	12.5
-11.35	64	-33.85	24.5
-11.65	163	-35.95	7.5
-12.05	35	-36.45	9.5
-12.35	32	-37.65	41
-12.55	97.5	-38.7	2
-14.15	10.5	-38.8	196
-14.35	32	-39.35	190.5
-14.75	16	-44.35	19.5
-14.95	102	-48.45	46
-15.55	4	-50.55	23
-16.35	25	-51.35	90
-16.55	3	-51.75	106
-16.6	43	-52.35	4
-17.4	1	-53.45	80.5
-17.5	2	-54.25	2
-18.25	1	-54.45	6
-18.55	6	-54.75	10
		-55.55	3

Table 24 The measured MS signal in borehole core G-1. Πίνακας 25. Η τιμές μαγνητικής επιδεκτικότητας στην γεώτρηση G-1

Core depth	**Mean value**	***Core depth***	**Mean value**
-3.85	159	-11.69	307
-4.65	371	-11.73	296
-5.00	475	-11.76	178
-6.00	493.5	-11.80	215
-6.30	475	-12.85	366
-6.33	357	-13.55	220.5
-6.36	339	-14.30	322
-6.39	473	-14.60	330
-6.41	305	-15.50	316
-6.44	582	-15.53	253
-6.47	408	-15.57	276

-6.50	289	-15.60	260
-6.53	251	-15.63	314
-6.56	282	-15.67	404
-6.59	289	-15.70	233
-6.61	308	-16.80	351.5
-6.64	343	-18.00	353
-6.70	314	-19.50	450
-7.60	207	-19.53	434
-7.62	225	-19.55	353
-7.64	209	-19.58	298
-7.66	161	-19.60	268
-7.68	185	-19.63	254
-7.70	171	-19.65	319
-7.72	145	-19.68	328
-7.74	111	-19.70	250
-7.76	145	-19.73	181
-7.78	77	-19.75	464
-7.80	75	-19.78	301
-7.90	164	-19.80	470
-8.65	321.5	-19.83	396
-8.85	311	-19.85	316
-10.20	161	-19.88	299
-10.90	350	-19.90	257
-11.45	434	-19.93	294
-11.61	371	-19.95	311
-11.65	373	-19.98	322
		-20.00	310

Table 25 The measured MS signal in borehole core GA-2. Πίνακας 26. Η τιμές μαγνητικής επιδεκτικότητας στην γεώτρηση GA-2

Core depth	**Mean value**	***Core depth***	**Mean value**
-5.00	27	-9.06	14
-5.04	38	-9.08	29
-5.08	14	-9.10	56
-5.11	14	-9.12	29
-5.15	11	-9.13	68
-5.19	40	-9.15	18
-5.23	17	-9.17	13
-5.26	29	-9.19	33

-5.30	30	-9.20	6
-5.34	97	-9.22	7
-5.38	27	-9.24	8
-5.41	19	-9.26	8
-5.45	13	-9.27	4
-6.20	10	-11.30	25
-6.23	5	-12.30	2
-6.27	9	-12.33	3
-6.30	3	-12.35	3
-6.33	5	-12.38	3
-6.37	3	-12.40	4
-6.40	4	-12.43	4
-7.30	5.5	-12.46	4
-7.40	7	-12.48	4
-7.47	6	-12.51	4
-7.53	5	-12.53	4
-7.60	4	-12.56	4
-8.30	7	-12.58	2
-8.80	6	-12.61	1
-8.82	6	-12.64	2
-8.84	16	-12.66	2
-8.85	15	-12.69	9
-8.87	13	-12.71	3
-8.89	10	-12.74	4
-8.91	12	-12.77	5
-8.92	11	-12.79	4
-8.94	7	-12.82	1
-8.96	12	-12.84	1
-8.98	14	-12.87	2
-8.99	13	-12.90	4
-9.01	21	-12.92	2
-9.03	12	-12.95	2
-9.05	9	-12.97	1
		-13.90	8

Table 26 *The measured MS signal in borehole core GA-3. Πίνακας 27. Η τιμές μαγνητικής επιδεκτικότητας στην γεώτρηση GA-3*

Core depth	Mean value
-6.75	204.5
-9.3	253.5
-9.5	220
-10.45	165.5
-11.65	75.5
-12.6	218
-13.4	184.5
-15.1	262

Table 27 *The measured MS signal in borehole core GA-4. Πίνακας 28 Η τιμές μαγνητικής επιδεκτικότητας στην γεώτρηση GA-4*

Core depth	Mean value	*Core depth*	Mean value	*Core depth*	Mean value
-11.60	168.5	-26.72	4	-37.95	8
-12.30	109.5	-26.74	5	-37.98	9
-15.30	127.5	-26.77	6	-38.01	9
-15.45	101	-26.79	3	-38.04	8
-15.48	93	-26.82	3	-38.07	6
-15.50	62	-26.84	2	-38.10	9
-15.53	56	-26.87	8	-38.13	8
-15.55	82	-26.89	5	-38.15	8
-15.58	105	-26.91	5	-38.18	8
-15.60	147	-26.94	5	-38.21	12
-15.63	71	-26.96	5	-38.24	5
-15.65	102	-26.99	4	-38.27	67
-15.68	96	-27.01	4	-38.30	50
-15.70	73	-27.03	3	-38.30	70
-15.73	99	-27.06	3	-38.33	66
-15.75	94	-27.08	4	-38.36	65
-15.78	102	-27.11	3	-38.39	62
-15.80	73	-27.13	4	-38.42	46
-15.83	84	-27.15	4	-38.45	19
-15.85	98	-27.18	5	-38.48	126
-17.50	50	-27.20	4	-38.51	154
-17.56	57	-27.23	3	-38.54	247
-17.61	12	-27.25	3	-38.57	215
-17.67	17	-27.27	3	-38.60	210

-17.72	13	-27.30	2	-38.62	240
-17.78	38	-29.45	7	-38.65	442
-17.83	110	-29.48	9	-38.68	327
-17.89	34	-29.51	9	-38.71	284
-17.94	77	-29.53	9	-38.74	361
-18.00	140	-29.56	9	-38.77	386
-18.08	61	-29.59	9	-38.80	430
-18.50	114	-29.62	8	-38.95	173
-18.53	125	-29.65	8	-39.00	4
-18.55	98	-29.68	9	-39.03	3
-18.58	136	-29.70	7	-39.06	2
-18.60	67	-29.73	7	-39.09	3
-18.63	164	-29.76	8	-39.12	5
-18.65	144	-29.79	8	-39.15	4
-18.68	62	-29.82	9	-39.17	4
-18.70	116	-29.84	9	-39.20	5
-18.73	135	-29.87	8	-39.23	3
-18.75	116	-29.90	10	-39.26	6
-18.78	62	-29.93	9	-39.29	5
-18.80	50	-29.96	22	-39.32	6
-19.20	109	-29.99	23	-39.35	6
-19.23	115	-30.01	21	-39.38	6
-19.27	100	-30.04	26	-39.41	7
-19.30	88	-30.07	32	-39.44	6
-20.70	109	-30.10	62	-39.46	8
-20.73	121	-30.95	69.5	-39.49	8
-20.76	127	-31.80	91	-39.52	9
-20.78	98	-31.82	119	-39.55	8
-20.81	110	-31.84	208	-39.58	8
-20.84	89	-31.85	108	-39.61	6
-20.87	162	-31.87	109	-39.64	8
-20.90	123	-31.89	133	-39.67	8
-20.92	90	-31.91	162	-39.70	8
-20.95	103	-31.92	156	-39.73	6
-20.98	101	-31.94	134	-39.75	9
-21.01	94	-31.96	246	-39.78	7
-22.35	191	-31.98	179	-39.81	8
-23.00	310	-31.99	148	-39.84	5
-23.03	192	-32.01	312	-39.87	5
-23.06	95	-32.03	146	-39.90	5
-23.08	68	-32.05	250	-41.50	3

-23.11	43	-32.06	162	-41.53	1
-23.14	92	-32.08	182	-41.56	2
-23.17	60	-32.10	154	-41.59	4
-23.19	37	-32.90	259	-41.61	6
-23.22	32	-32.93	185	-41.64	6
-23.25	33	-32.96	216	-41.67	5
-23.28	24	-32.99	341	-41.70	4
-23.30	55	-33.02	307	-41.73	4
-23.33	136	-33.05	263	-41.76	5
-23.36	104	-33.07	190	-41.79	4
-23.39	57	-33.10	316	-41.81	5
-23.42	163	-33.13	235	-41.84	4
-23.44	167	-33.16	343	-41.87	3
-23.47	107	-33.19	178	-41.90	3
-23.50	242	-33.22	232	-41.93	5
-23.53	107	-33.25	268	-41.96	5
-23.55	124	-33.28	153	-41.98	3
-23.58	120	-33.31	109	-42.01	4
-23.61	100	-33.34	22	-42.04	4
-23.64	61	-33.36	26	-42.07	5
-23.66	57	-33.39	28	-42.10	6
-23.69	37	-33.42	37	-42.13	3
-23.72	33	-33.45	34	-42.16	3
-23.75	38	-33.48	34	-42.18	4
-23.78	52	-33.51	34	-42.21	3
-23.80	104	-33.54	30	-42.24	4
-23.83	205	-33.57	31	-42.27	3
-23.86	119	-33.60	35	-42.30	2
-23.89	145	-33.63	40	-43.40	7
-24.80	170	-33.65	35	-43.43	8
-24.82	210	-33.68	36	-43.46	7
-24.84	251	-33.71	20	-43.49	8
-24.86	195	-33.74	25	-43.52	10
-24.88	160	-33.77	28	-43.55	12
-24.90	200	-33.80	16	-43.58	12
-24.92	184	-34.20	261	-43.61	13
-24.94	181	-34.24	50	-43.64	11
-24.96	174	-34.27	41	-43.67	10
-24.98	173	-34.31	38	-43.70	10
-25.00	183	-34.34	40	-43.73	11
-25.02	162	-34.38	37	-43.76	10

-25.04	210	-34.42	36	-43.79	12
-25.06	229	-34.45	42	-43.82	27
-25.08	182	-34.49	44	-43.85	14
-25.10	240	-34.52	42	-43.88	9
-25.12	187	-34.56	36	-43.92	10
-25.14	117	-34.60	46	-43.95	17
-25.16	76	-34.63	36	-43.98	11
-25.18	23	-34.67	42	-44.01	13
-25.20	28	-34.70	39	-44.04	9
-25.22	27	-35.70	11.5	-44.07	13
-25.24	26	-37.40	5	-44.10	8
-25.26	27	-37.43	3	-44.13	7
-25.28	27	-37.46	5	-44.16	7
-25.31	21	-37.49	6	-44.19	10
-25.33	20	-37.52	9	-44.22	9
-25.35	27	-37.55	6	-44.25	8
-25.37	38	-37.57	5	-45.00	3
-25.39	41	-37.60	6	-45.05	2
-25.41	39	-37.63	4	-45.09	1
-25.43	32	-37.66	7	-45.14	1
-25.45	10	-37.69	8	-45.18	2
-25.47	3	-37.72	9	-45.23	3
-25.49	3	-37.75	8	-45.27	5
-25.75	47.5	-37.78	7	-45.32	4
-26.60	11	-37.81	8	-45.36	6
-26.62	4	-37.84	9	-45.41	4
-26.65	3	-37.86	10	-45.46	3
-26.67	1	-37.89	11	-45.50	3
-26.70	4	-37.92	8		

Table 28 *The measured MS signal in borehole core GA-5. Πίνακας 29. Η τιμές μαγνητικής επιδεκτικότητας στην γεώτρηση GA-5*

Core depth	Mean value	Core depth	Mean value	Core depth	Mean value
-2.80	71.5	-10.63	242	-17.92	6
-2.93	85	-10.67	178	-17.95	6
-2.96	81	-10.71	161	-17.97	6
-2.99	55	-10.76	70	-18.00	6

-3.02	19	-10.84	127	-18.03	4
-3.05	39	-10.88	76	-18.06	5
-3.09	24	-10.93	63	-18.09	6
-3.12	38	-10.97	76	-18.12	6
-3.15	38	-11.01	62	-18.15	6
-3.18	59	-11.06	68	-18.18	6
-3.21	76	-11.10	93	-18.21	7
-3.24	106	-11.70	38	-18.24	8
-3.27	98	-11.74	25	-18.26	6
-3.30	107	-11.77	29	-18.29	7
-3.33	120	-11.81	31	-18.32	6
-3.36	178	-11.84	29	-18.35	7
-3.40	177	-11.88	25	-18.38	6
-3.43	208	-11.92	31	-18.41	8
-3.46	181	-11.95	27	-18.44	10
-3.49	133	-11.99	42	-18.47	21
-5.55	204.5	-12.02	38	-18.50	19
-5.57	170	-12.06	38	-18.53	10
-5.61	251	-12.10	29	-18.55	8
-5.65	151	-12.13	39	-18.58	7
-5.69	172	-12.17	32	-18.61	9
-5.73	179	-12.20	44	-18.64	10
-5.77	155	-12.24	139	-18.67	11
-5.81	123	-12.28	125	-18.70	12
-5.85	170	-12.31	138	-19.35	8
-5.89	185	-12.35	182	-20.75	15
-5.93	205	-12.38	158	-20.95	200
-5.97	174	-12.42	424	-22.55	91
-6.90	46	-12.46	210	-23.20	250
-6.94	48	-12.49	147	-25.30	322.5
-6.98	29	-12.53	142	-25.80	20
-7.02	22	-12.56	159	-25.83	20
-7.06	24	-12.60	299	-25.86	21
-7.10	13	-13.45	100	-25.90	23
-8.65	50	-14.30	10	-25.93	19
-8.68	44	-14.70	15	-25.96	22
-8.70	53	-14.74	12	-25.99	23
-8.73	60	-14.77	21	-26.02	25
-8.75	57	-14.81	22	-26.06	24
-8.78	52	-14.85	17	-26.09	25
-8.80	65	-14.89	14	-26.12	31

-8.83	59	-14.92	16	-26.15	32
-8.85	78	-14.96	16	-26.19	37
-8.88	45	-15.00	15	-26.22	45
-8.90	32	-15.03	14	-26.25	53
-8.93	23	-15.07	18	-26.90	45.5
-8.95	44	-15.11	16	-27.70	10
-8.98	58	-16.25	10	-27.73	11
-9.00	35	-16.43	8	-27.76	12
-9.03	26	-16.46	7	-27.79	15
-9.05	21	-16.49	7	-27.82	18
-9.08	30	-16.52	6	-27.85	18
-9.10	21	-16.56	7	-27.88	18
-9.13	23	-16.59	7	-27.91	20
-9.15	27	-16.62	5	-27.94	17
-9.18	24	-16.65	6	-27.96	8
-9.20	21	-16.68	6	-27.99	10
-9.23	21	-16.71	4	-28.02	8
-9.25	25	-16.75	5	-28.05	9
-9.28	25	-16.78	6	-28.08	7
-9.30	34	-16.81	5	-28.11	8
-10.20	83	-16.84	5	-28.14	4
-10.24	91	-16.87	4	-28.17	4
-10.29	46	-16.90	3	-28.20	3
-10.33	93	-16.94	4	-28.60	9
-10.37	96	-16.97	5	-28.68	10
-10.41	87	-17.00	7	-28.75	12
-10.46	164	-17.80	8	-28.83	8
-10.50	109	-17.83	8	-28.90	9
-10.54	108	-17.86	10	-29.75	429.5
-10.59	236	-17.89	11		

Appendix E (Extended abstract- in Greek). Εκτεταμένη περίληψη στα ελληνικά

I. Εισαγωγή

Η μορφολογία των παράκτιων περιοχών διαμορφώνεται κατά κύριο λόγο από την αλληλεπίδραση τριών παραγόντων. Την τεκτονική ανύψωση ή ταπείνωση τους, τις διαδικασίες της ιζηματογένεσης, και τις ευστατικές μεταβολές της στάθμης της θάλασσας, ενώ άλλοι παράγοντες (πχ. θαλάσσια ρεύματα) διαδραματίζουν δευτερεύοντα ρόλο (πχ. Emery & Myers, 1994; Nichols, 1999, εικ. 1-1). Η περιοχή του Ισθμού στην Κόρινθο, που είναι και η περιοχή μελέτης της παρούσας διδακτορικής διατριβής, αποτελεί ένα παράδειγμα που μπορούν να μελετηθούν και οι τρεις αυτοί παράγοντες. Η περιοχή ανυψώνεται τουλάχιστον κατά τα τελευταία 200 χιλιάδες χρόνια (πχ. Collier et al., 1992), με τις μεταβολές της στάθμης της θάλασσας να επηρεάζουν τις διαδικασίες της ιζηματογένεσης (πχ. Collier, 1990), ενώ το υδρογραφικό δίκτυο μεταφέρει χονδρόκκοκα υλικά προς την παράκτια περιοχή (πχ. Gawthorpe et al., 1994)

Η επιστημονική κοινότητα έχει αναπτύξει πληθώρα μεθοδολογιών για την πληρέστερη ανάλυση αυτών των διαδικασιών όπως την μελέτη βενθονικών και πλαγκτονικών τρηματοφόρων (πχ. Scott and Medioli, 1980; Triantaphyllou et al., 2003, 2010; Murray, 2007; Pavlopoulos et al., 2007; Koukousioura et al., 2012; Avnaim – Katav et al., 2012, 2013, 2015), την μαγνητική επιδεκτικότητα των ιζημάτων (e.g., Mullins 1977, Oldfield; 1991, Da Silva et al., 2009; Reicherter et al., 2010) κα.

Για την πληρέστερη μελέτη του παλαιοπεριβάλλοντος απαιτείται και το χρονικό πλαίσιο κατά το οποίο έγινε η ιζηματογένεση. Για το σκοπό αυτό έχουν αναπτυχτεί πολλές διαφορετικές μεθοδολογίες όπως χρονολόγηση κοραλλιών (πχ. Collier et al., 1992; Vita-Finzi, 1993; Dia et al., 1997; Kershaw et al., 2005; Roberts et al., 2009), υπολογισμός της φωταύγειας (πχ. Pope et al., 2008; Pawley et al., 2010; Reimann et al., 2011;

Ozturk et al., 2016), η μελέτη της βιοστρωματογραφίας βασισμένη σε νανοαπολιθώματα (πχ. Triantaphyllou et al., 2009; Dimiza et al., 2011; Triantaphyllou, 2014).

Η παρούσα εργασία έχει σαν στόχο την ανάλυση τόσο του παλαιοπεριβάλλοντος όσο και την μελέτη των τεκτονικών κινήσεων στην περιοχή του Ισθμού. Για τον σκοπό αυτό αναλύθηκαν ως προς το παλαιοπεριβάλλον, το περιεχόμενο σε νανοαπολιθώματα και την μαγνητική επιδεκτικότητα, 11 γεωτρήσεις συνολικού μήκους 373 μέτρων από το ανατολικό τμήμα του Ισθμού, στο ανερχόμενο και κατερχόμενο τέμαχος του ρήγματος Καλαμακίου-Ισθμίων. Σε συνδυασμό με την γεωλογική χαρτογράφηση και την ανάλυση δειγμάτων από την επιφάνεια, πραγματοποιήθηκε η μελέτη της παλαιογεωγραφίας της περιοχής, καθως και ο προσδιορισμός τόσο των τεκτονικών κινήσεων των σημαντικότερων δομών της περιοχής, όσο και του ρήγματος του Καλαμακίου-Ισθμίων.

II. Περιοχή μελέτης

Η περιοχή μελέτης της παρούσας διατριβής είναι το ανατολικό τμήμα του Κορινθιακού κόλπου και πιο συγκεκριμένα η περιοχή του Ισθμού. Το δυτικό τμήμα του Κορινθιακού κόλπου επεκτείνεται με ρυθμό περίπου 15-20 mm/yr, ενώ το ανατολικότερο τμήμα που είναι και η περιοχή ενδιαφέροντος περίπου 6-7 mm/yr (πχ. Clark et al., 1997; Avallone et al., 2004; Nystand Thatcher, 2004; McNeill and Collier, 2004; Chousianitis et al., 2013).

Η περιοχή δομείται από το αλπικό υπόβαθρο (ασβεστόλιθοι και δολομίτες ηλικίας από Τριαδικό έως άνω Ηώκαινο και Οφιολίθους), και μεταλπικά ιζήματα (κυρίως λιμναίες-θαλάσσιες μάργες και άμμοι) και αλλουβιακά ριπίδια (πχ. Hemelsdael & Ford, 2015; Ford et al., 2012; Jolivet et al., 2003, 2010; Papanikolaou & Royden, 2007; Taylor et al., 2011. Σήμερα τα ενεργά ρήγματα που ελέγχουν την μορφολογία του κόλπου έχουν διεύθυνση περίπου Α-Δ,, σχηματίζοντας μια ενεργή τεκτονική τάφρο (πχ. Myrianthis 1982; Brooks and Ferentinos, 1984; Keraudren and Sorel, 1987; Ori, 1989; Sorel, 2000; Stefatos et al., 2002; Moretti et al., 2003). Στο ανατολικό τμήμα του κόλπου τα κύρια

ενεργά ρήγματα είναι των Κεχριών (~0.2 mm/yr), του Αγίου Βασίλειου (~0.15 mm/yr) του Λουτρακίου (~0.5 mm/yr), η ρηξιγενής ζώνη των Αλκυονίδων (Σχοίνος, Πίσια καθως και τα υποθαλάσσια τμήματα τους) (~2 mm/yr) (εικ. 3-1) (πχ. Papanikolaou et al., 1988, Papanikolaou et al., 1989; Papanastassiou and Gaki-Papanastassiou, 1994; Armijo et al., 1996; Roberts, 1996; Koukouvelas et al., 2017; Deligiannakis et al., in press).

Η περιοχή ανυψώνεται (πχ. Ori, 1989; Gobo et al., 2013), με ρυθμό ~ 1.5 mm/yr στο κεντρικό τμήμα του κόλπου και ~ 0.3 mm/yr στο ανατολικό (πχ. Keraudren & Sorel, 1987; Collier, 1990; Collier et al., 1992; Keraudren et al., 1995; Pirazzoli et al., 2004; Westaway, 1996, 2002; Armijo et al., 1996; McMurray & Gawthorpe, 2000; Leeder et al., 2008).

Άξιο αναφοράς είναι η παρουσία της Διώρυγας του Ισθμού, καθως αποτελεί μια εξαιρετική ευκαιρία για την λεπτομερή παρατήρηση τόσο των στρωμάτων όσο και των τεκτονικών δομών του Ισθμού (π.χ. Freyberg, 1973; Collier, 1990; Collier & Dart, 1991; Collier & Thomson, 1991; Gawthorpe et al., 1994).

III. Μεθοδολογία

Για την παρούσα διατριβή χρησιμοποιήθηκαν δεδομένα από 11 γεωτρήσεις όλες στο ανατολικότερο άκρο του Ισθμού (συνολικό μήκος ~ 373 μ). Αναλύθηκαν ως προς το περιεχόμενο τους σε τρηματοφόρα (συνολικά 256 δείγματα), νανοαπολιθώματα συνολικά 63 δείγματα) και την μαγνητική επιδεκτικότητα των ιζημάτων (συνολικά 986 μετρήσεις). Έγινε ο προσδιορισμός της ηλικίας κοραλλιών που βρέθηκαν μέσα στην γεώτρηση Bh-7, ενώ έξι δείγματα από τρεις γεωτρήσεις (Bh-1, 5.25 m, 6.05 m, Bh-3, 20.5 m, 21.25 m, Bh-7, 20.65 m, 33.45 m) αναλύθηκαν ως προς την φωταύγεια των ιζημάτων. Χαρτογραφήθηκε επίσης η γεωλογία του Ισθμού και αναλύθηκαν 99 δείγματα από επιφανειακά στρωματά ως προς το μικρο- και ναννο περιεχόμενο τους. Μετά την στατιστική επεξεργασία των δεδομένων, έγινε ο προσδιορισμός του

παλαιοπεριβάλλοντος, της παλαιοβαθυμετρίας, και τις παλαιοοικολογίας των στρωμάτων.

IV. Δεδομένα από τις γεωτρήσεις

Συνολικά από τις 11 γεωτρήσεις που πραγματοποιήθηκαν 8 εξετάστηκαν λεπτομερώς, ενώ για τις τρεις (Bh-2, Bh-4, Bh-6) μόνο η λιθολογική περιγραφή ήταν εφικτή. Οι γεωτρήσεις Bh-3 και Bh-6 ήταν στο ανερχόμενο τέμαχος, ενώ οι υπόλοιπες στο κατερχόμενο τέμαχος του ρήγματος Καλαμακίου-Ισθμίων. Κατά κύριο λόγο μέσα στις γεωτρήσεις περιγράφηκαν εναλλαγές από χονδρόκκοκα (ποταμοχειμάρεια) με λεπτόκοκκα (θαλάσσια) ιζήματα (εικ. 5-1, 5-2).

Μέσω της λεπτομερούς παλαιοντολογικής ανάλυσης περιγράφηκαν 26 διαφορετικά είδη τρηματοφόρων (εικ. 5-3) και τρία είδη νανοαπολιθωμάτων (εικ. 5-4) small *Reticulofenestra* spp., small *Gephyrocapsa* spp., *Emiliania huxleyi*. Η μαγνητική επιδεκτικότητα των δειγμάτων μέσα στις γεωτρήσεις κυμαίνεται από ~1 σε ~600 $\times 10^{-5}$ (SI units). Στις εικόνες 5-5 έως 5-21 και στους πίνακες 3 έως 13 παρατίθενται η λεπτομερής περιγραφή της δειγματοληψίας, της λιθολογίας και τα αποτελέσματα της ανάλυσης των τρηματοφόρων, των νανοαπολιθωμάτων και της μαγνητικής επιδεκτικότητας μέσα στις γεωτρήσεις.

V. Χαρτογράφηση της περιοχής

Για τις ανάγκες της διατριβής χαρτογραφήθηκε η γεωλογία της περιοχής του Ισθμού όπου ελήφθησαν 149 δείγματα για περαιτέρω ανάλυση. Κατά κύριο λόγο περιγράφηκαν όμοιοι λιθολογικοί σχηματισμοί που είχαν περιγραφεί και στις γεωτρήσεις, δηλαδή εναλλαγές από λεπτόκοκκα και χονδρόκοκκα ιζήματα (θαλάσσιο / χερσαίο περιβάλλον).

Περιγράφηκαν επίσης ανδεσίτες και εκτεταμένες εμφανίσεις μάργας στο κέντρο του ρήγματος του Καλαμακίου-Ισθμίων (πχ. Collier & Dart, 1992), αποκαλυμμένες τόσο από τις διαδικασίες διάβρωσης όσο και από την δράση του ρήγματος (εικ. 6-1). Η ανάλυση των τεκτονικών στοιχείων που περιγράφηκαν δείχνει μια δομή ΒΒΑ-ΝΝΔ και κλίση προς ΝΝΑ ~ 55^o – 70^o (εικ. 6-4). Η ανάλυση των δειγμάτων τόσο ως προς την μίκρο- αλλά και την νάννο πανίδα έδειξε εναλλαγές μεταξύ χερσαίων και θαλάσσιων περιβαλλόντων (εικ. 6-8).

VI. Στατιστική ανάλυση

Σημαντικό τμήμα της παρούσας εργασίας αποτελεί η στατιστική ανάλυση των αποτελεσμάτων τόσο των τρηματοφόρων όσο και των τιμών της μαγνητικής επιδεκτικότητας. Μέσω της δι-παραμετρικής (two way cluster analysis, εικ. 7-1, 7-2) και της μη παραμετρικής (MDS, εικ. 7-3) ανάλυσης των μετρημένων τρηματοφόρων στις γεωτρήσεις και στα επιφανειακά δείγματα, έγινε ο προσδιορισμός τριών ομάδων. Η πρώτη ομάδα εκφράζει λιμνοθαλάσσια περιβάλλοντα με εκτιμώμενο παλαιοβάθος λιγότερο από 20 μέτρα, η δεύτερη ρηχά θαλάσσια περιβάλλοντα με εκτιμώμενο παλαιοβάθος έως τα 40 μέτρα και η τρίτη ενδιάμεσες θαλάσσιες συνθήκες μεταξύ των δυο με εκτιμώμενο παλαιοβάθος μεταξύ 20 και 40 μέτρων (π.χ. Pallikarakis et al., Cor. Proof.).

Μέσω στατιστικής ανάλυσης επίσης, έγινε ο συσχετισμός μεταξύ των λιθολογιών και παλαιοπεριβαλλόντων μέσα στις γεωτρήσεις, με τις τιμές της μαγνητικής επιδεκτικότητας (πινάκες 14, 15). Έτσι συσχετιστήκαν με μεγαλύτερη ακρίβεια και εγκυρότητα οι υψηλότερες τιμές μαγνητικής επιδεκτικότητας με τα χερσαία και οι χαμηλότερες τιμές με τα θαλάσσια περιβάλλοντα (εικ. 7-4).

VII. Προσδιορισμός του παλαιοπεριβάλλοντος

Με βάση την στατιστική ανάλυση του προηγούμενου κεφαλαίου έγινε η περιγραφή του παλαιοπεριβάλλοντος στα δείγματα. Με την βοήθεια δεικτών που χρησιμοποιήθηκαν (πυκνότητα δείγματος (FD), ποσοστό σπασμένων τρηματοφόρων επί του συνόλου του δείγματος (BR), ποικιλομορφία του δείγματος (A-Fisher) και ο λόγος μικρής/μεγάλης *Ammonia* spp. (A-ratio), καθως και την εκτίμηση του παλαιοβάθους, έγινε ο προσδιορισμός των εναλλαγών του παλαιοπεριβάλλοντος από χερσαία σε θαλάσσια περιβάλλοντα τόσο στις γεωτρήσεις όσο και στα επιφανειακά δείγματα (π.χ. Pallikarakis et al., Cor. Proof.). Οι περισσότερες εναλλαγές παρατηρήθηκαν στην γεώτρηση Bh-3 (5), ενώ οι λιγότερες στην GA-2, που απλά από ένα σχετικά βαθύτερο περιβάλλον στο κατώτερο τμήμα της γεώτρησης, κατέληξε σταδιακά σε λιμνοθαλάσσιο περιβάλλον στο ανώτερο τμήμα της (εικ.8-1, 8-7).

VIII. Προσδιορισμός της ηλικίας των ιζημάτων

Απαραίτητη προϋπόθεση για την ολοκληρωμένη μελέτη των δειγμάτων είναι ο χρονικός προσδιορισμός της ιζηματογένεσης. Για τον λόγο αυτό χρησιμοποιήθηκαν τρεις ανεξάρτητες διαδικασίες για τον προσδιορισμό της ηλικίας. Οι δυο αφορούσαν την απόλυτη και η μια την σχετική χρονολόγηση των ιζημάτων.

Αρχικά μετρήθηκε η φωταύγεια σε έξι δείγματα, δυο σε κάθε μια από τις γεωτρήσεις Bh-1, Bh-3 και Bh-7, στις εγκαταστάσεις του εργαστηρίου Αρχαιομετρίας «Ε.Κ.Ε.Φ.Ε. Δημόκριτος». Αφού ακολουθηθήκαν οι τυπικές διαδικασίες (πχ. Thiel et al., 2011; Tsakalos et al., 2016), υπολογίστηκε η εκλυόμενη ακτινοβολία τόσο σε κόκκους αστρίου, όσο και χαλαζία. Τα αποτελέσματα όμως δεν ήταν τα αναμενόμενα καθώς στους κόκκους χαλαζία παρουσιάστηκε το φαινόμενο του κορεσμού, ενώ στους αστρίους το φαινόμενο του ασθενούς σήματος (εικ. 9-1, 9-2).

Στην συνεχεία στάλθηκαν κοράλλια που βρέθηκαν στην γεώτρηση Bh-7 (δείγμα Bh-7, 18.25 m) στο ινστιτούτο Max Planck στο Mainz (Γερμανία) για χρονολόγηση με ^{230}Th/U (πίνακας 17). Οι εκτιμώμενες ηλικίες όπως φαίνονται στον πίνακα 17 έχουν εύρος από 241 μέχρι 358 χιλιάδες χρόνια με αποκλίσεις έως και τα ± 80 χιλιάδες χρόνια (εικ. 9-3). Το μεγάλο εύρος τιμών καθώς και η σχετικά μεγαλύτερη ηλικία από την αναμενόμενη (Pallikarakis et al., Cor. Proof.) μπορεί να εξηγηθεί με την διαγέννεση, διαδικασία η οποία αλλάζει την αρχική χημική σύσταση των κοραλλιών.

Για τον λόγο αυτό αναλύθηκαν συνολικά 63 δείγματα ως προς το περιεχόμενο τους σε νανοαπολιθώματα. Η παρουσία κοκκόλιθων από small *Reticulofenestra* spp. (~45%), small *Gephyrocapsa* spp (~33%) και σε κάποια δείγματα από *E. huxleyi* specimens (5-8%) βοήθησε στην βιοστρωματογραφία των ιζημάτων. Έτσι, με την συμβολή της καμπύλης μεταβολής της στάθμης της θάλασσας, έγινε ο διαχωρισμός των δειγμάτων σε δυο κατηγορίες, νεώτερα από 240 χιλιάδες χρόνια και από 240 έως ~ 450 χιλιάδες χρόνια. Η εκτιμώμενες ηλικίες των κοραλλιών παρά το εύρος τους δείχνουν μια ηλικία από ~ 175 χιλιάδων χρόνων και άνω, αποκλείοντας έτσι το ενδεχόμενο να προέρχονται από το μεσοπαγετώδη διάστημα των 125 χιλιάδων χρόνων (MIS 5e). Το γεγονός αυτό συμφωνεί με τα στρωματογραφικά δεδομένα από τις γεωτρήσεις που αναλύθηκαν, τα επιφανειακά στρώματα που χαρτογραφήθηκαν, καθώς και με την βιβλιογραφία.

IX. Σαρωνικός Κόλπος

Για την εξαγωγή πιο αξιόπιστων και έγκυρων συμπερασμάτων έγινε η σύγκριση του παλαιοπεριβάλλοντος μεταξύ των αποτελεσμάτων των δειγμάτων του Ισθμού και δεδομένων γεωτρήσεων από την περιοχή του Πειραιά (εικ. 10-1) (Goiran et al., 2011, Triantaphyllou et al., 2016), συγκρίνοντας τα τρηματοφόρα και το εκτιμώμενο παλαιοπεριβάλλον από δυο διαδοχικές μεσοπαγετώδεις περιόδους. Τρεις γεωτρήσεις (P-2, P-4, P-5) όλες στο δελταικό πεδίο του Κηφισού αναλύθηκαν ως προς την μικροπανίδα, ενώ η P-4 αναλύθηκε και ως προς το περιεχόμενο τους σε κόκκους γύρης και την μαγνητική επιδεκτικότητα των ιζημάτων (εικ. 10-3, 10-5, πίνακες 18-20).

Οι γεωτρήσεις αυτές πραγματοποιήθηκαν σε διαφορετικό περιβάλλον ιζηματογένεσης, με την μεταβολή της στάθμης της θάλασσας να διαδραματίζει μικρότερο ρόλο, με σαφώς πιο έντονη την επίδραση του υδρογραφικού δικτύου ενώ έγιναν σε μια περιοχή τεκτονικά σχετικά σταθερή. Σημαντική παράμετρος είναι επίσης και το γεγονός πως η ιζηματογένεση έλαβε χώρα κατά το Ολόκαινο, σε αντίθεση με τα δείγματα του Ισθμού που έγινε κατά το Πλειστόκαινο.

Και σε αυτές τις γεωτρήσεις περιγράφηκαν διαφορετικά περιβάλλοντα απόθεσης, από ρηχά θαλάσσια έως χερσαία χωρίς όμως να παρατηρηθούν οι έντονες εναλλαγές που περιγράφηκαν στις γεωτρήσεις από τον Ισθμό. Τα δεδομένα αυτά υποστηρίχθηκαν τόσο από παλυνολογικά δεδομένα όσο και από τις τιμές της μαγνητικής επιδεκτικότητας για την γεώτρηση P-4.

Σε σχέση με τα δεδομένα από τις γεωτρήσεις του Ισθμού, επιβεβαιώθηκε η συσχέτιση ειδών όπως *Ammonia tepida* σε λιμνοθαλάσσια περιβάλλοντα και η ύπαρξη θαλάσσιων ειδών όπως τα miliolids και *Rossalina* spp. σε βαθύτερα θαλάσσια περιβάλλοντα. Και στις δυο περιπτώσεις η πυκνότητα του δείγματος σε συνδυασμό με τις τιμές μαγνητικής επιδεκτικότητας χρησιμοποιήθηκε για τον καθορισμό χερσαίων περιβαλλόντων.

Χ. Συσχέτιση και τρισδιάστατη απεικόνιση των ιζημάτων

Μέσω της μικροπαλαιοντολογικής ανάλυσης των γεωτρήσεων στην περιοχή του Ισθμού περιγράφηκαν εναλλαγές από χερσαία/θαλάσσια ιζήματα. Συσχετίζοντας τα δεδομένα αυτά με την καμπύλη μεταβολής της στάθμης της θάλασσας προκύπτει πως μέσα στις γεωτρήσεις υπάρχουν εναλλαγές από παγετώδη/μεσοπαγετώδη διαστήματα. Η συνεχόμενη μεταβολή της θαλάσσιας στάθμης σε συνδυασμό με την τεκτονική ανύψωση της περιοχής έχει καθορίσει την στρωματογραφία, με διαδοχικές αλληλουχίες επίκλησης και απόσυρσης (πχ. Emery and Myers, 1994; Nichols, 1999; Nagendra et al., 2011).

Στην συνέχεια έγινε η συσχέτιση των γεωτρήσεων, καθως και των επιφανειακών στρωμάτων που διακρίνονται στην Διώρυγα του Ισθμού (εικ. 11-1, 11-3). Μέσω αυτής της συσχέτισης δημιουργήθηκε το τρισδιάστατο μοντέλο απεικόνισης των στρωμάτων για το ανατολικότερο τμήμα του Ισθμού.

XI. Ανάλυση των αποτελεσμάτων

XI. α) Ηλικία των στρωμάτων

Συσχετίζοντας τον ρυθμό ανύψωσης της περιοχής (0,3 mm/yr Collier et al., 1992) και την καμπύλη της μεταβολής της στάθμης της θάλασσας από Siddall et al. (2003), προκύπτει πως η ιζηματογένεση ήταν πιθανή μόνο κατά συγκεκριμένα διαστήματα (MIS 5e, ~125, MIS 6e, ~175, MIS 7 ~(190-240) και MIS 9 ~310 χιλιάδες χρόνια). Η παρουσία της *E. huxleyi* τόσο στα επιφανειακά δείγματα όσο και στο σύνολο των δειγμάτων των γεωτρήσεων περιορίζει σημαντικά τα πιθανά σενάρια σε νεώτερα από 240 χιλιάδες χρόνια, ενώ λόγω των ηλικιών των κοραλλιών δεν δύναται να είναι από το διάστημα MIS 5e στα 125 χιλιάδες χρόνια (εικ. 12-1).

Στα επιφανειακά δείγματα που παρατηρήθηκαν μόνο small *Gephyrocapsa* spp. και *Reticulofenestra* spp. χωρίς κοκκόλιθους από *E. Huxleyi,* Large *Gephyrocapsa* (>4 μm) και *Pseudoemiliania lacunose* η εκτιμώμενη ηλικία τους κυμαίνεται από 240 έως 430 χιλιάδες χρόνια (Backman et al., 2012).

XI. β) Τεκτονική δραστηριότητα

Ο ρυθμός ανύψωσης της περιοχής του Ισθμού 0.3 mm/yr τα τελευταία 205 χιλιάδες χρόνια έχει υπολογιστεί με απόλυτη χρονολόγηση U/Th από τους Collier et al. (1992), Dia et al. (1997) and Pierini et al. (2016) με δεδομένα από μακροαπολιθώματα. Μέσω των νανοαπολιθωμάτων όμως μπορεί να εκτιμηθεί εκ νέου ο ρυθμός αυτός με μια εντελώς διαφορετική μεθοδολογία. Συνυπολογίζοντας το παλαιοβάθος όπως εκτιμήθηκε στην γεώτρηση GA-2 και την παρουσία της *E. Huxleyi* προκύπτει μια ηλικία από 125 έως τα 265 χιλιάδες χρόνια. Με βάση το απόλυτο υψόμετρο της γεώτρησης προκύπτει ένας ρυθμός ανύψωσης ~0.34 ± 0.12 mm/yr (εικ. 12-2).

Επιπλέον με βάση την παρουσία της *E. Huxleyi* στα επιφανειακά δείγματα S.23.9/2, S.25.9./3, S.25.9/2 και S.12/7/3, εκτιμάται η ίδια ηλικία και κατά συνέπεια ένας ρυθμός ανύψωσης ~0.27 ± 0.12 mm/yr. Η απουσία της *E. Huxleyi* στα δείγματα 17/7/5 και S.17/7/6 οδηγεί στο συμπέρασμα πως η πιθανή τους ηλικία είναι από 280 έως 410 χιλιάδες χρόνια και κατά συνέπεια ένας ρυθμός ανύψωσης ~0.33 ± 0.12 mm/yr (εικ. 12-2, 12-3). Άξιο αναφοράς είναι πως οι εκτιμώμενοι ρυθμοί είναι πολύ κοντά σε αυτούς που είχαν προτείνει οι προηγούμενοι ερευνητές, επιβεβαιώνοντας τους ρυθμούς ανύψωσης η γνώση των οποίων παίζει καθοριστικό ρόλο στην απεικόνιση του παλαιοπεριβάλλοντος.

Εντονότερη τεκτονική δραστηριότητα στον Ισθμό παρατηρείται στο ανατολικό τμήμα του, όπως φαίνεται τόσο από την τοπογραφία όσο και από τα ρήγματα στην Διώρυγα (πχ. Collier, 1990; Collier et al., 1992; McMurray and Gawthorpe, 1994 και η παρούσα εργασία) (εικ. 12-4). Με βάση τους διαφορετικούς ρυθμούς ανύψωσης όπως έχουν υπολογιστεί από τα νανοαπολιθώματα (τομή C-C', εικ. 12-3), εκτιμάται ένας μέγιστος ρυθμός ολίσθησης για το ρήγμα Καλαμακίου-Ισθμίων ~0.07±0.02 mm/yr.

XI. γ) Τεκτονικές κινήσεις στην τάφρο Λουτρακίου-Κεχριών

Τα βασικά ρήγματα που επηρεάζουν την περιοχή του Ισθμού είναι τα ρήγματα των Κεχριών, της ρηξιγενούς ζώνης των Αλκυονίδων, του Λουτρακίου και του Αγίου Βασίλειου (εικ. 12-5). Το ρήγμα των Κεχριών, μια δομή συνολικού μήκους ~ 24 km, έχει ρυθμό ολίσθησης ~0,15-0,20 mm/yr και ταπεινώνει την περιοχή του Ισθμού (πχ. Koukouvelas et al., 2017; Deligiannakis et al., in press) (εικ. 12-6). Το ρήγμα του Λουτρακίου (εικ. 12-7) έχει περίπου 15 km μήκος, ταπεινώνει την περιοχή του Ισθμού και έχει ρυθμό ολίσθησης περίπου 0.50 mm/yr (Roberts et al., 2011). Το ρήγμα του Αγίου Βασιλείου (εικ. 12-5) έχει μήκος περίπου 38 km, ρυθμό ολίσθησης περίπου 0,20 mm/yr και επίσης ταπεινώνει την περιοχή του Ισθμού. Η περιοχή του Ισθμού ανυψώνεται από την επίδραση τη ζώνης των Αλκυονίδων. Η σεισμική ακολουθία το '81 ανύψωσε την περιοχή κατά 2 εκατοστά περίπου (Mariolakos & Stiros, 1987).

Για την μοντελοποίηση του ρυθμού ανύψωσης και ταπείνωσης από κάθε ένα κανονικό ρήγμα στην περιοχή, χρησιμοποιήθηκε η επίδραση του σεισμού του 2009 στην L'Aquila (Ιταλία) (εικ. 12-8), σεισμός που προκλήθηκε από την δράση επίσης κανονικού ρήγματος (πχ. EMERGEO Working Group, 2009, 2010; Papanikolaou et al., 2010; Goudarzi et al., 2011; Cheloni et al., 2014; Livio et al., 2017). Έτσι με βάση την επίδραση κάθε δομής στην περιοχή υπολογίστηκε η εκτιμώμενη ανύψωση και ταπείνωση της περιοχής του Ισθμού, από τα ρήγματα (εικ. 12-9, με 12-13).

Στην συνέχεια έχοντας σαν βάση τους εκτιμώμενους ρυθμούς ανύψωσης της περιοχής (εικ. 12-14) από τους Collier et al. (1992), Collier and Thomson (1992), Dia et al. (1997), Pierini et al. (2016), υπολογίστηκε η διαφορά με τα αποτέλεσμα του μοντέλου και κατά συνέπεια, πόσο είναι ο ρυθμός της γενικότερης ανύψωσης της περιοχής που απαιτείται ώστε να ισχύουν οι υπολογισμένοι ρυθμοί ανύψωσης με βάση την βιβλιογραφία. Αξιοσημείωτο είναι πως παρατηρείται μια μείωση του ρυθμού αυτού προς τα βόρεια βορειοανατολικά.

Για να γίνει πιο εμφανής η σημασία της γενικότερης ανύψωσης της περιοχής κατασκευάστηκαν οι χάρτες της υποθετικής παλαιογεωγραφίας της περιοχής με βάση

μόνο την επίδραση των ρηγμάτων πριν από 125 και 200 χιλιάδες χρόνια (εικ. 12-15). Χωρίς την επίδραση της γενικότερης ανύψωσης στην περιοχή, ο Ισθμός φαίνεται να ήταν μονίμως αναδυμένος, ενώ σύμφωνα τόσο με την βιβλιογραφία όσο και τα αποτελέσματα της παρούσας εργασίας, η περιοχή του Ισθμού χαρακτηρίζεται από εναλλαγές θαλάσσιων/χερσαίων ιζημάτων.

XI. δ) Παλαιογεωγραφία της περιοχής

Το τελικό προϊόν αυτής της διατριβής είναι η παλαιογεωγραφική εξέλιξη της περιοχής του Ισθμού. Για την παλαιογεωγραφική εξέλιξή του χρησιμοποιήθηκαν η μεταβολή της στάθμης της θάλασσας, ένα υψηλής ανάλυσης μοντέλο του ανάγλυφου, ο ρυθμός ανύψωσης της περιοχής καθως και τα δεδομένα από την παρούσα εργασία και δημιουργήθηκε η παλαιογεωγραφία της περιοχής του Ισθμού τα τελευταία 350 χιλιάδες χρόνια (εικ. 12-17). Έτσι θωρείται πως υπήρχε δίαυλος επικοινωνίας των δυο κόλπων (Κορινθιακός και Σαρωνικός) πριν από ~310 και πριν από 200 χιλιάδες χρόνια (MIS 9 και 7 αντίστοιχα), ενώ από τότε και μετά η συνεχόμενη ανύψωση της περιοχής οδήγησε στον σχηματισμό του Ισθμού. Αξιοσημείωτο είναι πως με βάση την λεπτομερή βυθομετρία του Σαρωνικού και την μεταβολή της στάθμης της θάλασσας είναι πιθανόν σε κάθε παγετώδη περίοδο να σχηματίζεται μια παλαιολίμνη (εικ. 12-6).

XI. ε) Περιορισμοί και δυνατότητες της παρούσας διατριβής

Ένα βασικό αποτέλεσμα της παρούσας διατριβής είναι η σημασία της μεθοδολογίας που ακολουθήθηκε. Βασισμένη σε διαφορετικά επιστημονικά αντικείμενα έγινε δυνατόν να προσδιοριστεί με μεγάλη ακρίβεια και αξιοπιστία η περιγραφή του παλαιοπεριβάλλοντος, καθώς και ο σχετικός προσδιορισμός της ηλικίας των ιζημάτων με την χρήση διαφορετικών μεθοδολογιών. Παρόλο που εκτιμήθηκε η σχετική ηλικία

των ιζημάτων, λόγω της απουσίας της απολυτής χρονολόγησης των ιζημάτων οι εκτιμώμενες ηλικίες έχουν σχετικά μεγάλο εύρος.

Για την καλύτερη περιγραφή της επίδρασης των ρηγμάτων που επηρεάζουν τις τεκτονικές κινήσεις στην περιοχή, αναλύθηκαν διαφορετικά σενάρια σχετικά με την αναλογία της τεκτονικής ανύψωσης/ταπείνωσης ρηγμάτων καθως και κλίση αυτών.

XII. Συμπεράσματα

Η παρούσα διατριβή παρουσιάζει τόσο την παλαιογεωγραφική εξέλιξη του Ισθμού κατά το Τεταρτογενές, όσο και τις διαδικασίες εκείνες (ευστατικές και τεκτονικές κινήσεις), που οδήγησαν στις συνεχόμενες αλλαγές της γεωμορφολογίας.

Αρχικά μέσα από δεδομένα 11 γεωτρήσεων και επιφανειακών δειγμάτων από την περιοχή του Ισθμού προσδιορίστηκε το παλαιοπεριβάλλον τόσο με την στατιστική ανάλυση των αποτελεσμάτων όσο και με την βοήθεια της λιθολογίας και της μαγνητικής επιδεκτικότητας των ιζημάτων. Με την βοήθεια των νανοαπολιθωμάτων έγινε ο σχετικός προσδιορισμός της ηλικίας των στρωμάτων (από 125 έως 240 χιλιάδες χρόνια για τις γεωτρήσεις και από 125 έως ~410 χιλιάδες χρόνια για τα επιφανειακά ιζήματα) και στην συνέχεια η συσχέτιση των διαφορετικών οριζόντων.

Έπειτα ακολούθησε η τρισδιάστατη απεικόνιση των ιζημάτων του ανατολικού τμήματος του Ισθμού, καθώς και ο προσδιορισμός του ρυθμού ανύψωσης (~0.3 ± 0.12 mm/yr) της περιοχής. Μέσω της λεπτομερούς χαρτογράφησης του ρήγματος Καλαμακίου-Ισθμίων και με βάση τα νανοαπολιθώματα προσδιορίστηκε ένας ρυθμός ολίσθησης για το ρήγμα ~ 0.07±0.2 mm/yr κατά τα τελευταία 200 χιλιάδες χρόνια.

Πραγματοποιήθηκε η ανάλυση της ανύψωσης και της ταπείνωσης των σημαντικότερων ρηγμάτων της ευρύτητες περιοχής. Με βάση τα αποτελέσματα αυτά, εκτιμήθηκε ο ρυθμός της γενικότερης τεκτονικής ανύψωσης της περιοχής.

Τέλος, με βάση τόσο τα δεδομένα από αυτήν την εργασία, τον ρυθμό ανύψωσης της περιοχής, το λεπτομερές μοντέλο του ανάγλυφου της περιοχής και τις ευστατικές κινήσεις της θάλασσας, έγινε η ανακατασκευή του παλαιοπεριβάλλοντος κατά το Τεταρτογενές.